Fall 12-5-2011

Rational Design and Development of Anti-Angiogenic Protein Agents

Lu Yin
Georgia State University

RATIONAL DESIGN AND DEVELOPMENT OF ANTI-ANGIOGENIC PROTEIN AGENTS

by

LU YIN

Under the Direction of Dr. Zhi-Ren Liu

ABSTRACT

Inhibition of angiogenesis is an effective and low toxic therapeutic avenue for the treatment of cancer patients in addition to traditional interventions. Majority of current available angiogenesis inhibitors for cancer therapies are growth factor inhibitors and small molecule tyrosine kinase inhibitors. A number of endogenous proteins and/or proteolytic fragments of extracellular matrix proteins are shown to have the activity of inhibition of angiogenesis by directly targeting endothelial cells. Structural analyses have indicated that a common structure of anti-parallel β-sheet with a highly positively charged surface presents in many of those inhibitors. This common structural feature is critical for the maintenance of their anti-angiogenic

function. With this structural information, we have designed and developed a new class of anti-angiogenic proteins by integrating the short anti-parallel β-sheet forming sequences of endogenous anti-angiogenic proteins into a stable host protein, the extracellular domain-1 of cluster of differentiation 2 molecule (CD2D1). 1D ^{1}H NMR spectra analyses indicated that the designed anti-angiogenic protein (ref to as ProAgio) folded as a β-sheet structure similar to that of the parental protein, CD2D1. ProAgio inhibited the growth of human umbilical vein cells (HUVECs) without affecting the growth of epithelial cells, suggesting a specific effect to endothelial cells. ProAgio effectively reduced endothelial tubules formed by the co-culture of HUVECs and PC3 cells on matrix gel *in vitro*. The designed anti-angiogenic protein was further site-specifically PEGylated in order to improve PK/PD properties and reduce immunogenicity. Examinations with PC3 xenografts showed that both ProAgio and the PEGylated ProAgio dramatically inhibited tumor growth. Immunofluorescence staining analyses of the endothelial marker CD31 indicated dramatic decreases in tumor vessels in lengths and branching points. Histological and immunofluorescence staining analyses of tissue slices of major organs indicated that there were no pathological damages to the tissue structure or disruption of normal vessels associated with the treatment of our designed anti-angiogenic agent. Overall, our studies developed a novel anti-angiogenesis agent that may have great clinical potentials. Our concept of protein design can be extended to the development of other novel protein drugs.

INDEX WORDS: Anti-angiogenesis, Rational design, VEGF, VEGFR inhibitors, Endogenous angiogenesis inhibitors, β-Sheet protein, CD2D1,

RATIONAL DESIGN AND DEVELOPMENT OF ANTI-ANGIOGENIC PROTEIN AGENTS

by

LU YIN

A Dissertation Submitted in Partial Fulfillment of the Requirements for the Degree of

Doctor of Philosophy

in the College of Arts and Sciences

Georgia State University

2011

RATIONAL DESIGN AND DEVELOPMENT OF ANTI-ANGIOGENIC PROTEIN AGENTS

by

LU YIN

Committee Chair: Dr. Zhi-Ren Liu, PhD

Committee: Dr. Jenny J. Yang, PhD

Dr. Julia Hilliard, PhD

Dr. Hans E. Grossniklaus, MD

Electronic Version Approved:

Office of Graduate Studies

College of Arts and Sciences

Georgia State University

December 2011

DEDICATION

This dissertation is dedicated to my parents, Mr. and Mrs. Ming-Liang Yin who always believe in me to achieve my dream.

ACKNOWLEDGEMENTS

First, I would like to thank Dr. Zhi-Ren Liu for giving me this opportunity to broaden my knowledge in science. I sincerely thank him for teaching and mentoring me throughout my graduate career with great patience. His dedication and constant encouragement is the key for me to fulfill this study. I would especially like to thank Dr. Jenny J. Yang who has been a role model for me and all her graduate students. She has encouraged each one of us marching toward the goal to become a well-trained scientist and a better person. I wouldn't be determined to practice giving presentations in front of audiences without her encouragement, which was the biggest breakthrough that I've ever made. I also thank her for the momentous roles in my project and numerous help that she kindly offered whenever I needed. I would like to especially acknowledge my exceptional doctoral dissertation committee member, Dr. Julia Hilliard. Her continuous support and thoughtful suggestions helped me to make great improvements in this dissertation work. I would particularly thank Dr. Hans Grossniklaus for willing to become a member of my doctoral dissertation committee member. He generously in shared his tremendous knowledge in the field of angiogenesis as well as useful laboratory resources were indispensable in this study. It was especially appreciated that he would answer every single one of my questions with great patience and even examined tissue slides with me in person. I would also like to thank Dr. Hua Yang for her many discussions with me, helpful suggestions and hand-on trainings that facilitated this study greatly. I would like to thank Dr. Phang C. Tai for his help in accepting me to the Department of Biology at Georgia State University. His successive support throughout my graduate career brought me great encouragement to fulfill my degree. I

would also thank Dr. Delon W. Barfuss, Dr. Susana Greer and Dr. Andrew Clancy for kindly helping me through my doctoral qualifying examination. What they showed me helped me build my confidence to succeed in my graduate study.

Next, I would specially thank for my husband, Dr. Hsiau-Wei Lee for his consequential roles in designing and modeling all the proteins in this study, advices on protein purification as well as ideas that helped this project keep moving forward. Without him, I wouldn't be able to accomplish my study in many ways. I am so proud of what we've been through together and who we are now. I would especially thank my father, Mr. Ming-Liang Yin. I wouldn't be determined to pursue the higher education in a doctoral degree without his influences. I particularly thank my mother, Mrs. He-Yi Li. It is her who built the foundation for me to enter the field of science and enjoy it all along. I owe Dad and Mom for missing out on the past 6 years of their lives. I would also like to thank my parent-in laws, Major General and Mrs. Rong-Chang Lee. Without their tremendously emotional and financial help, I wouldn't be able to continue my graduate study and complete my degree. I also would like to specially thank my sister, Ms. Chang Yin and her family for always supporting me. Dear sister, you are one cool person who I can never repay. I would also like to thank my brother and sister in-law, Dr. and Mrs. Shao-Chien Lee for always being there for me and my family.

Then, I would specially thank Mrs. LaTesha Warren who was always cheerful and kind. Her great assistance facilitated my study and made me feel like home. I would also like to thank Dr. Yubin Zhou, Dr. Yun Huang, Dr. Shun-Yi Li, Dr. Jian-Hua Yang, Ling Wei, and Dr. Hing-Cheung Wang, for their specialties and kind help when I carried out this study. I would particularly like to thank Dr. Anna W. Maniccia and her husband, John. They have been awesome friends to me.

I would specially thank Dr. Christ Carter for helping me improve my writing techniques and being helpful in my study. I would also like to thank my other current and past lab members, Dr. Xue-Liang Gao, Dr. Li-Xia Wei, Hai-Zhen Wang, Heena Day, Liang-Wei Li, Xiao-Wei Liu, Chia-Yi Liu, Yinwei Zhang, Bing Xu, Ravi Turaga and Hui-Wen Lue for their continuous support and help through the years. I especially appreciate all of them for respecting on the "rules" that I made in ordering lab supplies. They have kindly had my back when I tried to help our laboratory be more organized. I really enjoyed these years working with them.

And finally, I would like to thank all the current lab members from Dr. Jenny J. Yang's laboratory. Thank Yan-Yi Chen for his kind discussions about my protein purification experiments. He always has sparkling ideas that make things work. I would like to thank Dr. Jing-Juan Qiao for always being so patient and helpful whenever I needed her. Adriana Castiblanco, Dr. Mike Kirberger, Yu-Sheng Jiang, Dr. Jie Jiang, Sheng-Hui Xue, Chen Zhang, Jie Feng, You Zhuo, Fan Pu, and all others, I would like to thank them for answering every question that I asked and I know that I'd asked a lot of help from every one of them. Without their generous help throughout these years, I wouldn't be able to master the protein purification and other techniques and made this project possible.

In the end, I would thank National Stutter Association (NAS) for their continuous and exceptional efforts in making this world a better place for non-fluent and fluent speakers. I also thank for the scholarships sponsored me for NSA conferences with life-changing experiences.

TABLE OF CONTENTS

LIST OF TABLES

LIST OF FIGURES

LIST OF ABBREVIATIONS

Abbreviations Chemistry and Biochemistry

BrdU	5-bromo-2-deoxyuridine
BSA	Bovine serum albumin
CD	Circular Dichroism
cDNA	complementary DNA
D1-CD2	Domain 1 of cluster of differentiation 2
DNA	Deoxyribonucleic acid
DTT	Dithiothreitol
ED_{50}	Half maximal effective concentration
EDTA	Ethylenediaminetetraacetic acid
FPLC	Fast performance liquid chromatography
GAG	Glycosaminoglycan
GS4B	Glutathione sepharose 4B
GST	Glutathione-S-transferase
HBSS	Hank's Buffered Salt Solution
H&E	Hematoxylin and Eosin
HEPES	4-(2-hydroxyethyl)-1-piperazineethanesulfonic acid
HRP	Peroxidase
IPTG	Isopropyl β-D-thiogalactoside
K_d	Dissociation constant
kDa	Kilodalton
K_{on}	Association rate constant
K_{off}	Dissociation rate constant
LB medium	Luria-Bertani medium
MES	2-morpholin-4-ylethanesulfonate
MTT	3-(4,5-Dimethylthiazol-2-yl)-2,5-diphenyltetrazolium bromide
mg	Milligram
µg	Microgram
ml	Milliliter
mM	10^{-3} mol/dm^3
µM	10^{-6} mol/dm^3
MW	Molecular weight
ng	Nanogram
nm	nanometer
nM	10^{-9} mol/dm^3
NMR	Nuclear magnetic resonance
NO	Nitric oxide
O. D.	Optical Density
OD	Absorbance
PBS	Phosphate buffer saline
PCR	Polymerase chain reactions

PDB	Protein databank
PEG	Polyethylene glycol
PGI	Prostacyclin
pM	10^{-12} mol/dm^3
SDS-PAGE	Sodium dodecyl sulfate polyarcylamide gel electrophoresis
Tris	2-Amino-2-(hydroxymethyl)-1,3-propanediol
UV	Ultraviolet

Abbreviations in Biology

APC	Antigen presenting cell
Ang	Angiopoietin
bps	base pairs
CD2	Cluster of differentiation 2
CD31	Cluster of differentiation 31
CD48	Cluster of differentiation 48
CD58	Cluster of differentiation 58
CD2D1	Extracellular domain 1 of CD2
CHO	Chinese hamster ovary
CRD	Carbohydrate recognition domain
CTLs	Cytotoxic T lymphocytes
EC	Endothelial cell
E. coli.	*Escherichia coli*
ECM	Extracellular matrix
EGF	Epidermal growth factor
FBS	Fetal bovine serum
FGF	Fibroblast growth factor
FGFR	Fibroblast growth factor receptor
EPC	Endothelial progenitor cell
FIGF	Fos-induced growth factor
FLK	Fms-like tyrosine kinase
FN	Fibronectin
FU	Fluorouracil
Gal-1	Galectin-1
GFR	Growth factor reduced
GIST	Gastrointestinal stromal tumor
HCC	Hepatocellular carcinoma
HIF	Hypoxia-inducible factor
hPRL	N-terminal fragment of human prolactin
HUVEC	Human umbilical cord vein endothelial cell
IF	Immunofluorescence
IgSF	Immunoglobulin superfamily
INF	Interferon

IL	Interleukin
i.p.	Intraperitoneal
KIT	V-kit Hardy-Zuckerman 4 feline sarcoma viral oncogene homolog
LV	leucovorin
mAb	Monoclonal antibody
MAPK	Mitogen-activated protein kinase
MHC	Histocompatibility complex
MMP	Metalloproteinase
mTOR	Mammalian target of rapamycin
MVD	Mean vascular density
NAP-2	Neutrophil-activating protein-2
NC domain	Non-collagenous domain
NK cell	Natural killer cell
NMD	Non-Matrix-Derived
NSCLC	Non-small-cell lung cancer
PCR	Polymerase chain reaction
PC	Prostate cancer
PDGF	Platelet-derived growth factor
PDGFR	Platelet-derived growth factor receptor
PEDF	Pigment epithelium-derived factor
PEX	MMP-2 hemopexin domain
PF-4	Platelet factor-4
PHS	Public Health Service
PIGF	Placental-induced growth factor
PK/PD	Pharmacokinetic/Pharmacodynamic
PKC	Protein kinase c
PLC-γ	Phospholipase C-γ
Raf-1	V-raf-1 murine leukemia viral oncogene homolog 1
Rb	Retinoblastoma
RCC	Renal cell carcinoma
RET	Rearranged during transfection
RGD	Arginine-glycine-aspartic acid
RTK	Receptor tyrosine kinase
SRBC	Sheep red blood cell
TcR	T cell receptor
TGF	Transforming growth factor
TIMP	Tissue inhibitors of matrix metalloproteinases
TKI	Tyrosine kinase inhibitor
Tum	Tumstatin
TSP-1	Thrombospondin-1
TSR	Thrombospondin-1 type 1 repeat
VEGF	Vascular endothelial growth factor
VEGFR	Vascular endothelial growth factor receptor

Others

ATCC	American type Culture Collection
DAR	Department of Animal Research
1D	1 dimensional
2D	2-dimensional
3D	3-dimensional
FDA	Food and Drug Administration
IACUC	Institutional Animal Care and Use Committee
GSU	Georgia State University
Obj.	Objective
rpm	Revolutions per minute
SOP	Standard operating procedure

CHAPTER 1

GENERAL INTRODUCTION

1.1 Angiogenesis in Life and Diseases

Blood vessels distribute oxygen and nutrients, and remove waste from distant organs. Understanding the mechanism of blood vessels formation is a primary yet challenging field (reviewed in [1]). Most vasculature is developed during embryogenesis under multiple tightly regulated processes involved in vasculogenesis, angiogenesis and arteriogenesis (reviewed in references 1 – 11 and 13 – 16). Vasculogenesis gives rise to a primitive vascular network where mesodermal angioblasts proliferate, migrate, differentiate to endothelial cells (ECs) and align to tubular structures [2, 3]. These primitive vessels are further expanded by sprouting or splitting, then pruned and remodeled into a functional circulatory system, termed as angiogenesis [3]. Subsequent arteriogenesis coats vessels with pericytes and smooth muscles, and forms mature blood vessels [4]. After birth till adolescence, angiogenesis becomes the main mechanism that produces new blood vessels for organ growth and development [1].

In normal adult tissues, vasculature is quiescent except for female reproductive cycles [1-5]. Despite an extremely low turnover rate, ECs respond quickly to tissue stimuli and divide rapidly to turn on angiogenesis facilitating wound healing and tissue repair [1, 6]. Prolonged stimuli lead to excessive angiogenesis, which have been implicated in many pathological processes, such as inflammatory and autoimmune disorders, tumor growth and metastasis, ocular diseases, obesity, asthma, diabetes, bacterial infections and other conditions [1, 7]. Conversely, insufficient angiogenesis prevents revascularization and tissue regeneration, a condi-

tion that is related to ischaemic diseases, cardiac failure, preeclampsia, Alzheimer's disease [1]. To date, anti- and pro-angiogenic therapies have prominent roles in treatments of malignant diseases, myelodysplastic syndrome, and age-related macular degeneration [8]. With increasing in depth insights into how angiogenesis affects health and diseases, angiogenesis is considered as an important target that will enable us to combat a broad range of human diseases [7-11].

1.2 Angiogenesis is a Multi-step Process

Under normal physiological conditions, angiogenesis is a complex multi-step process [3, 5]. Wound, hypoxia, and inflammation are signals that activate angiogenesis. Vascular endothelial growth factor (VEGF), also referred as VEGF-A, is a critical player for angiogenesis initiation. In mature blood vessels, EC lining is surrounded by a mural capsule composed of basement membrane and a layer of pericytes. VEGF increases vascular permeability, promotes ECs entering mitotic cycles, and leads to dissociation of pericytes [8, 12, 13]. Simultaneously, matrix metalloproteinases (MMPs) and other enzymes locally degrade the basement membrane and extracellular matrix (ECM), which allows ECs to disconnect with each other, change shapes and migrate toward the stimulus. Only ECs in the leading edges continuously proliferate, while ECs along the trail reattach to each other and form intact monolayer capillary tubes. Then different tubes are connected into loops. At last, blood flows into the newly formed vasculature and establishes circulation. In large blood vessels, fibroblasts and smooth-muscle like cells are also recruited to the nascent vessels to recoat them.

1.3 Angiogenesis Switch during Tumorigenesis

In addition to serial genetic and epigenetic events, angiogenesis is a prerequisite for transformation of normal tissue into cancers [14, 15]. Several lines of evidence observed from transgenic animal models, human breast, cervical and skin cancers have demonstrated that angiogenesis switch is a critical rate limiting step for tumor malignancy and metastasis [5, 7, 14]. Virtually all cells in human tissue are situated within the range of 100 μm around blood vessels for adequate oxygen and nutrient supplies. Before neovascularization occurs, a stage defined as avascular phase, most solid tumors enter a dormant state and will not exceed 1 to 2 mm^3 in size [16-18]. Inadequate access to vasculature leads to necrosis and/or apoptosis inside solid tumors, therefore restrains them from continuously expanding despite the high proliferation rates of unaffected cancer cells [19] and reviewed in [5, 19, 20]. Exponential growth of tumors only occurs in the following vascular phase when new blood vessels are established [5, 18]. These principles also apply to metastatic tumors.

Angiogenesis switch is controlled under the balance between pro- and anti-angiogenic factors (reviewed in [5, 21]). Once formed, vasculature quickly matures and is stabilized by endogenous inhibitors. Interferon α/β (IFN-α/β) and platelet factor-4 (PF-4) are the first identified anti-angiogenic factors that inhibit ECs migration and proliferation [22-24]. Thrombospondin-1 (TSP-1) is an endogenous anti-angiogenic protein secreted by platelets [25]. Notably, a variety of endogenous angiogenesis suppressors is released from extracellular matrix proteins by proteolytic degradation to inhibit ECs migration and adhesion. For example, endostatin and angiostatin are fragments of type XVIII collagen and plasminogen, respectively [26, 27]. Dormant tumor lesions have to adapt disparate methods to break through the avascular phase supervised

by all those known and unknown inhibitory mechanisms. In contrast, many growth factors and cytokines secreted or induced by tumor cells have been proven to promote angiogenesis. Among them, VEGFs and their receptors (VEGF/VEGFRs) are crucial stimulants that promote ECs proliferation and increase vessel permeability and remolding [28, 29] and reviewed in [28]. Integrins (especially intergrin $\alpha_v\beta_3$ and $\alpha_v\beta_{5)}$, extracellular matrix metalloproteinases-3 and -9 (MMP-3 and -9), angiopoietin-1 and -2 (Ang-1 and -2) and their receptor Tie2 are important regulators of angiogenesis [4, 29]. Besides, many growth factors and chemokines such as platelet-derived growth factor β (PDGF-B), epidermal growth factor (EGF), fibroblast growth factors (FGFs), and interleukin-6 and -8 (IL-6 and -8) also promote angiogenesis and their distinct mechanisms were reviewed by Wang and coworkers [11].

Depending on different origins and microenvironments, tumor cells adapt unique mechanisms to tip this balance in favor of switching on angiogenesis: either by silencing endogenous anti-angiogenic proteins for example TSP-1 gene mutations, or secreting/inducing pro-angiogenic factors such as growth factors and MMPs (reviewed in [5]). In many cases both are applied.

1.4 Tumor Vasculature Morphology

Tumor vasculature are formed by angiogenesis (sprouting for existing vessels), co-opting host vessels, and postnatal vasculogenesis (recruiting endothelial progenitors from bone marrow) (reviewed in [30]). A broken balance between negative and positive angiogenic factors in tumors results in a constant growth of new blood vessels, a condition described as “wounds that never heal” (reviewed in [31]). In the presence of excessively increased levels of VEGF, an-

giopoietin-1 and -2, and other pro-angiogenic stimulants, newly formed tumor vessels are structurally and functionally abnormal: (i) they are often dilated and leaky as a consequence of missing cell-cell adhesion junctions between ECs with discontinuous basement membranes [12, 32-34]; (ii) vessels are also disorganized with tortuous paths, haemorrhages, dead ends, and without a clear hierarchy of arterioles, venules and capillaries [15]; (iii) cancer cells occasionally integrate into the vessel walls (reviewed in [35]); (iiii) structural abnormalities along with compression from proliferating cancer cells contribute to heterogeneous and insufficient blood flows [34].

1.5 Molecular Pathways of Tumor Angiogenesis

1.5.1 VEGF Signaling Pathways

VEGFs and their receptors are the most important mediators of angiogenesis. In 1983, Serger and coworkers first reported a vascular permeability factor (VPF) secreted by a tumor cell line significantly increases vascular permeability [12]. Later on, its cDNA sequence proved that it is the same protein as VEGF (or VEGF-A) isolated by Ferrara *et al* in 1989 [36]. So far, five other glycoproteins are identified to be products of the VEGF gene family members, including VEGF-B, C (also known as c-fos-induced growth factor, FIGF), D, E, and placental-induced growth factor (PIGF, also referred as PGF) [37-39]. Among them, VEGF is the most potent EC-specific mitogen that promotes both physiological and pathological angiogenesis. VEGF strongly induces angiogenesis *in vitro* and *in vivo* [40-42]. Studies in transgenic mice embryonic studies show that loss of a single VEGF allele is lethal accompanied with severe abnormalities in angiogenesis and blood vessel formation [43].

The VEGF gene (vegf) located in chromosome 6 is formed by eight exons and seven introns [44-46]. Exon 7 codes for an Arginine (Arg) and Lysine (Lys) enriched c-terminal motif, meanwhile exon 6 is translated into a 24 amino acids long insertion that is also highly positively charged [44]. Alternative splicing of exons 6 and 7 generates different length of isoforms with or without the binding ability to the highly negatively charged glycosaminoglycans (GAGs) (heparin, for example) and ECM. So far, the identified isoforms mainly are $VEGF_{121}$, $VEGF_{145,}$ $VEGF_{148,}$ $VEGF_{165}$, , $VEGF_{183}$, $VEGF_{189}$ and $VEGF_{206}$ [44, 47-49]. The diversity of those isoforms is believed to mediate the biological function and tissue specificities of VEGF [50-52]. $VEGF_{165}$ is the predominant and most characterized VEGF isoform. Many studies have demonstrated that $VEGF_{165}$ is responsible for specific receptor binding and VEGF bio-functions [51-57]. With the basic motif coded by exon 7, 50-70% secreted VEGF-A_{165} binds to ECM creating an extracellular VEGF storage pool [51]. Plasminogen, an extracellular protease and MMPs, especially MMP-3 and -9, can cleave $VEGF_{165}$ and $VEGF_{189}$, which produces shorter VEGF fragments that are active and diffusible [29, 54]. During tumor angiogenesis, degradation of ECM and proteolytic cleavage of VEGF-A have been considered as two important mechanisms that upregulate VEGF signaling pathways by releasing sequestered VEGF [29, 54].

Two tyrosine kinase receptors can be recognized by VEGF: VEGFR-1 (also known as Flt-1) and VEGFR-2 (also known as Flk-1 or KDR) [58, 59]. Although VEGFR-1 has 10-fold higher binding affinity than VEGFR-2 does, VEGFR-2 is the major receptor for VEGF angiogenic signaling [60-62]. Certain tumor types and ECs also express Neuropilin-1 (NPR-1) as co-receptor that enhances the binding of $VEGF_{165}$ to its receptor VEGFR-2 [63]. The protease cleaved VEGF isoforms without the c-terminal basic motif encoded by exon 7 cannot bind to NPR-1, thus do not have

the enhancement effect. The 40 -kDaa glycoprotein VEGF binds to VEGFR-2 in a homodimeric form. Upon ligand binding, VEGFR-2 undergoes conformational changes and dimerization, which activates its receptor tyrosine kinase (RTK) activity that leads to receptor autophosphorylation followed by a cascade of downstream signaling [64, 65]. VEGF strongly stimulates proliferation of ECs from arteries, veins and lymphatics via activation of the protein kinase c (PKC) and Raf-Mek-Erk pathway [66]. It also protects ECs from apoptosis by inducing the expression level of anti-apoptotic proteins, suppressing pro-apoptotic proteins such as p53, p21, Bax, and up-regulating the phosphatidylinositol-3' kinase (PI3K)-Akt signaling pathway [40, 67]. VEGF potently enhances vascular permeability by rearranging and loosing cell adhesion junctions between ECs [68]. VEGF also promotes ECs migration by enhancing the expression of urokinase- and tissue-type plasminogen activator (uPA and tPA) in ECs [69, 70]. Both uPA and tPA convert plasminogen to its active form plasmin. The proteolytic activity of plasmin degrades ECM components paving the way for ECs migration and vessel remodeling. In addition, VEGF also mobilizes bone marrow-derived (BM) endothelial progenitor cells (EPCs) to promote postnatal vasculogenesis in different types of tumors [71-73].

Other VEGFs and VEGFRs have their distinct biological functions. VEGF-B and PIGF selectively bind to VEGFR-1, but not other VEGFRs [74, 75]. VEGFR-1 does not have established role in angiogenesis yet. Early studies show that VEGFR1 may function as a "decoy" receptor for VEGFR-2 that negatively regulates its function by reducing its ligand binding. Recent studies suggest a role of VEGFR-1 in pathological angiogenesis like tumor metastasis via activation of MMP-9 [76, 77]. A more recent study draws a contrary conclusion on inhibition of VEGFR-1 as a valid target to reduce spontaneous metastasis in mouse models [78]. VEGF-C and -D mainly

recognize VEGFR-3 (also known as Flt-4) and mediate lymphangiogenesis. VEGF-C and -D also bind to VEGFR-2 after protease cleavage [38, 79].

1.5.2 Angiopoietins

In addition to VEGF/VEFGR, early studies also demonstrated that Angiopoietin-1 and -2 (Ang-1 and -2) and their receptor Tie-2 (also known as Tek) also have crucial roles in mediating angiogenesis [80-82]. Tie-2 is an RTK expressed in the surfaces of ECs, smooth muscle, fibroblast and some immune cells [83, 84]. Ang-1 is the primary agonist of Tie-2. Unlike VEGF, Ang-1 alone does not induce *in vitro* angiogenic effects [83]. Transgenic mouse embryos that lack Ang-1 or Tie-2 developed relatively normal vasculature, but eventually died at late stage due to defects in blood vessel remodeling [83]. The physiological roles of Ang-1 lay in recruiting pericytes and mediating the interactions between ECs and their surrounding environment, stabilizing the newly formed blood vessels [85]. Ang-1 also prevents blood vessel leakage countering the potent permeable effect of VEGF [86]. Ang-2, however, has a rather complex role in angiogenesis. It functions partially as an antagonist to Tie-2, which promotes ECs detachment from smooth muscle cells and ECM [81, 87]. The destabilization effect of Ang-2 either leads to vessel regression, or increases in EC sprouting under excessive level of VEGF-A and other growth factors [88, 89]. The ratio of Ang-1/Ang-2 can function as a check-point for tumorigenesis. Recent studies show that elevated Ang-2 expression levels correlate with poor prognosis in patients with tumors [90-92]. Furthermore, specific inhibition of Ang-2 reduces tumor growth in xenograft models [93, 94].

1.5.3 Fibroblast Growth Factor

In an early review, Folkman and a coworker pointed out that many EC growth factors have strong affinity to heparin [95]. The acid fibroblast growth factor (aFGF/FGF-1) and basic fibroblast growth factor (bFGF/FGF-2) are among the first identified angiogenic growth factors that separated by heparin-affinity chromatography. As suggested by a review of this family, there are more than 20 different FGF isoforms that bind to four different types of FGF receptors (FGFRs) regulate a range of physiological and pathological functions such as organ development, neurogenesis, angiogenesis, and cancer growth (reviewed in [96]). In addition to receptor binding, the interaction between FGFs to cell-surface associated heparan sulfate proteoglycans plays an important role in transduction of FGFs signaling. FGF1 and -2 have similar angiogenic functions as VEGF-A during tumorigenesis (reviewed in [96, 97]). Both FGF-1 and -2 promote EC proliferation and migration. Up-regulation of FGF-2 protects ECs from apoptotic stimuli via distinct mechanisms such as expression of Bcl-XL and Bcl-2, or activation of Raf-1 [98, 99]. FGF-1 and -2 facilitate blood vessel remodeling through mediation of uPA, MMPs, and collagenase [11, 97, 100]. FGF-2 also indirectly promotes angiogenesis by increasing VEGF and VEGFR expression level in ECs (reviewed in [97]). Although studies using monoclonal antibodies that neutralize FGF-2 did not produce anti-tumor effect, a recent study has shown that up-regulation of FGF signaling is one of the possible causes for resistance of anti-VEGFR2 tumor treatment in RIP-Tag mouse model [101, 102].

1.5.4 Platelet-derived Growth Factor

Platelet-derived growth factor (PDGF) family and their receptors (PDGFR-α and PDGF-β) share great structural and amino-acid sequence similarity with that of the VEGF/VEGFR family (reviewed in [103]). PGDF was initially found to be released into circulation from α-granules in platelets but subsequent studies show that fibroblasts, ECs, osteoblasts, and many other cell types also secret PDGF (reviewed in [97, 103]). There are four individual PDGF polypeptide chains encoded by different genes: PGDF-A, -B, -C, and D. Homo- or hetero-dimerization between those polypeptide chains produces five active isoforms, including PDGF-AA, BB, AB, CC, and DD (reviewed in [103]). Hoch and workers suggested that formation of the heterodimeric PDGF-AB is rare *in vivo* and without clear known biological significance [104]. PDGFs isoforms initiate signaling pathways via binding to the two RTKs (PDGFR-α and –β); for example, PDGF-AA activates PDGFRα, whereas PDGF-BB mainly activates PDGFR-β. PDGFs play essential roles in organogenesis during embryonic development, but they are expressed in low levels under normal physiological conditions in adults (reviewed in [103]). Similar to other growth factors, all four homodimeric PDGFs promote carcinogenesis via activation of a variety of cellular signaling molecules such as Ras, PI3K, phospholipase C-γ (PLC-γ), and Akt (reviewed in [103, 105]). The PDGF-BB/PDGFR-β signaling is one of the major regulatory molecules of angiogenesis. PDGF-BB is mainly expressed in ECs and neurons, while PDGFR-β is expressed in vascular smooth muscle cells and pericytes (reviewed in [103]). PDGF-BB and PDGFR-β knockout mice died prenatally with widespread hemorrhage and edema as consequences of vascular pericytes losses, suggesting the crucial role of PDGF-BB/PDGFR-β in recruiting vascular pericytes and promoting blood vessel maturation [106]. PDGFs also contribute to tumor growth and angiogenesis also by re-

cruiting either PDGFR-β^+ or PDGFR-α^+ fibroblasts to tumor stroma [107-109]. PDGF-BB also induces ECs to secret VEGF and successively stimulates tumor angiogenesis [110, 111]. Several lines of evidences have demonstrated that inhibition of PDGF/PDGFR signaling pathways are potential avenues to inhibit tumor angiogenesis [112-115]. In addition, Suzuki and colleagues suggested that PDGF-B may have more dominant role than VEGF does in the maintenance of angiogenesis in certain types of gastric carcinomas. Therefore stratified anti-angiogenic remedies may favor the overall survival rate in patients with gastric cancer [114].

1.5.5 Other Growth Factor Signal Pathways

Besides the above described signaling pathways, many other growth factors have been demonstrated to promote angiogenesis via different mechanisms (reviewed in [11, 97, 116]). Both epidermal growth factor (EGF) and transforming growth factor-α (TGF-α) promote angiogenesis via epidermal growth factor receptor (EGFR). EGF signaling and EGFR inhibitors will be introduced in 1.7.2.2. Although transforming growth factor-β (TGF-β) family is reported to have multiple physiological functions including angiogenesis, the roles in angiogenesis is context-dependent with both anti- and pro-angiogenic effects documented. By switching downstream signaling transduction pathways in different cell types, TGF-β may prevent angiogenesis in early stage of tumorigenesis, while becoming pro-angiogenic as cancer progresses into late stages when the growth factor is usually expressed at high levels (reviewed in [117, 118]). Recent studies have demonstrated that inhibition of TGF-β by different methods reduces tumor angiogenesis and tumor growth (reviewed in [117, 119]).

1.5.6 Integrins

Integrins are a group of transmembrane glycoproteins that regulate cell adhesion, mobility and survival. Integrins are heterodimers composed of distinct α and β chains [120]. Different combinations between 18 α-subunits and 8 β-subunits by non-covalent interactions generate 24 mammalian integrins (reviewed in [120, 121]). The αv and α5β1 integrins are receptors for a variety of ECM components, such as fibrinogen (αvβ3, α5β1), fibronectin (αvβ3, α5β1), osteopontin (αvβ3), and activated vitronectin (αvβ3, αvβ5). A conserved tripeptide sequence, Arg-Gly-Asp (RGD), is displayed in those ECM proteins, and is required for the ligand-receptor reorganization. Integrin αvβ3, αvβ5 and α5β1 have roles in tumor angiogenesis. They are not expressed or expressed in low levels in normal tissues, but induced or up-regulated in a wide range of tumor types, particularly in tumor ECs [122, 123]. Studies have shown that integrins crosstalk with specific growth factors that are crucial for tumor angiogenesis. For example, blockage of integrin αvβ3 abolishes the angiogenic effects of TNF-α and bFGF, whereas integrin αvβ5 is required for the effects of TGF-α and VEGF on angiogenesis [124]. Different antagonists targeting αvβ3, αvβ5 and α5β1, including monoclonal antibodies, RGD mimetic peptides, non-peptide compounds and antisense RNAs, have shown significant anti-angiogenic and anti-tumor effects by inhibiting tumor cell and EC growth (reviewed in [120]). Many of them are under clinical trials for treatment of patients with different types of cancers. Integrins and RGD mimetic peptides are also under extensive investigations as targeting moieties for tumor imaging and drug delivery (reviewed in [125]).

1.5.7 Matrix Metalloproteinase

Matrix metalloproteinases (MMPs) are zinc-dependent endopeptidases with a broad spectrum of activities which control ECM remolding by degrading all known EC proteins (reviewed in [126]). A total of 23 human MMPs have been characterized as either secreted MMPs or transmembrane-type MMPs (MT-MMPs) that together regulate tissue remodeling, organ development, inflammatory processes, and pathological conditions such as cancer (reviewed in [127]). MMPs are not or expressed in low levels in quiescent ECs, but are strongly induced and activated during pathological angiogenesis such as tumor and inflammation (reviewed in [126]). Depending on their expression patterns and availability of substrates, MMPs tightly regulate tumor angiogenesis by exerting dual functional effects (reviewed in [127, 128]). On one hand, MMPs, particularly MMP-2, MMP-9 and MMP-14, are essential for the formation of tumor vasculature as they degrade ECM, which clears the way for EC migration and also proteolytically activates angiogenic factors (reviewed in [128]). MMP-9 serves as an example; in addition to degradation of ECM components, it potently accelerates the angiogenic switch by releasing ECM-bound VEGF isoforms to activate VEGFR-2 [129]. MMP-9 also catalytically induces the activation of TGF-β and bFGF-2 signaling pathways [130, 131]. On the other hand, MMPs cleave ECM proteins to generate a diverse range of endogenous protein fragments to block active angiogenesis. For example, MMPs cleave type IV, XVII collagen, plasminogen and perlecan, which respectively produce tumstatin, endostatin, angiostatin and endorepellin that strongly inhibitor tumor angiogenesis (reviewed in [128]).

1.6 Tumor Angiogenesis as a Therapeutic Target

In 1971, Dr. Judah Folkman first proposed “anti-angiogenesis” as a tumor therapy given the fact that tumor growth depends largely on new vasculature formation [16]. This hypothesis has greatly driven an enthusiastic wave of pursuing therapeutic angiogenesis inhibitors as effective cancer therapies. In past three decades, a great body of knowledge regarding mechanisms of angiogenesis has been gained as a result of studying tumor angiogenesis. In 2004, avastin (also known as bevacizumab, Genentech Inc.) became the first U.S. Food and Drug Administration (FDA) approved anti-angiogenic drug by for the treatment of advanced colorectal cancer, which opened a new era for targeting tumor vasculature as an anti-cancer therapy.

Back in 2004, anti-angiogenic therapy was predicted as “the fourth modality” for cancer treatment. Compared to traditional chemotherapy, radiotherapy, and surgery, it has several clinical advantages. Firstly, anti-angiogenic therapies mainly target the proliferating ECs, thus they are less likely to lead to side effects related to inhibition of actively dividing cells, such as bone marrow suppression, gastrointestinal (GI) disturbances, and hair loss. Secondly, clinical data clearly show that anti-angiogenic reagents significantly lower the dose ranges of cytotoxic and radioactive cancer therapies, thus reduces side effects among cancer patients [132-134]. Thirdly, data support that anti-angiogenic therapies also normalize tumor vasculature and promote drug delivery (reviewed in [135]). Lastly, a broad spectrum of malignant and benign tumors can be treated because angiogenesis is a universal mechanism for tumorigenesis and metastasis (reviewed in [136]).

1.7 Overview of Anti-angiogenic Reagents in Cancer Therapy

1.7.1 VEGF and VEGFR inhibitors

Current development of anti-angiogenic therapies for cancer treatment is heavily focused on inhibition of VEGF/VEGFR signaling pathway. Several inhibitors targeting this pathway have been developed into clinical usage including the humanized anti-VEGF monoclonal antibody, Bevacizumab, and small molecular inhibitors such as Sunitinib (Sutent®) and Sorafenib (Nexavar®).

1.7.1.1 Monoclonal Antibodies

1.7.1.1.1 Bevacizumab

Bevacizumab (rhuMab A.4.6.1, Avastin; Roche) is the first U. S. FDA approved anti-cancer drug that specifically target angiogenesis. Bevacizumab neutralizes all VEGF isoforms preventing their activation of VEGFR-2. In 1993, Kim and coworkers first demonstrated that blockage of VEGF signaling pathway by the murine precursor of bevacizumab (muMab A.4.6.1) sufficiently suppressed different types of human cancers implanted in immunodeficient mice [137]. Later studies show that bevacizumab has the same *in vitro* and *in vivo* anti-angiogenic effects as Mab A.4.6.1 [138]. A final three armed phase III clinical trial led to the approval of bevacizumab in combination of 5-fluorouracil (FU)/leucovorin (LV) as the first-line therapy for patients with previously untreated metastatic colorectal cancer [132]. Bevacizumab is also approved to treat nonsquamous non-small-cell lung cancer (NSCLC), glioblastoma, and renal cell carcinoma (RCC). Its application for treatment of metastatic HER-2 negative breast cancer is under FDA repeal process.

1.7.1.1.2 VEGF Trap

Soluble VEGF traps represent another approach to specifically inhibit VEGFR signaling pathway. Aflibercept (Regeneron and Sanofi-Aventis) is a recombinant protein created by fusion of the Fc fragment of human IgG_1 with both the extracellular domains of VEGFR1 and VEGFR2 [139]. In contrast to the VEGF neutralizer, bevacizumab, aflibercept has three major differences. First, it acts as a soluble VEGF receptor that traps all three types of VEGFs (VEGF, VEGF-B, and PIGF). Second, the binding affinity of aflibercept to VEGF is greatly enhanced with a K_d value around 1 pM compared to 800 pM of bevacizumab [139]. Third, it has improved pharmacokinetic behavior with prolonged circulating half-life [139]. It shows potent anti-tumor activities in a number of pre-clinical animal models, such as pancreatic carcinomas, neuroblastoma, and human ovarian cancer [140-142]. In pre-clinical animal models, aflibercept not only inhibits formation of new blood vessels, but also promotes vascular remodeling and regression of pre-existing vasculatures [139, 143-145]. Similar to bevacizumab as a single-agent, in a number of phase II clinical trials, treatment with aflibercept in patients with recurrent or metastatic urothelial cancer, pretreated lung adenocarcinoma, and recurrent malignant glioma have showed minimal response rates [146-148]. As reported by Regeneron and Sanofi-Aventis in 2011, aflibercept in combination with chemotherapy achieved positive results in phase III clinical trial in patients with metastatic CRC, but failed to improve overall survival rate when it was combined with docetaxel to treat patients with NSCLC (www.genengnews.com and company report). An aflibercept ophthalmic solution (Eylea) has been approved by FDA for treatment of age-related macular degeneration.

1.7.1.1.3 VEGF Intraceptor

Intracellular disruption of VEGF secretion is a novel method to inhibit tumor angiogenesis. A C-terminal KDEL (Lys-Asp-Glu-Leu) motif is an endoplasmic reticulum (ER) retention signal for ER-resident proteins [149]. Flt23k plasmid was designed by Singh and colleagues as an anti-angiogenic gene therapy [150]. It encodes Flt23k, a recombinant protein composed of domain 2 and 3 (VEGF binding domains) of VEGFR1 coupled with KDEL. Intracellulary expressed Flt23k binds VEGF in ER, and prevents its secretion, which will down-regulate VEGF signaling. Intrastromal injection of Flt23k plasmid sufficiently inhibits injury-induced corneal neovascularization in a marine model [150]. Nanoparticles have been used to delivery Flt23k plasmid and increase its expression duration [151]. A dual targeting tumor endothelium by nanoparticles carrying RGD (Arg-Gly-Asp) peptide and Flt23k plasmid has further enhanced its effects *in vivo* [152]. Compared to antibodies, it represents a novel approach to sequester VEGF from VEGFR.

1.7.1.1.4 Other VEGF Antibodies

Many other monoclonal antibodies are under clinical development. CDP791 (UCB Pharma) and IMC-1121B (ImClone Systems Inc) are VEGFR-2 antibodies that under phase II and phase III clinical trials (reviewed in [153]). In addition to aflibercept, pegaptanib sodium (Macugen®, Eyetech Pharmceuticals), a VEGF aptamer and ranibizumab (Lucentis®, Roche), an antibody fragment have been approved by FDA for the treatment of age-related macular degeneration [154, 155].

1.7.1.2 Small-molecule VEGFR Inhibitors

Sunitinib (SU11248, Sutent®; Pfizer) and Sorafenib (Bay-43-9006, Nexavar®; Bayer/Onyx) are small-molecule tyrosine kinase inhibitors (TKIs) that prevent phosphorylation of RTKs by targeting their intracellular ATP-binding pockets. Functioning as ATP analogues, TKIs usually have multiple targets by competitively binding to the ATP-binding pockets of different RTKs. They are considered "selectively" but not specifically as inhibitors of VEGF signaling pathways, so their anti-tumor effects are complex rather than just suppression of tumor angiogenesis alone (reviewed in [153]). Sunitinib blocks signal transduction from a variety of RTKs including all three types of VEGFR, colony stimulation factor receptor type 1 receptor, Fms-like tyrosine kinase 3 (FLK-3), PDGF-α and –β, glial cell line-derived neurotrophic factor receptor (RET), and stem cell receptor (KIT) (reviewed in [156]). Beside inhibition of angiogenesis induced by PDGF-β and VEGFR-2, sunitinib also represses tumor cell proliferation. Sunitinib is approved to treat imatinib (ST11571, Gleevec; Novartis)-resistant gastrointestinal stromal tumor (GIST), RCC, NSCLC, and thyroid cancer (reviewed in [156-159]). Different from bevacizumab, sunitinib is used as a stand-alone therapy for RCC and GIST. Sorafenib is a Raf-1 (a serine/thereonine protein kinase belong to RAF kinase family) inhibitor that blocks the Raf-Mek-Erk MAPK signaling pathway [160]. The anti-angiogenesis and anti-tumor effects of sorafenib are mainly involved in VEGFR-2 and -3, PDGF-β, Flt-3, and c-kit inhibition. Sorafenib is approved by U.S. FDA as an anti-cancer therapy for advanced RCC and unresectable hepatocellular carcinoma (HCC) (reviewed in [161]).

Many other small-molecule TKIs inhibit the VEGFR, EGFR, PDGFR, RET, and c-kit signaling pathways are under clinical development (reviewed in [153]). Some successful examples

are axitinib (Pfizer), motesanib (Amgen), cediranib (AstraZeneca), and vandetanib (AstraXeneca).

1.7.2 Other Reagents that Inhibit Angiogenesis

1.7.2.1 Mammalian Target of Rapamycin (mTOR) Inhibitors

Temsirolimus (CCI-779, Torisel®; Wyeth) is an mTOR inhibitor derived from rapamycin. mTOR is a serine/threonine kinase that controls cell growth, proliferation, and response to hypoxic stress by regulating ribosome function and tRNA synthesis. In addition to anti-tumor effects, temsirolimus prevents tumor angiogenesis through the down-regulation of hypoxia-inducible factor-1α (HIF-1α) induced VEGF synthesis in cancer cells and direct inhibition of EC proliferation (reviewed in [162]). Temsirolimus is used for the treatment of patients with advanced RCC [163].

1.7.2.2 Epidermal Growth Factor Receptor Inhibitors

Several lines evidence have shown that anti-angiogenesis is part of the tumor suppressive mechanisms of EGFR inhibitors (reviewed in [164]). First, EGFRs and their two major ligands, EGF and TGF-α, potently activate proliferation and survival pathways in ECs (reviewed in [97]). Secondly, EGFR signaling also increases the secretion of VEGF and a series of other angiogenic factors [165, 166]. Furthermore, VEGFRs and EGFRs activate common pathways such as MAPK and PI3K [167]. Therefore, treatments of cancer patients with EGFR inhibitors can also be considered as anti-angiogenic therapies. The main category of EGFR inhibitors are monoclonal antibodies such as trastuzumab (Herceptin; Roche), panitumumab (Vectibix; Amgen) , and

cetuximab (Erbitux; Bristol-Myers Squibb and Imclone). Other are small-molecule TKIs, for example erlotinib (Tarveca, Roche).

1.7.2.3 Immuno-modulatory Agents and Others

Thalidomide (Thalomid; Celgene) and its derivative lenalidomide (Revlimid; Celgene), interferon (IFN-α) and IL-12 are immuno-modulatory agents that have anti-inflammatory and anti-angiogenesis effects [153, 168, 169]. Their angiogenic inhibitory mechanisms are not clear yet. Some research links them with regulation VEGF expression (reviewed in [153]). Thalidomide in combination of dexamethasone is approved for treatment of multiple myeloma.

1.8 Pitfalls for Using Current Anti-angiogenesis

After bevacizumab was approved by FDA, anti-angiogenic therapy has quickly integrated into traditional anti-cancer treatments. In contrast to the fact that angiogenesis is an effective and low toxicity target for a broad range of solid tumors and non-malignant diseases, three decades of numerous pre- and clinical studies only provide us with a handful of anti-angiogenesis reagents that approved by FDA for clinical usage. Among them, as introduced above, most are monoclonal antibodies or small molecular TKIs that specifically or selectively block VEGF/VEGFR and other pro-angiogenic signaling pathways. As suggested by clinical data compiled within past several years of experience with this novel anti-cancer strategy, several drawbacks of currently available anti-angiogenic reagents have clearly emerged.

First, no matter VEGF/VEGFR, EGF/EGFR or other growth factors that promote angiogenesis, all are widely expressed in various normal tissues with diverse physiological roles.

Inhibition of those signaling pathways yields adverse effects. Inhibition of VEGF/VEGFR was initially assumed to only block developmental and pathological angiogenesis sparing ECs in normal tissues (reviewed in [170]). Interference with wound healing is a common risk related to angiogenesis inhibition; however, other systematic adverse events have become evident with VEGF/VEGFR inhibitors treatment. Since profound cardiovascular side effects were associated with administration of VEGF/VEGFR inhibitors, more and more studies have demonstrated that VEGF is essential in maintaining normal cardiovascular function (reviewed in [171]). VEGF induces endothelial type nitric oxide (NO) and prostacyclin (PGI_2) in endothelium, which are essential for endothelial-dependent vasodilation in coronary arteries [172-174]. Lee and colleagues also show that autocrine of VEGF is required for EC survival and blockage of this signaling pathway by small molecule kinase inhibitors results in increased ECs apoptosis in normal tissues, and subsequent rarefaction in small arteries and arterioles [175]. VEGF/VEGFR inhibitors also increase arterial stiffness possibly by interaction with endothelin, a vasoconstrictor [176, 177]. Therefore, hypertension is the most common side effects associate with VEGF/VEGFR inhibitors due to defects in vessel vasodilation, rarefaction and increase in vessel stiffness (reviewed in [171]). From 11 to 32% of patients under bevacizumab treatment have been reported to experience elevated blood pressure (reviewed in [178]). Around half of those who develop to hypertension require pharmacologic interventions. The incidence of hypertension with VEGF TKIs treatment is about 15% to 60% (reviewed in [171]). Data have also shown a tendency of increasing in incidents of hypertension when patients are treated with higher potency TKIs (reviewed in [171]). More serious cardiac side effects, such as myocardial infarction (MI) and congestive heart failure, and bevacizumab treatment-related deaths during clinical

trials have been reported (reviewed in [178]). Those events may be related to microvascular rarefaction upon VEGF inhibition. Outside the cardiovascular system, VEGF is also plays important roles in maintaining mucosal homeostasis, platelet function, and neuron protection, so that bleeding, gastrointestinal perforation, thromboembolism, voice change, upper and lower digestive tract mucositis, and neurological complications are also reported with inhibition of VEGF/VEGFR (reviewed in [179]). VEGF is expressed in normal renal cortex and mediates glomerular inflammation and repair, which is possible reason that bevacizumab and VEGFR TKIs treatments are associated with proteinuria and oedema [170, 180]. Small molecular TKIs inhibits many other receptors other than VEGFR, and therefore are accompanied by more complications other just inhibition of VEGF signaling pathway alone.

Resistance to VEGF/VEGFR inhibitors has been observed in preclinical and clinical studies. Bergers and coworkers developed a two-mode theory to explain the phenomena (reviewed in [181]). In general, there are two outcomes after treatment with VEGF/VEGFR inhibitors, either initial disease regression followed by restoration of tumor growth (referred as “evasive resistance”), or no beneficial effects in tumor inhibition (referred as “intrinsic resistance”). Among many possible mechanisms responsible for these two types of drug resistance, up-regulation of alternative pro-angiogenic signaling pathways play essential roles. Ferrara pointed out that other signaling pathways mediating VEGF-independent tumor angiogenesis exist in various types of preclinical and clinical tumor models (reviewed in [182]). Treatments with VEGFR inhibitors in cancer patients are reportedly increase circulating pro-angiogenic growth factors such as FGF and PIGF. In some cases, FGF leads to a new wave of revascularization that enables tumor to escape treatment with VEGFR inhibitors. Tumors that intrinsically resist treatment

with VEGF/VEGFR inhibitors may due to pre-existing redundant pro-angiogenic signals. For example, in early stage of human breast cancer biopsies VEGF is the major pro-angiogenic signal, but in late stage FGF and other growth factors become dominant. Recently, FDA is considering withdrawal of bevacizumab from breast cancer treatment due to adverse effects and controversial benefits in patient survival rates.

At last, large efforts have been made to overcome the resistance to VEGF/VEGFR inhibitors, such as developing multi-targeting TKIs and combinatory therapy with reagents that target parallel pro-angiogenic signaling pathways. Selective TKIs usually cause more side effects due to off-target inhibitory effects. In addition, they may not necessarily increase clinical efficacy as expected. For example, a phase 3 clinical trial showed that axitinib (AG013736; Pfizer), a potent selective inhibitor of VEGFR-1, 2, and 3, cKIT and PDGFR does not improve overall survival in advanced pancreatic cancer when it is combined with gemcitabine [183]. Both VEGF and EGFR are over-expressed in advanced NSCLC, colorectal carcinoma, RCC and many other solid cancers. Although VEGF and VEGFR are considered valuable therapeutic targets for NSCLC treatment, the introduction of monoclonal antibodies (mAbs) that target either of these two signaling pathways have marginally increased survival rates in certain types of cancer, for example in advanced NSCLC patients eligible for these agents (reviewed in [184]). Several clinical trials demonstrated that even the combination of bevacizumab with anti-EGFR inhibitors produces controversial benefits (reviewed in [185]). Many preclinical models showed promising effects when VEGF/VEGFR inhibitors are combined with other pro-angiogenic inhibitors targeting PDGF, mTOR and FGF, but their efficacies require further clinical investigation [102, 186, 187]. Hence, resistance to VEGR/VEGFR inhibitors may not be solved simply by blocking multiple pro-

angiogenic signaling pathways, which urges the development of agents with novel anti-angiogenic mechanisms that will further validate angiogenesis as a therapeutic target.

1.9 Endogenous Angiogenesis Inhibitors and their Therapeutic Implications

As discussed above, current anti-angiogenic therapies for cancer have highly focused on inhibition of VEGF/VEGFR and other pro-angiogenic growth factors. Since most growth factors function in a wide range of physiological processes or distributed outside the endothelium, this approach brings drug resistance and unnecessary sides effects. Furthermore, collective clinical evidence has shown that tumor cells develop drug resistance to those therapies by producing multiple redundant angiogenic growth factors. Recent advances in identification of endogenous angiogenesis inhibitors shed light on development of low toxicity, EC-specific protein agents with a broad spectrum of angiogenesis targets.

In 1989, Bouck and coworkers first demonstrated that tumor angiogenesis is a result of a shift in balance between pro- and anti-angiogenic factors in a tumor (reviewed in [188]). Based on this study, Dr. J. Folkman proposed the angiogenesis switch theory and initiated diligent efforts to discover endogenous angiogenesis inhibitors (reviewed in [189]). From 1980 to 2003, his laboratory reported 11 angiogenesis inhibitors with 5 of them being novel molecules. To date, many endogenous angiogenesis inhibitors are documented. Those molecules can be roughly divided into two major categories, matrix-derived and non-matrix-derived endogenous inhibitors (reviewed in [21]). Most of them are matrix-derived proteins, such as thrombospondin-1 (TSP-1), endostatin, and protein fragments derived from collagens and fibronectins. The non-matrix-derived endogenous inhibitors are compromised of growth factor,

cytokines, and fragments of blood coagulation factors such as platelet factor-4, ILs, interferons (INFs), and angiostatin. Other endogenous inhibitors could not be classified into either above, for example tissue inhibitors of metalloproteinases (TIMs) and 16-kDa prolactin fragment.

1.9.1 Matrix-Derived Endogenous Inhibitors of Angiogenesis

1.9.1.1 Endostatin

As one of the first documented ECM-derived endogenous angiogenesis inhibitors, endostatin is the only clinically approved therapeutic agent in this category. In comparison with VEGF/VEGFR inhibitors, endostatin has low toxicity and EC-specific angiogenesis inhibition with a broad spectrum of anti-angiogenic targets. Instead of blocking specific signaling pathways, microarrays studies suggested that endostatin affects about 10% of the genes in human micro-vascular ECs genome. In September 2005, Chinese State FDA approved the human recombinant endostatin (Endostar®) for the treatment of NSCLS [190]. Endostatin was initially separated from the urine of tumor-bearing mice by O'Reilly and colleagues in Dr. Judah Folkman's laboratory [26]. This discovery was inspired by Dr. Judah Folkman's hypothesis that certain primary tumors release angiogenesis inhibitors to suppress remote metastases (reviewed in [7]). The same theory also led to the earlier discovery of angiostatin (a plasminogen fragment) [191].

The 20-kDa endostatin is a proteolytic fragement from C-terminal NC1 domain of collagen XVIII cleaved by elastase or by cathepsin-L [26, 192-195]. The initial purified endostatin was not soluble, but showed dramatic tumor inhibitory effects when the protein pellets were injected subcutaneously into mice on daily bases [26]. Hundreds of literatures demonstrated that endostatin inhibits more than 20 different types of murine and human tumors with tumor re-

sponse rates from 47% to 91% at doses from 10mg/kg to 100 mg/kg/day (reviewed in [196]). Endostatin inhibits proliferation of ECs, hence suppresses tumor angiogenesis. Several studies reported that endostatin also inhibits migration and invasion of human head and neck squamous cell carcinoma cells and AIDS-related Kaposi's sarcoma cells so that it may also exert anti-tumor effect *in vivo* [197, 198].

The role of circulating endostatin in preventing angiogenesis related diseases is well demonstrated within the population with Down's syndrome. Individuals with Down's syndrome have an extra copy of collagen XVIII due to chromosome 21 trisomy. The serum endostatin level in the individuals with Down's syndrome is 39±11 ng/mL compared to 20±11 ng/mL in normal controls [199]. This slight increase in circulating endostatin not only significantly decreases incidences of all types of solid tumors except for testicular cancer but also decreases occurrences of other angiogenesis-related disease such as diabetic retinopathy and atherosclerosis [199]. In transgenic mice over-expressing endostatin, a similar level (1.6 fold) of increase in circulating level of endostatin is sufficient to slow down tumor growth [200].

The mechanisms of how endostatin inhibits tumor angiogenesis remain elusive. The proposed mechanisms include inducing G1 rest in ECs, blocking activities of MMP-2, 9 and 13, preventing VEGF isoforms binding to VEGFR, and stabilizing adhesion junctions [201-205]. Endostatin contains RGD motifs and is known to associate with integrin αvβ3, αvβ5 and α5β1 [206, 207]. Cell surface glypicans and the actin-binding protein, tropomyosin, are also possible receptors for endostatin [208]. Although endostatin affects about 10% of genes in EC genome and induces EC apoptosis, endostatin does not interfere with wound healing [196, 209]. Toxicities have not been observed in animal models or in clinical settings. Four cancer patients with

continuous self-administration of a daily dose of endostatin for more than 3.5 years did not report any side effects (Reviewed in [196]).

1.9.1.2 Thrombospondin-1

The 450-kDa thrombospondin-1 (TSP-1) is a homotrimeric protein initially found to be the most abundant protein in the platelet α granule (reviewed in [210]). It stabilizes platelet aggregates in blood clots and wounds. The secreted TSP-1 is also incorporated into basement membrane, vessel walls and other interstitial tissues with multiple biological roles involved in mediating cell adhesion, cell cycle, and angiogenesis. Unlike other anti-angiogenic protein fragments, the full length TSP-1 potently inhibits *in vitro* and *in vivo* angiogenesis, but its large size and multifunctional character hinders it from being used directly as an anti-angiogenic reagent [211]. Many efforts focus on development of TSP-1 fragments that could effectively inhibit angiogenesis, which will be further discussed in section 1.9.3.2. Studies have demonstrated that the inhibitory effect of native TSP-1 lies in its properdin type I repeats and procollagen homology region (PHR) [212].

1.9.1.3 Other Matrix-Derived Endogenous Angiogenesis Inhibitors

The vascular basement membrane, composed of thin layers of insoluble extracellular matrix proteins, also mediates angiogenesis in addition to its structural roles. Type IV collagen is the major component in vascular basement membrane, and it forms a scaffold network for other macromolecules (reviewed in [213]). A total of six genes encode distinct collagen IV α-chains, known as α1- α6. Each α-chain comprises three domains: the N-terminal 7S domain, the

middle triple helical domain, and the c-terminal globular non-collagenous (NC1) domain [214]. Similar to type XVIII collagen with cryptic endostatin, the NC1 domain of type IV collagen produces varies of anti-angiogenic fragments through proteolytic degradation of the α1, α2, α3 and α6 chains. For example, arresten is a 26-kDa anti-angiogenic protein derived from the NC1 domain of the α1 chain with selectively inhibitive effects in EC proliferation and tube formation, whereas canstatin is a 24-kDa fragments from the α2 chain of type IV collagen [215, 216]. The NC1 domain in α3 chain of type IV collagen contains a 28-kDa fragment named as tumstatin [217]. Systematic administration of tumstatin demonstrates anti-tumor and anti-angiogenic activities in mouse xenograft models. Although, arresten, tumstatin, and endostatin are all derived from the NC1 domains of basement membrane collagens, their anti-angiogenic mechanisms are different. All three proteins recognize integrin but arresten blocks the binding of integrin α1β1 to the type I collagen, tumstatin inhibits tumor angiogenesis via integrin αvβ3, and endostatin decreases EC migration by binding to integrin α5β1. Furthermore, tumstatin only shares 14% amino acid sequence similarity to endostatin [217].

Another example is anastellin, a 76-amino-acid anti-angiogenic fragment from the first type III repeat in fibronectin [218]. Anastellin inhibits angiogenesis by inducing the polymerization of soluble fibronectins to form fibril. Because the first type III repeat domain has a similar function and structure as that of the NC1 domain from collagen IV, it is suggested that proteolytic degradation of ECM is a common mechanism to produce structurally related endogenous angiogenesis inhibitors with unique downstream signaling networks. This information has been utilized to facilitate the discovery of new anti-angiogenic molecules. For example, restin is a 22-

kDa endostatin-like anti-angiogenic fragment protein fragment from collagen XV discovered by computational homology search using endostatin as a model [219].

1.9.2 Non-Matrix-Derived Endogenous Angiogenesis Inhibitors

1.9.2.1 Angiostatin

Angiostatin was identified in Dr. Judah Folkman's laboratory using the same method as the discovery of endostatin from Lewis lung carcinoma-bearing mouse [220]. Its parental protein, plasminogen, contains five kringle domains (kringle 1-5). Plasminogen does not inhibit angiogenesis. Proteolytic degradation of plasminogen produces 38–45-kDa anti-angiogenic peptides that contain different kringle domains [221]. They are collectively called angiostatin. Recent studies showed that different kringle domains contribute differently to its function in inhibition of angiogenesis. Kringle-1 potently inhibits EC proliferation, whereas kringle-4 only inhibits EC migration with no effects on cell growth [222]. Cao and coworkers also suggested that, although Kringle-5 is not included in angiostatin, it also inhibits angiogenesis [223].

1.9.2.2 Pigment Epithelium-derived Factor

Pigment epithelium-derived factor (PEDF) is a 50-kDa naturally secreted glycoprotein that was first identified and isolated from human retinal pigmented epithelial (RPE) cell-conditioned medium [224]. The biological functions of PEDF have been indicated in inducing neuronal differentiation in retinoblastoma (Rb) cells [224], neurotrophic activity in embryonic retina and cerebellar granule cells [225, 226], and maintenance of retinal and ureal avascularity [227, 228]. PEDF has been documented as one of the most potent natural anti-angiogenic pro-

teins. It inhibits EC-proliferation and prohibits *in vitro* EC-migration with an ED_{50} of 0.4 nM, which is more potent than these of angiostatin, TSP-1, and endostatin [227]. PEDF inhibits angiogenesis via down-regulation of VEGF signaling [229, 230]. A balance between levels of PEDF and VEGF is importance in mediating tissue and tumor angiogenesis. For example, a low PEDF/VEGF ratio contributes to ischemia-induced angiogenesis in retina [231]. Yang and colleagues have shown that angiostatin decreases VEGF/PEDF mRNA ratio in murine ocular melanoma [228]. In addition to inhibition of angiogenesis, PEDF also exerts direct anti-tumor effects [232-234]. Overexpression of PEGF reduces tumor angiogenesis and inhibits tumor growth in a wide range of tumor types, such as Rb, melanoma, gastric carcinoma, cervical carcinoma, and osteosarcoma [227, 234-237]. The role of PEDF in inhibition of tumor metastasis is also been investigated. Studies have demonstrated that overexpression of PEDF prevents liver metastasis in pancreatic adenocarcinoma, human melanoma, and mouse uveal melanoma [234, 238, 239].

1.9.2.3 Interferons and Interleukins

Interferons (IFNs) and interleukins (ILs) are multi-functional cytokines released by lymphocytes. Besides regulating immune responses to infections and tumors, IFNs and ILs also mediate angiogenesis in embryos and under pathological conditions. IFN-α is the first identified endogenous anti-angiogenic regulators [22]. Since 1988, IFN-α has been used for the treatment of hemangiomatosis, pediatric hemangiomas, angioblastomas and high-grade giant cell tumors [240, 241]. IFN-α and -β have direct anti-proliferative effects by promoting G1 and S phases arrest of the cell cycles [242]. The anti-angiogenic mechanisms of IFN-α and -β are not well understood. Studies suggest that they partially rely on inhibition of bFGF-2, VEGF, and MMP-9 in-

duced tumor angiogenesis [243-245]. IL-12 and IL-18 also suppresses FGF-regulated angiogenesis. Their expressions are induced by IFN-γ [246, 247]. Other ILs, such as IL-1β and IL-4, also prevent bFGF induced angiogenesis [248, 249]. Although IFNs have showed promising anti-angiogenic effects, their short half-lives and systemic side-effects have restricted their clinical applications [241].

1.9.2.4 CXC Chemokines

CXC Chemokines are a group of heparin-binding proteins with distinct functions in mediating angiogenesis. CXC family members share a similar 3D structure. Each member contains four conserved cysteine (Cys) residues with the first two separated by one non-conserved residue (reviewed in [250]). A second conserved N-terminal glutamic acid-leucine-arginine (ELR) motif determines receptor selectivity and angiogenic effects. Members with the ELR motif (ELR^+), such as IL-8, granulocyte chemotactic protein-2 (GCP-2), and growth-related gene alpha-α, β, γ (GRO-α, β, γ), strongly promote angiogenesis via CXC receptor-1 and-2 (CXCR-1 and -2) in many tumor models (reviewed in [251]). By contrast, PF4, neutrophil activating protein-2 (NAP-2) and interferon-γ-inducible protein 10 (IP-10) are CXC chemokines that lack the ELR motif (ELR^-) which potently inhibits angiogenesis by mediating signaling pathways downstream of CXCR-3 (reviewed in [250, 252]). This unique structure-function characterization has drawn growing interest in studies of the regulatory roles of the CXC chemokines in tumor angiogenesis. PF4 is the first identified endogenous angiogenesis inhibitor, and also the most studied CXC chemokines family member (reviewed in [253]). PF4 inhibits EC proliferation, migration, and formation of endothelial tubes *in vitro* [254]. Systematic administration of PF4 also inhibits dif-

ferent types of tumor growth in animal models. Different mechanisms have been proposed to explain the anti-angiogenic effect of PF4 (reviewed in [255]). First, as a strong heparin binding protein, PF4 is able to displace VEGF and FGF-2 from interacting with glycosaminoglycans (GAGs). Since GAGs serve as low-affinity binding co-receptors for these growth factors, PF4 could partially block VEGF and FGF-2 from binding to their high-affinity receptors. Second, PF4 may directly associate with those growth factors and reduce their activities. Last, PF4 binds to its receptor CXCr3, which reduces ECs proliferation by mediating the expression of a cell cycle protein, $p21^{Cip1}$ [256].

1.9.2.5 Tissue Inhibitors of Matrix Metalloproteinases and PEX

Tissue inhibitors of matrix metalloproteinases (TIMPs) can block the activity of MMPs, therefore play a critical role in regulation of the homeostasis of ECM (reviewed in [257]). However, TIMPs have paradoxical effects during tumorigenesis and angiogenesis. On one hand, because MMP-2 and -9 significantly contribute to angiogenesis switch during tumorigenesis, TIMPs can inhibit angiogenesis by blocking protease activities of MMP-2 and -9 [257]. It also has been reported that TIMP-2 down-regulates angiogenesis in an MMP-independent manner through directly suppressing ECs proliferation [258]. On the other hand, TIMPs can promote angiogenesis because the protease activity of the MMPs is required to produce many endogenous angiogenesis inhibitors such as angiostatin and endostatin [193, 259]. In addition, TIMPs are multifunctional proteins that stimulate cell growth and protect cells from apoptosis (reviewed in [260]). The net effect of TIMPs during tumor angiogenesis may depend on the tis-

sue type, local TIMPs concentration and the disease progression. Elevated plasma TIMPs levels are also considered as a sign for poor prognosis in many types of cancers (reviewed in [257]).

A naturally occurring MMP-2 inhibitor, PEX, is able to inhibit *in vivo* angiogenesis [261]. PEX is a breakdown product consisting of the C-terminal hemopexin-like domain of MMP-2. Detectable amounts of PEX are located in vivo in conjunction with αvβ3 and reach peak levels during the late-stage of vessel maturation. Compared to TIMPs, PEX inhibits angiogenesis *in vitro* and *in vivo* through the direct blockage of MMP-2 binding to αvβ3.

1.9.2.6 Other Non-Matrix-Derived Endogenous Angiogenesis Inhibitors

Many other endogenous proteins have a role in reducing angiogenesis (reviewed in [21]). For example, pigment epithelium-derived factor (PEDF) is responsible for the avascularity of ocular compartments and it selectively inhibits the growth of new vessels in normal prostate, pancreas, and murine xenograft tumors [262]. Vasostastin is the N-terminal fragment of calreticulin that specifically inhibits ECs attachment to laminin and blocks EC proliferation [263]. A peptide hormone, prolactin, is associated with lactation with pro-angiogenesis effect. Its naturally occurring breakdown product, a 16-kDa N-terminal fragment of human prolactin (16k hPRL), can inhibit angiogenesis 100 times more potently than endostatin does [264]. The increasing number of endogenous inhibitors discovered has colored a bright future for the development of anti-angiogenic reagents for cancer patients.

1.9.3 Peptide-based Anti-angiogenic Peptide Drugs

1.9.3.1 Development of Peptide-based Anti-angiogenic Peptide Drugs

Currently, synthesis of peptides originated or modified from endogenous angiogenesis protein inhibitors has become the most common approach to develop novel anti-angiogenic reagents. There are several reasons for using peptides instead of the whole protein: a) to reduce side effects by avoiding undesired protein functions; b) to increase solubility; c) to facilitate large-scale productions. First, most discovered endogenous anti-angiogenic inhibitors are fragments derived from parental proteins with or without anti-angiogenic property. Strikingly, in majority of these inhibitors, only a small portion or region is responsible for blocking the complex angiogenesis networks. Since most of those proteins have “default” functions in mediating a number of biological events instead of specifically inhibiting angiogenesis, utilizing the anti-angiogenic portion will not only enhance the anti-angiogenic function, but reduce the risk of side effects in most case. Second, many endogenous anti-angiogenic proteins are derived from large, insoluble ECM proteins. Dissecting them into small peptides will solve the solubility issue and make them more suitable for therapeutic treatments. In addition, production of short peptides by solid-phase synthesis can avoid the batch differences produced by protein biosynthesis through bacterial, yeast or mammalian expression. Those reasons have encouraged a worldwide wave of development of synthetic peptides derived from existing endogenous inhibitors.

1.9.3.2 TSP-1 Peptides

TSP-1 was the first endogenous angiogenesis inhibitor recognized in 1990 [25]. Although the whole protein potently inhibits angiogenesis, it is difficult to use a 450-kDa extracellular glycoprotein that regulates various biological processes directly as a valuable therapeutic reagent. Tolsma and colleagues located the angiogenesis-inhibitory region of TSP-1 into two separate domains in the 70-kDa central region of each of the polypeptide chains, the procollagen domain and the three type 1 repeats (TSRs) [212]. Peptides derived from both domains have confirmed anti-angiogenic properties, but peptides derived from the TSRs are more potent than that derived from the procollagen domain. The smallest peptide that retains the anti-angiogenic activity is a 9-residue fragment from the procollagen-like region. Small synthetic TSP-1 peptides from the second and third TSRs of TSP-1, Mal II (residues 424-442) and Mal III (residues 481-499), block new vessel formation in rat cornea and granulation tissues. Peptides derived from TSRs of other TSR-containing proteins, such as spondin 1, CYR61, connective tissue growth factor (CTGF), and WISP-3 have also shown potential to inhibit angiogenesis *in vitro* and *in vivo*, which suggests that TSRs is a conserved protein structure that inhibits angiogenesis [265].

Therapeutic TSP-1 peptides have been developed for clinical studies. The original Mal II peptide contains amino acid mutations SPWSSA*SVTA*GDGVITRIR (where A* indicates cysteine was replaced by alanine when peptides were synthesized), and Mal III contains similar amino acid mutations SPWDIA*SVTA*GGVQKRSK when tested [212]. The intact TSP-1 protein inhibits a variety of *in vitro* angiogenesis assays at a concentration range of 0.5 – 20 nM, but Mal II failed to show inhibitory effects. Dawson and coworkers improved the *in vitro* activity of Mal II

by 100 – 1000- fold by substituting either three of the L-amino acids 4, 5, and 14 with their D-enantiomers [266]. They also confirmed that the anti-angiogenic activity of Mal II is fully retained by its last seven amino acids (GVITRIR), known as peptide 1. However, the modified peptide (NAc-Gly-Val-DILe-Thr-Arg-Ile-ArgNHEt) has no therapeutic effects because of short half-life in rodents [211]. Haviv and colleagues further modified the peptide at positions 5 and 7 with N- and C-terminal capping to create two heptapeptides mimetics, ABT-526 (NAc-Sar-Gly-Val-DIle-Thr-Nva-Ile-Arg-ProNHEt) and ABT-510 (NAc-Sar-Gly-Val-DalloIle-Thr-Nva-Ile-Arg-ProNHEt) [211, 267]. Both heptapeptides have improved pharmacodynamic/pharmacokinetic (PD/PK) profiles and increased activities compared with Mal II. ABT-510 has increased water solubility compared to ABT-526 and is formulated as an acetate salt. It blocks TSP-1 binding to its receptor CD36, suggesting that it inhibits angiogenesis by the mechanism similar as TSP-1 does [267]. In a human bladder carcinoma xenograft mouse model, continuously administration of 30 – 90 mg/kg ABT-50 by osmotic minipumps reduced neovascularization in tumor tissues [211]. A phase II clinical study showed that, when administrated subcutaneously with doses of 20mg once a day or 200mg twice a day, ABT-510 failed to meet the objective response rate (ORR), which suggested that ABT-510 is not suitable to be used as a single-agent [268, 269]. A similar phase II clinical study in patients with previously untreated advanced renal cell carcinoma also leads to the same conclusion that ABT-510 is not sufficient as a stand-alone agent although it has a favorable safety profile [270].

1.9.3.3 Tumstatin Peptides

The 28-kDa tumstatin is an endogenous anti-angiogenic protein fragment of the NC1 domain of type IV collagen α3 chain [271]. Tumstatin inhibits tumor growth by reducing new blood vessel formation and directly repressing the growth of tumor cells. The anti-angiogenic effect of tumstatin is located between N-terminal amino acid residues 54 and 132 (known as Tum-5), while the anti-tumor activity is possessed between residues 185-203 [217, 271]. Tum-5 is 10-fold more effective than endostatin does in inhibition of human prostate cancer (PC-3) xenografts in nude mice [271]. A series of overlapping synthetic peptide further narrowed its anti-angiogenic region to even smaller peptides, T3 (amino acids 69-88) and T7 (amino acids 74-98) [272] .

1.9.3.4 PF4 Peptides

PF4 was identified as a heparin-binding protein released from platelet α-granules in 1950s [273]. The major recognized physiologic role of PF4 is to neutralize heparin and other heparin-like molecules such as GAGs on endothelial cell surfaces; therefore, it plays an important role in thrombosis, immune modulation, and angiogenesis (reviewed in [274]). PF4 was originally developed as a clinical alternative to protamine for heparin neutralization. With a confirmed tumor-suppressive effect by reducing angiogenesis in different xenograft animal tumor models, PF4-derived peptides have become a popular pipeline to produce new alternative venues to current anti-angiogenic therapies (reviewed in [275]). Development of PF4-derived peptides has been focused on reducing toxicity and improving bioactivity. PF4 is a homo-tetramer composed of four 70 amino acids subunits. The C-terminal of PF4 is critical to its anti-angiogenesis effect.

The naturally occurring PF4 fragment $PF4_{17-70}$ is a proteolytic cleavage product by elastase between Thr-16 and Ser -17. Although the two cleavage fragments (amino acid 1-16 and amino acid 17-70) still remained attached together through disulfite bonds, it is reported to be 30 – 50 folds more potent than the full length PF4 [276]. Another 24-amino-acid fragment, $PF4^{47-70}$ (NGRKICLDLQAPLYKKIIKKLLES), possesses anti-angiogenic effects and also blocks the binding of either FGF-2 or VEGF to ECs [255, 277]. Further stabilizing the C-terminal PF4 fragments by leucine zipper motif also produces anti-angiogenic peptides [278]. Nesmelova and colleagues showed that a heterodimic hybrid peptide derived from both PF4 and the pro-angiogenic IL-8 sequences has stronger anti-proliferation effects than PF4 alone [279].

1.9.3.5 Anginex

As growing numbers of anti-angiogenic peptides are derived from endogenous proteins. Van der Schaft and coworkers engaged in designing combinatorial peptides from different endogenous anti-angiogenic β-sheet proteins [280]. In contrast to PF4 peptides discussed above, anginex is 33-amino-acid peptide that forms anti-parallel amphipathic β-sheet structure [281]. The amino acid sequence of anginex is originated from analysis of the β-sheet hydrophobic core part of PF4 family proteins including PF4, IL-8, and bactericidal-permeability increasing protein (BPI) [281, 282]. The hydrophobic core parts of those described proteins have several common features: 1) ratio of positive to negative charge residues falls between 4/2 and 6/2, the non-charged polar residues (N,Q, T, S) are around 20%, 2) there are 40% - 50% of hydrophobic residues (e.g. I, L, V, M and A), 3) there is alternation between those charged/ polar residues and hydrophobic residues with specific turns between β-sheet strands, and 4) there is

proper placement and pairing of the hydrophobic residues in the sequences [283]. The synthetic peptide anginex inhibits *in vitro* ECs proliferation, induces ECs apoptosis, and inhibits tumor growth in xenograft mice models [281, 284]. The β-sheet structure is the bioactive form of anginex suggesting that the β-sheet structure is critical to inhibit angiogenesis [285]. Further sequence scanning study also demonstrated that the critical N-terminal SVQMKL and the C-terminal IIVKLN are the most essential residues for maintaining its anti-angiogenic activity [286].

1.9.4 Drawbacks of Anti-angiogenic Peptides

Currently, dissecting endogenous angiogenesis inhibitors or even stimulators into small peptides that are less than 50-amino-acid in length dominates the field of developing therapeutic agents. Compared to drugs that are acting on specific pro-angiogenic signaling pathways such as VEGF/VEGFR, FGF, or EFG inhibitors, those peptides effectively block angiogenesis produced by a variety of *in vitro* and *in vivo* models. The rising concerns about the side effects seen for the available VEGF/VEGFR inhibitors and the emergence of drug-resistances made the peptide-based drugs attractive. The biological and chemical nature of small peptide-based drug, however, could impede the clinical application or therapeutic outcomes in cancer patients.

First, peptide drugs by nature have unfavorable pharmacological properties. Enzymatic degradation in serum and oral bioactivity could make them less effective than predicted (reviewed in [287]). Secondly, short length often gives the peptides less defined secondary structures that are required for their targeting and function. Thirdly, although the modifications such as N-terminal capping or substitution with non-nature amino acids confer protease-resistance

to peptide drugs, those so called designer peptide drugs are expensive for synthesis. The cost of inclusion of one or two non-natural amino acids could reach up to $1,000 per gram (reviewed in [287]). Occasionally, it is necessary to substitute non-natural amino acids in order for peptide drugs to be fully effective. For example, as discussed above, ABT-510 (NAc-Sar-Gly-Val-DalloIle-Thr-Nva-Ile-Arg-ProNHEt) is the modified version of a TSP-1 derived peptide. In contrast to the nanomolar range medium effective dose (ED50) reported for ABT-510, its natural counterpart was not active in angiogenesis assays [266].

In summary, although peptide-based drugs remain a valuable approach to develop new therapeutic anti-angiogenic reagents, limitations such as high cost, restrictions on production and lack of pharmacological properties largely impede their development. Numerous investigations have been productive in producing potent peptides with demonstrated *in vitro* effects, but few have succeeded in the clinical trials. Most of them showed no beneficial effects when applied to cancer patients.

1.9.5 A structural link of Endogenous Angiogenesis Inhibitors

It is noted that many of these endogenous angiogenesis inhibitors share distinguishable regional structural similarity. As pointed out by Dings and coworkers a majority of them fold as or contain anti-parallel β-sheet structures with highly positively charged lysine/arginine-rich surfaces (Reviewed in [288]). The 3D structure of a protein's determined by its amino acid sequence, which in turn conveys biological activity. This proposed structural information may provide important benefits for *de novo* design of peptides and proteins with desired anti-angiogenesis effect.

As shown in Figure 1.1, a number of endogenous angiogenesis inhibitors are derived from ECM proteins depicted with highly positively charged β-sheet structure (reviewed in [288]). ECM proteins usually are composed of frequent repeats within the same molecule or similar structured modules shared between different ECM families (reviewed in [213]). One such example is the C-terminal NC1 domain of XVIII that contains a 180 amino acids globular domain known as endostatin [26]. The crystal structure of endostatin shows that it folds into predominantly an anti-parallel β-sheet structure with extended loops and two α-helices [289]. This structure is distantly related the C-type lectins and LINK domains in CD44 and TSG-6 (reviewed in [213]). Two clusters of arginines (Arg155, 158, 184, and 270; Arg193 and 194) composing an extensive basic patch on its surface is responsible for bFGF binding [208].

Another such example is anastellin, an all-β-sheet endogenous angiogenesis inhibitor derived from fibronectin. Fibronectin is another ECM protein that exits as a soluble protein in plasma and also as self-assembled fibrils in the ECM (reviewed in [213]). The 250-kDa fibronectin are assembled by multiple copies of three types of repeated modules: type I (FN1), II (FN2) and III (FN3) repeats. Anastellin is derived from the first FN3 repeat in fibronectin [218]. The full length FN3 has a well characterized 3D structure that can be described as a "β-sandwich". It consists of two sets of anti-parallel β-sheets enclosing a hydrophobic core. One set of the sheet comprises three (A, B and E) β-strands, whereas the other has four (C, D, F and G) strands. Anastellin is a truncated FN3 without the first two β-strands (A and B) and also highly positively charged with an array of solvent exposed lysines and arginines on both sides of its surfaces.

A third example of such endogenous angiogenesis inhibitors is the extensively positively charged chemokine PF4. Native PF4 exits as a homo-tetramer composed of two asymmetric

dimers. Each 70-amino-acid PF4 polypeptide chain contains an N-terminal glutamate-rich aperiodic region. A central core part consists of three anti-parallel β-strands and a C-terminal amphipathic α-helix [273]. The N-terminal region is constrained to the central core by two disulfide bridges, Cys10-Cys36 and Cys12- Cys52. One of the unique structural features of PF4 is the existence of an array of three basic amino acids clusters in its sequence (reviewed in [255]). The first cluster of basic residues is located in the N-terminus (Arg20, Arg22, and His23). The central β-sheet core region hosts the second basic cluster (Arg49 and Lys50). The last distinct basic area is in the C-terminal helix (residues 61-68) featured by the alternation of lysines and pairs of hydrophobic leucines or isoleucines (Lys61-Lys62-Ile63-Ile64-Lys65-Lys66-Leu67-Leu68) [273]. The central anti-parallel β-sheets regions of two PF4 subunits associate with each other and form a dimer. The central β-sheets regions are then further positioned laterally to the another dimer and stabilize the tetrameric structure [290]. This structural arrangement makes the lysine residues (Lys61, 62, 65 and 66) of the four α-helices of the teramer forming an equatorial cationic ring that is responsible for heparin binding [255, 278]. Butcher and colleagues showed that when a PF-4 sequence unrelated leucine zipper motif was crafted with the residue 61-68 of PF4 featured with Lysine 61, 62, 65 and 66, it showed significant heparin binding activity [278]. Those structure characters of endogenous anti-angiogenesis inhibitors could serve as enlightenment for novel protein drug design.

1.10 Rational for Design Anti-angiogenic β-sheet Proteins

1.10.1 Rational for Design Anti-angiogenic Protein using a Stable Host

Angiogenesis has been proven to be a valuable target for inhibition of tumor growth by numerous investigations and clinical studies. As reviewed above, most available FDA approved anti-angiogenic reagents are humanized monoclonal antibodies, or small molecular VEGF/VEGFR kinase inhibitors, or inhibitors that targeting other growth factor pathways. There are growing numbers of growth factors that have been demonstrated to mediate tumor angiogenesis dependent or independent on VEGF, which is the primary mechanism of which tumors to escape current treatment leading to a "second wave of angiogenesis". As discussed above, emerging number of endogenous inhibitors have been shown to effectively induce proliferating EC apoptosis and block tumor angiogenesis. In contrast to inhibiting growth factors that stimulated ECs, this method represents new revenue to directly reduce the building blocks (ECs) of tumor angiogenesis. Because tumor vessels have disrupted structure with less-to-no protection from pericytes or basement membranes, these agents are less likely to disrupt normal vessels. In addition, VEGF or other growth factors, such as PDGF, EGF, usually play important roles in the maintenance of normal body homeostasis. Inhibition any of those pathways bring consequent side effects. To this end, endogenous proteins or fragments are less likely to affect functions of normal organs and are well tolerated by cancer patients.

To date, only one recombinant endogenous protein, endostatin, is further modified and approved for clinical applications. Instead of developing protein fragments or peptides derived from endogenous anti-angiogenic proteins, we proposed to rational design of an anti-angiogenic protein using a stable host protein, CD2D1. Anti-angiogenic peptides are crafted into

an angiogenic unrelated β-sheet host protein. The rational is based on two facts: first, amphipathic β-sheet structure is critical for endogenous anti-angiogenic protein; second, the β-sheet structure has to be well-maintained for angiogenic inhibition. In the following section, we will discuss in detail on the choice of the host protein and strategy of design. CD2D1 is a suitable choice to maintain the critical β-sheet structure of anti-angiogenic peptides. After being crafted to the host protein, not only the anti-angiogenic peptides exit as an amphipathic β-sheet folding but their hydrophilic surface is fully solvent-exposed to function in blocking angiogenesis.

One major goal of dissecting endogenous anti-angiogenic protein is to avoid possible side-effects since most of the parental proteins have "default" physiological functions in the cases like TSP-1 or PF4. In other cases, even the parental proteins have unknown physiological roles, which brings up the possibility of occurrences of unexpected side-effects. In our designed model, the host protein, CD2D1 is the most extensively studied adhesion molecule to date. The stable structural features and defined roles in immune processes make it easy to predict the expected function of our designed protein. Since the host protein has very low affinity to its target, it is less likely to cause any non-targeting effect except inhibit angiogenesis in growing tumor. Even if there is any, it could be avoided by altering the designed model.

1.10.2 The CD2 Adhesion Molecule

Cluster of differential 2 (CD2) is one of the most extensively studied cell surface adhesion molecules (reviewed in [291, 292]). CD2 is a transmembrane glycoprotein expressed on T lymphocytes, natural killer (NK) cells and thymocytes [293]. The binding partner of CD2 is CD48 and CD58. The biological function of CD2 is mainly as a cell surface co-receptor molecule for T

cell receptor (TcR) that mediates T cell activation and adhesion to antigen presenting cells (APC), therefore mediating immune responses (reviewed in [294]). In addition to cell adhesion, it is also known that CD2 triggers IL-2 production in T cells upon binding to CD58 in human [295]. CD58 is not found in marine species, so that CD48 is recognized as the primary ligand in marine. The binding affinity between CD2 and CD48 is weak (Kd = 60 – 90 μM), but monoclonal antibodies that blocks CD2-CD48 interaction inhibits marine T-cell activation [296, 297].

1.10.3 Structure of the Host Protein CD2D1

Both rat and human CD2, and their ligands (CD48 and CD58, respectively) consist of two extracellular domains, a transmembrane domain, and a proline-rich cytoplasmic tail. CD2 belongs to the well-studied immunoglobulin superfamily (IgSF) [292, 298]. The overall extracellular portions of CD2 have an Ig-fold illustrated in Figure 1.2 [298]. The N-terminal extracellular Domain 1 of CD2 (denoted as CD2D1) consists of nine anti-parallel β-strands named as A, B, C, C', C'', D, E, F and G. Two layers of GFCC'C'' and ABED strands compromise a β-sheet sandwich structure that was described as a Greek Key architecture [298]. The GFCC'C'' strands form the adhesion surface that is critical for CD48 binding. This binding surface is fully solvent exposed. It also has 45% of charged residues in this region compared to average of 29% charged residues in most endogenous proteins. Extensive mutagenesis and structural studies have demonstrated that the binding between CD2 and CD48 is mostly due to charge-charge interaction [299].

1.10.4 CD2D1 as a Host Protein

The N-terminal domain of CD2 was selected as the host protein for several reasons. First, CD2D1 is small (10-kDa, 99 amino acids) with several resolved crystal and NMR structures at high resolutions [298, 300-303]. Second, CD2D1 is highly mutation tolerant. Previous studies have reported that single mutations at 40 different locations on the CD2D1 have no apparent effects on the expression, solubility, and structural integrity of the protein [304-306]. Using computational design methods, Yang and coworkers created *de novo* Ca(II) binding sites in CD2D1 that were shown to maintain their native-like conformations [307]. The grafting approach established in the same laboratory also demonstrated that mutations at the terminal-end and 22-23, 52-53, and 83-84 do not alter the folding or conformation of the CD2 [308]. Third, high resolution NMR studies show that CD2D1 is able to maintain its native structure and conformation in a pH range from 1 to 10, suggesting that electrostatic interactions play a minor role in the folding of CD2 [304]. Fourth, the dynamic properties of CD2 are well studied by Driscoll and coworkers [303, 309]. Yang and colleagues have previously reported the dynamic properties of CD2 with a designed Ca(II) binding site. These important features and knowledge of CD2D1 allow us to specifically explore the conformational and dynamic properties of the host protein with the engineered anti-angiogenic sites [310].

1.10.5 Our Designed Model

Our designed model is base on the host protein CD2D1 N- and C-terminus β-sheets. The designed agent is denoted as ProAgio. A total of 8-amino-acid differences between CD2D1 and ProAgio are shown as bold in Table 1.1 and Figure 1.3. Several reasons led us to choose this re-

gion as the engineer site for incorporating the anti-angiogenic peptides. First, as shown in Table 1.1, this region has the highest sequence similarity to the anti-angiogenic peptides. Secondly, all the side chains of hydrophilic residues will be exposed to solvent, so that the amphipathic features of the anti-angiogenic peptides will be well maintained. Thirdly, those two β-sheets have less side-chain interactions between the hydrophobic core located near Trp32, which will allow the highest structure stability after alteration.

The simulated model structure was shown in Figure 3.1. In our designed model, anti-angiogenic peptides (TVQMKL and NLKVII) are crafted into the 5-10 of N-terminal β-strand A and 94-99 of and C-terminal β-strand G of CD2D1, respectively. The complete amino acid sequence of ProAgio was illustrated in Figure 1.5. Since the hydrophobic core region of CD2D1 located near Trp32 is not disrupted by this design, the overall β-sheet sandwich structure will be maintained and remain as a structural restraint to the crafted peptides. Individual residues involved in the anti-angiogenic function were illustrated in a simulated ProAgio model as Figure 1.4. In the simulated structure, the side chains of Thr5 pairs with Asn94, Glu7 pairs with Lys96, and these side chains are facing the solvent surface of CD2D1. Lys9 and Ile99 in the end of A and G β-strands form interaction and their side chains are expected to face the same direction of Thr5, Glu7, Asn94, and Lys96 although with greater flexibility. Most other designed residues (Val6, Met8, Leu10, Leu95, Val97 and Ile99) are hydrophobic residues expected to be facing the opposite direction (to the β-sandwich core region). A Met23Cys mutation is further designed into the BC loop region that will not interfere with the structural stability and anti-angiogenic function of our designed ProAgio.

1.11 Significance and an Overview of this Study

Angiogenesis is a rate limiting step for tumor growth and metastasis. Although it has been 40 years since angiogenesis was proposed as a valuable target for cancer therapy, only a limited number of agents were developed in this field. Angiogenesis is mediated by a fine balance between pro- and anti-angiogenic factors. Current therapeutic drugs have been heavily focused on inhibition of pro-angiogenic factors especially VEGF/VEGFR inhibitors. Many of those developed agents have shown undesired side-effects. In addition, inhibition of single or several signaling transduction pathway(s) could not effectively prevent tumor cells from releasing alternative stimulants that initiate new waves of angiogenesis. In contrast, endogenous angiogenesis inhibitors have emerged as a new category of anti-angiogenic therapy. Compared to growth factor inhibitors, they usually target ECs with a broader range of mechanisms. Furthermore, these endogenous angiogenesis inhibitors show low toxicity and high selectivity toward ECs. Most endogenous angiogenesis inhibitors are proteolytic fragments derived from ECM proteins, so that they are limited to drug development because of solubility and structural stability.

In this study, a novel anti-angiogenic protein agent was developed to specifically target ECs. Different from existing strategies, we used rational design of peptide sequences derived from native angiogenic proteins in a stable β-sheet host protein. This is not only the first agent development of this kind, but these studies also shed lights on applying a novel approach to tackle challenges in clinical anti-angiogenic drug research and development. Compared to VEGF/VEGFR and other growth factor inhibitors, our designed agent directly exerts anti-angiogenic effects by direct targeting ECs, which is more efficient and minimizes drug resistance. As far as other endogenous anti-angiogenic proteins and monoclonal antibodies are con-

cerned, our designed agent has a molecular weight of 10-kDa, which allows it to have better tissue penetration. In addition, the stable host protein will enable the crafted anti-angiogenic peptides to adopt a β-sheet structure and increase their biological effects. Furthermore, our host protein resists extensive mutations, so that multiple functional sites could be easily incorporated. For example, a single mutation of Met23Cys allows PEGylation of our designed protein, which significantly improves its solubility, increases blood circulation half-life, and decreases immunogenicity.

Chapter 2 in this dissertation documents material and methods used to carry out this research project. Different techniques are categorized as below. First, techniques include molecular cloning to create mutations in the wild type and mutant CD2D1 host proteins, protein expression and purification procedures utilizing ion-exchange and size exclusion chromatographies, cell culture techniques, and site-specifically PEGylation of the designed protein using a 20-kDa maleimide-PEG. Second, evaluation of the anti-angiogenic functions of designed proteins utilizes cell viability assays, BrdU cell proliferation assays, and tube formation assays. Each of these *in vitro* models use human umbilical cord vein cells (HUVECs) and their procedures are discussed in detail. Third, *in vivo* evolution of anti-tumor effect uses a xenograft human prostate cancer cell line PC3 in immunodeficient nude mice. Procedures of tumor cell implantation and methods of monitoring tumor growth are documented. Furthermore, studies are performed to investigate the mean vessel density (MVD) using fluorescence labeled anti-CD31 antibody. Procedures of immunofluorescence (IF) staining and imaging process are also listed. In additional, organ toxicities of treated mice are analyzed by hematoxylin and eosin (H&E) stain-

ing of fixed organs. Pathological examines of HE stained organ slides were done by Dr. Hans Grossniklaus. The vessel integrity of each major organ was also examined by CD31 IF staining.

Chapter 3 focused on our designed anti-angiogenic protein, ProAgio. First, detailed strategies used for rational designs are discussed and illustrated in great details by simulated computational model structures. Side-chain directions of each amino acid residues involved in the anti-angiogenic region and site-specific PEGyaltion are examined one by one in order to demonstrate the best design strategy. Molecular cloning, purification, and site-specific PEGylation of ProAgio enabled us to carry on *in vitro* and *in vivo* evaluations of ProAgio on its anti-angiogenesis effect are discussed.

In Chapter 4, humanization of ProAgio using a human homologue of rat CD2D1 (huCD2D1) are discussed in detail. Side-chain directions of each amino acid in rat and human CD2D1 are compared one-by-one in order to provide detailed structural information for humanization of ProAgio. The 3D structures of both host proteins are aligned to confirm the regions for crafting of anti-angiogenic peptides. The final designed model contains several aspects of mutations with different purposes including anti-angiogenesis, glycosylation, and PEGylation. The designed huProAgio is expressed, purified, and further tested using *in vitro* and *in vivo* angiogenesis models. Since the protein showed limited solubility, protein refolding under pH gradients and buffer selections are also discussed.

In Chapter 5, molecular cloning, protein purification, PEGylation, and evaluation of designed anti-angiogenic protein agents are summarized. Our initial designed model using a CD2D1 variant 6D31 is discussed and summarized. A set of *in vivo* anti-angiogenesis assays using ProAgio-PEG is also documented in this chapter.

Conclusions were drawn and summarized in Chapter 6. The future clinical outlook of ProAgio and significance of this study was also discussed in this chapter.

Proteins expressed and purified in this dissertation and their related sections or chapters were listed in Table 1.2.

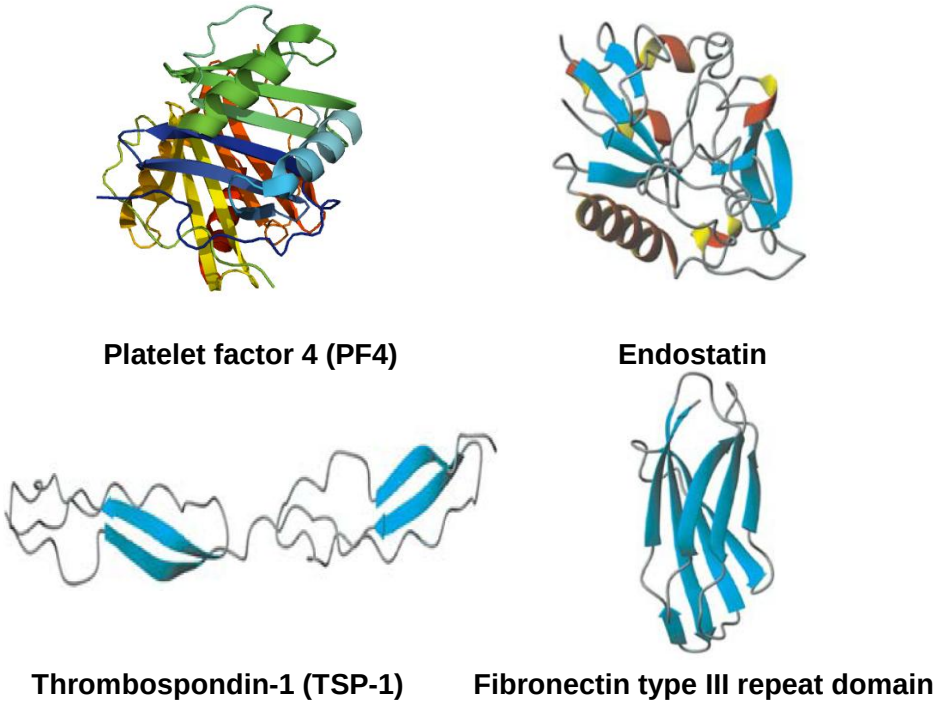

Figure 1.1 Structural Similarity between Endogenous Anti-angiogenic Proteins. A number of endogenous angiogenesis inhibitor share similar β-sheet structure [288]. β-sheet structures usually consist the hydrophobic core region of those proteins as highlighted. The platelet factor structure 4 is from PDB (access ID: 1RHP). Other structures were illustrated by R. Dings and colleagues [288].

Figure 1.2 Crystal Structure of Rat CD2D1. The rat CD2D1 folds as a β-sheet structure with 9 β-strands (PDB accession ID, 1hng). The D, E, B and A β-strands consist one layer of β-sheet. G, F, C and C' strands compose a second layer of β-sheet [298]. There is a hydrophobic core region in between.

Table 1.1 N- and C- Terminal Residues of CD2D1 and ProAgio

Amino Acid	5	6	7	8	9	10	94	95	96	97	98	99
CD2D1	Thr	Val	Trp	Gly	Ala	Leu	Asp	Leu	Arg	Ile	Leu	Glu
*ProAgio	Thr	Val	**Glu**	**Met**	**Lys**	Leu	**Asn**	Leu	**Lys**	**Val**	**Ile**	**Ile**

*: Amino Acids in ProAgio that are different from CD2D1 are shown in bold.

```
         10          20          30          40          50          60
RDSG**TVQMKL** GHGINLNIPN FQCTDDIDEV RWERGSTLVA EFKRKMKPFL KSGAFEILAN

         70          80          90
GDLKIKNLTR DDSGTYNVTV YSTNGTRILN KAL**NLKVII**
```

Figure 1.3 The Protein Sequence of ProAgio with a Cysteine PEGylation Site. Total 8 mutations in ProAgio compared to CD2D1. Anti-angiogenic peptides (TVQMKL and NLKVII) were grafted into the C- and N- terminal of CD2D1 and shown in bold. A M23C mutation was made to facilitate site-specific PEGylation of ProAgio.

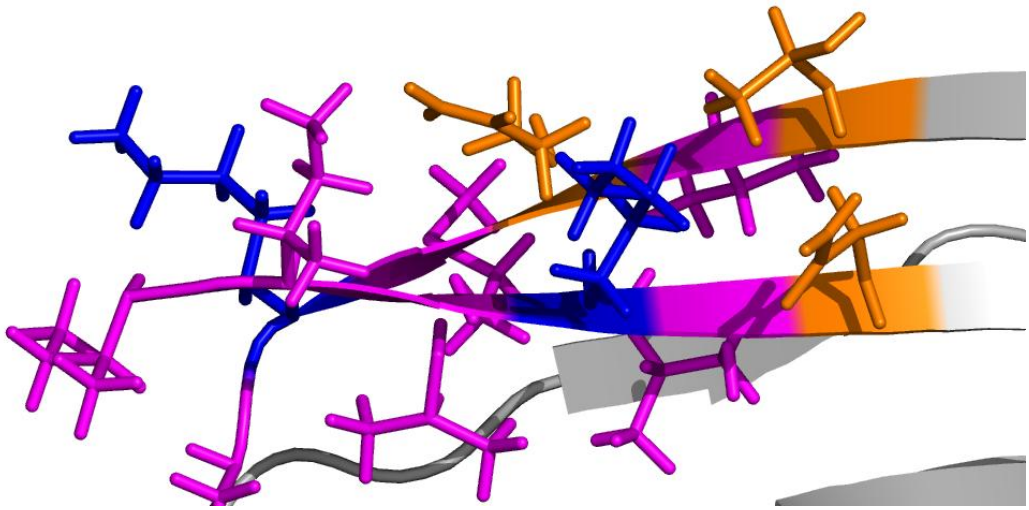

Figure 1.4 Designed Anti-angiogenic Region in ProAgio. The homology model of ProAgio was built by a computer program, Modeller, using the C-ray crystal structure of CD2D1 (PDB accession ID, 1HNG) as a template. Amino acids involved in anti-angiogenic function are color coded. Orange represents polar residues, magenta represents hydrophobic residues, and blue indicates positively-charged residues. (B and C) Different views of the ProAgio model structure.

Table 1.2 Index for Protein Expressed and Studied in this Dissertation

*Abbreviation	Description	Related Contents
CD2D1	Extracellular domain 1 of rat cluster of differential 2 with CD48 as its natural ligand [298]	1.10.4
HuCD2D1	Extracellular domain 1 of human cluster of differential 2 as CD58 its major natural ligand [302]	4.1.3
6D31	A *de novo* designed metal-binding protein using rat CD2D1 as the parental host protein [311]	5.1
6D31-ProAgio	Initial designed anti-angiogenic protein using 6D31 as the parental host protein	5.1 – 5.4
ProAgio	The de novo designed anti-angiogenic protein using rat CD2D1 as a parental host protein	1.10.5; Chapter 3; and 5
Met23Cys-ProAgio	ProAgio with a Met23Cys mutation	5.9
ProAgio-PEG	ProAgio was conjugated with a Y-shaped 20-kDa maleimide-PEG at the Cys23 residue in order to improve PK/PD parameters	5.9 and Chapter 3
huProAgio	Based on ProAgio, the anti-angiogenic peptide regions were re-designed into huCD2D1 for future clinical studies	Chapter 4
His-huProAgio	A purified his-tagged huProAgio	4.5
CD2D1-PEG	A Met23Cys CD2D1 mutant with with a Y-shaped 20-kDa maleimide-PEG at the cys23 residue	Chapter 3

*: Only proteins expressed and purified in this dissertation were listed.

1. Driscoll, P.C., et al., *Structure of domain 1 of rat T lymphocyte CD2 antigen.* Nature, 1991. **353**(6346): p. 762-5.
2. Withka, J.M., et al., *Structure of the glycosylated adhesion domain of human T lymphocyte glycoprotein CD2.* Structure, 1993. **1**(1): p. 69-81.
3. Li, S., et al., *Rational design of a conformation-switchable Ca2+- and Tb3+-binding protein without the use of multiple coupled metal-binding sites.* FEBS J, 2008. **275**(20): p. 5048-61.

CHAPTER 2

METHODS AND MATERIALS

2.1 Cell lines

Human umbilical vein endothelium cells (HUVECs) (Invitrogen, Grand Island, NY) cryopreserved at the end of the primary culture in a frozen medium containing 10% dimethyl sulfoxide (DMSO) were recovered into cell culture flasks at a density of 1.25×10^4 viable cells/mL. Cells were maintained at a 37˚C, 5% CO_2, and humidified cell culture incubator in medium 200 (Invitrogen, Grand Island, NY) supplied with 1× low serum growth supplement (LSGS) (Invitrogen, Grand Island, NY). When 500 mL of medium 200 was supplemented with 10 mL of LSGS, the final concentrations of the components in the full growth medium for HUVECs were: 2% v⁄v of fetal bovine serum (FBS), 1 µg⁄mL of hydrocortisone, 10 ng⁄mL of human epidermal growth factor (EGF), 3 ng⁄mL of basic fibroblast growth factor (bFGF), and 10 µg⁄mL of heparin. Initial cultures were maintained for 5 – 6 days until they were 80% confluent with medium-changing every other day. Confluent cultures could be maintained by changing medium every day. Subculturing HUVECs was performed by digesting cells with 0.25% trypsin/EDTA (Mediatech, Manassas, VA) and seeding cells into a new culture vessel at a cell density of 2.5×10^3 cells/cm^2. Cryopreserved HUVECs (Invitrogen, Grand Island, NY) showed reduced viability compared to the primary culture.

A human prostate cancer cell line, PC-3M-luc-C6 (PC3) (Caliper Life Sciences, Hopkinton, MA) was a kind gift from Dr. Ritu Aneja from Georgia State University (GSU). PC-3M-luc-C6 is a bioluminescent light producing cell line derived from PC3M human adenocarcinoma cells by stable transfection of the North American Firefly Luciferase gene expressed from the SV40

promoter. PC3 cells were maintained in MEM medium (Mediatech, Manassas, VA) supplied with 10% FBS (HyClone, Waltham, MA), 1mM glutamine. Cells were passed at 1:5 to 1:10 ratios every 2-3 days using 0.25% Trypsin/EDTA.

Other human cell lines including HCT-116 (Catalog #CCL-247, human colon carcinoma) and M4A4 (Catalog #CRL-2915, human metastatic breast ductal carcinoma) were purchased from the American type Culture Collection (ATCC, Manassas, VA). All above cell lines were maintained and preserved in ATCC recommended culture medium and protocols.

2.2 Site-directed Mutagenesis to Produce Anti-angiogenic Protein cDNA

2.2.1 Site-directed Mutagenesis

Desired mutations were introduced to plasmids of interest using QuikChange® II XL Site-Directed Mutagenesis Kits (Stratagene, Santa Clara, CA). Complementary mutagenic primers were designed either by placing desired point mutation, deletion or insertion in the middle of the primer flanked with 10 – 15 unmodified base pairs (bps) on both sides or using the online software, QuikChange primer design application (www.genomics.agilent.com). Site-directed mutagenesis polymerase chain reactions (PCR) were carried out following the manufacturer's exact instructions. After the reactions were complete, an amount of 10 units of *Dpn I* was add-ed to each reaction, which was incubated for 1 hour at 37˚C to digest the parental plasmid DNA. The mutated DNA plasmids were then transformed into *XL-1*-Blue competent cells provided by the kit. Bacterial were applied to a LB agar plate containing 100ng/mL ampicillin and allowed to grow overnight. Usually 3 – 6 colonies were chosen to be mini-cultured in 1 – 5 mL of ampicillin

containing LB medium. Plasmids were purified and sent for sequencing in a DNA sequencing core facility located at GSU.

2.2.2 Multi Site-directed Mutagenesis

QuikChange® Multi Sit-Directed Mutagenesis kits (Stratagene, Santa Clara, CA) were used to generate multiple mutations that were located in the separate termini of the parental cDNAs. Different from QuikChange® II *XL* Site-Directed Mutagenesis Kits, a single mutagenic primer instead of a pair is required to mutagenize each site, using a double-stranded DNA template. The kit contains a PCR enzyme blend featured with a unique *Pfu* fusion-based DNA polymerase that provides a one step mutation at multiple sites. Mutagenic primers were designed using online software, QuikChange primer design application (www.genomics.agilent.com). The protocols were provided by the manufacturer.

2.2.3 Transformation *Escherichia coli* (*E. coli*) strains

The JM109 (Promega, Madison, WI) competent cells and *XL*-blue Super competent Cells were used for amplifying a particular plasmid in large quantities. BL-21 (DE3), BL-21 (DE3) *pLysS* competent cell lines were kind gifts from Dr. Jenny Yang from the Chemistry Department at GSU. A BL-21 CodonPlus® (DE3) competent cell line was purchased from (Stratagene, Santa Clara, CA). All three BL-21 cell lines were used to express the proteins of interest in this study. When transformations were performed, suitable competent cells were thawed on ice in pre-chilled 14 mL polypropylene tubes (BD). BL-21 CodonPlus® (DE3) competent cells were incubated with β-mercaptoethanol for 10 minutes prior to transformation as suggested by the

manufacturer. Next, 10-100 ng of desired plasmids were added into 50-100 µl of competent cells followed by incubation on ice for 30 minutes. Then the mixture was heat shocked by 20-90 seconds water bath at 42˚C as recommended by manufacturers or established protocols. A volume of 500 µl of pre-warmed S.O.C medium was added to each tube. After cooling for 2 minutes on ice, the tubes were incubated at 225 rpm for 1 hour in a shaker set at 37˚C. Each bacteria culture was then spread onto individual LB agar plate containing a proper concentration of antibiotics for different plasmids. LB plate was incubated overnight at 37˚C.

2.3 Cloning of the CD2 variants into pGEX-2T Expression Vector

2.3.1 Mini Prep

DNA purification from bacterial culture in Small scales (0 – 20 µg) was performed using Qiaprep® spin Mini Kit (Qiagen, Hamburg, Germany). A single colony from the freshly transformed plate of bacteria was added to 1 – 5 mL of LB media containing proper concentrations of antibiotics. The culture was incubated overnight in a shaker set at 37˚C and 225 rpm. The bacterial pellet was collected by centrifugation at 8,000 rpm for 5 minutes at room temperature followed by removal of the LB media. Next, cells were re-suspended in 250 µL of buffer P1. An equal volume of Buffer P2 (the cell lysis buffer) was then added to the solution. The tube was gently inverted 4-6 times to mix followed by immediately adding 350 µL of Buffer N3 (the neutralization buffer). The solution was further mixed by gentle inversion for 4-6 times. The cell debris was clarified from the mixture by centrifugation at 13,000 rpm for 10 minutes at room temperature. Then the supernatant was transferred to a spin column and centrifuged at 13,000 rpm for 1 minute, which allowed the plasmid DNA bound to the column membrane. For *endA*$^+$

bacteria strains, the column was washed once with 500 µL buffer PB by centrifugation at 13,000 rpm for 1 minute to remove trace nuclease activities. The column was then washed with buffer PE and dried by centrifugation for additional 1 – 2 minutes after washing. The plasmids were eluted with elution buffer (10Mm Tris-HCl, pH 8.5) or distilled water if further restriction digestion or ligation was desired. The purified DNA usually was used for DNA sequencing to verify the construction.

2.3.2 Midi prep

Moderate amounts (10 µg – 200 µg) of plasmids were purified using the Wizard® Plus DNA Purification System (Promega, Madison, WI). The purification procedures were performed according to the manufacturer's instruction. An overnight plasmid-containing bacterial culture of 50-100 mL was collected by centrifugation at 8,000 rpm for 10 minutes at 4˚C. The cell pellet was completely re-suspended by pipetting in 3 mL of suspension buffer and transferred in an autoclaved centrifuge tube (Nalgene, Rochester, NY). A volume of 3 mL of the lysis buffer was added into the tube. Then the tube was gently inverted 4-6 times followed by immediately adding 3 mL of the neutralization buffer. The mixture was further gently inverted 4-6 times to mix. The cell debris was clarified from the solution by centrifugation for 15 minutes at 14,000 rpm at 4˚C. The resultant supernatant was transferred into a clean 50 mL conical tube and mixed with 10 mL of DNA purification resins. The DNA/resin mixture was then loaded to a midi prep column connected to a Vac-Man® Laboratory Vacuum (Promega, Madison, WI). The supernatant was removed by vacuuming followed by washing twice with 15 mL of Column Wash Solution. When the last run of wash was complete, the vacuum was allowed to run for additional 30

seconds to dry the resins. The column reservoir was then separated from the column, and excess Column Wash Solution was removed by centrifugation at 13,000 rpm for 2 minutes. A volume of 300 µL of pre-hearted (65˚C) Elution buffer (Tris-HCl, pH 8.5) or distilled water was added to each the column and incubated for 1 minute. Next, the eluate was collected by centrifugation at 13,000 rpm for 1 minute. The residual amount of ethanol that might interfere with following enzymatic reactions was removed from the sample using an evaporation method by leaving the cap open overnight at room temperature. The purified plasmids were then stored at -20˚C or -80˚C for longer time.

2.3.3 DNA Concentration and Quality Measurement

The OD_{260} and OD_{280} of DNA solutions were measured using a spectrophotometer. DNA concentrations were calculated based on the following formula using common extinction coefficient of 50 $(\mu g/mL)^{-1}cm^{-1}$ for DNA as DNA concentration (µg/mL) = (OD_{260}) × (dilution factor) × (50 µb DNA/mL)/(1 OD_{260} unit). The ratio of OD_{260} and OD_{280} was calculated for each sample to determine the purity. The accepted purity value is between 1.65 and 1.85. DNA plasmids or fragments were further verified by agarose gel electrophoresis. Usually intact DNA plasmids or fragments should appear as sharp bands without smear.

2.3.4 Agarose Gel Electrophoresis

Separation of DNA molecules was performed by agarose gel electrophoresis and DNA bands were visualized using double stranded DNA binding dyes such as SYBR Safe (Invitrogen, Grand Island, NY) or ethidium bromide (Sigma-Aldrich, St. Louis, MO). Low percent gels (0.8 –

1%) usually used for analyses of DNA plasmids or DNA fragments of large MWs, while higher percent gels (> 2%) were used for separation of small molecular weight DNA fragments such as PCR products. An appropriate amount of electrophoresis grade agarose (EMD Chemicals, Gibbstown, NJ) was weighed and mixed with 50 – 100 mL of 1X TAE (Tris-Base, Glacial Acetic Acid, EDTA, pH 8.0). The agarose was melted by heating the mixture using an electronic micro-wave. Then, the mixture was allowed to cool down below 68˚C before adding ethidium bromide at a final concentration of 0.5 μg/mL. Then the liquid was poured into a casting apparatus with an appropriately sized and numbered comb. The comb was removed after the agarose became firmly solidified at room temperature, and then the gel was properly placed into an electropho-resis device filled with 1 X TAE buffer. Each DNA sample was mixed with an appropriate volume of 5 X DNA loading dye (Fermentas, Glen Burnie, Maryland) to make the final loading dye con-centration to 1 X. A volume of 5 – 20 μL of such sample was loaded to each well. The gel was then subjected to electrophoresis for 45 – 90 minutes at 100 – 120 volts at room temperature. DNA fragments in the gel were visualized under the UV light with a wavelength of 302 nm using a UV transilluminator equipped with a CCD camera.

2.3.5 Agarose Gel Extraction of DNA

Following gel electrophoresis, the DNA fragment of interest was extracted from the gel for applications such as ligation, mutagenesis, and restriction enzyme digest. All gel extractions were performed using the QIAquick Gel Extraction Kit (Qiagen, Hamburg, Germany) according to the manufacturer's instruction. The band of interest was excised from the agarose gel with UV safety screens and protective eyewear during gel excision. The excised gel piece was

weighed in a pre-weighed microcentrifuge tube. Then buffer QG was added to the tube in a 3:1 ratio (for example, 300 µL buffer QG to 100 mg gel). A 6:1 ratio of QG buffer was added to higher percent gels (> 2%). Then, the mixture was incubated at 50˚C for 10 – 15 minutes in order to completely dissolve the gel. The pH of the resultant solution is indicated by a pH indicator contained in buffer QG. The dissolved DNA only efficiently binds QIAquick membrane when the color of the mixture shows yellow color, a color similar to buffer QG. Orange of purple color after the gel was dissolved indicates a higher pH that has to be returned ≤ 7.5 by adding 10 µL of 3 M sodium acetate, pH 5.0 to the tube. After 1 gel volume of 100% isopropanol was added to the sample and mixed, the solution was then transferred to a QIAquick column and centrifuge at 13,000 rpm for 1 minute. In order to remove any residual agarose, 0.5 mL of Buffer QG was added to and the column was centrifuged again at 13,000 rpm for 1 minute. The column was then washed with 0.75 mL of buffer PE to remove any excess salt by centrifugation at 13,000 rpm for 1 minute. The column was dried by centrifugation for an additional 1 minute, and then the DNA was eluted with pre-warmed (65˚C) Buffer EB (10 mM Tris-HCl, pH 8.5) or distilled water. The eluate was stored at -20˚C until use.

2.3.6 Restriction Enzyme Digestion

All restriction enzymes were purchased from Fermentas, Glen Burnie, MD. Optimal conditions and protocols followed manufacturer's instructions. A typical restriction reaction system usually is composed of 2 µg of plasmid DNA, 1 µL of restriction enzyme, 2 µL of 10X appropriate restriction digest buffer, 16 µL of distilled water. Scaled up reactions usually were performed in 50 µL or 100 µL reactions with 5 µg or 10 µg of plasmid DNA as substrates separately. When

PCR products were digested, 0.2 µg of DNA were used in a 20 µL reaction system. If double digest was desired, proper buffer that suitable for both restriction enzymes was used. Sequential digest was performed otherwise. A typical double digest with BamHI and EcoRI was composed of 2 µg of plasmid DNA, 1 µL of BamHI, 1 µL of EcoRI, 2 µL of 10X Tango™ buffer (Fermenta, Glen Burnie, MD), and 14 µL of distilled water. Reaction mixtures usually were incubated for 1-16 hours at 30-42 ˚C following manufacturer's recommendations. The digested fragments were separated by agarose gel electrophoresis for extraction or analysis of plasmid constructions.

2.3.7 Ligation of CD2 Variants and pGEX-2T Expression Vector

Desired CD2D1 cDNA or mutants purified from agarose gel were inserted into pGEX-2T expression vector (GE Life sciences, Piscataway, NJ). A 3:1 to 5:1 cDNA to pGEX-2T was used for the ligation reaction. To a 1.5 mL Eppendorf tube, 50-100 ng of digested and purified pGEX-2T vector, proper calculated amount of cDNA fragments, 1 to 2 µL of ligase buffer, 1 µL of T4 DNA ligase, and distilled water were mixed together to a total volume of 10 to 20 µL. The reaction was placed at room temperature and then at 16 ˚C overnight for maxima ligation. The ligation mixture was then transformed to JM109 competent cells. Correct clones were confirmed by DNA sequencing or restriction enzyme digestion after mini DNA purification.

2.4 Expression of the Glutathione (GST)-tagged Proteins

2.4.1 Optimization of Expression for the GST-tagged Proteins

Each expression vector construction was test in different cell lines for maxima expression level. The BL-21 (DE3), BL-21 (DE3) *pLysS* and the BL-21(DE3) CodonPlus® competent

cell lines were used in this project for protein expression. Usually 5-6 health colonies were chosen from plates with transformed bacterial. Each colony was added to 2 mL LB medium with 100 µg/mL and incubated 225 rpm for 2 to 3 hours in a shaker. Then isopropyl-β-D-thiogalactoside (IPTG) was added to a final concentration of 0.2 mM. The cultures were incubated for another 3 to 4 hours. An aliquot of 1 mL of each culture was centrifuged in a 1.5 mL Eppendorf tube and pellets were collected. Sample buffer (50 µL, 1X SDS buffer) were added to each tube and boiled for 10 minutes. Samples were then analyzed by SDS gel electrophoresis. The colony with highest expression level was chosen for further large scale protein expression. If desired expression level was not achieved, the chosen colony was subjected to further optimization on temperature (18˚C to 37˚C), induction time (2 to 16 hours), and IPTG concentration (0.1 to 1mM).

2.4.2 Expression of CD2 Variants in Luria Bertani (LB) Medium

ProAgio cDNA bearing pGEX-2T expression plasmid was transformed into BL-21(DE3) Codon-Plus® competent cells. A healthy colony was inoculated into 3 mL LB medium with 100 µg/mL of ampicillin, which was incubated at 37 ˚C until the optical density (O. D.) 600 nm reaches 0.6 - 0.8. 50 µl of culture were transferred to 50 mL LB medium and incubated at 37 ˚C overnight with agitations. 15mL of such culture were added into 1L LB medium and incubated at 250rpm, 37 ˚C. When the reading of O. D. 600 nm reached 0.8 - 1.0 (roughly 2 to 2.5 hours), a final concentration of 0.2mM IPTG was added to the flask. Then temperature was decreased to 30 ˚C and protein expression was induced and incubated for 4 to 5 hours until the O. D. reach 1.8 - 2.0. Bacteria were collected by centrifugation at 6000 rpm for 15min. Pellets were transferred to a 50 mL centrifuge tube and temporarily stored at -20 ˚C until usage.

2.5 Purification of CD2D1 and ProAgio

The cell pellet was defrosted and suspended in lysate buffer (30 mL of lysate buffer per each liter growth). DTT was added to the pellet mixture to reach a final DTT concentration of 5 mM. EDTA was added to the pellet mixture to reach final EDTA concentration of 10 mM. The mixture was blended for 30 seconds.The blended mixture was separated into multiple small plastic beakers (< 25 mL per beaker) and each beaker was sonicated 6 times. The duration of each sonication cycle is 10 seconds with a 10 minute interval between sonication cycles. For lysis of ProAgio pellets, a light sonication was applied. Lysates were further disrupted by passing through a French press 40k cell. Once the sonication cycles were complete, the content was centrifuged for 30 minutes at 17,000 rpm. The supernatant was filtered using 0.45 μm syringe filter while the remaining pellet was re-suspended in lysate buffer to repeat above purification steps. After cell lysis, the fusion proteins in the supernatant were loaded onto a column of GS4B resin (GE lifesciences, Piscataway, NJ). After binding, each column was washed with 50 mL of 1x PBS buffer. The fusion proteins were cleaved by thrombin (2.5 mL of 1x PBS buffer with 30 μL of thrombin (1 unit/μL) on the beads following elution of waste materials. The column was first kept at 4 °C with agitation for 14 hours, and then placed at room temperature for two hours before elution. The proteins were eluted using 20 mL of 1x PBS buffer per column. The eluted proteins were further purified using a superdex 75 column (GE lifesciences, Piscataway, NJ) in the FPLC and 10 mM Tris elution buffer at pH 7.4. The size exclusion purification was used to further purify ProAgio with 1XPBS buffer, while a SP Sepharose column (GE lifesciences, Piscataway, NJ) was applied for the further purification of CD2D1. The protein was bound to the cationic exchange column using 20 mM acetate buffer at pH 3.5. The protein was eluted with an

increasing pH gradient from 3.5 to 8.0 (50 mM Tris buffer). The identities of CD2 variants were confirmed by SDS–PAGE. The protein concentration was measured with ε_{280} = 11700 M^{-1} cm^{-1} for CD2D1 and ε_{280} = 8480 M^{-1} cm^{-1} for ProAgio. Concentrations were further confirmed by a Bradford protein assay using bovine serum albumin (BSA) as a standard.

2.6 Purification of ProAgio-PEG

2.6.1 Site-specific PEGylation of ProAgio

After cleavage, Y-shaped maleimide PEG (Jenkem Technology, Allen, TX) powders were directly added to column at molar ratio of 1:5 to 1:8 (protein to PEG). The molar concentration of ProAgio protein was determined by Bradford protein assay using BSA as a standard. Molar concentration was calculated same as section 2.5 because each fusion protein molecule only contain 1 molecule of ProAgio recombinant protein. Typical binding for each column required an average of 100 – 250 mg of PEG. Mixture was incubated at room temperature for 1 hour or at 4 ˚C overnight. PEGylated protein was eluted using 1XPBS.

2.6.2 Purification of ProAgio-PEG Using Ion Exchange Chromatography

ProAgio-PEG recombinant protein was dialyzed to 5 mM MES sodium Salt pH 6.0 at 4 ˚C. Further purify the protein by an AKTA FPLC system (GE Life Sciences, Piscataway, NJ) equipped with a SP high performance Sepharose ™ Column (GE Life Sciences, Piscataway, NJ). The purification program was performed as following program with flow rate at 5 mL/minute. All fractions were collected at 2 mL/tube. First, the instrument was equilibrated with 2 CV (column volume) of Buffer A (5 mM MES sodium salt, pH 6.0). Samples were injected into a 10 or 50 mL

sample loop. Fractions were collected from this point onward. Most free PEG and PEGylated GST did not bind to column and form major UV280 absorbance peaks were discarded. Non-specific bound proteins were washed off with 5 CV of Buffer B gradients (5 mM MES sodium salt, 1M NaCl, pH 6.0) from 0% to 10% to remove non-specific bound proteins. Elution of ProA-gio-PEG started around 50% Buffer B, fraction 35-40.The column was washed with 3 CV of 100% of Buffer B and re-equilibrated with 5 CV of 100% of Buffer A.

A volume of 20 µL of fractions from each UV absorbance peak was loaded into a SDS-PAGE gel analysis using coomassie blue staining. PEGylation was visualized by iodine staining. The 20,000 Y-shape maleimide PEGylated ProAgio migrated between molecular weight (MW) of 55-kDa to 70-KDa, which was much slower than the calculated MW of 31-kDa. Protein fractions with ProAgio-PEG or CD2D1-PEG were pooled together (usually were fractions 36, 37, 38, and 39), concentrated, and further dialyzed to 1XPBS for further biology functional assays and animal experiments.

2.6.3 Protein stability test

Purified ProAgio was mixed with FBS in a 1:1 ration. The mixture was incubated at 37˚C for desired time. Sodium dodecyl sulfate polyacrylamide (SDS-PAGE) gel electrophoresis was performed to determine the degradation of ProAgio. The disappearance of ProAgio protein band was attributed completely to degradation.

2.7 Determination of Protein Concentration

The concentration of ProAgio and ProAgio-PEG was determined using UV absorbance at 280 nm and calculated using an estimated extinction coefficient of 8480 M^{-1} cm^{-1}. For example, an UV absorbance 280 nm of 0.848 was equal to 100 μM (11.28 mg/L) of ProAgio or (31.28 mg/L) of ProAgio-PEG, because that the PEG chain increased the molecular weight of ProAgio but did not affect the protein composition. Protein concentrations were further confirmed using Bradford protein assay using bovine serum albumin as a standard.

2.8 Conformational Analyses by 1D ^{1}H NMR

For 1D ^{1}H NMR studies on ProAgio and CD2D1, NMR samples were prepared by diluting proteins in 10 mM Tris-HCl with 10% D_2O at pH 7.4. Protein concentrations were varied from 150 to 300 μM. Dioxane was used as an internal reference for the NMR spectra (3.743 ppm). All NMR spectra were recorded using Varian Inova 500 MHz and 600 MHz NMR spectrometers. Spectra widths of 6600 Hz and 8000 Hz were used at 500 MHz and 600 MHz, respectively. A water suppression pulse sequence from Varian Biopack was used with 8 K complex data points at 25 ºC. All the 1D NMR experiments were collected with 1024 scans.

The data were processed with the program FELIX98 (MSI). After Fourier transformation, typically a squared sinebell window function shifted over 75º was used. Post acquisition suppression of the water signal was achieved by deconvolution of a Gaussian function with a function width of 20.

2.9 Assays to determine the *in vitro* effects of ProAgio

2.9.1 Determination of Cell Growth

HUVEC cells were typsinized and seeded into a 96-well plate at $4x10^4$ cells /mL. After 16 – 18 hours of attachment, cells were treated 0 – 40 µM of ProAgio-6D31 or CD2D1 for 48 hours. Cell proliferation rates were measured by Thiazolyl blue tetrazolium bromide (MTT) (Sigma-Aldrich, St. Louis, MO) assay. MTT power was diluted in Hank's balanced salt solution at 5mg/mL. 1/Tenth of the total culture volume of MTT solution of added to each well and incubator for additional 4 hours. Then the supernatant was carefully removed and DMSO was added to dissolve the formed crystal. Photometry at 490nm was performed using a PerkinElmer Victor 3 microplate reader (PerkinElmer, Waltham, MA). The absorbance of cell control was designated as 100%. The proliferation rates were calculated using the equation: proliferation rate of treated cells = absorbance of treated cells/absorbance of cell control. The values were plotted using Microsoft Excel.

2.9.2 Cell proliferation Assay (BrdU)

Cell proliferation rates were determined using BrdU cell proliferation kit (Calbiochem, La Jolla, CA). All procedures followed the manufacturer's instruction. Briefly, HUVECs or M4A4 cells were trypsinized and seeded into 96 well plates at $4x10^4$ cells/mL. Cells were allowed to attach for overnight, and then treated with protein and peptide reagents at desired concentrations for 48 hours. Each concentration was tested in triplet wells. BrdU label was 1:2000 diluted into fresh tissue culture media, and 20 µL of this working solution were added to each well to be labeled. After incubation for an additional 12 hours, cells were fixed, and then incubated

with 100 µL of 1:100 diluted anti-BrdU antibodies at room temperature for 1 hour. After washing 3 times with wash buffer, a peroxidase goat anti-mouse IgG HRP conjugated antibody was added to each well for 30 minutes followed by 3 times washes. Tetra-methylbenzidine substrate solution was incubated with each well for 15 minutes and the reaction was stopped by 2.5N sulfuric acid. The absorbance in each well was measured a PerkinElmer Victor 3 microplate reader (PerkinElmer, Waltham, MA) at dual wavelengths of 450 – 540 nm. The proliferation rates of different treatment were compared as folds change of control. Each treatment was repeated in triplicate, and experiments were repeated 3 times.

2.9.3 Tube Formation Assay

The *in vitro* angiogenesis studies were performed using tube formation assay. HUVCs were seeded into a 96 well plate coated with 50 µl of martigel (BD Biosciences, San Jose, CA) for each well. Before usage, the coated plates were incubated for 30 minutes at 37°C and 5% CO2 environment to allow matrix to polymerize. A volume of 50 µL of HUVEC cell suspension ($2x10^4$ cells) was added to each well. For examine HUVECs and PC3 cells co-culture (1:1 mixture) formed tubules, a volume of 50 µL of HUVEC suspension containing $1x10^4$ cells was added to each well. Stimulators, such as 10% FBS or $1x10^4$ cells PC3 cells were supplied with the culture media to promote the formation of endothelial tubules. At the same time, protein and peptide reagents were added at desired concentrations in duplicate wells for each concentration. Then the angiogenesis assay plate was incubated for 6 – 8 hours at 37°C, 5% CO2 atmosphere. Tube formations were observed under a light microscope at 50 X magnification (10 X Ocular lens and 5 X Obj. Lens). Three digital pictures were taken from each well. Experiments were repeated for

three times. The total tubule length per 5X Obj. field for each picture was measured using the ImageJ software (National Health Institution, Bethesda, Maryland). Branch points were counted manually.

2.9.4 GST Pull-down Assay

GST pull-down assays were performed according to protocols described by Kaelin and colleagues [312]. GST fusion proteins (GST, GST-CD2D1, and GST-ProAgio) were expressed and conjugated to GS4B beads as described in section 2.5. Freshly thawed and routinely maintained HUVECs at 80% confluence were rinsed with 1 x Hanks Balanced Salt Solution (HBSS), and incubated with 25 ng/mL human recombinant VEGF (Invitrogen, Grand Island, NY) supplied in full-culture medium without bFGF described in section 2.1 for additional 16 hours at 37 ˚C, 5% CO_2. Then cells were washed three times with cold 1 X PBS, pH 7.4. All following procedures were performed on ice or under 4 ˚C. Cell pellets were collected by centrifugation at 8,000 rpm for 5 minutes after cells were physically detached from culture flasks by scraping. Cell pellets were resuspended and incubated for 2 hours in NETN lysis buffer supplied with 1 X protease inhibitor cocktail (20 mM Tris, pH 8.0; 100 mM NaCl; 1 mM EDTA; 10 µg/nl phenylmethylsulfonyl fluoride; 0.1% Nonident P-40; 500 µM 4-(2-Aminoethyl) benzenesulfonyl fluoride hydrochloride; 150 nM aprotinin; 1 µM E-64; and 1 µM leupeptin hemisulfate). EDTA-free protease inhibitor cocktail set V was purchased from Calbiochem, La Jolla, CA. Chemical reagents were purchased from Sigmal-Aldrich, St. Louis, MO. The lysates were centrifuged at maximum speed for 2 minutes in a microcentrifuge. Clear supernatant was transferred to a clean microcentrifuge tube.

Total proteins in supernatant were diluted to 1 μg/μL, pre-cleared by GS4B beads for 2 hours, and then used for pull-down assay.

GS4B beads conjugated with 500 μg of GST, GST-CD2D1, or GST-ProAgio was incubated with a total of 500 μg of above HUVEC lysate in a volume of 500 μL for overnight by end-over-end mixing. Beads were washed three times in lysate buffer. Proteins were eluted by boiling at 95 ˚C for 8 minutes in 1 X SDS sample buffer (50 mM Tris-HCl, pH 6.8; 2% SDS; 10% glycerol; 1% βmercaptoethanol; 12.5 mM EDTA; and 0.02% bromophenol blue). For each sample, 20 μL of eluates were loaded to SDS-PAGE gel electrophoresis analysis.

2.9.5 Western Blot

Proteins in SDS-PAGE gel were transferred to a PVDF membrane by an electronic transfer device (Bio-Rad, Hercules, CA) for 2 hours at 100 Volts at room temperature in transfer buffer. Protein bands in PVDF membrane were visualized by staining in 2% Ponceau Solution (Sigma-Aldrich, St. Louis, MO) for 1 minute, and then destained by repeated washing in water. Membranes were incubated at room temperature for 30 minutes in 1 X TBST blocking buffer (50 mM Tris-HCl, pH 7.6; 150 mM NaCl; 0.1% Tween 20; and 5% bovine serum albumin). A primary mouse anti-human Galectin-1 (anti-Gal-1) monoclonal antibody (Abcam, Cambridge, MA) was incubated with the membrane at 1:500 dilutions for overnight at 4 ˚C. Membrane was washed three times for 5 minutes each in 1 X TBST washing buffer (50 mM Tris-HCl, pH 7.6; 150 mM NaCl; and 0.1% Tween 20). A radish peroxidase (HRP)-conjugated goat anti-mouse IgG secondary antibody (Thermo Fisher Scientific, Waltham, MA) was incubated with the membranes at 1:2000 dilutions for 1 hour at room temperature. Membranes were then washed again for

three times in washing buffer and briefly dried. Luminata Western HRP substrates were added to each membrane (Millipore, Billerica, MA) and developed for 5 minutes. Membranes were then examined using a UV transilluminator with an attached CCD camera.

2.10 *In Vivo* Effects of ProAgio and ProAgio-PEG Using Xenograft Nude Mice Model

2.10.1 Animal Care

Athymic Nude-*Foxn1*^{nu} mice (Nude mice) at age of 3-4 weeks were purchased from Harlan Laboratories, Indianapolis; IN. Animals were housed in animal facilities located at GSU animal research center. Experimental procedures for all animal studies were reviewed and approved by Institutional Animal Care and Use Committee (IACUC) at GSU according to the Public Health Service (PHS) guide for care and use of laboratory animals (Protocol approval # 2007-0126). A standard operating procedure (SOP) for working with laboratory animals were followed for routine animal handling, intraperitoneal (i.p.) injection, tumor inoculation, tumor measurement, and endpoint euthanasia.

Animals were routinely monitored every day for any potential abnormality including movement, food intake, body weight, alertness, and skin color. For tumor-bearing mouse, all tumors must be measured at least twice a day. Any animal with a tumor size exceeding in any direction than 1.5 cm, as stated in the IACUC protocol, should be euthanized. Pain levels from all procedures were recorded and reported to staff members at the Department of Animal Research (DAR) at GSU. Pain levels were categorized following the U.S. Department of Agriculture (USDA) classifications for pain as follows: B represents that animal are being bred, conditioned, or held for teaching, testing, experiments, and research; C means that tests will be conducted

involving no pain; and D indicates that procedures will be conducted involving accompanying pain or distress that will be relieved by treatment with anesthetic, analgesic, or tranquilizing drugs.

2.10.2 *In Vivo* Xenograft Model

PC-3M-luc-C6 cells were cultured in MEM medium with 8% FBS. Cells were trypsinized and suspended in 1 X HBSS mixed with 50% volume of matrix gel. The mixture was kept on ice until injection. Animals were placed in an anesthesia induction chamber in a bio-safety II cabinet located in a standard operating room in DAR facilities. Animals were anesthetized using isoflurane administrated by a vaporizer. Anesthetized animals were kept in a warm re-circulating water heating pad during anesthesia. The injection area was sanitized with ethanol pads. A volume of 100 μL this suspension containing $5X10^6$ cells was subcutaneously injected into one flank of each nude mouse. Five to seven days after tumor cell inoculation, treatments were initiated when the xenografts were clearly established and had reached a volume of 50–100 mm^3. All reagents were administered by i.p. injection at desired doses (buffer: 1 X PBS; ProAgio: 5 mg/kg/day; ProAgio-PEG: 2.5 – 20 mg/kg/day; CD2D1-PEG: 20 mg.kg/day; Avastin: 20 mg/kg/twice weekly). Tumor sizes and mice weights were measured and recorded every other day with a digital caliper and a digital balance. Tumor volumes were measured using formula: Tumor volume (mm^3) = $\pi/6$ x (length x width x width).

2.10.3 Determination of Tumor Weights

At the end of treatment, animals were euthanized according to the established SOP approved by DAR. Briefly, animals were placed in a plastic CO_2 gas chamber in the DAR facility procedure room. CO_2 gas valve was slowly turned on, and gas flow will be maintained for at least 1 minute after apparent clinical death. Then, the gas valve was turned off. After animals were removed from the gas chamber, unintended recoveries were voided by physical euthanasia. Then, tumors were carefully dissected from the tumor-bearing mice without adjacent tissues or skins. Tumors ware weighed using a digital balance individually.

2.10.4 CD31 Immunofluorescence (IF) Staining of Frozen Slides

Fresh dissected normal mouse organs and tumor tissues were placed into cryo-molds, covered with OCT compound, and then snap-frozen in liquid nitrogen. Tissue blocks were sliced into 10 or 20 µM thick sections using a cryostat. For staining of the endothelial marker, CD31, 10 – 20 µM thick sections were used. Sections were dried on Superfrost Plus slides (VWR International, Radnor, PA) for I hours. Specimens were permeabilized with TBST buffer (0.1 % Triton X-100 (Sigma-Aldrich, St. Louis, MO), 50mM Tris-HCl, 150 mM NaCl, pH 7.5) and incubated in blocking buffer (5% bovine serum albumin in TBST buffer) for 1 hour at room temperature to block nonspecific antibody binding. Then ECs were stained using a rat anti-mouse CD31 (BD Pharmingen, San Diego, CA) and a green fluorescence conjugated anti-rat IgG second antibody. Briefly, sections were washed three times with TBST buffer for 5 minutes each time with gentle agitation. Then, 100 - 200 µl of rat anti-mouse CD31 (1:1000 diluted in TBST buffer) antibodies were added to each section and incubated at room temperature for 1 hour or 4 ˚C overnight.

Specimens were rinsed again with TBST buffer and mounted in ProLong® Gold Antifade Reagent with DAPI (Invitrogen, Grand Island, NY) after briefly drying in air.

2.10.5 Mean Vessel Density (MVD) Determination of in Xenograft Tumors

Specimens were examined with a Zeiss 700 Axiophot fluorescence microscope (Carl Zeiss Optical, Thornwood, NY). In each mouse, three sections were chosen from top and middle points of each xenograft. CD31 stained slides were scanned under low magnification (5X objective and 10X ocular lens). After the highest vessel density was determined in the slides, an area of 319.8 X 319.8 μM with the highest amount of vessels was scanned under a 20X objective lens and 10X ocular lens. For comparison, all slides were stained under same conditions, and all images were taken under the same device setting. Images of from each section were analyzed for MVD, vessel count, and branching points. The total number of vessel length within each of the image was measured using a Zeiss LSM image browser (Carl Zeiss Optical, Thornwood, NY). MVD were determined using methods described by Weidner and coworkers [313]. Briefly, any clear pattern of green fluorescent stained EC or EC cluster within the tumor tissue that separated from connective-tissues was counted as one vessel. Microvessels in sclerotic areas or adjacent to connective tissues were not considered. At least three MVD from different sections within a tumor were examined and counted for statistic analysis. A vessel branching point was defined as any green fluorescent staining with a pattern of 3 branches connected into one dot.

2.10.6 Determination of Organ Toxicity

General toxicity was evaluated by measuring body weight changes and observing daily behavior and food intakes. In order to determine organ toxicity, major organs including heart, kidney, liver, and spleen were dissected out. One set of organs from each mouse were fixed in 4% paraformaldehyde/PBS solution. Hematoxylin and eosin (H&E) staining of these fixed organs were processed in the laboratory of Dr. Hans Grossniklaus at the department of Ophthalmology and Pathology at Emory University. Pathological examinations were performed by Dr. H. Grossniklaus. In order to determine the vessel toxicity, one set of major organs from each mouse were snap frozen into liquid nitrogen with O.C.T imbedding. Organs were then sliced and processed for CD31 IF staining using methods described above. At least three different sections from each organ were examined for H&E and CD31 IF staining respectively.

2.11 Statistics Analysis

Quantitative data from cell proliferation and MTT cell viability assays were described in mean ± S.D. (standard deviation). In animal experiments, quantitative data were described in mean ± S.E.M. (standard error of mean). Statistic evaluations of data from cell proliferation, tube formation, and CD31 IF-staining were performed with unpaired student's *t* tests (two-tailed). For evaluation of *in vivo* data with normal distributions, ANOVA one way tests were performed using SPSS (IBM, Armonk, NY), a statistic software. Otherwise, Welch's *t* tests were used in order to compare the tumor growth curves of two different treatment groups. In any case, a calculated possibility value less than 0.05 ($P < 0.05$) was considered statistically significant.

CHAPTER 3

Development of A protein Anti-angiogenic Agent by *de novo* Protein Design

Lu Yin [1], Hsiau-Wei Lee[3], HuaYang[4], Ravi Chakram[1], Hans E. Grossniklaus[4], Jenny J. Yang[2*] and Zhi-Ren Liu [1*]

[1]Department of Biology, Georgia State University, Atlanta, GA 30303, USA

[2]Department of Chemistry, Georgia State University, Atlanta, GA 30303, USA

[3]Complex Carbohydrate Research Center, the University of Georgia, Athens, GA30602, USA

[4]Department of Ophthalmology and Pathology, Emory University, Atlanta, GA30322, USA

*Corresponding Author:

Zhi-Ren Liu, Ph.D.
Department of Biology
Georgia State University
University Plaza
Atlanta, GA 30303 USA
(biozrl@langate.gsu.edu)

Jenny J. Yang, Ph.D.
Department of Chemistry
Georgia State University
University Plaza
Atlanta, GA 30303 USA
(chejjy@langate.gsu.edu)

Key words: Anti-angiogenesis/Protein engineering/CD2/

Running title: Protein Anti-angiogenesis agent

Inhibition of angiogenesis is a promising avenue for cancer treatment. Substantial efforts have been made to develop agents that target vascular endothelial growth factor (VEGF) and other growth factor pathways. We have developed a new class of anti-angiogenesis proteins by integrating the short anti-parallel β-sheet forming sequences of the endogenous anti-angiogenesis proteins into a stable host protein, the domain 1 of rat CD2 (CD2D1). The designed protein exhibits strong *in vitro* activity in inhibition of human umbilical vein endothelial cell (HUVEC) proliferation with no effects on epithelial cells. Tests with PC-3 xenografts showed that the designed protein strongly inhibits tumor growth. Histological analyses indicated that tumor mean vascular count is dramatically reduced, while the vessels in other organs are not affected, upon the treatments with the developed agents.

Solid tumors will not grow beyond 3 – 4 mm in diameter without building up their own blood supply. The establishment of tumor blood vessels is also essential for cancer metastasis [7, 16, 30]. Anti-angiogenesis, mono-therapy or in-combination with other therapeutic agents, represents a very promising approach for cancer treatment (reviewed in [314, 315]). Successes have been achieved, such as bevacizumab (avastin, Roche), a FDA approved anti-angiogenesis drug [28, 137]. However, clinical studies have revealed that the cancer patient survival benefits of anti-angiogenic drugs have thus far been insignificant (reviewed in [316]). In addition, most studies in development of anti-angiogenesis agents have been mainly focused on strategies of blocking vascular endothelial cell growth factor and its receptor (VEGF/VEGFR) signaling or other receptor tyrosine kinase (RTK) pathways that play a role in promoting endothelial cell proliferation and migration (reviewed and investigated in [317-322]).

Studies have revealed a fine balance between endogenous pro-angiogenic factors, such as VEGF, FGF, PDGF, and endogenous angiogenesis inhibitors, such as many anti-angiogenic peptides generated from ECM (reviewed in [215, 323, 324]). Tipping the balance of pro-angiogenic and anti-angiogenic will have profound effects on tumor growth. Substantial efforts were made in attempting to harness the natural anti-angiogenesis activity to starve cancers. Many endogenous polypeptides, such as endostatin, angiostatin, platelet factor 4 (PF4), and thrombospondin, in blood circulation have been isolated and identified. Studies indicate that these endogenous anti-angiogenesis polypeptides play a critical role in controlling tumor angiogenesis that are vital for growth of primary tumors and metastases [223, 323, 325-327]. The detailed molecular mechanism by which these endogenous anti-angiogenic polypeptides exert their anti-angiogenesis activity is not well understood. It was noted that a common structure

moiety, a short anti-parallel β-sheet with certain amino acid sequence consensus, exists in most of these anti-angiogenesis polypeptides. It was revealed that anti-parallel β-sheet is critical for the anti-angiogenesis activity [281, 282]. Thus, efforts were made to use short peptides that would mimic the structure of the short anti-parallel β-sheet. Experiments demonstrate that the peptide mimics indeed has good anti-angiogenesis activity [281]. However, due to *in vivo* instability and pharmacological disadvantage, the peptide is not dose effective in the *in vivo* applications.

We employed an approach of rational protein design by integrating the short anti-parallel β-sheet forming amino acid sequences into a β-sheet region of a stable host protein, domain one of rat CD2 (CD2D1) (Figure 3.1). The engineered protein (named as ProAgio thereafter) was expressed in bacterial *E. coli. ,* and subsequently purified (Figure 3.S1A). The resulting protein exhibited structural properties very similar to that of the host protein CD2D1 as demonstrated by the 1D ^{1}H-NMR analyses (Figure 3.S1B). To increase protein solubility and blood circulation time, the designed ant-angiogenesis protein agent was site-specifically PEGylated using 20-kDa maleimide polyethylene glycol (PEG), a molecule with Y-shaped PEG chain (denoted as ProAgio-PEG), at an introduced cysteine residue (Figure 3.S1C).

To determine the effects of our developed protein agent on the endothelial cells, we carried out cell proliferation assays using the HUVEC cells. The cells were treated by various concentrations of developed protein, ProAgio, buffer, and the host protein, CD2D1. Bevacizumab, a FDA approved anti-angiogenesis drug, was also used in our test as a comparison. It was

clear that the ProAgio inhibits endothelial growth media (containing 3 μg/mL of bFGF and 10 of μg/mL EGF) induced HUVEC cell proliferation, whereas bevacizumab does not (Figure 3.1B). We further tested whether the effects were specific to endothelial cells. To this end, the same cell proliferation assays were carried out with HUVECs, endothelial cells and M4A1, an epithelial cell type the presence of 5 and 10 μM of ProAgio. It was clear that strong anti-proliferation effect was induced by the agent with HUVEC cells, while no effects were observed with M4A1 cells (Figure 3.1C). The observations indicated that the effects of ProAgio were endothelial cell specific. To further verify the *in vitro* anti-angiogenesis activity, we carried out the *in vitro* endothelial cell tube formation assay using HUVEC cells. It was evident that the ProAgio almost completely disrupted the endothelial tube formed by the PC3 and HUVEC co-culture formed tububles at concentration of 20 μM (Figure 3.1D).

We next asked whether the developed protein would have activity in inhibition of tumor growth in animal models of human cancer cells. To this end, we created a xenograft model of PC3 cells using immunodeficient mice. Tumor bearing mice were treated with various concentrations of ProAgio-PEG and PEGylated CD2D1 (CD2D1-PEG) (20 mg/kg), and buffer saline for 20 days via one dose per day (i.p. injection). The treatments were started when the tumor volumes reach 50 mm^3 (at the seventh day post tumor inoculation). It was clear that ProAgio-PEG inhibited the tumor growth almost completely at the dose of 20 mg/kg, while as controls did, the tumors grew at the normal rate in the mice treated with buffer saline and the PEGylated host proteins, CD2D1-PEG, at 20 mg/kg (Figure 3.2A). There was a clear dose dependent increase in tumor growth inhibition. However, the dose dependence became less dramatic after the dose

of 10 mg/kg. To further test the effectiveness of our developed protein agent, we carried out treatment experiments with the PC-3 xenograft using ProAgio-PEG and avastin bevacizumab side-by-side. We used 20 mg/kg i.p. (twice/weekly) for avastin and 10 mg/kg i.p. daily dose for the protein ProAgio-PEG with the same treatment scheme as above. The results demonstrated that the ProAgio-PEG was significantly more effective in inhibition of tumor growth than the avastin bevacizumab treatment course at the designed doses (Figure 3.2C). By the end of the treatment course, tumors in each treatment group were excised and weighed. There were substantial differences in the tumor weights of the ProAgio-PEG and PEGylated host protein treatment groups. There were also significant differences in tumor sizes between the ProAgio-PEG and avastin bevacizumab treatment groups (Figure 3.2B and D). To analyze the anti-angiogenesis effects of the treatment of the designed agent, we carried out Immunofluorescence (IF) staining of CD31, an endothelial marker, with the frozen tissue sections prepared from tumors that were collected at the end of each treatment course. IF staining (Table 3.1A) showing examples of staining slides demonstrated that the blood vessels were dramatically reduced (both in density and length). Statistical analyses of CD31 stains indicated that upon the treatment by ProAgio-PEG there were dramatic reductions in micro-vessel density (MVD), including branch points, and vessel lengths (Table 3.1). The ProAgio-PEG treatment led to a much large MVD reduction compared to that of avastin treatment group (Table 3.1B).

In principle, a good anti-angiogenesis agent should be less toxic to existing blood vessels in normal tissue/organs. To assess whether the designed protein disrupted the non-tumor blood vessels, we prepared tissue sections from liver, kidney, and spleen that were collected

from the mice that were treated by the different agents. The tissue sections were analyzed by hematoxylin and eosin (H&E) staining and immunostaining. HE staining revealed that there was no obvious abnormality in tissue anatomy structure, and no damage lesion/necrosis was observed (Figure 3.3A). IF staining using the anti-CD31 antibody suggested that there was no significant disruption and reduction of blood vessels in the liver, kidney, and spleen upon the treatments with ProAgio-PEG and avastin compared to those in the groups that were treated with the and PBS buffer saline. We further analyzed any possible cardiovascular damages upon the treatment with the designed agents. Hearts were excised at the end of the treatment course. The cardiac tissues were sectioned. The tissue sections were analyzed by either H&E staining or by IF staining using anti-CD31 antibody. The histology analyses indicated that there was no cardiovascular damage upon the treatment with the ProAgio-PEG as compared to those in the treatment groups with PEGylated CD2D1 and buffer saline (Figure 3.3B).

We have successfully developed an anti-angiogenesis agent by rational protein design. The *in vitro* and *in vivo* experiments demonstrate the effectiveness of our designed protein. The developed agent is not toxic to normal blood vessels and other tissue/organs, providing a promising potential for future clinical applications. Most current available anti-angiogenesis agents target VEGF/VEGFR or other RTK pathways. Such agents often cause unwanted biological side effects [328, 329]. In addition, many cancers are resistant to the inhibition of VEGF/VEGFR [330]. Our developed protein is one of a very few examples that do not act through targeting VEGF/VEGFR or any other RTK pathways. Importantly, our study provides an example of proof-of-concept to harness the natural anti-angiogenesis activity to starve cancers. In addition, our

study introduced a new strategy to integrate a small bio-active structural motif or an unstable short circulating peptide into a stable host protein. The resultant protein overcomes the major disadvantage of therapeutically peptides e.g. *in vivo* instability and unfavorable pharmacological properties. This concept can be extended to the design and development of other protein drugs. Our system certainly will create a new platform for design of therapeutic agents by *de novo* protein design.

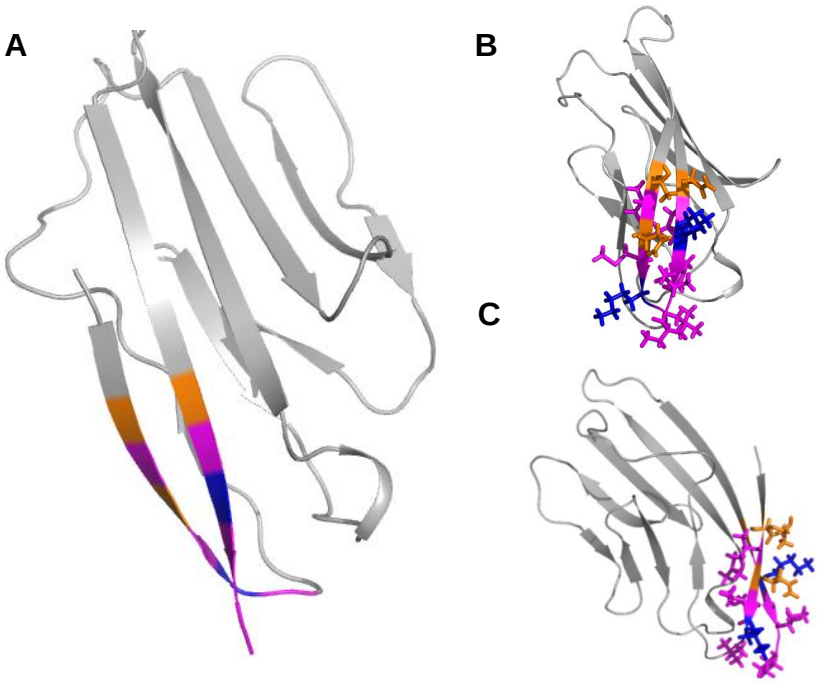

Figure 3.1 ProAgio is a *De Novo* Designed Anti-angiogenic Agent.

(A) Anti-angiogenic peptide sequences (TVQMKL and NLKVII) were de novo designed into the N- and C-terminal β-strands of CD2D1 separately. The homology model of ProAgio was built by a computer program, Modeller, using the X-ray crystal structure of CD2D1 (PDB accession ID, 1hng) as a template. Amino acids involved in anti-angiogenic function are color coded. **Orange** represents polar residues, **magenta** represents hydrophobic residues, and **blue** indicates positively-charged residues. (B and C) Different views of the ProAgio model structure.

Figure 3.S1 Molecular Cloning and Protein Generation

The anti-angiogenic peptides sequence (TVQMKL and NLKVII) were designed into the N- and C-terminal of CD2D1 separately. Mutations of W7Q, G8M, A9K, D94N, R96K, I97V, L98I, and E99I were created by replacing correspondent deoxyribonucleic acids in the cDNA sequence of D1-CD2 using a Site-directed® mutagenesis kit (Stratagene, Santa Clara, CA). The ProAgio cNDA was inserted into a pGEX-2T vector (GE lifesciences, Piscataway, NJ). The ProAgio protein was expressed with a glutathione (GST) tag fused into the N-terminal and purified by GS-4B column. Then the GST tag was removed from ProAgio via thrombin cleavage, and the protein was further purified by size-exclusion column (Fig. S1A). ^{1}H-NMR analysis showed that ProAgio has an anti-parallel β-sheet structure that is similar to that of CD2D1 (Fig. S1B). A cysteine mutation (M23C) was introduced into CD2D1 and ProAgio in order to site specifically PEGylate both proteins by conjugate a 20-kDa maleimide polyethylene glycol (PEG) to the cysteine site. The ProAgio-PEG and CD2D1-PEG were purified by cation exchange column (Fig. S1C).

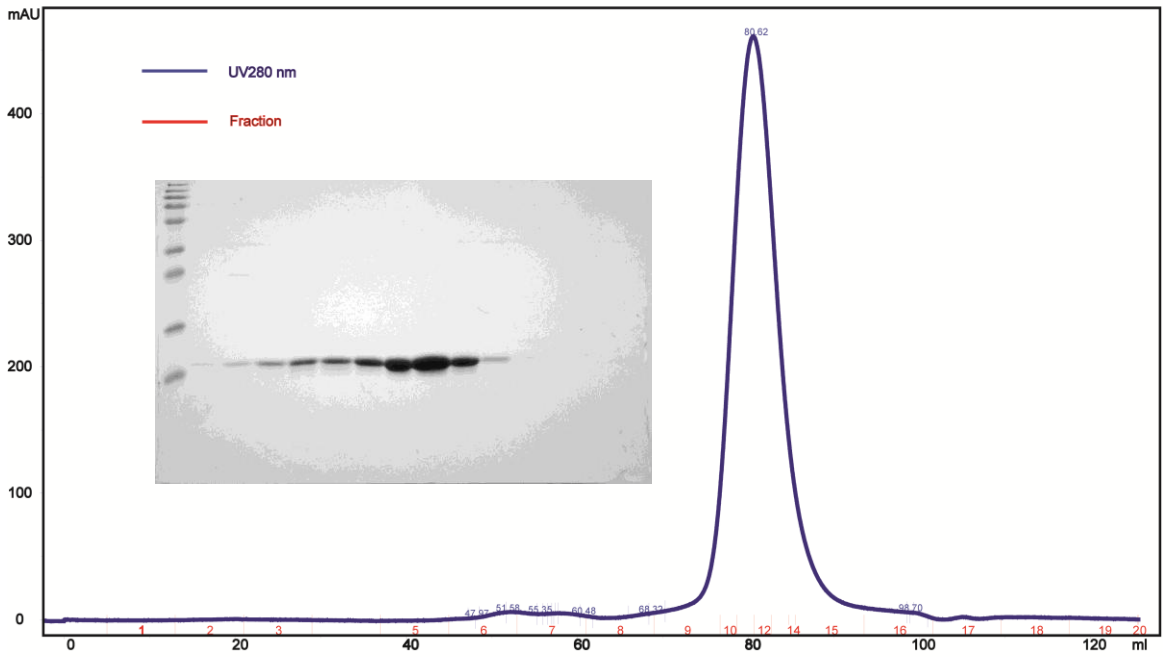

Figure 3.S1A Purification of ProAgio by Gel filtration chromatography. Gel filtration chromatography was performed using PBS buffer, pH 7.4 with a flow rate of 1 mL/min. ProAgio was eluted in the major peak composed of fraction 9 – 15. Insert figure: SDS gel electrophoresis of fraction 6 – 19.

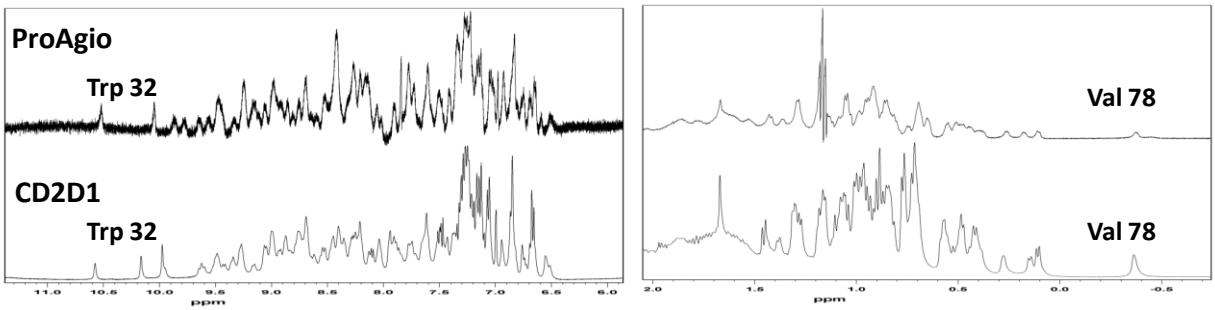

Figure 3.S1B Comparison between the 1D H^1-NMR Spectra of ProAgio and CD2D1. NMR samples were prepared by diluting proteins in 10 mM Tris-HCl with 10% D_2O at pH 7.4. Dioxane was used as an internal reference for the NMR spectra (3.743 ppm). All NMR spectra were recorded using Varian Inova 500 MHz and 600 MHz NMR spectrometers.

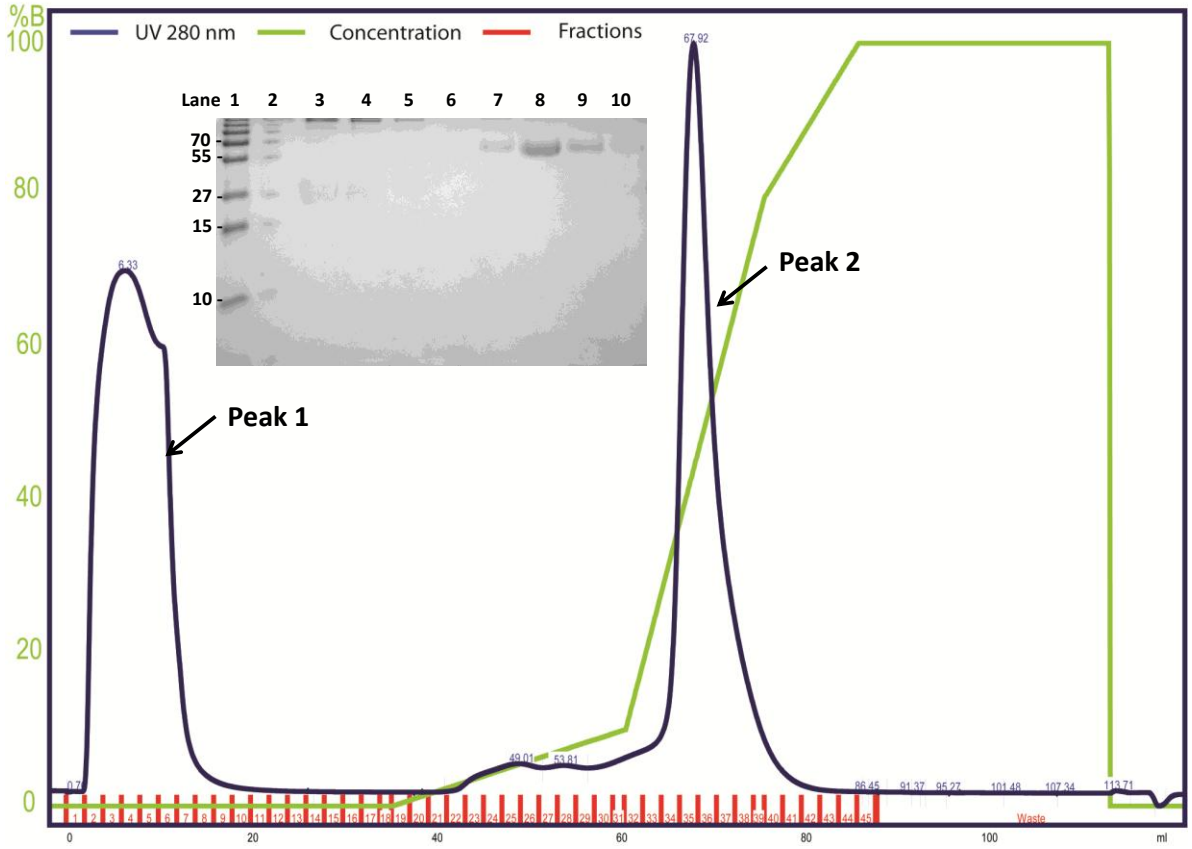

Figure 3.S1C Purification of ProAgio-PEG by Cation-exchange Chromatography.

Figure 3.S1C Purification of ProAgio-PEG by Cation-exchange Chromatography. PEGylated ProAgio (ProAgio-PEG) was purified using binding buffer (5 mM MES, pH 6.0) and elution buffer (5 mM MES, 1 M NaCl, pH 6.0). Two major UV-280 absorbance peaks (1 and 2) were observed in cation-exchange chromatography. Fractions from each peak were collected and analyzed by SDS electrophoresis and coomassie blue staining (insert picture). In the insert picture, Lane 1: pre-stained protein marker (Fermentas, Glen Burnie, MD), Lane 2 – 5: elution fraction 3 – 7 from peak 1, and Lane 7 – 10: elution fraction 25 – 28 from peak 2 containing ProAgio-PEG. In SDS gel, ProAgio-PEG migrated between 55- and 79-KDa molecular markers, which was slower than actual its actual molecular weight (31-kDa).

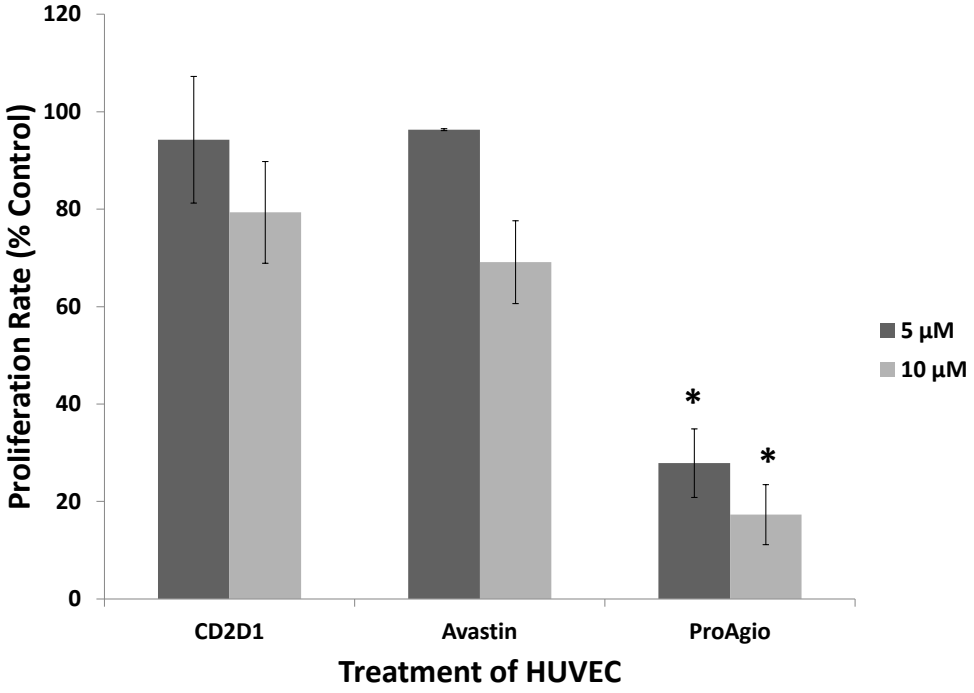

Figure 3.1B **ProAgio Inhibits EC Proliferation.** 4x10^4 cells/mL of HUVECs were seeded into a 96 well plates. Cells were allowed to attach for overnight, then treated with proteins at 5 or 10 µM for 48 hours. BrdU label was added to each well for 12 additional hours. Proliferation rates were measured under dual wavelengths of 450 – 540 nm. The experiment was repeated 3 times.

*: ProAgio (5 µM) versus CD2D1 (5 µM), and ProAgio (10 µM) versus CD2D1 (10 µM) showed statistically significant differences ($P < 0.001$, unpaired student's *t* test, two-tailed).

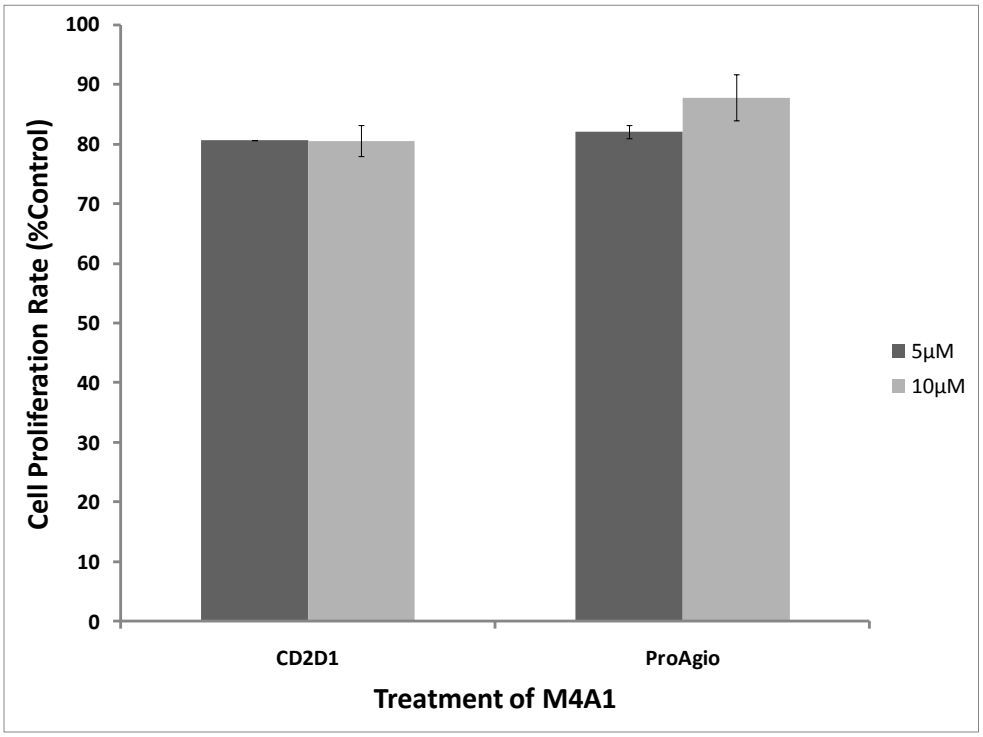

Figure 3.1C ProAgio has no Anti-proliferation Effects on M4A1 Cells. Cells were seeded into a 96 well plates at 4 – 1 X 10^5/ mL overnight in order to gain same confluence as HUVECs (Invitrogen, Grand Island, NY). Then cells were treated with proteins at 5 or 10 µM for 48 hours. BrdU label was added to each well for 12 additional hours. Proliferation rates were measured under dual wavelengths of 450 – 540 nm. The experiment was repeated 3 times.

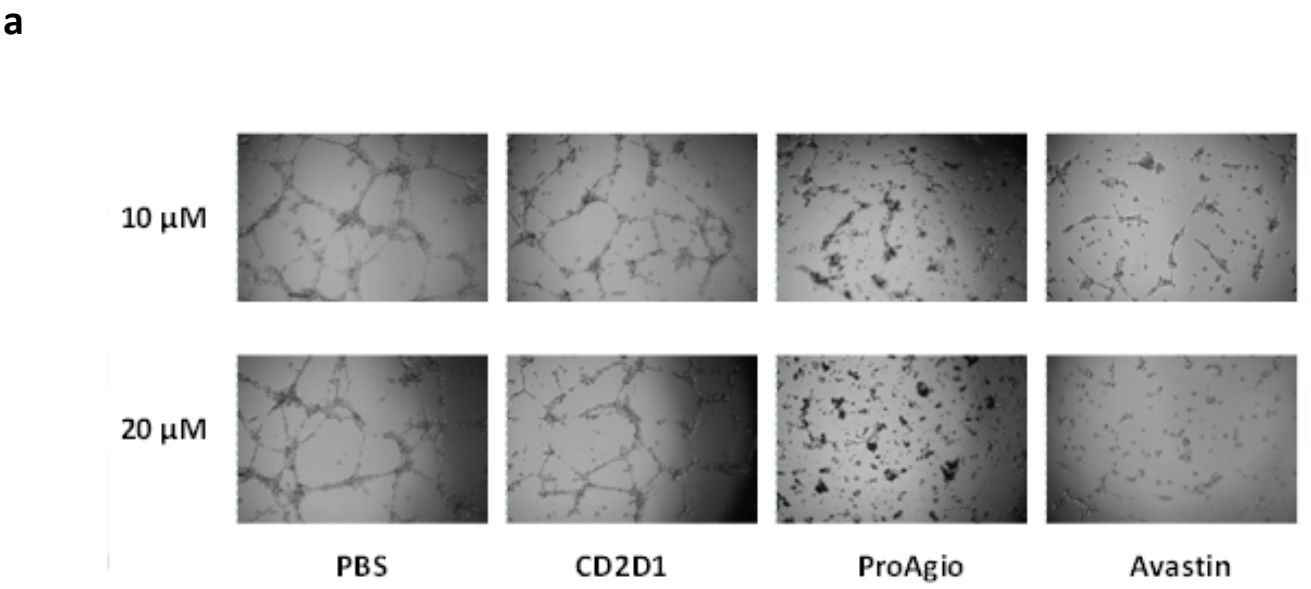

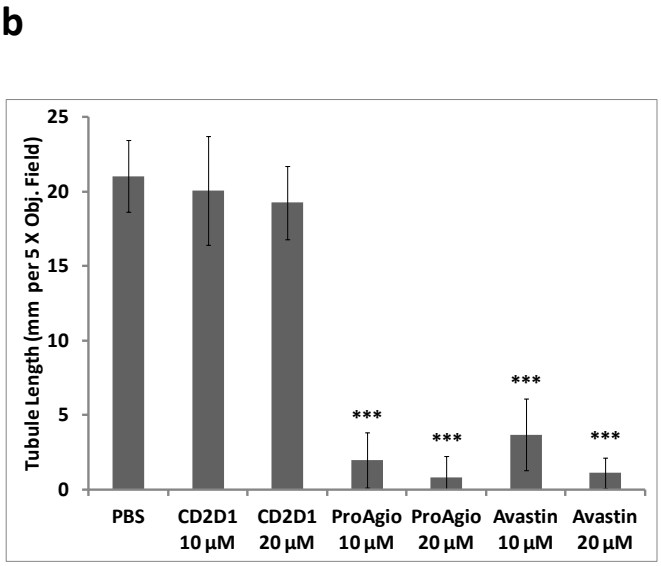

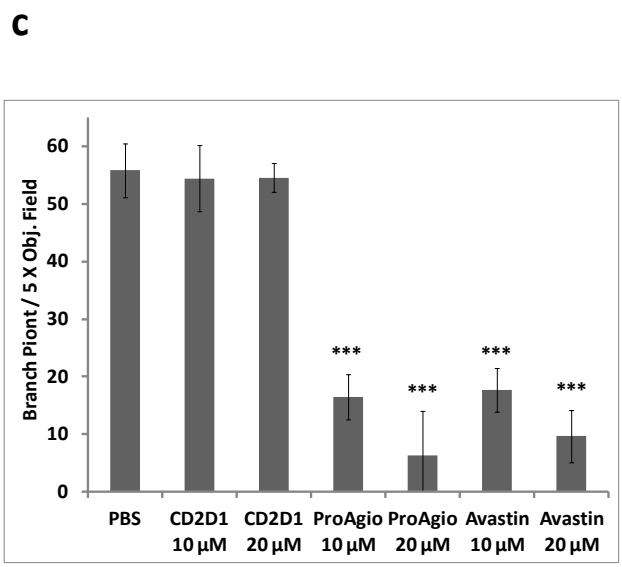

Figure 3.1D ProAgio Inhibits *In Vitro* HUVEC-PC3 Tube Formation.

Figure 3.1D ProAgio Inhibits *In Vitro* HUVEC-PC3 Tube Formation. (a): A total number of $1x10^4$ HUVEC cells and $1x10^4$ PC3 cells were seeded into a 96-well plate coated with 50 µl of matrigel (BD Biosciences, San Jose, CA) each well. Endothelial tubules were allowed to form at 37°C, 5% CO2 atmosphere. Formation of endothelial tubules was observed from 6-8 hours. Pictures were taken using 10 x ocular and 5 x objective (Obj.) lenses. A typical picture from each treatment group was shown in upper figures. (**b):** Tubule lengths (mm/5 x Obj. field) were measured using ImageJ (NIH, Bethesda, MD) (the lower left panel). (**c):** Numbers of branch point/5 x Obj. field were manually counted (the lower right panel). The experiment was repeated 3 times. Data was shown as mean ± S.D..

*******: $P < 0.001$, unpaired student's *t* test, two-tailed (experimental group versus PBS buffer control group).

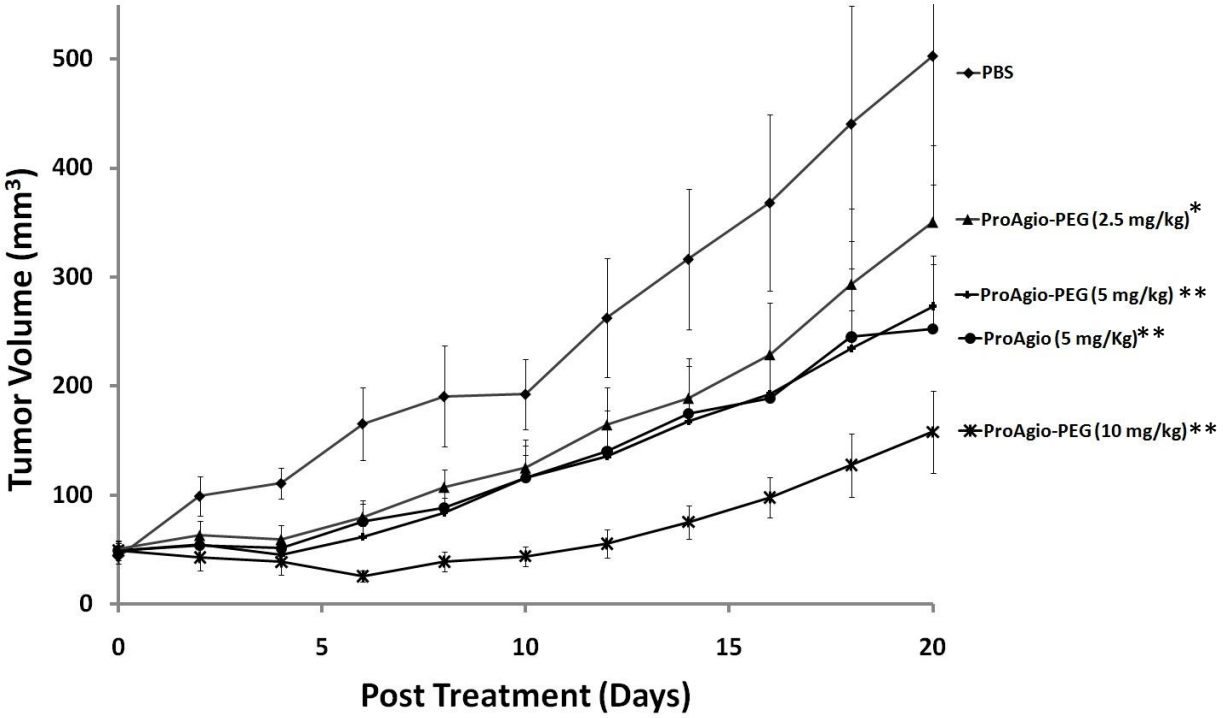

Figure 3.2A ProAgio Blocks Growth of PC3 Xenografts in a Dose-dependent Manner.

Figure 3.2A ProAgio Blocks Growth of PC3 Xenografts in a Dose-dependent Manner. A volume of 100 µl ($5X10^6$) PC3 cells were subcutaneously injected into nude mice. Treatments were initiated when the xenografts were clearly established and had reached a volume of 50 – 100 mm^3. All reagents were administered by intraperitoneal injection (i.p.) at desired doses (buffer: 1 X PBS; ProAgio: 5 mg/kg/day; ProAgio-PEG: 2.5 – 20 mg/kg/day). Tumor dimensions were measured every other day. Tumor volume were calculated using formula: Tumor volume (mm^3) = $\pi/6$ x (length x width x width). Statistic significances were evaluated using Welch's *t* tests. $P < 0.05$ was considered significant (n = 6 for each group).

*: ProAgio-PEG (2.5 mg/kg/day) versus Buffer treated group was not significantly different, $P > 0.05$.

**: ProAgio (5 mg/kg/day) versus buffer treated, ProAgio-PEG (5 mg/kg/day), and ProAgio-PEG (10mg/kg/day) versus buffer treated group were significantly different, $P < 0.05$.

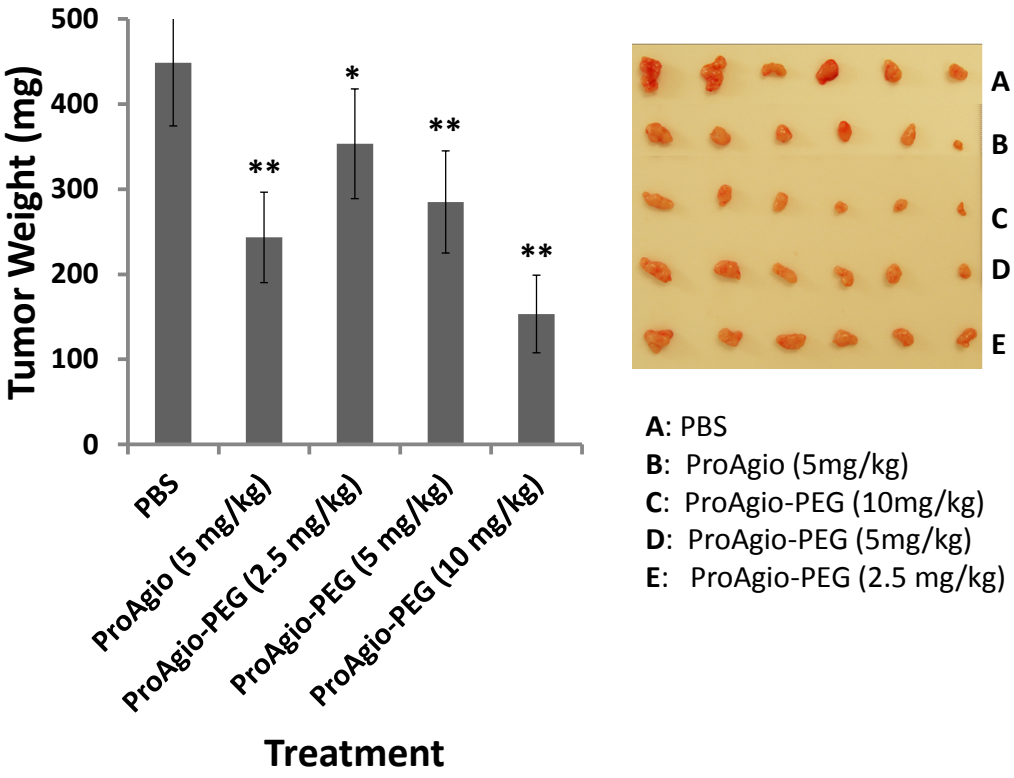

Figure 3.2B ProAgio-PEG Reduces End-point Tumor Weights.

Figure 3.2B ProAgio-PEG Reduces End-point Tumor Weights. A volume of 100 µL ($5X10^6$) PC3 cells were subcutaneously injected into nude mice. Treatments were initiated when the xenografts were clearly established and had reached a volume of 50–100 mm^3. All reagents were administered by intra-peritoneal injection (i.p.) at desired doses (buffer: 1 X PBS; ProAgio: 5mg/kg/day; ProAgio-PEG: 2.5 – 20 mg/kg/day). Tumor from each mouse was dissected in the last day of treatment and weighed by a digital balance. Tumor dimensions were measured every other day. Tumor volume were calculated using for-mula: Tumor volume (mm^3) = $\pi/6$ x (length x width x width). Statistic significances between groups were evaluated using ANOVA one way test (n = 6). $P < 0.05$ was considered significant.

*: ProAgio-PEG (2.5 mg/kg/day) versus Buffer- treated group was not significantly different, $P > 0.05$.

**: ProAgio (5 mg/kg/day) versus buffer treated, ProAgio-PEG (5 mg/kg/day), and ProAgio-PEG (10mg/kg/day) versus buffer-treated group were significantly different, $P < 0.05$.

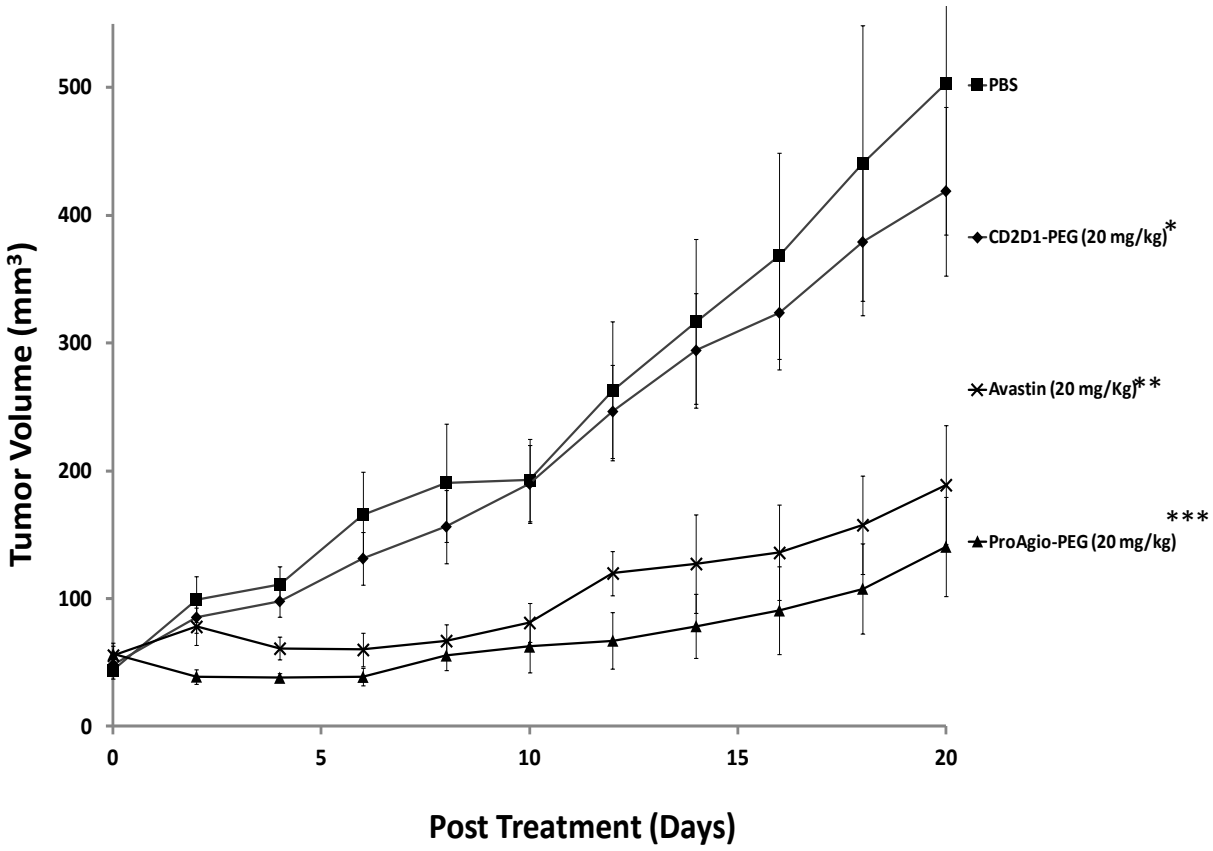

Figure 3.2C Comparison between ProAgio-PEG and Avastin Treated PC3 Xenografts.

Figure 3.2C Comparison between ProAgio-PEG and Avastin Treated PC3 Xenografts. Human PC3 cells were subcutaneously injected into nude mice. Treatments were initiated when the xenografts were clearly established and had reached a volume of 50–100 mm^3. All reagents were administered by intraperitoneal injection (i.p.) at desired doses (buffer: 1 X PBS, pH 7.4, 200 µL/day; ProAgio-PEG 20 mg/kg/day, CD2D1-PEG: 20 mg.kg/day; Avastin: 20 mg/kg/ twice weekly). Tumor from each mouse was dissected in the 20th day of treatment and weighed by a digital balance. Tumor dimensions were measured every other day. Tumor volume were calculated using formula: Tumor volume (mm^3) = $\pi/6$ x (length x width x width). Statistic significances between groups were evaluated using Welch's *t* test (n=6). $P < 0.05$ was considered significant. *: $P > 0.05$ for CD2D1-PEG (20 mg/kg/day) versus Buffer-treated group; **: $P < 0.05$ for avastin (20 mg/kg, twice weekly) versus buffer treated group; ***: $P < 0.001$ for ProAgio-PEG (20 mg/kg/day) versus buffer-treated group; and $P > 0.05$ for Avastin (20 mg/kg/ twice weekly) versus ProAgio-PEG (20mg/kg/day).

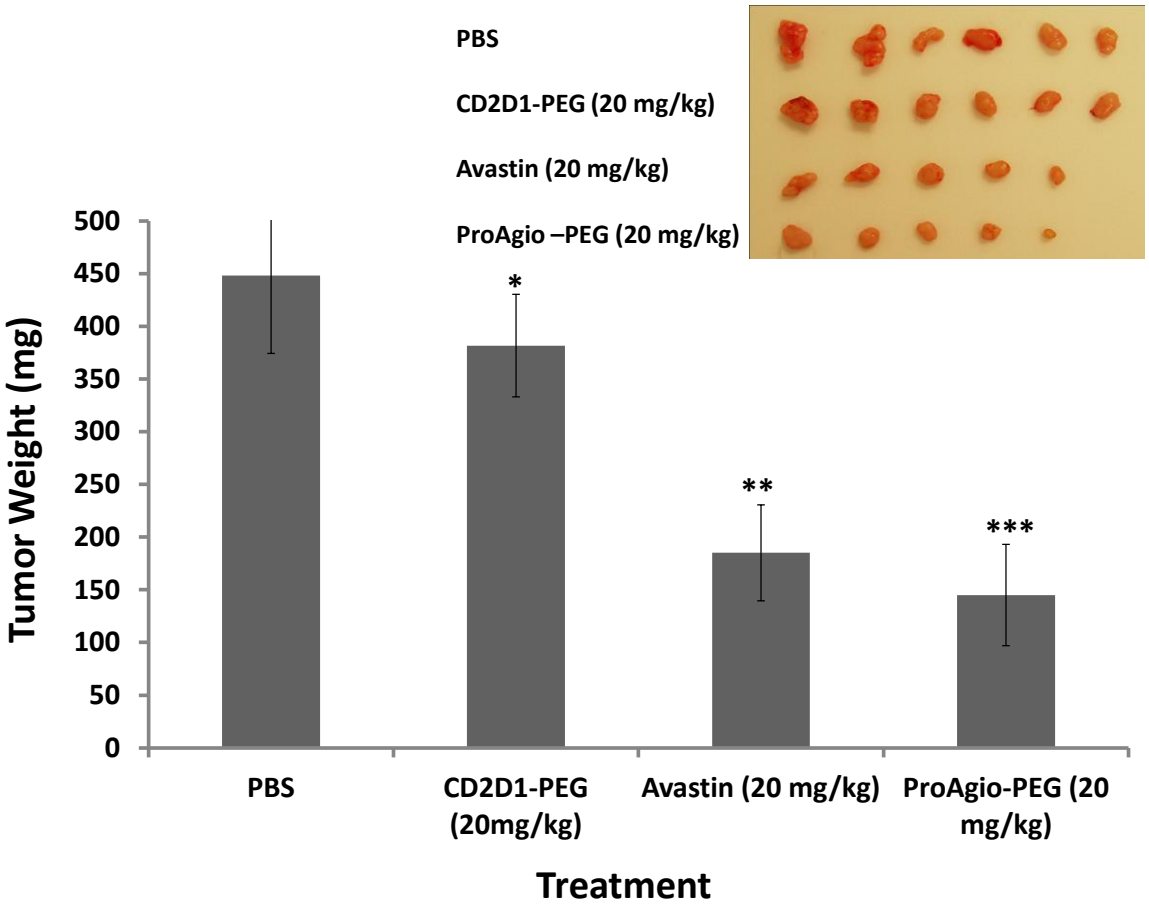

Figure 3.2D ProAgio-PEG and Avastin Reduces End-point Tumor Weights.

Figure 3.2D ProAgio-PEG and Avastin Reduces End-point Tumor Weights. A volume of 100 μL ($5X10^6$) PC3 cells were subcutaneously injected into Nude mice. Treatments were initiated when the xenografts were clearly established and had reached a volume of 50–100 mm^3. All reagents were administered for 20 days by intraperitoneal (i.p.) injection at desired doses (buffer: 1 X PBS; ProAgio-PEG 20 mg/kg/day, CD2D1-PEG: 20 mg.kg/day; Avastin: 20 mg/kg/twice weekly). Tumor from each mouse was dissected in 20th day of treatment and weighed by a digital balance. Statistic significances between groups were evaluated using ANOVA one way test. $P < 0.05$ was considered significant ($n = 6$ for each group).

*: $P > 0.05$ for CD2D1-PEG (20 mg/kg/day) versus Buffer treated group; **: $P < 0.05$ for Avastin (20 mg/kg/ twice weekly) versus buffer treated group; ***: $P < 0.01$ for ProAgio-PEG (20 mg/kg/day) versus the buffer treated group; and $P > 0.05$ for Avastin (20 mg/kg/twice weekly) versus ProAgio-PEG (20mg/kg/day).

Table 3.1A. MVD Comparison between ProAgio and ProAgio-PEG treated PC3 Xenografts.

	PBS	ProAgio (5mg/kg)	ProAgio-PEG (2.5 mg/kg)	ProAgio-PEG (5 mg/kg)	ProAgio-PEG (10 m/kg)
***Vessel Length (μM)**	1326.59 ± 157.53	[b] 569.86 ± 64.67	[a] 1044.63 ±105.94	[a] 548.57 ± 69.0	[b] 441.29 ± 80.8
****MVD**	15.83 ± 1.78	[a] 12.17 ± 1.75	[a] 16.93 ± 1.48	[C] 10.11 ± 1.06	[C] 8.5 ± 1.41
Branching Point	8.28 ± 1.98	[c] 1.39 ± 0.16	[a] 5.8 ± 1.28	[b] 2.78 ± 0.51	[C] 1.56 ± 0.44

Table 3.1A. MVD Comparison between ProAgio and and ProAgio-PEG Treated PC3 Xenografts.

Human PC3 xenograft-bearing nude mouse were treated for 20 days by intraperitoneal (i.p.) injection at desired doses (buffer: 1 X PBS; ProAgio-PEG 20 mg/kg/day, CD2D1-PEG: 20 mg.kg/day; Avastin: 20 mg/kg twice weekly). Snap frozen tumor tissue blocks were sliced into 10 µM thick sections using a cryostat. ECs were stained using a rat anti-mouse CD31 (BD Pharmingen, San Diego, CA) and a green fluorescence conjugated anti-rat IgG second antibody. After the highest vessel density within a section was determined under lower objective lens (5X), an area of 319.8 X 319.8 µM with the highest amount of vessels was scanned under a 20X objective lens and 10X ocular lens.

***Vessel Length:** the total number of vessels length within each of the image was measured using a Zeiss LSM image browser. Data were shown in µm/319.8 X 319.8 µm area.

****** Mean Vessel Density (MVD):** MVD were determined using methods described by Weidner and co-workers [330]. Briefly, any clear pattern of green fluorescent stained EC or EC cluster within the tumor tissue that separated from connective-tissues was counted as one vessel. Microvessels in sclerotic areas or adjacent to connective tissues were not considered.

a, b, c :Statistic significances were evaluated using unpaired Student's *t* test (two-tailed).). All values represented as mean ± S.E. (n=6 for each group). $P < 0.05$ was considered significant. a: $P > 0.05$, b: $P < 0.05$, and c: $P < 0.01$. All P values were compared between each treatment group versus buffer treated group.

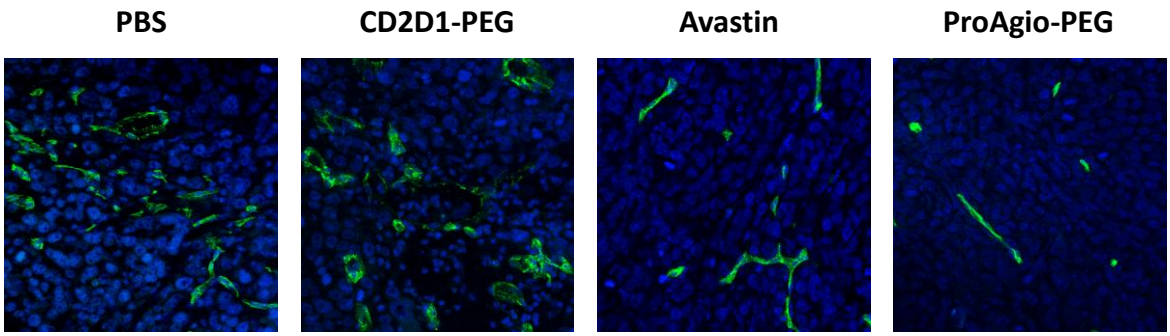

	PBS	CD2D1-PEG (20 mg/kg)	Avastin (20 mg/kg)	ProAgio-PEG (20 mg/kg)
*Vessel Length (µM)	1326.59 ± 157.53	[a] 1119.02 ± 169.84	[C] 545.61 ± 147.8	[C] 269 ±79.32
**MVD	15.83 ± 1.78	[a] 14.33 ± 1.22	[a] 8.44 ±2.10	[C] 5.50 ± 1.27
Branching Point	8.28 ± 1.98	[a] 8.05 ± 1.72	[b] 2.2 ± 0.91	[C] 0.44 ± 0.16

Table 3.1B MVD Comparison between ProAgio and Avastin Treated PC3 Xenografts.

Table 3.1B MVD Comparison between ProAgio and Avastin Treated PC3 Xenografts. Human PC-3 xenograft-bearing nude mouse were treated for 20 days by intraperitoneal (i.p.) injection at desired doses (buffer: 1 X PBS; ProAgio-PEG 20 mg/kg/day, CD2D1-PEG: 20 mg/kg/day; Avastin: 20 mg/kg /twice weekly). Snap frozen tumor tissue blocks were sliced into 10 µM thick sections using a cryostat. ECs were stained using a rat anti-mouse CD31 (BD Pharmingen, San Diego, CA) and a green fluorescence conjugated anti-rat IgG second antibody. After the highest vessel density within a section was determined under lower objective lens (5X), an area of 319.8 X 319.8 µm with the highest amount of vessels was scanned under a 20X objective lens and 10X ocular lens. The upper panel showed CD31 IF staining images of PBS, CD2D1-PEG, ProAgio-PEG and avastin treated tumor tissue. Each picture represented mean vessel count (MCV) for each treated group. CD31 was labeled with **green** fluorescence. Nucleus was labeled with DAPI and showed in **blue** color).

***Vessel Length:** the total number of vessels length within each of the image was measured using a Zeiss LSM image browser. Data were shown in µm/319.8 X 319.8 µm area.

**** Mean Vessel Density (MVD):** MVD were determined using methods described by Weidner and co-workers [313]. Briefly, any clear pattern of green fluorescent stained EC or EC cluster within the tumor tissue that separated from connective-tissues was counted as one vessel. Microvessels in sclerotic areas or adjacent to connective tissues were not considered.

a, b, c :Statistic significances were evaluated using unpaired Student's *t* test (two-tailed). All values represented as mean ± S.E. (n=6 for each group). $P < 0.05$ was considered significant. a: $P > 0.05$, b: $P < 0.05$, and c: $P < 0.01$.

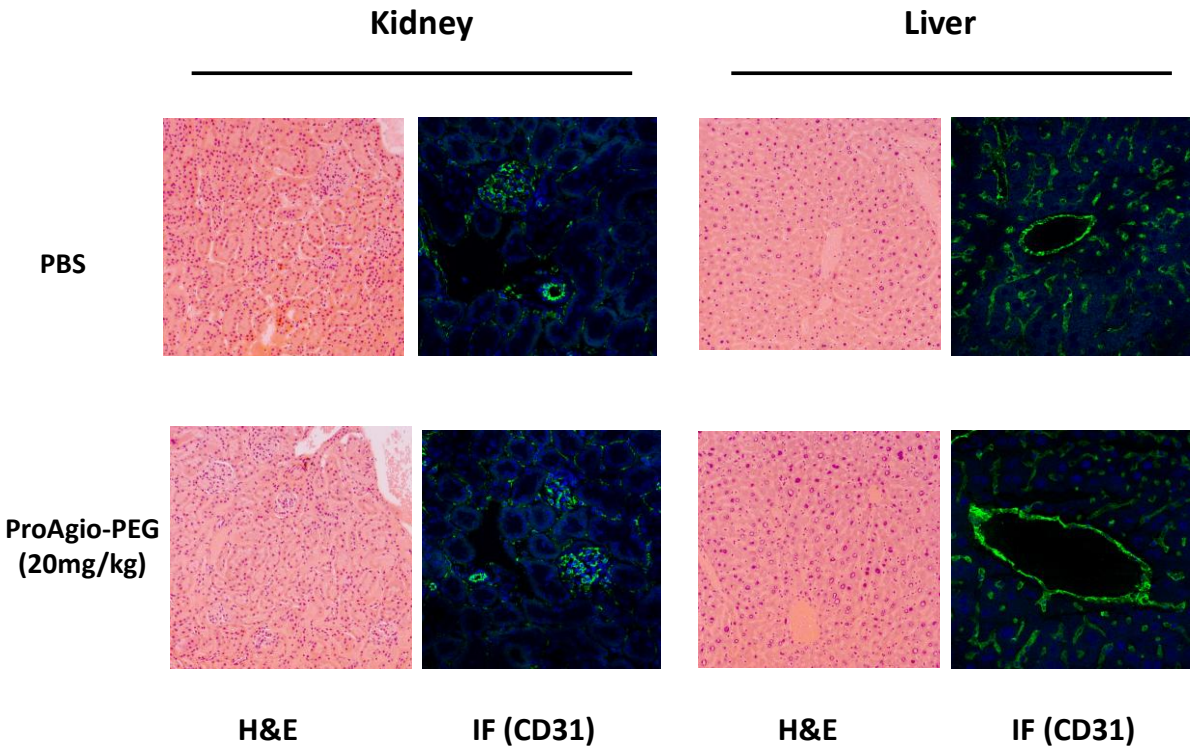

Figure 3.3A ProAgio-PEG has No Organ Toxicities. One set of organs from each mouse were fixed in 4% paraformaldehyde/PBS solution. Hematoxylin and eosin (H&E) staining of these fixed organs was processed in a pathology laboratory at the department of Ophthalmology and Pathology at Emory University. Pathological examinations were performed by Dr. Hans Grossniklaus. Vessel staining was performed using CD31 IF staining (CD31 labeled with green fluorescence, nucleus labeled with DAPI and showed in blue color).

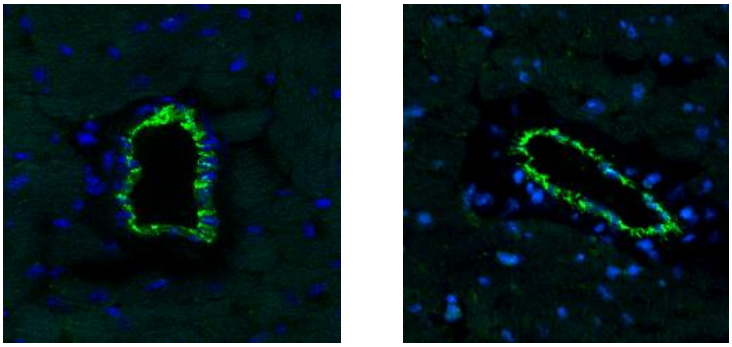

PBS

ProAgio-PEG
(20 mg/kg)

Figure 3.3B ProAgio-PEG does not Disrupt Normal Organ Blood Vessels. Snap frozen tissue blocks were sliced into 10 µM thick sections using a cryostat. ECs were stained using a rat anti-mouse CD31 (BD Pharmingen) and a green fluorescence conjugated anti-rat IgG second antibody. This picture showed the EC pattern (labeled in **green** fluorescence) of microvessels in PBS and ProAgio-PEG (20mg/kg) treated heart tissues. Nucleus were labeled with DAPI and showed in **blue** color.

CHAPTER 4

HUMANIZATION OF ProAgio

4.1 Introduction

4.1.1 Humanization of ProAgio

Humanization of ProAgio is aiming to aid potential clinical applications of the designed protein agent. As introduced in chapter 1, the initial design of ProAgio is based on the 99-amino-acid CD2D1 from rat. The advantage of using the rat protein instead of the human CD2 is largely due to concerns on protein stability. Decades of structure studies have been done using the CD2D1 from rat as discussed in chapter 1. The typical two-layered anti-parallel β-sheet sandwich folding conveys incredible structure stability, allowing the protein to withhold a wide of range of pH variation and sequence mutations [291]. In addition, rat CD2D1 is able to be expressed in bacterial *E. coli* systems with a high protein yield with well-folded 3D structure. In contrast, the human CD2 (denoted as huCD2 in this chapter) requires an N-linked glycosylation in its domain 1 region to stabilize its folding, so that the protein expression of huCD2 in a laboratory level has been problematic. Similar strategies have been widely adopted in producing antibody drugs, for example in the case of bevacizumab. Humanization, however, is necessary for our designed ProAgio to be applied to clinical therapies with minimal immunological responses.

In this chapter, the similarity between the domain 1 of rat CD2 and huCD2, applied strategies for re-design of rat ProAgio into the human host protein, preliminary data using *in vitro* and *in vivo* models will be discussed. The designed ProAgio using the human host protein is named as huProAgio.

4.1.2 Biological Functions of huCD2

The human homologue of rat CD2, huCD2, is a 50 – 55-kDa transmembrane glycoprotein receptor mainly expressed in T lymphocytes and NK cells [331]. In 1980s, the cell adhesion function of huCD2 was first identified when anti-CD2 antibody disrupted the T lymphocyte aggregation with sheep red blood cells (SRBC), a phenomenon is known as “rosette” [291]. Rosetting with SRBC had been widely accepted as a marker to identify T lymphocytes in 1970s. Later on studies have shown that huCD2 specifically recognizes CD58 expressed on the surface of antigen-presenting cells (APC) and functions as a co-receptor to TCR during the major histocompatibility complex (MHC)-mediated antigen recognition process [332]. Therefore, huCD2 plays a role in initiating cellular immune responses. Except for its adhesion function, huCD2 has also been indicated in signaling transduction. Hünig and colleagues have demonstrated that huCD2 serves as an alternative activation signaling molecule to T lymphocytes [333]. This activation is usually accompanied with the subsequent release of IL-12 by T lymphocytes, and it is suggested that cytoplasmic tail part of huCD2 is required for transduction of the stimuli [334].

4.1.3 Comparison of the Domain 1 of huCD2 and Rat CD2

The cell adhesion function of huCD2 is located in the domain 1 of its extracellular region [335]. Withka and coworkers reported the 3D structure of the 105-amino-acid adhesion domain of huCD2D1 ($huCD2_{1-105}$) calculated from 2D homonuclear NMR data in 1993 [302]. The $huCD2_{1-105}$ protein folds into a typical Ig-folding that is very similar to its rat homologue [302]. Basically, there are total 9 anti-parallel β-sheet strands (named as A, B, C, C’, C’’, D, E, F, and G separately) connected by flexible loop regions. Anti-parallel strands (G, F, C’’, C’, C, and E) are

leveled in one layer, whereas the other three strands (B, D, and E) compose a second layer of β-sheet on the opposite side [302]. The A β-strand is next to strand G, and they are parallel to each other. In the middle of these two layers, a hydrophobic core is constituted by a serial of conserved hydrophobic residues from both layers. The ligand binding region is involved in strands G, F, C and C'', while a glycosylation at Asn65 on the opposite layer of β-sheets is required for its folding and structural stability [336].

Detailed protein sequence alignments between human and rat CD2 are shown in Table 4.1. The amino acid similarity between these two proteins is relatively low. A total number of 42 out 105 amino acids in huCD2$_{1-105}$ are same as those of rat CD2$_{1-99}$, which gives them a ~40% identity. Within these 42 identical amino acids, 22 of them are hydrophobic residues, especially those amino acids contributed to the hydrophobic core region. For example, amino acids Leu19, Tyr60, Leu68, and ILE70 located on the D, E, and B strands, and residues Trp35, Ala45, Phe47, and Tyr81 on the C, C' F, and G strands are identical to the correspondent amino acids in rat CD2$_{1-99}$.

Although their sequence identity is low, the 3D structure alignment between these two proteins is surprisingly high [300, 301]. Alignment of the crystal structures of rat CD2$_{1-99}$ (PDB accession ID, 1hng) and huCD2$_{1-105}$ (PDB accession ID, 1hnf) carried out using software program, Pymol, are shown as Figure 4.1A – C. It is notable that not only the backbone but also the side chain directions of each aligned amino acid are highly agreeable. The overlay 3D structure indicates that the N and C-terminal regions correspondent to the rat ProAgio anti-angiogenic region have similar side chain distribution. Side chains of Glu8, Trp10, and Ala12 on β-strand A, and those of Asp99, Lys101, and Gln 103 shown as red in Figure 4.1C are all facing toward the sur-

face of the protein. This feature is critical for humanization of rat ProAgio using the huCD2$_{1\text{-}105}$ as a host protein, especially when maintain the certain side chain direction is desired for the design of anti-angiogenic peptides.

4.2 Design of the huProAgio

4.2.1 Rational for Design of the huProAgio

Rational for design of huProAgio is based on our knowledge and experiences obtained from the successful design of rat ProAgio. The key of our rat ProAgio design greatly depends on the structural similarity between the domain 1 of rat CD2 and other endogenous anti-angiogenic proteins, such as PF4, TSP-1, and endostatin et al. As discussed above, the 3D structures of the domain 1 of rat and human CD2 are highly identical, so that changes in the same region of huCD2 are much likely to convey the same structural and biological effects.

Several facts have to be taken into consideration when design huProAgio using rat ProAgio as a reference. First, whether or not the chosen region for anti-angiogenic function will maintain the same side chain directions as rat ProAgio did. Second, factors that affect the protein stability such as the glycosylation and PEGylation should also be paid close attention to, so that protein production will be feasible. At last, since CD2 is an adhesion molecule, its ligand interaction should be abolished in order to avoid undesired side effects. Design strategies aiming to solve each of those concerns will be address one by one as follows.

4.2.2 Design of the Anti-angiogenic Regions in huProAgio

The host protein is the first 1 – 104 amino acids in of the human CD2 molecule (sequence is shown in Table 4.1). In order to differentiate this host protein from the tradition 1 – 105 amino acids domain 1 of human CD2, the host protein huCD2$_{1\text{-}104}$ will be denoted as huCD2D1 here after. This one amino acid change is less likely to bring out any structural alterations since Arg105 is located in the end of the C-terminal region of the protein, and has few NOE constrains.

The anti-angiogenic function of ProAgio relies on amino acids positioned from 5 – 10 in β-strand A and 94 – 99 in β-strand G as listed in Table 1.1. Those residues are aligned to amino acids 8 – 13 and 99 – 104 individually. There are total 12 amino acids in these two regions. Among them, only 4 are different residues. By calculation, it is 67% identical to the same region of rat CD2, a much higher rate compared with the overall 40% identity between the whole domain 1 regions of these two proteins. These comparison comparisons further supported the hypothesis to design the anti-angiogenic short sequences by mutating those particular amino acids. The anti-angiogenic sequences used to design huProAgio are similar as those of ProAgio, and they are SVQMKL and NLKVII. The N- and C-terminal sequences of original huCD2D1 and the designed huProAgio are listed as Table 4.2. As shown in the same table, mutations of Glu8Ser, Thr9Val, Trp10Gln, Gly11Met, Ala12Lys, Ile102Val, Gln103Ile, and Glu104Ile have to be made in order to create the desired anti-angiogenic sequences.

4.2.3 Glycosylation and PEGylation of huProAgio

Unlike rat CD2D1, the domain 1 of huCD2 is glycosylated at Asn65, and it is critical for the protein folding and stability [302, 336]. Due to this reason, purification of the domain 1 of huCD2 relies on two different expression systems, either using mammalian system such Chinese hamster ovary (CHO) cells or bacterial *E. coli.* cells. CHO cells will allow huCD2 to be expressed with a single N-linked high mannose glycosylation chain attached to Asn65 [302, 337]. Another widely adopted method is to express the domain 1 of huCD2 in *E. coli* systems without the N-linked glycan. Although enzymes required to make this post-translational modification are absent in *E. coli* cells, mutations are necessary to be made in order to obtain a stable expression and folded protein. In this study, three mutations (Lys61Glu, Phe63Leu, and Thr67Ala) are introduced to facilitate expression and purification using *E. coli* cells [338].

As discussed in Chapter 3 and 5, a site-specific PEGylation of ProAgio is via a mutation, Met23Cys. Residue Met23 in rat CD2 is aligned to Met26 in human CD2, so that mutation of Met26Cys is also introduced into the huProAgio protein sequence for the same purpose. Same as Met23 in rat CD2, Met26 in human CD2 is also located in the flexible loop region and exposed to the solvent as referred to the PDB file, 1hnf [300]. Since ProAgio can be successfully PEGylated, it is presumed to be able to be modified by maleimide PEG in the same manner.

4.2.4 Abolish the Ligand Recognition between CD2-CD58

The nature ligand of huCD2 has been proven to be the CD58 molecule (also known as LFA-3, lymphocyte function-associated antigen 3) [332, 339]. The CD2-CD58 interaction has been well studied [338, 340]. The affinity between these two cell surface adhesion molecules

was reported at 1 – 10 μM range with fast K_{on} (association) and K_{off} (dissociation) rates, which suggest that huCD2 binds to CD58 at a relatively low affinity, but the binding is very dynamic manner [341]. The human CD2 also reported to binds to other ligands, such as CD48 and CD59, in a very low affinity with a Kd value ranged around 0.5 mM [341, 342]. To this end, only the CD2-CD58 interaction is consider in this project to abolish the biological functions of CD2.

Our strategy to abolish the biological functions of huCD2 is set by introducing mutation(s) in the ligand binding surface that will disrupt the CD2-CD58 interaction. The binding surface between CD2 and CD58 was investigated by Wang et al [338]. Several pairs of amino acids on the interface are critical for CD2-CD58 interaction by forming hydrogen bonds and charge-charged interactions. A detailed summary of each amino acids involved in the counter interaction is listed in their paper. Briefly, Lys43, Tyr86, Asp32, Arg48, Lys51, and Lys34 of huCD2 are among the most essential residues that contribute to the binding. Generally, the least amount of mutations helps to avoid structural mis-foldings, so that we intended to choose a single mutation that effectively abolishes the CD2-CD58 interaction while brings minimal affects to structural integrity. First of all, Kim et al produced a serial of huCD2 mutants with each of them harboring one alanine substitution to each interface residues [340]. Secondly, as demonstrated by their studies, a single Tyr86Ala mutation totally disabled the CD2-CD58 interaction indicated by rosetting and binding assays [340]. Thirdly, ^{1}H NMR spectra of this Tyr86Ala mutant indicates a similar 2D folding to that of the wild type protein. These facts determined that Tyr86Ala mutation is a suitable candidate in order to evade the biological consequences of the host protein, huCD2D1.

4.3 Protein Sequence of the Designed huProAgio

The complete protein sequence of the designed huProAgio is shown as Figure 4.2. This protein is intended to be expressed and purified from *E. coli* expression systems without the N-linked glycan chain. Several mutations for individual purposes discussed through this chapter 4.1 are summarized as follows. First, As listed in Table 4.1, mutations of Glu8Ser, Thr9Val, Trp10Gln, Gly11Met, Ala12Lys, Ile102Val, Gln103Ile, and Glu104Ile are introduced in order to create the desired anti-angiogenic sequences (SVQMKL and NLKVII) at positions 5 – 10 in β-strand A, and 94 – 99 in β-strand G in the host protein. Second, three amino acids mutations (Lys61Glu, Phe63Leu, and Thr67Ala) will be made so that the designed huProAgio could be expressed in *E. coli* cells the in non-glycosylated form. Third, an amino acid mutation (Tyr86Ala) will abolish the interaction between huCD2D1 and CD258 [340]. At last, an amino acid mutation (Met26Cys) will allow huProAgio to be site-specifically PEGylated in Cys26 for elongation of blood circulation retention time, increase in protein solubility, and possible improvement of protein stability.

The high mannose N-glycan linked to the domain 1 of huCD2 has been demonstrated to not only facilitate its folding but also stabilize the 3D structure [336]. Although the glycosylated $huCD2_{1\text{-}105}$ has been produced in mammalian CHO cells, the cost of this method is high compared to alternative expression systems such as yeast. An additional model was designed for expression huProAgio in the *pichia pastoris*, and it complete amino-acid sequence was shown in Figure 4.3. In this model, except for Lys61, Phe63, and Thr67 were kept so that Asn65 can be modified with N-glycan, all other mutations are same as that of the designed model for the bacterial system shown as Figure 4.2. Yeast *pichia pastoris* system, if properly optimized, is a su-

preme choice for expression of human recombinant proteins. With an additional secretion signals, proteins are secreted, which greatly accelerates purification processes [343]. In addition, protein yield is much higher compared to using *E. coli* and mammalian expressions. For example, protein yield of human serum albumin using *pichia pastoris* expression could reach as high as 3.6g/L, while the yield of non-glycosylated huCD2$_{1\text{-}105}$ in *E. coli* cells was reported at 15 mg/L [338, 343].

4.4 3D Structure of the designed huProAgio

Figure 4.1 illustrated the designed model structure of huProAgio built by a computer program (Modeller) using the X-ray crystal structure of huCD2 (PDB accession ID, 1hng). Anti-angiogenic sequences (SVQMKL and NLKVII) are introduced at amino acid positions 5 – 10 in β-strand A, and 94 – 99 in β-strand G in the host protein. The predicted structure is highly agreeable with the crystal structure of human CD2$_{1\text{-}105}$ [300]. The β-strand A and G parallel pairs next to each other. Since strand G also has side chain interactions with strand F and G, the designed anti-angiogenic short peptides will be restrained as a β-sheet structure. The simulated 3D structure also predicts that side chains of Ser8 pairs with Asn99, Glu10 pairs with Lys101, and their side chains are facing toward the protein surface. Lys12 in the end of β-strand A and Ile104 forms interactions, and their side chains are expected to be at the same level of that of Ser-Asn99 and Glu-Lys101.

The designed mutation site (Met26Cys) for site-specific PEGylation is designed at the long BC loop region. It side chain is expected to be well solvent-exposed, which will increase the PEGylation rate. In addition, the BC loop are on the at opposite direction to where the anti-

angiogenic short peptides are located, so that PEG chain linked to Cys28 is less likely to affect the designed anti-angiogenic function. Other mutations, such as Lys61Glu, Phe63Leu, and Thr67Ala for abolishing N-glycosylation, Tyr86A for evading CD2-CD58 interaction are mutation sites that are well studied, and their correspondent mutants were expressed as folded proteins [338, 340]. For those reasons, these additional mutations are expected to bring minimal affects to the structure stability of ProAgio.

4.5 Preliminary Data for HuProAgio

4.5.1 Optimization of cDAN Sequences for Expression

The cDNAs coding for huProAgio designed for *E. coli* and yeast *pichia pastoris* were synthesized by Epoch Life Science, INC at Missouri City, TX. Codons were optimized for expression in *E. coli* and yeast expression systems by Epoch Life Science using their proprietary software. Several strategies were used to create optimized codons for each species. As shown in Figure 4.5, when aligned by online program, LALIGN, the optimized cDNA sequences of huCD2D1 and that of huProAgio aiming for *E. coli* expression have 78.5% identity and 85.9% similarity. Figure 4.6 showed that the cDNA sequences of human versus that of the yeast expression optimized huProAgio have slightly less identity, 79.1%. These two different cDNAs are expected to improve the huProAgio expressions in *E. coli* or yeast cells. The synthesized huProAgio cDNA were further cloned to a bacteria expression vector, pET30a (Novagen, Madison, WI) and expressed in bacterial BL-21(DE3) cells (unpublished data by R. Chakram). Figure 4.7 indicated that both huCD2D1 and huProAgio had high level of protein expression.

4.5.2 Refolding and Buffer Selection

The bacterial expressed huProAgio (named as his-huProAgio) tagged with an N-terminal histidine hexamer designed for purification using Ni-NTA columns. Urea refolding of the expressed huProAgio from inclusion bodies produced proteins with limited stability. According to different buffer recipes tested by Ravi Turaga in our lab, under neutral pH condition (pH 7.4), the refolded protein precipitated in the presences of a variety compounds, such as 10 – 20 % glycerol, 0.5 – 1 M arginine, 1% N-laurycyl sarcosine. The same set of experiments also indicated that his-tag huProAgio was soluble under pH higher than 10. These results prompted us to examine the possibility of refolding huProAgio by gradually decreasing pH instead of urea concentrations. In addition, our previous experience with rat ProAgio showed that a buffer containing a combination of glycine and arginine might increase protein solubility (Table 5.2). Taken these two concerns together, a buffer recipe consisted of 5 mM Tris, 50 mM arginine, 50 mM glycine, 150 mM NaCl and 2 mM DTT was designed as a basal buffer for pH refolding of huProAgio. A low concentration of Tris (5 mM) with 150 mM NaCl was used with expections to bring minimal side effects when the protein is injected into nude mice.

A batch of huProAgio protein resuspended in 0.5 M arginine, pH 10.8 was gradually dialyzed into buffers at pH 9.5, pH 8.5, and then to pH 7.5. All buffers are composed of the same basal recipe indicated as above with adjusted pH levels. The huProAgio protein was soluble under each step till pH 7.5. As shown in Figure 4.8, the protein concentration was around 40 μM. There was no difference in protein concentration between pH 8.5 and pH 7.5. A fraction of protein sample at pH 8.5 was tested for thrombin cleavage. Protein was incubated with 20 units of thrombins (GE lifesciences, Piscataway, NJ) for 2 hours at room temperature. The mixture was

then passed through a benzamidine Sepharose 6B (GE lifesciences, Piscataway, NJ) packed column 10 times to remove thrombin. Upon removal of his- tag, huProAgio did not show obvious precipitation but the final concentration was less than his-tagged form (28 μM compared to 44 μM).

This method was repeated with the same batch of protein. Results indicated as Figure 4.9 showed that his-huProAgio reached a maximum concentration of 100 μM. The protein showed obvious precipitation when concentrated beyond 100 μM. In this second experiment, the concentration after refolding was consistent with the previous one, 38 μM versus 44 μM. A similar recipe composed of 50 mM arginine, 50 mM glycine, and 2 mM DTT in PBS buffer (pH 8.0) was selected for purification of his-tagged huProAgio proteins that were applied for drug efficacy testing using PC3-Luc xenograft model.

4.5.3 Evaluation of the *In Vitro* Effect of His-huProAgio

Above refolded his-huProAgio was subjected to in vitro testing using HUVECs. Proliferation rates were shown in Figure 4.10. At 10 μM concentration, his-huProAgio exhibited higher anti-proliferation rate compared to ProAgio. A 96% reduction in proliferation rate was observed compared to buffer treated controls. At higher concentration, however, proliferation rate was inhibited by 32% compared to 73% of ProAgio treated group. This result not only suggested that the bacterial expressed huProAgio has comparable *in vitro* anti-angiogenesis effect as ProAgio but also demonstrated that our humanization strategy was successful. The reason why his-huProAgio dropped inhibitive effects at lower concentration is worth investigating. It might suggest that his-tag interferes with the secondary structure of his-ProAgio.

4.5.4 Evaluation of the *In Vivo* Effect of huProAgio

The in vivo effect of huProAgio was evaluated using the same PC3 xenograft model as did with ProAgio. Purified huProAgio was soluble up to 100 μM in buffer conditions indicated as above: 50 mM arginine, 50 mM glycine, and 2 mM DTT in PBS buffer (pH 8.0). The experiment was initiated when volumes of tumor implants reached 50 – 100 mm^3, the 5^{th} day in this case. A total of 16 doses of buffer control, 10 mg/kg/day of endostar and huProAgio were administrated via i.p. injection.

As shown in Figure 4.11, huProAgio demonstrated significant anti-tumor effect over the treatment course. The average tumor volume of huProAgio treated group was significantly reduced during the first week of treatment. HuProAgio slowed down tumor growth by 6 days. At the end of treatment, the average end tumor volume was 263.74 and 109.92 mm^3 for buffer and huProAgio group separately, which indicated a 59.3% reduction rate ($t = 3.53$, $P = 0.0054$, unpaired student's *t* test, two-tailed) in tumor volume comparing the huProAgio treated group to the buffer control. Since the starting tumor volumes were 80 mm^3 for both groups, buffer control group gained 2.2 times in tumor volume while there was 0.5 times increase in huProAgio treated group. Those measurements were further demonstrated by the end point tumor weights indicated in Figure 4.12. There was up to a 40% reduction rate ($t = 2.78$, $p = 0.02$, unpaired student's *t* test, two-tailed) in the end-point tumor mass when compared with huProAgio treated and buffer control groups.

The toxicities of his-huProAgio were monitored by observation of physical, behavior, and weight changes of each experimental mouse. No mice behaved abnormally. No sign of illness for each mouse until the end point treatment. Figure 4.13 indicated that there were no

body abnormal body weight changes during the whole course of treatment. These observations suggested that our designed huProAgio is not toxic, but the actual toxicities have to be demonstrated in further pre-clinical animal models.

4.6 Conclusion

In this chapter, a detailed design strategy of using human $CD2_{1-104}$ as a host protein was discussed. Although there is only 40% amino acid similarity between rat $CD2_{1-99}$ and human $CD2_{1-104}$, these two proteins are aligned well in 3D structures. Two *a*nti-angiogenic sequences (SVQMKL and NLKVII) were introduced at amino acid positions 5 – 10 in β-strand A, and 94 – 99 in β-strand G in human $CD2_{1-104}$. The predicted model structure was highly agreeable with the crystal structure of human $CD2_{1-105.}$ The designed his-huProAgio was expressed in bacteria and purified. Using i*n vitro* and *in vivo* xenograft models, it was demonstrated that his-huProAgio inhibited HUVECs proliferation and tumor growth. These results not only shed light on further clinical application of ProAgio, but also highlighted the significance of *de novo* protein design strategy as a novel approach for drug discovery and development.

Future challenges of huProAgio will include optimization of protein expression, solubility, formulation, and *in vivo* evaluation of pharmacological and pharmacokinetic properties of huProAgio.

Table 4.1 Comparison of Rat CD21-99 and huCD21-105

Rat $CD2_{1-99}$	$hCD2_{1-105}$	Side Chain Direction
D2	N5	N-Terminal
S3	A6	N-Terminal
G4	L7	Inside
*T5	*E8	Outside
*V6	*T9	Inside
***W7**	***W10**	Outside
***G8**	***G11**	Inside
***A9**	***A12**	Loop
***L10**	***L13**	Loop
G11	**G14**	Loop
H12	Q15	Loop
G13	D16	Outside
I14	**I17**	Inside
N15	**N18**	Outside
L16	**L19**	Inside
N17	D20	Outside
I18	**I21**	Inside
P19	**P22**	Inside
N20	S23	Loop
F21	**F24**	Inside
Q22	**Q25**	Loop
M23	**M26**	Loop
T24	S27	Loop
D25	**D28**	Loop
D26	**D29**	Loop
I27	**I30**	Inside
D28	**D31**	Outside
E29	D32	Outside
V30	I33	Inside
R31	K34	Outside
W32	**W35**	Inside
E33	**E36**	Outside
R34	K37	Loop
G35	T38	Loop
	S39	Loop

	D40	Loop
S36	K41	Loop
T37	K42	Sideway
L38	K43	Outside
V39	I44	Inside
A40	**A45**	Inside
E41	Q46	Outside
F42	**F47**	Inside
K43	R48	Outside
R44	K49	Loop
K45	E50	Loop
M46	K51	Loop
K47	E52	Sideway
P48	T53	Inside
F49	**F54**	Outside
L50	K55	Inside
K51	E56	Loop
S52	K57	Loop
G53	D58	Loop
A54	T59	Loop
F55	Y60	Inside
E56	K61	Outside
I57	L62	Inside
L58	F63	Outside
A59	K64	Loop
N60	**N65**	Loop
G61	**G66**	Loop
D62	T67	Outside
L63	**L68**	Inside
K64	**K69**	Outside
I65	**I70**	Inside
K66	**K71**	Outside
N67	H72	Loop
L68	**L73**	Inside
T69	K74	Loop
R70	T75	Outside
D71	**D76**	Outside
D72	**D77**	Inside
S73	Q78	Outside
G74	D79	Inside
T75	I80	Outside

Y76	**Y81**	Inside
N77	K82	Outside
V78	**V83**	Inside
T79	S84	Outside
V80	I85	Inside
Y81	**Y86**	Outside
S82	D87	Loop
T83	**T88**	Loop
N84	K89	Loop
G85	**G90**	Loop
T86	K91	Loop
R87	N92	Loop
I88	V93	Loop
L89	**L94**	Inside
N90	E95	Outside
K91	**K96**	Sideway
A92	I97	Outside
L93	F98	Inside
***D94**	***D99**	Outside
***L95**	***L100**	Inside
*R96	*K101	Outside
***I97**	***I102**	Inside
*L98	*Q103	Outside
***E99**	***E104**	C-terminal
	R105	C-terminal

Table 4.1 Protein Sequence Comparison between Rat $CD2_{1-99}$ and $huCD2_{1-105}$. The 1-99 amino acids of rat CD2 are listed in the first column. The 1-105 amino acids are listed in the second column. The directions of both sequences are indicated in the last column. Amino acids that are same in rat $CD2_{1-99}$ and $huCD2_{1-105}$ are shown in bold. Amino acids located in the loop regions are labeled as loop. All other amino acids are located within different β-sheet strands. Side chain directions of amino acids located within β-sheet strands are indicated as following. **Outside:** amino acid side-chain is facing toward the protein surface; **Inside:** amino acid side-chain is facing opposite of the protein surface; **Sideway:** amino acid side chain is parallel with the β-sheet strand at which it is located.

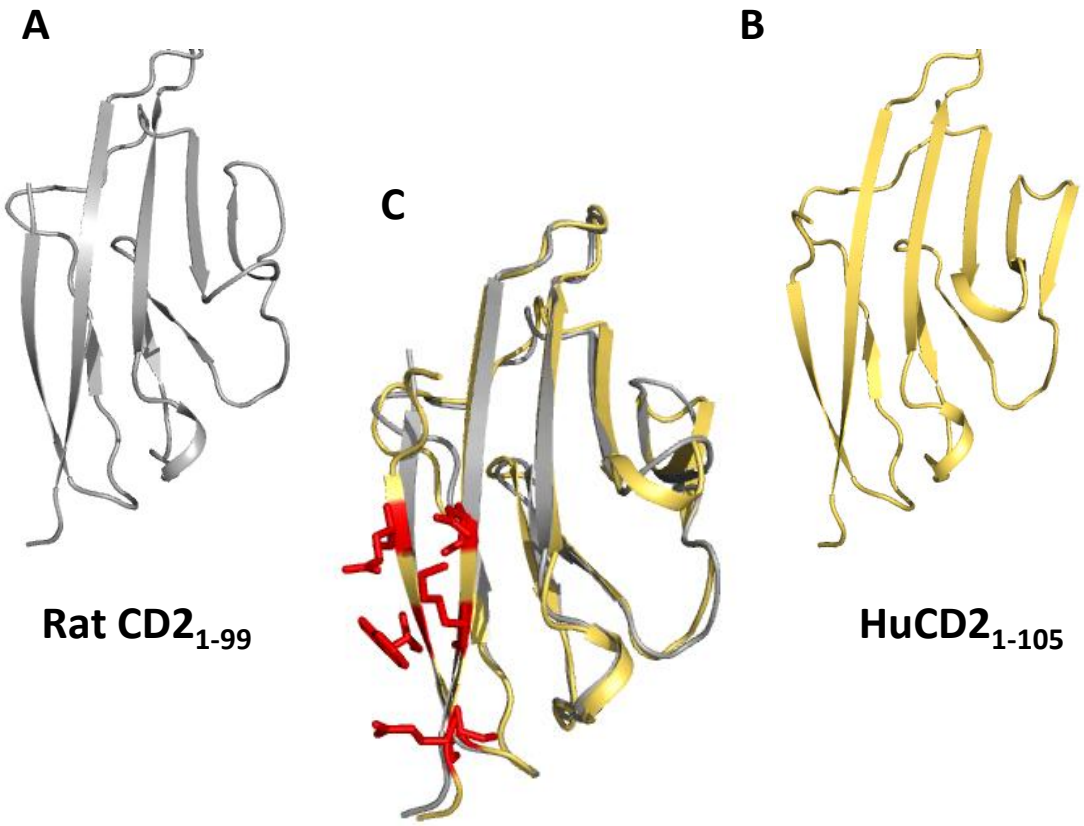

Figure 4.1 Structural Comparisons of Rat CD2$_{1-99}$ and huCD2$_{1-105}$. (A and B) The overall ribbon diagrams of rat CD2$_{1-99}$ (PDB accession ID, 1hng) and huCD2$_{1-105}$ (PDB accession ID, 1hnf) are shown in gray and yellow colors separately. **(C)** 3D Structural alignment of rat CD2$_{1-99}$ and huCD2$_{1-105}$. Side chains of amino acids involved in design of the anti-angiogenic sites are shown in red color (only side-chains facing toward the protein surface are shown here). Sequences are aligned by Dr. Hsiau-Wei Lee using a computer program, Pymol.

Table 4.2 N- and C- Terminal Amino Acids of huCD2D1 and huProAgio

Amino Acid	8	9	10	11	12	13	99	100	101	102	103	104
huCD2D1	Glu	Thr	Trp	Gly	Ala	Leu	Asp	Leu	Lys	Ile	Gln	Glu
***huProAgio**	**Ser**	**Val**	**Gln**	**Met**	**Lys**	Leu	Asn	Leu	Lys	**Val**	**Ile**	**Ile**

***:** Mutated amino acids in huProAgio are shown in bold.

```
        10          20       *  30          40          50          60
KEITNALSVQ MKLGQDINLD IPSFQCSDDI DDIKWEKTSD KKKIAQFRKE KETFKEKDTY

        70          80       ** 90         100
ELLKNGALKI KHLKTDDQDI YKVSIADTKG KNVLEKIFNL KVII
```

Figure 4.2 Protein Sequence of huProAgio for *E. coli* Expression Systems. Amino acids involved in anti-angiogenic sites are underlined. The three amino acids mutations (Lys61Glu, Phe63Leu, and Thr67Ala) that stabilize the non-glycosylated protein in *E. coli* expression systems are shown in bold [338]. An amino acid mutation (Tyr86Ala) that abolishes the interaction between huCD2D1 and CD58 are labeled with double stars [340]. An amino acid mutation (Met26Cys) that allows huProAgio to be site-specifically PEGylated in Cys26 is labeled with single star.

```
        10         20       *  30         40         50         60
KEITNALSVQ MKLGQDINLD IPSFQCSDDI DDIKWEKTSD KKKIAQFRKE KETFKEKDTY

        70         80      **  90        100
KLFKNGTLKI KHLKTDDQDI YKVSIADTKG KNVLEKIFNL KVII
```

Figure 4.3 **Protein Sequence of huProAgio for Yeast Expression Systems.** Amino acids involved in anti-angiogenic sites are underlined. An amino acid mutation (Tyr86Ala) that abolishes the interaction between huCD2D1 and CD258 are labeled with double stars [340]. An amino acid mutation (Met26Cys) that allows huProAgio to be site-specifically PEGylated in Cys26 is labeled with single star.

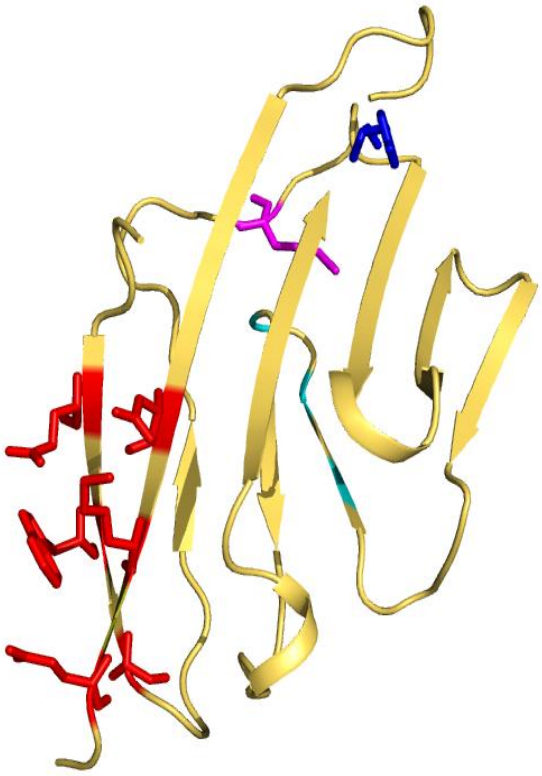

Figure 4.4 Overall Ribbon Structure of the Designed huProAgio. The homology model of huProAgio is built by a computer program, Modeller, using the X-ray crystal structure of huCD2 (PDB accession ID, 1hnf) as a template. Amino acids involved in huProAgio design are color coded as following. **Red:** side chains of amino acids involved in anti-angiogenic sites (only side chains facing toward the protein surface are shown here); **Cyan:** three amino acids mutations (Lys61Glu, Phe63Leu, and Thr67Ala) that stabilize the non-glycosylated protein in *E. Coli* expression systems[338]; **Blue:** an amino acid mutation (Tyr86Ala) that abolishes the interaction between huCD2D1 and CD258 [340]; **Magenta:** an amino acid mutation (Met26Cys) that allows huProAgio to be site-specifically PEGylated in Cys26. This computer model is simulated by Dr. Hsiau-Wei Lee.

```
Orig   AAAGAGATTACGAATGCCTTGGAAACCTGGGGTGCCTTGGGTCAGGACATCAACTTGGAC
       :::::::: :: :: ::  :::::::::::::: ::  :::::::::: :::::  :::::
Opti   AAAGAGATCACTAACGCACTGGAAACCTGGGGCGCGCTGGGTCAGGATATCAATCTGGAC

Orig   ATTCCTAGTTTTCAAATGAGTGATGATATTGACGATATAAAATGGGAAAAAACTTCAGAC
       ::::: :: ::::::..  .  :: :: :: :::::::: :::::::.:::::::.::
Opti   ATTCCGAGCTTTCAGTGCTCCGACGACATCGACGATATCAAATGGGAGAAAACTTCTGAT

Orig   AAGAAAAAGATTGCACAATTCAGAAAAGAGAAAGAGACTTTCAAGGAAAAAGATACATAT
       :::::.:::::::: ::.::: :.:::::::::::.:: :::::.::::::.:: :: ::
Opti   AAGAAGAAGATTGCCCAGTTCCGTAAAGAGAAAGAAACCTTCAAAGAAAAGGACACCTAC

Orig   GAGCTACTGAAAAATGGAGCGCTGAAAATTAAGCATCTGAAGACCGATGATCAGGATATC
       :::::.::::::.:: ::.:::::::::::: ::.:::::::::.::::::::::::.:: :::
Opti   GAGCTGCTGAAGAACGGTGCGCTGAAAATCAAACATCTGAAAACCGATGATCAAGACATC

Orig   TACAAGGTATCAATATATGATACAAAAGGAAAAAATGTGTTGGAAAAAATATTTGATTTG
       ::::::.::.:: ::    ::::::.::::: ::.:: ::  ::::::::.:: :::::  ::
Opti   TACAAAGTGTCCATCGCGGATACTAAAGGCAAGAACGTTCTGGAAAAGATCTTTGACCTG

Orig   AAGATTCAAGAG
       ::.:: ::::::
Opti   AAAATCCAAGAG
```

Figure 4.5 Comparison of Optimized cDNA Codons of huProAgio for *E. coli* Expression. Sequence alignment of the original (upper panel) and codon-optimized (lower panel) cDNA sequences was done using an online software, LALIGN. An estimated 78.5% identity (85.9% similarity) in 312 base pairs (bps) was shown between the original and optimized sequences. The codon optimization for expression in *E. coli* systems were perforeed by Epoch Life Science, INC located at Missouri City, TX using their pro-prietary software.

```
E.      AAAGAGATCACTAACGCACTGTCCGTGCAAATGAAACTGGGTCAGGATATCAATCTGGAC
        ::::::.:: :::::::::.:::.  :::::::::::::::::.::.:: :::::  :.:::
Yeast   AAAGAAATTACTAACGCTCTGAGTGTGCAAATGAAACTGGGACAAGACATCAACTTAGAC

E.      ATTCCGAGCTTTCAGTGCTCCGACGACATCGACGATATCAAATGGGAGAAAACTTCTGAT
        :: ::.:: :::::::: :: :: :: :: :: :: ::::::::::::.::.:::::::: 
Yeast   ATCCCAAGTTTTCAGTGTTCTGATGATATTGATGACATCAAATGGGAAAAGACTTCTGAC

E.      AAGAAGAAGATTGCCCAGTTCCGTAAAGAGAAAGAAACCTTCAAAGAAAAGGACACCTAC
        :::::::::.::::: ::.::: :.::.::::::.::::: :::::.:::::::: ::::::
Yeast   AAGAAGAAAATTGCTCAATTCAGAAAGGAGAAGGAAACTTTCAAGGAAAAGGATACCTAC

E.      GAGCTGCTGAAGAACGGTGCGCTGAAAATCAAACATCTGAAAACCGATGATCAAGACATC
        .:. :: : ::::: :::.:. ::::::: ::.:: :: ::.:: ::::::::::::::
Yeast   AAATTGTTTAAGAATGGTACATTGAAAATTAAGCACCTTAAGACAGATGATCAAGACATC

E.      TACAAAGTGTCCATCGCGGATACTAAAGGCAAGAACGTTCTGGAAAAGATCTTTAACCTG
        :::::::: :: :: :: ::::::.::.:: ::::::::  ::::.::::::::: :: ::
Yeast   TACAAAGTCTCAATTGCCGATACAAAGGGTAAGAACGTGTTGGAGAAGATCTTCAATCTT

E.      AAAGTGATCAT
        ::.:: :::::
Yeast   AAGGTTATCAT
```

Figure 4.6 Comparison of Optimized cDNA Codons of huProAgio for Yeast Expression. Sequence alignment of the cDNA codon sequences optimized for *E. coli* (upper panel) and yeast (lower panel) expression systems using the online software, LALIGN. An estimated 79.1% identity (87.1% similar) in 312 bps was shown between the original and optimized sequences. The cNDA codons were optimized for expression in yeast expression systems by Epoch Life Science, INC. using their proprietary software.

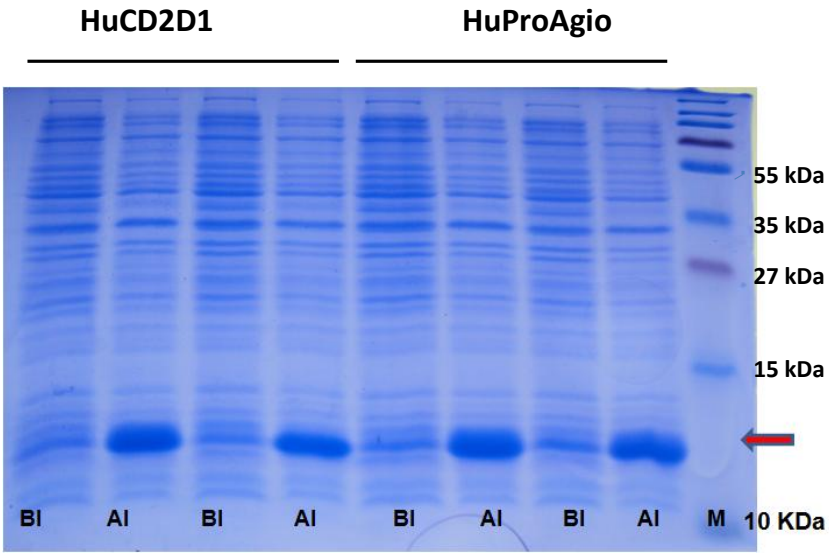

Figure 4.7 Bacterial Expression of HuCD2D1 and HuProAgio. Expression levels of different bacterial clones were analyzed by SDS-PAGE gel electrophoresis of bacteria lysates. Lane 1 – 4 (from left) BL-21(DE3) clones before and after (BI, AI) IPTG induction. Lane 5 – 8) BL-21(DE3) clones before and after (BI, AI) IPTG induction. Courtesy of R. Chakram.

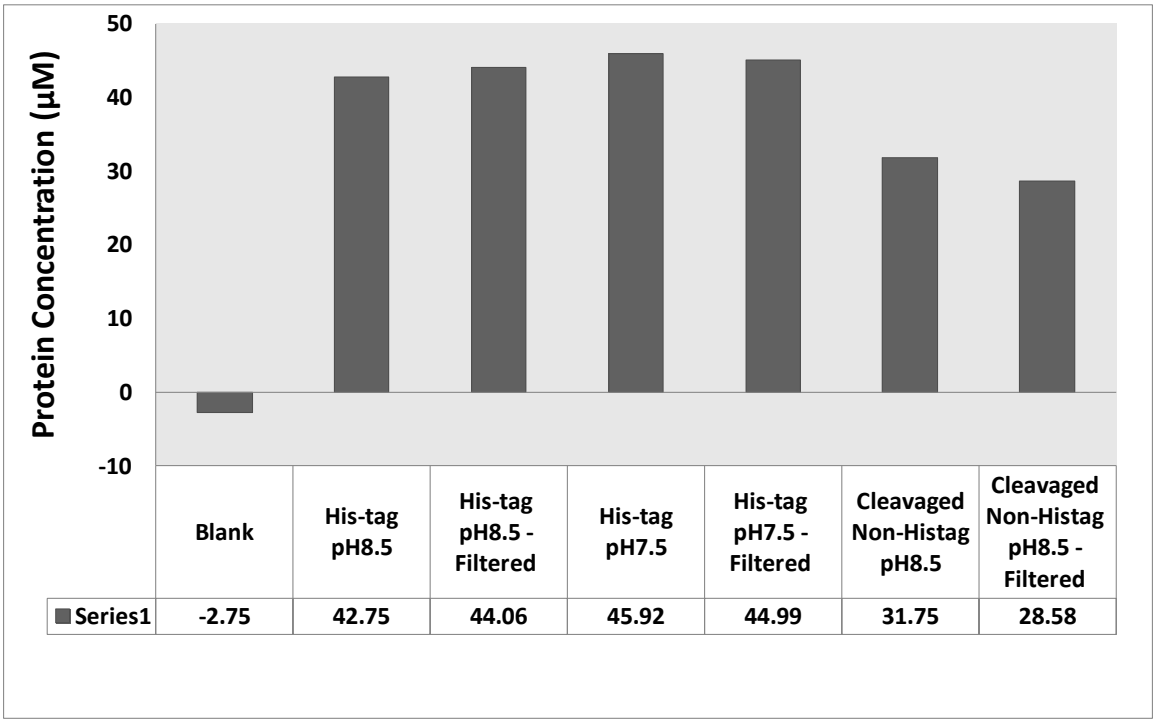

Figure 4.8 Concentration of HuProAgio after pH Refolding. His-tagged huProAgio were refolded in 50 mM arginine, 50 mM glycine, and 2 mM DTT in PBS buffer at indicated pH values. Protein concentrations were measured by Bradford protein assay using BSA as a standard. Concentrations were indicated in micromoles.

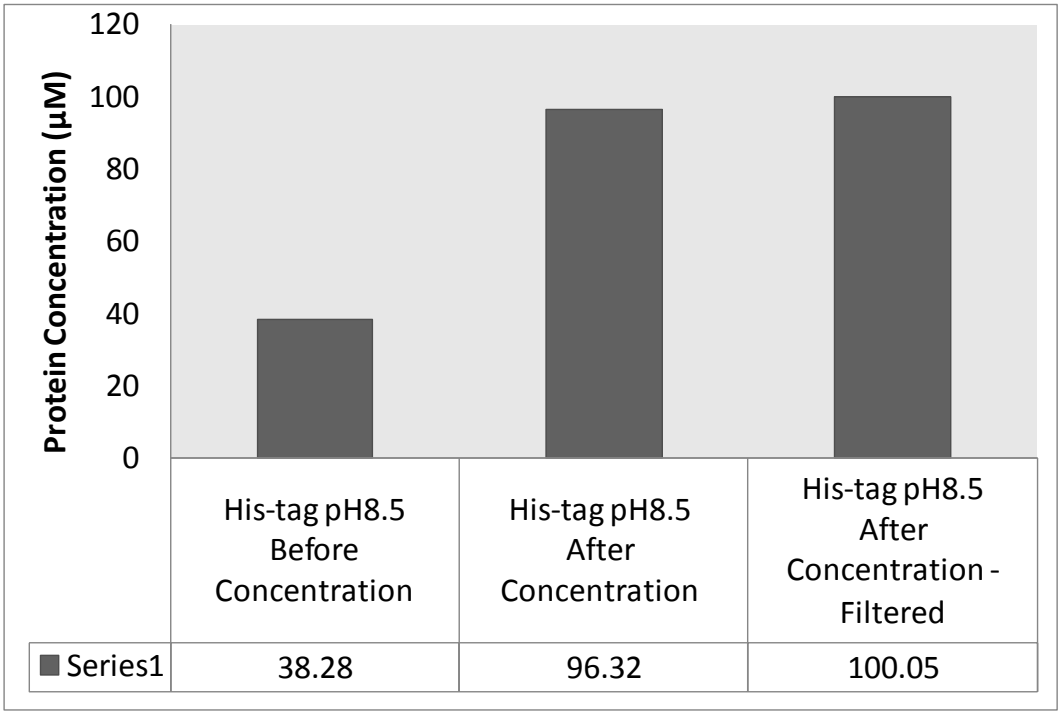

Figure 4.9 Maximum Concentration of HuProAgio after pH Refolding. His-tagged huProAgio were *refolded in* 50 mM arginine, 50 mM glycine, and 2 mM DTT in PBS buffer (pH 8.0) at indicated pH values. At the end of refolding process, protein was concentrated by centrifugation at 8,000 rpm in a centrifugal filter unit (Millipore, Billerica, MA). Protein concentrations were measured by Bradford protein assay using BSA as a standard. Concentrations were indicated in micromoles.

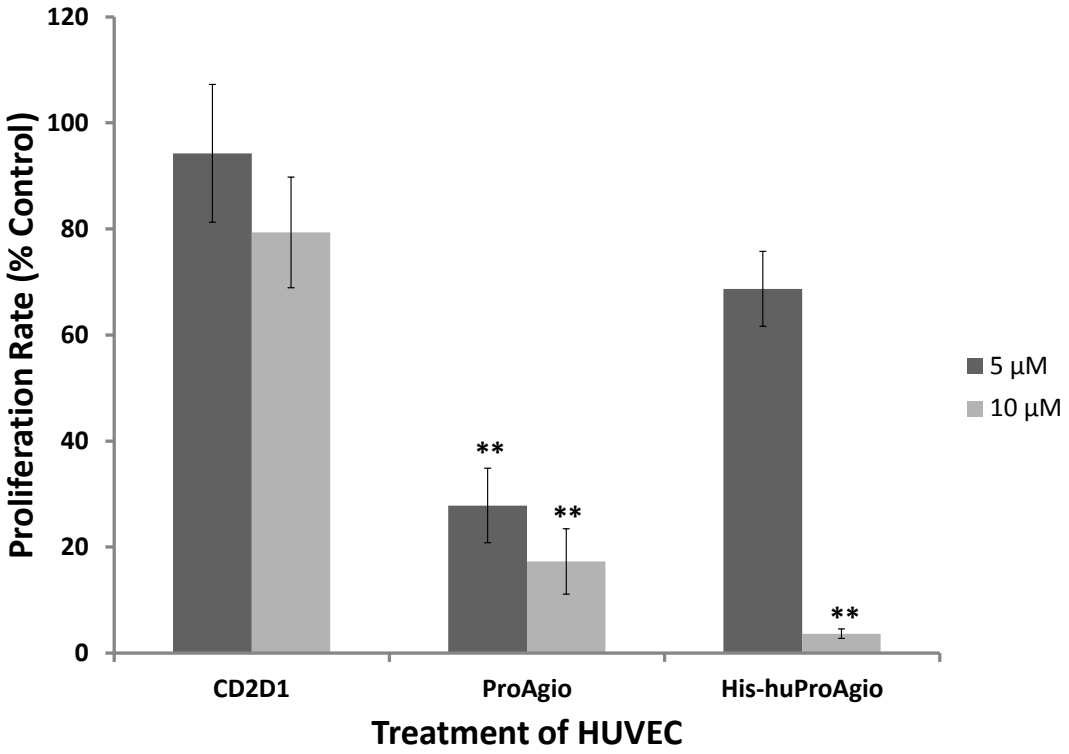

Figure 4.10 His-huProAgio Inhibits Proliferation of HUVECs. HUVEC cells were treated with CD2D1, ProAgio, and his-huProAgio for 48 hours at 5 and 10 μM separately. 20 μL of 1:2000 diluted BrdU were added to each well for additional 12 hours. Proliferation rates were measured by under absorbance 450 – 540 nm and shown as percentage of buffer control. Data were shown as mean ± S.D.. The experiments were repeated 3 times.

**: ProAgio (5 μM) versus CD2D1 (5 μM), ProAgio (10 μM) versus CD2D1 (10 μM), and his-HuProAgio (10 μM) versus CD2D1 (10 μM) showed statistically significant differences ($P < 0.001$, unpaired student's *t* test, two-tailed).

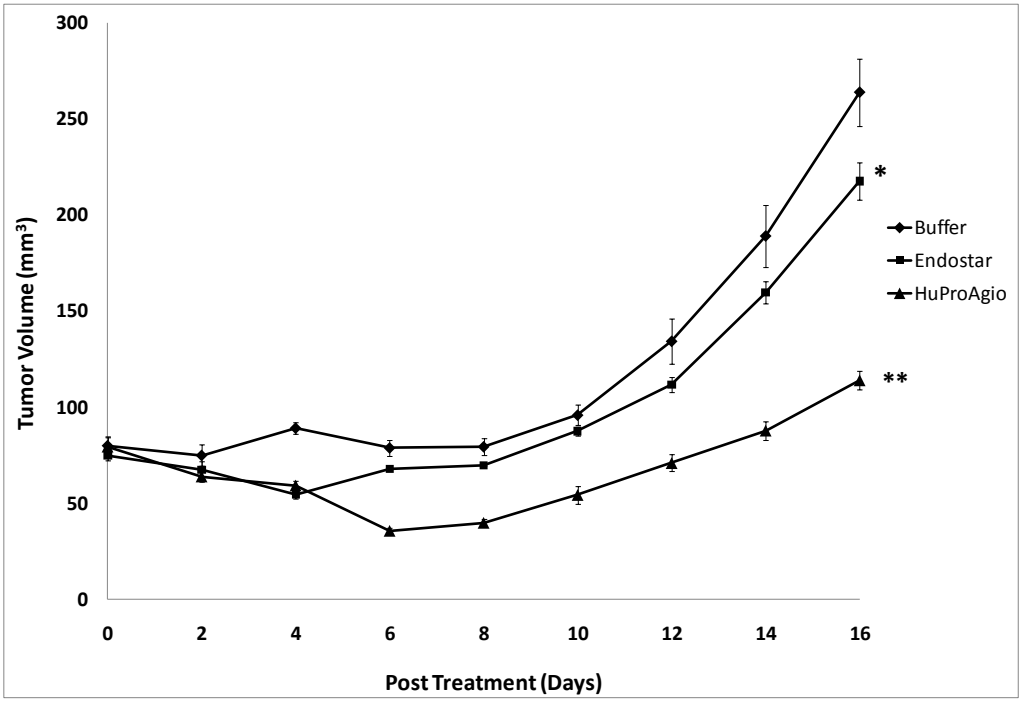

Figure 4.11 Tumor Growth Curve of ProAgio Treated PC3 Xenografts. $5x10^6$ of PC3 cells were implanted subcutaneously into nude mice (n = 6 for each group). All agents were administered for 16 days by intraperitoneal injection (i.p.) at desired doses (buffer: 1 X PBS, pH 7.4, 200 µL/mouse/day; Endostar: 10 mg/kg/day; and huProAgio: 10 mg/kg/day). Treatments were started until tumor volume reached 50 – 100 mm^3. Tumor dimensions (length and width) were measured using a caliper every other day. Tumor volume were calculated as π/6 x (length x width x width). Data were shown as mean ± S.E.. Statistic significances were evaluated using Welch's *t* test. $P < 0.05$ was considered significant.

*: Endostar (10 mg/kg/day) versus Buffer treated group was not significantly different, $P > 0.05$.

**: HuProAgio-PEG (10 mg/kg/day) versus buffer treated group was significantly different, $P < 0.05$.

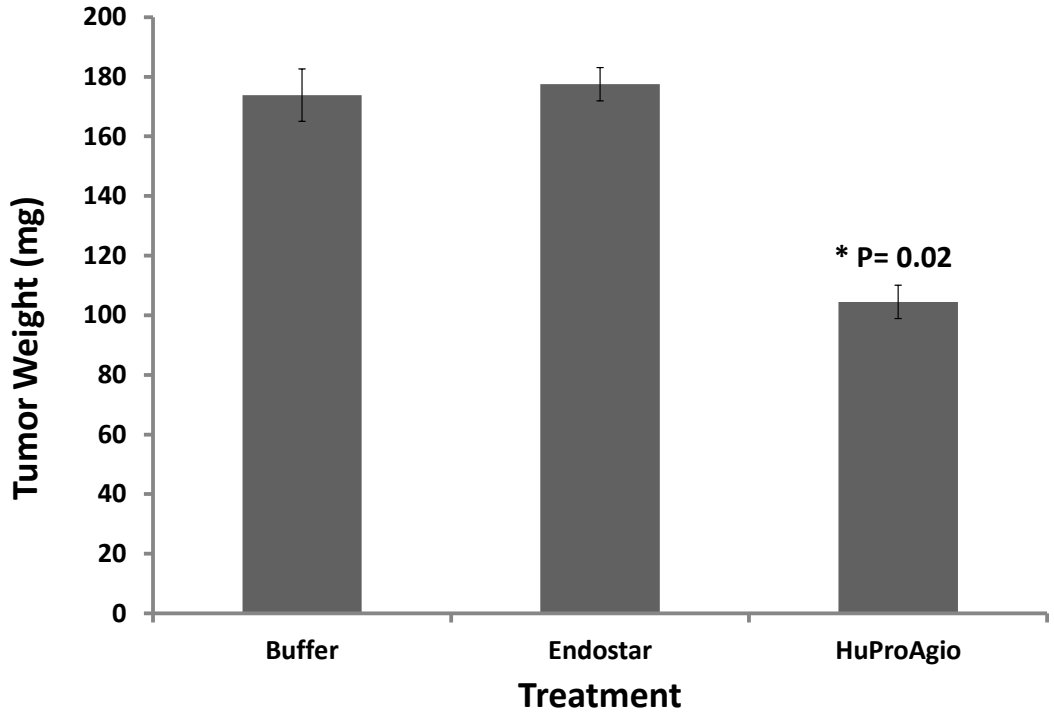

Figure 4.12 Tumor Weights of HuProAgio Treated Xenografts. $5x10^6$ of PC3 cells were implanted subcutaneously into nude mice (n = 6 for each group). All agents were administered for 16 days by intraperitoneal injection (i.p.) at desired doses (buffer: 1 X PBS, pH 7.4, 200 µL/mouse/day; Endostar: 10 mg/kg/day; and huProAgio: 10 mg/kg/day). On the last day of treatment, xenografts were dissected and measured individually. Data were shown as mean ± S.E..

*: huProAgio (10 mg/kg/day) versus buffer treated group showed statistically significant differences ($P < 0.05$, unpaired student's *t* test, two-tailed).

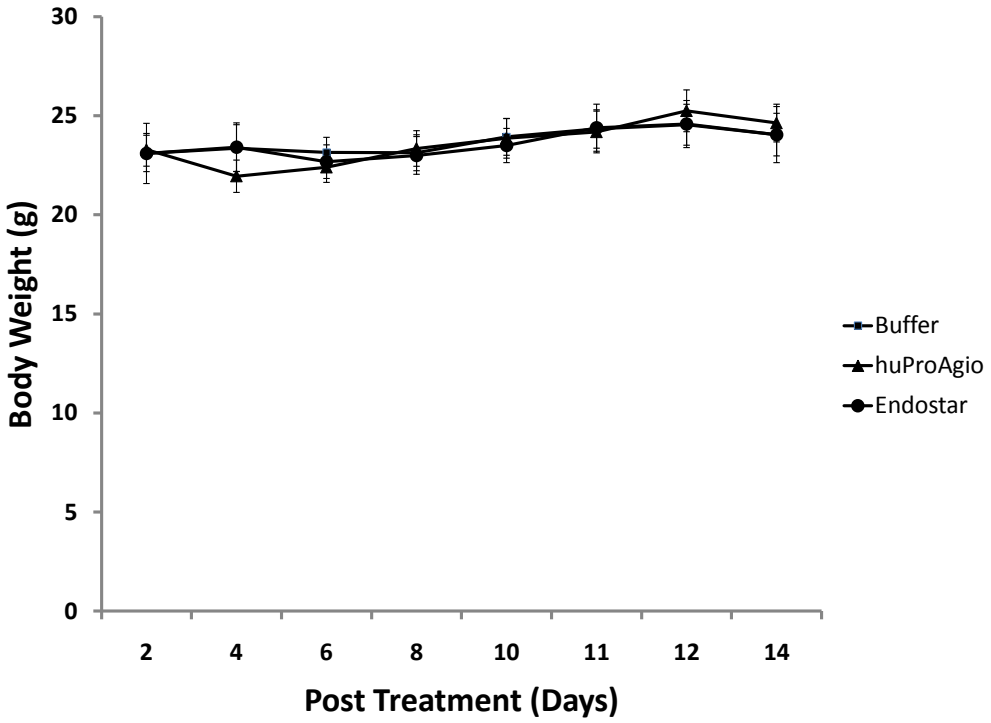

Figure 4.13 Body Weights of Treated Nude Mouse. $5x10^6$ of PC3 cells were implanted subcutaneously into nude mice (n = 6 for each group). All agents were administered for 16 days by intraperitoneal injection (i.p.) at desired doses (buffer: 1 X PBS, pH 7.4, 200 µL/mouse/day; Endostar: 10 mg/kg/day; and huProAgio: 10 mg/kg/day). The body weight of each mouse was monitored every other day. Weight were shown as mean ± S.E. .

CHAPTER 5

CLONING, PROTEIN PURIFICATION, AND PEGYLATION

5.1 Introduction of 6D31-ProAgio

In our initial design, the anti-angiogenic peptides (TVAQMKL and NLKVII) were framed separately into the N- and C- termini of a CD2D1 variant protein, 6D31 instead of the wild type CD2D1. 6D31 (also named as CD2.trigger) was designed and constructed as a Ca^{2+}- binding protein by the research group led by Dr. Jenny J. Yang from GSU [311]. Li and colleagues reported that two reverse electronic charge mutations (Arg31Asp and Lys43Asp) together with Glu29 and Glu41 coordinately formed a Ca^{2+}- binding pocket on the surface of GFCC'C'' β-sheet strands of CD2D1 [311]. This designed metal binding pocket allowed 6D31 to adopt reversible conformational changes induced by positively charged metal ions. Li and coworkers suggested that 6D31 was structurally unfolded in the absence of positively-charged metal ions [311]. Upon binding to $Ca2^{+}$, $La3^{+}$, or $Tb3^{+}$, charge-charge interactions between metal irons and the negatively-charged metal binding pocket triggered refolding of 6D31 into a β-sandwich structure same as that of wild type CD2D1.

The difference between using 6D31 versus wild type CD2D1 as a host protein mainly focused on metal binding capability. Our initial hypothesis was to design a dual function protein with anti-angiogenic function and radio-toxicity. In the 6D31-ProAgio model, anti-angiogenic peptides were framed into the same position as we did later on with the wild type CD2D1. Since the metal binding pocket of 6D31 is far from the N- and C- terminal strands, it should still function if the overall 3D protein structure remains the same. The metal binding feature will provide

a possibility to load the designed 6D31-ProAgio with radioactive metal ions that are toxic to the local tumor tissues. Preliminary studies in this chapter suggested that wild type CD2D1 surpasses 6D31 in structural stability, so that the final version of ProAgio discussed throughout this dissertation was designed using wild type CD2D1 as a host protein. Since early experiences of expression and purification of 6D31-ProAgio helped to pave the way for ProAgio studies, in this chapter, molecular cloning, protein purification, and PEGylation of 6D31-ProAgio and ProAgio were both summarized.

5.2 Molecular Cloning of 6D31-ProAgio

The 6D31 cDNA was a gift from Dr. Jenny J. Yang from GSU. It was cloned into a pGEX-2T bacterial expression vector (GE lifesciences, Piscataway, NJ) between restriction enzyme recognition sites, BamH I and EcoR I, indicated in Figure 5.1. A thrombin cleavage site is located right before BamH I restriction recognition site. A 26-kDa glutathione S-transferase (GST) gene is located in the 5'-end of the cleavage site as a fusion tag. In order to create 6D31-ProAgio cDNA, a series of mutations was introduced into the parental cDNA using primers listed as Table 5.1. Total 18 base pairs were substituted, which resulted in 8 amino acids mutations (Trp7Gln, Gly8Met, Ala9Lys, Asp94Asn, Arg96Lys, Ile97Val, Leu98Ile, and Glu99Ile) in the N- and C-terminal β-strands of 6D31 separately.

5.3 Expression and Purification of 6D31-ProAgio

6D31-ProAgio was expressed as a GST-fusion protein in a BL-21 (DE3) bacteria strain, BL-21(DE3) CodonPlus® competent cell line (stratagene, Santa Clara, CA). Purification procedures

were adapted from protocols developed for CD2D1 and 6D31 by members of Dr. Jenny J. Yang's research group from GSU [291, 311]. IPTG concentrations were optimized using 2 mL-scale cultures. In Figure 5.2, it showed that 0.1 - 0.3 mM of IPTG was sufficient to induce protein expression. Larger scale protein expressions were done using 1 L culture induced under a relative low IPTG concentration (0.2 mM) at temperature (30˚C) for 4 hours. These precautions were intended to increase the soluble forms of 6D31-ProAgio to be expressed. The GST tag was utilized to purify the fusion protein from cellular extracts using a Glutathione 4B affinity (GS4B) column (GE lifesciences, Piscataway, NJ), and then removed by on beads thrombin cleavage. Further purification using different methods including ion or cation exchange, gel filtration and other chromatographies would by applied if separation of thrombin was desired. Normally, after thrombin cleavage, GST tags remained bound to the affinity column while CD2D1 or 6D31 were able to be eluted using buffered saline at neutral pH. In this case, however, after thrombin cleavage 6D31-ProAgio was not eluted from the GS4B column as expected using phosphor buffered saline (PBS) at pH 7.4. Major efforts were drawn to overcome this challenge using a variety of elution conditions, such as gradually increasing salt concentration up to 1 M, or higher pH to 10.0, but none of them yielded satisfying results. Finally, a combination of reducing condition and higher pH (50 mM Tris buffer, 10 mM reduced glutathione, 150 mM NaCl, and pH 10.0) successfully eluted all proteins including the cleavage GST tags and 6D31-ProAgio as shown in Figure 5.2. Clearly, the 6D31-ProAgio was separated by thrombin cleavage, but it still attached to the GST affinity column together with GST. This phenomenon resulted in two major separated bands at 11-kDa (represented 6D31-ProAgio) and 26-kDa (represented GST) exhibited by SDS-PAGE gel stained with coomassie blue.

The eluted mixture was further separated by Gel filtration Chromatography (GFC) (Figure 5.3 A and B). Two major elution peaks were observed: fractions 6 – 7 and 12 – 13. SDS-PAGE gel electrophoresis analysis showed that the first peak (fraction 6 – 7) consisted of GST while the second peak (fraction 12 – 13) contained majority of 6D31-ProAgio. It was possible that GST had conformational changes that provoked the protein to be continuously eluted out until fraction 11 – 12. Although fractions 12 – 14 were mixed with trace amount of GST, those fractions were collected and further used for *in vitro* testing of biological function.

5.4 Evaluation of the *In Vitro* Effect of 6D31-ProAgio

The *in vitro* biological effect of 6D31-ProAgio was evaluated by MTT cell viability assay using HUVECs and an epithelial colon cancer cell line, HCT116 (Figure 5.4 and 5.5). A final concentration of 4 μM 6D31-ProAgio and control proteins including GST, CD2D1, and 6D31 were incubated with the cells seeded into 96-well plates for 48 hours. Cell viabilities were determined by MTT assays. Figure 5.5 suggested that compared to control proteins (GST and CD2D1), 6D31-ProAgio showed significant inhibitive effect on HUVECs but not HCT116 cells. Because 6D31-ProAgio showed obvious precipitation, half of the protein sample was filtered through a 0.2 μM syringe filter. The filtered 6D31-ProAgio sample still significantly reduced viability of HUVECs except for being less effective, which is expected because the filtered sample contained lower concentration of protein compared to the non-filtered one. The host protein, 6D31, also showed inhibitive effect. It was not clear whether 6D31 truly affected growth of HUVECs because this experiment was not repeated due to difficulties in low protein yield and quick precipitation.

5.5 Molecular Cloning of ProAgio

As discussed above, 6D31-ProAgio showed significant precipitation when its concentration exceeded 50 μM. This low concentration brought challenges to determine its structure and biological functions. It was highly possible that this precipitation was due to poor structural stability after extensive mutation. In order to solve this problem, the wild type CD2D1 was chosen to be the host protein instead of 6D31, which was discussed in chapter 1 and following sessions. Compared to 6D31, the wild type CD2D1 is stable in a wide range of pH, temperatures, and salt concentrations. In addition, purification of CD2D1 has produced high yield of proteins with well established protocols explored by Dr. Jenny J. Yang's research group. Those advantages were expected to improve the protein stability and increase solubility. This protein was designated as ProAgio in all chapters of this dissertation.

Molecular cloning of ProAgio was based on 6D31-ProAgio cDNA. Since the anti-angiogenic region contained 8 amino acids mutations already being produced in 6D31 cDNA, mutations were made in the metal binding site in order to mutate the 6D31 host into wild type CD2D1. Site-directed mutagenesis reactions were carried out using primers indicated as Table 5.2. Two back mutations Asp31Arg and Asp43Lys were made, which abolished the metal binding property. Another deletion was made to remove a restriction enzyme recognition site that was designed for insertion of other peptide sequences.

5.6 Expression and Purification of ProAgio

ProAgio was expressed as a GST-fusion protein same as 6D31-ProAgio did. ProAgio was expressed in high level and purified using GS4B columns. Expression and purification were

shown as Figure 5.6. Analysis by SDS-PAGE gel electrophoresis indicated that the GST-ProAgio had high affinity for GS4B columns. After on column cleavage by thrombin, proteins were eluted with 10 mM reduced glutathione in 50 mM Tris buffer (pH 8.0) and further purified using gel filtration chromatography. Figure 5.7 showed the UV 260 nm absorbance of each fraction. Similar to 6D31-ProAgio, two major peaks containing GST and ProAgio separately were eluted. Analyses of gel filtration fractions (Figure 5.8) suggested that majority of GST was separated from ProAgio. The separation was much more improved compared to that of 6D31-ProAgio but the resolution of gel filtration chromatography was still not able to completely remove GST from ProAgio. Although the amount of GST was much less than separation of 6D31-ProAgio, it interrupted with further structural studies of ProAgio (data not shown). In order to solve this problem, this method was further improved by elution of ProAgio using PBS instead of reduced glutathione. Without competition from reduced glutathione, GST remained bound to GS4B so that only ProAgio was eluted. One technical challenge for PBS elution was the local ProAgio concentration. Up to 10 mg of GST fusion protein could bind to 1 mL of GS4B beads. Frequently, precipitation of ProAgio was observed after thrombin cleavage. This aggregation could be significantly improved by increasing the NaCl concentration up to 500 mM. The high salt was able to successfully elute ProAgio without GST, which resulted in high protein purity upon gel filtration chromatography separation as shown in Figure 3.1SA. This phenomenon suggested that ProAgio might have a preference to aggregate, and high salt concentration facilitated the disassociate process.

As the expected, the purified ProAgio shows higher stability than 6D31-ProAgio but less than CD2D1. Without freezing, the concentration of 6D31-ProAgio reached 100 – 120 μM, but

storage of this protein in -20˚C resulted in protein precipitation, which posed a challenge to functional studies that require high concentration of protein stock.

5.7 Evaluation of the *In Vitro* Effect of ProAgio

The purified ProAgio was used for in vitro evaluation of the anti-angiogenic function of ProAgio. Figure 5.9 clearly demonstrates that ProAgio inhibits HUVEC cell growth by 80% compared with CD2D1 at the concentration of 5 – 10 μM. HUVECs treated with CD2D1 shows slightly decrease of viability at higher concentration. The possible reason is probably the fact that most endogenous anti-angiogenic proteins have β-sheet structure and CD2D1 is a well formed β-sheet protein. This experiment illustrates that CD2D1 as a host protein is able to support the anti-angiogenic peptides and enhance their effect in inhibition of endothelial cell growth but not cancerous epithelial cells.

5.8 Solubility and Stability of ProAgio

In order to increase the solubility of ProAgio, individual or a combination of sucrose, trehalose, lactose, mannitol, arginine, glutamatic acid, trehalose dehydrate, Tween 20, PEG8000 and NaCl were added to the HEPES and PBS buffer solutions indicated as Table 5.3. All those recipes were studied by Dr. J. H. Yang from Dr. Jenny J. Yang's laboratory from GSU. Protein was diluted in low concentration and concentrated by vacuum-frozen drying. After thawing at room temperature, the soluble protein in all recipes were around 10 – 20 μM, which was consistent with previous observations. To this end, all these ingredients failed to significantly

increase protein solubility. In later studies, ProAgio proteins were either fresh purified or diluted to concentration < 10 μM, and then stored at -20˚C and re-concentrated after thawing.

Protein stability of ProAgio was tested by incubation with fetal bovine serum (FBS). When mixed with serum at 1:1 ratio (volume), most ProAgio proteins were degraded by four hours (Figure 5.10).

5.9 PEGylation of ProAgio

As discussed in section 5.6, ProAgio showed limited protein solubility and stability, which prompted us to PEGylate ProAgio. PEGylation has been widely adopted as an effective method to prolong half lives of proteins and peptides, improve their solubility, and decrease immunogenicity [344]. Different amino acid residues such lysine, arginine, cysteine residue, N- and C-termini were mostly used PEGylation site. In the case of ProAgio, PEGylation on lysine, arginine and terminal residues risked losing anti-angiogenic function because our designed mutation sites were located in the N- and C- terminal β-strands with lysine and arginine mutations. After a comparison of different PEGylation methods, we chose to site-specifically PEGylate ProAgio with maleimide-PEG maleimide reagents with different molecular weight. Maleimide-PEG chains of 20-kDa were used to PEGylate ProAgio and the PEGylated protein, ProAgio-PEG was used for animal studies. Since original ProAgio did not include any cysteine residue, a Met23Cys mutation was made in order to facilitate the site-specific PEGylation and its simulated model structure was shown as Figure 5.11. Met23 was chosen as the PEGylation site is because several reasons. First, it was located in the flexible loop region that was less likely to affect overall protein structure compared to residues involved in the hydrophobic core region.

Secondly, Met23 was laid in opposite to the framing region, which reduced the possibility of blocking biological functions of ProAgio. In addition, methionine and cysteine have the most structural similarity. All these criteria made Met23 the best choice as a site-specific PEGylation site. The PEGylated ProAgio was designated as ProAgio-PEG in this dissertation.

Met23Cys mutated ProAgio showed less stability compared to ProAgio. After thrombin cleavage, proteins were precipitated on GS4B columns. High concentration of L-arginine (500 mM) in PBS was used to solubilize ProAgio. As shown in the first left lane in Figure 5.13, not only ProAgio mutant but also GST was eluted from GS4B. PEGylation was successful as showed by other lanes in Figure 5.12. There are 4 cysteine residues on GST protein, so it was also PEGylated during the procedure. In later experiment, it showed that high concentration of arginine eluted a large amount of GST, which posed difficulties to separate GST-PEG from ProAgio-PEG by cation-exchange chromatography. An on column PEGylation was developed to efficiently PEGylate ProAgio as described in Chapter 2. This method sufficiently solubilized ProAgio. Furthermore, GST-PEG was also eluted in a smaller amount compared to L-Arginine elution. The mixture was subjected to further purification using cation exchange chromatography. As shown in Figure 3.1SC, at pH 6.0, PEG and GST-PEG did not bind to cation exchange column, which led to sufficient separation. The purified ProAgio-PEG showed extensive solubility with concentration that reached up to 1 mM. It was used for later animal studies to investigate its anti-angiogenesis functions during tumorigenesis.

5.10 GST Pull-down Assay

Galectin-1(Gal-1) has been shown as an important target for synthetic anti-angiogenic peptide, Anginex [345]. In order to determine if Gal-1 is the possible target for ProAgio, a GST pull-down assay was performed As shown in Figure 5.13, Cell lysates from VEGF-activated HUVECs were mixed with GST, GST-CD2D1, GST-ProAgio conjugated GS4B beads. Pull-down of Gal-1 was tested by a mouse monocolonal antibody against human Gal-1. Panel C showed that a equal amount of GST, GST-CD2D1, and GST-ProAgio were added to HUVEC-lysate. A minor protein degradation was observed in GST-ProAgio. Panel B indicated that Gal-1 was constitutively expressed in VEGF-activated HUVECs. Panel A showed that Gal-1 was associated with ProAgio. GST or CD2D1 did not precipitate with Gal-1. This result suggested that Gal-1, an important pro-angiogenesis protein was a possible target for ProAgio. Further experiments are needed in order to confirm this targeting in huProAgio.

5.11 Evaluation of *In Vivo* Effects of ProAgio-PEG

The Cys23 PEGylated ProAgio was used for in vivo evaluation using PC3 xenograft model (Figure 5.14A-C). As shown in Figure 5.14, when treated at 10 mg/kg/day, it was clear that ProAgio-PEG effectively slowed down the growth of xenograft tumors, while the control protein CD2D1-PEG did not. ProAgio-PEG reduced the end point tumor mass by 35% ($P < 0.05$, unpaired student's *t* test, two tailed). Compared to buffer control group, it significantly reduced tumor angiogenesis as indicated by CD31 IF staining shown in Figure 5.14C.

In this set of animal experiment, the starting point was 4 weeks post inoculation compared to 7 and 5 days post inoculation in the same models discussed in Chapter 3 and 4 respec-

tively. Together with these findings with early treatment with ProAgio and humanized ProAgio, it was convincing that ProAgio sufficiently inhibited tumor angiogenesis at early and late stage of tumor growth.

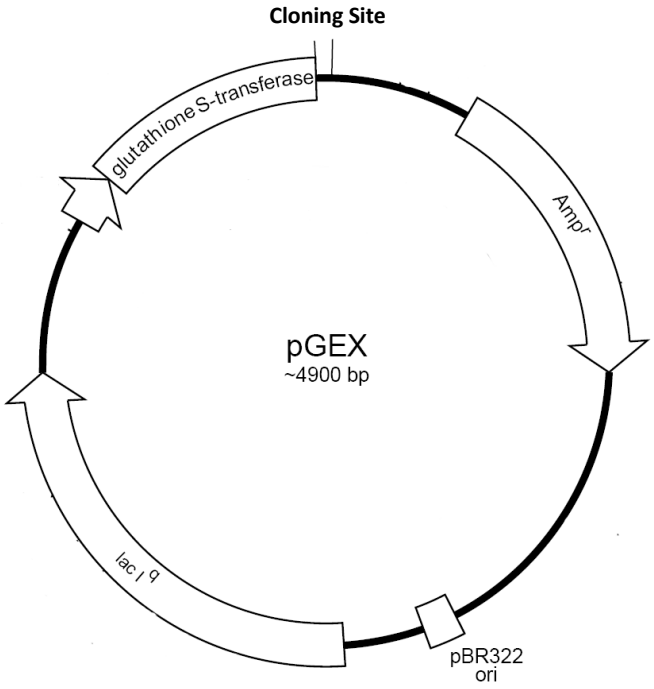

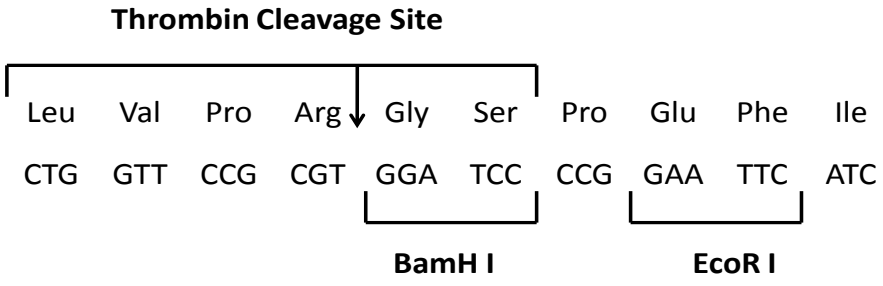

Figure 5.1 Expression Vector pGEX-2T With Thrombin Cleavage and Cloning Sites. The 6D31 or CD2 cDNAs were inserted between the two indicated cloning sites with a stop codon (TAG) before EcoR I. The pGEX-2T image was adapted from www.gelifesciences.com/pGEX.

Table 5.1 Synthetic Primers for Generating 6D31-ProAgio cDNA

Mutations	Primer
W7Q	5’-GAGACAGTGGGACCGTC**CA**GATGAAACTGGGTCATG
G8M, A9K	5’-CCAGAGACAGTGGGACCGTCTGG**ATGAAA**CTGGGTCATGGCATCAACCTGAA
D94N, R96K, I97V	5’-GACACGTATCCTGAACAAGGCACTG**A**AT**T**TTGA**AAG**TTCTAGAGTAGAATTCCCGGGTCGA
L98I, E99I	5’-ACGTATCCTGAACAAGGCACTGAATTTGAAAGTT**A**T**TATC**TAGAATTCCCGGGTCGAC

Table 5.1 Synthetic Primers for Generating 6D31-ProAgio cDNA. Total 18 base pairs were substituted, which produced 8 amino acid mutations at the N- and C- terminal strands of the parental 6D31.

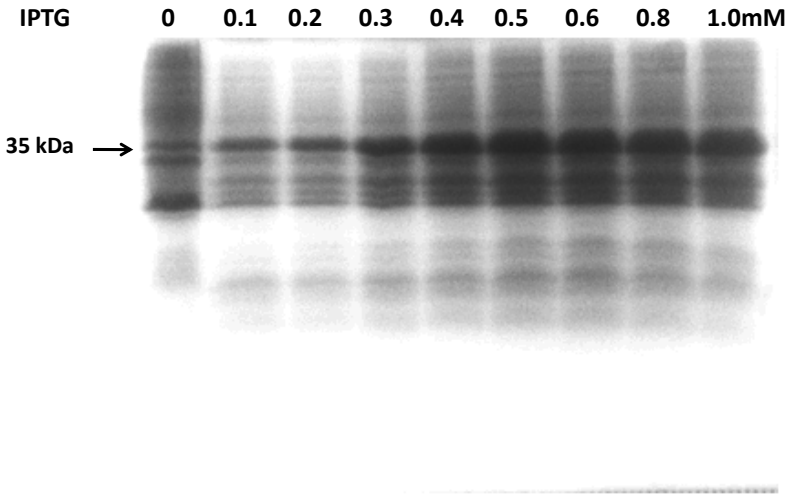

Figure 5.2 Optimization of IPTG Concentration for 6D31-ProAgio Expression. Different concentrations of IPTG (0 – 1 mM) were incubated with BL-21(DE3) bacteria for 4 hours at 30˚C. 20 µl of sample from 1 mL lysate were loaded to each lane. The molecular weight of GST-ProAgio was shown at 35-kDa.

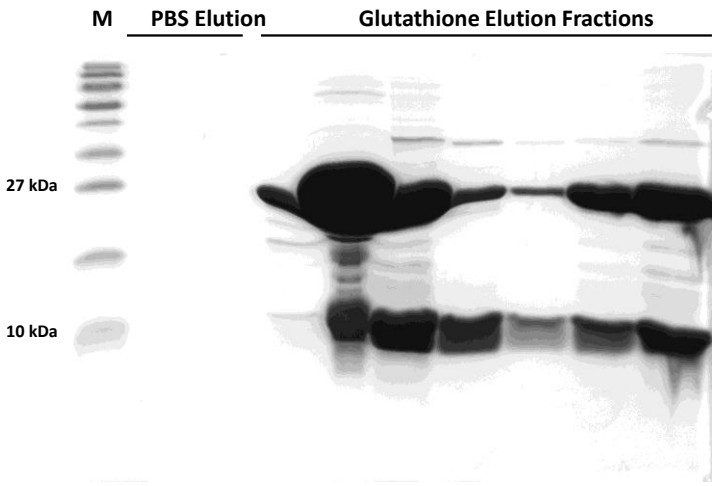

Figure 5.3A Glutathione Elution of 6D31-ProAgio. Elution fractions were examined by SDS-PAGE gel electrophoresis and coomassie blue staining. The first two lanes from left indicated the PBS elution. Other lane showed proteins (cleavage GST and 6D31-ProAgio) that were eluted from glutathione 4B affinity column (GE lifesciences, Piscataway, NJ) using 10 mM reduced glutathione. The upper bands at 26-kDa were GST cleaved from GST-ProAgio fusion protein. The lower bands at 11-kDa were ProAgio after cleaved from GST-6D31-ProAgio fusion protein.

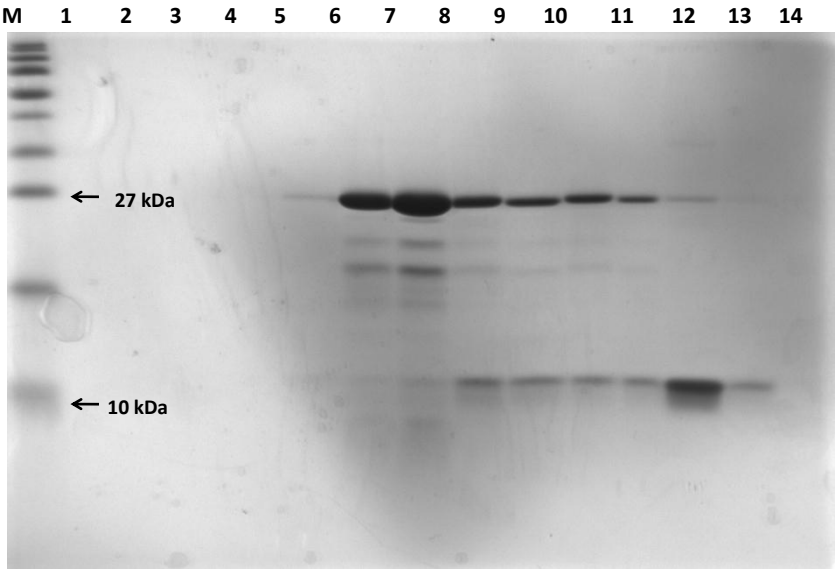

Figure 5.3B Elution fractions of 6D31-ProAgio Using Gel Filtration Chromatography. Fractions (1 to 14) were examined by SDS-PAGE gel electrophoresis and coomassie blue staining. Upper bands (26-kDa) represented GST. Lower bands (11-kDa) were 6D31-ProAgio.

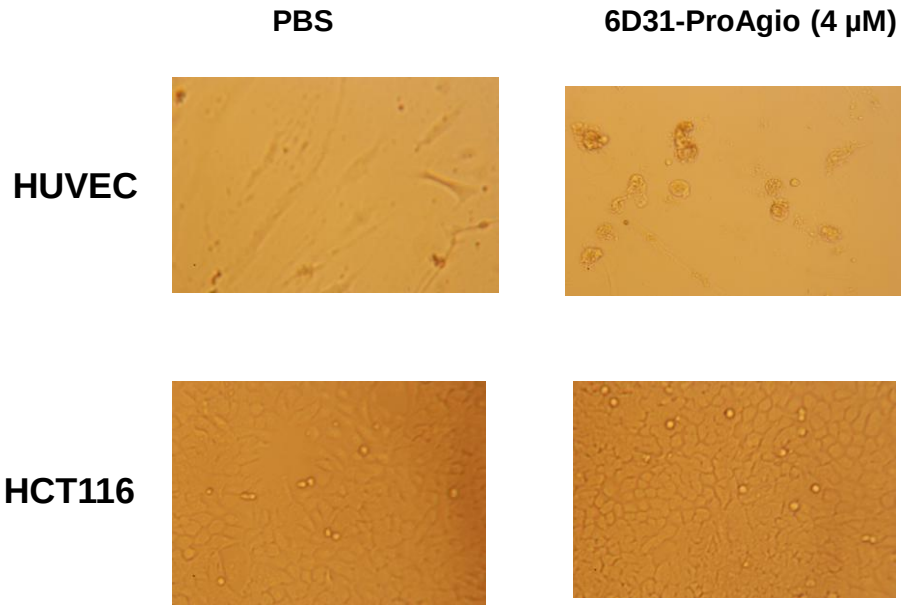

Figure 5.4 6D31-ProAgio Inhibited HUVEC Growth. HUVECs and HCT116 cells were seeded into a 96-well plate. Cells were treated with 6D31-ProAgio for 48 hours. Pictures were taken under 400X magnification.

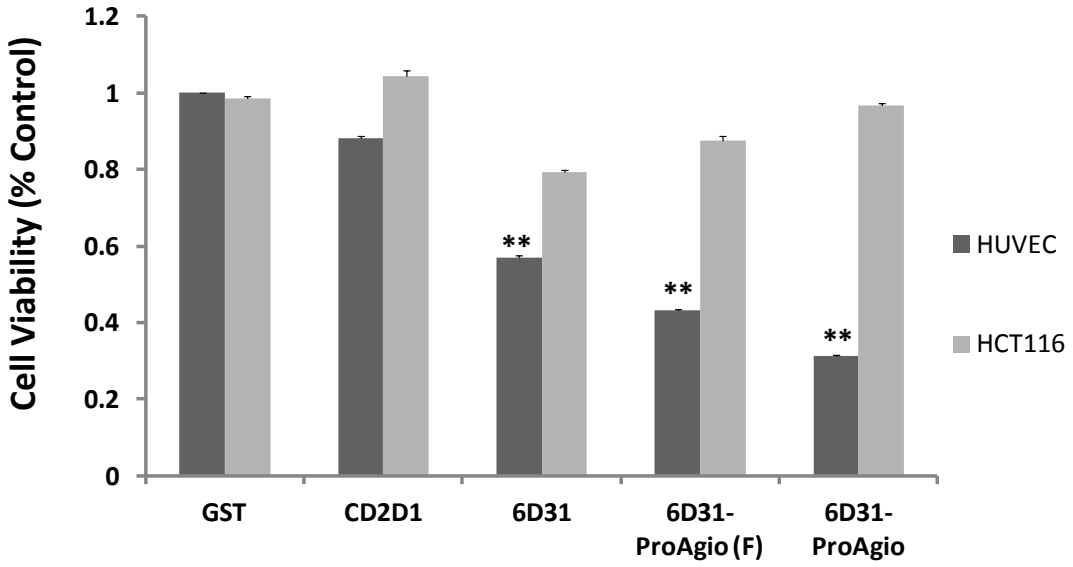

Figure 5.5 6D31-ProAgio Reduced HUVEC Viability. HUVEC were seeded into 96-well plates and treated with GST, CD2D1, 6D31, filtered 6D31-ProAgio (6D31-ProAgio (F)), and 6D31-ProAgio. All proteins were added to cells at a final concentration of 4 μM except for the filtered 6D31-ProAgio. **: 6D31-ProAgio (4 μM) versus CD2D1 (4 μM) and the filtered sample of 6D31-ProAgio (10 μM) versus CD2D1 (10 μM) showed statistically significant differences ($P < 0.05$, unpaired student's *t* test, two-tailed). P values were based on three triplicate wells. The experiment was performed only once because of limited protein solubility.

Table 5.2 Synthetic Primers for Generating ProAgio cDNA.

Mutations	Primer
D31R	5’- GATGATATTGATGAGGTG**CGA**TGGGAGAGGGGGCACC
D43K	5’- CACCCTGGTTGCCGAGTTTAA**A**AGGAAGATGAAG
DelCCAAGGCCT	5’- GAAGATGAAGCCTTTTTTGAAATCGGGAGCATTTGAGATCTTAGCAAATG

Table 5.2 Synthetic Primers for Generating ProAgio cDNA. Reactions of site-directed mutagenesis were carried out using 6D31-ProAgio cDNA as a template using indicated primers.

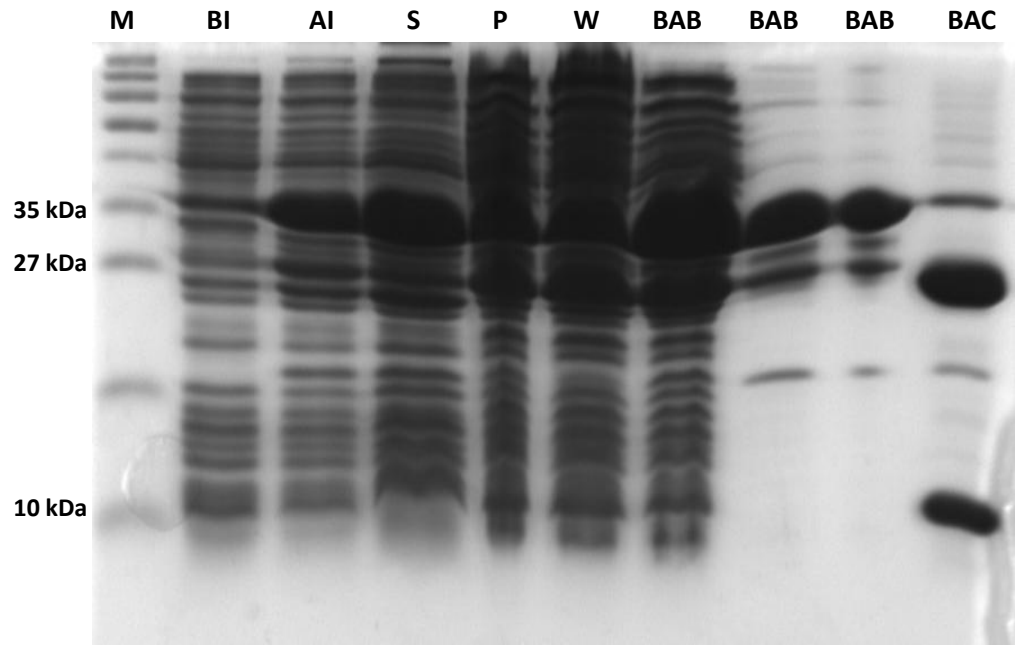

Figure 5.6 Expression and Purification of ProAgio. ProAgio was expressed as a GST fusion protein (37-kDa) in BL-21(DE3) bacteria and purified by GST 4B affinity columns. The GST tag was removed by thrombin cleavage. From left to right, each lane represented: before induction (BI), after induction (AI), supernatant of cell lysates (S), pellet of cell lysate (P), unbound waste (W), GS4B beads bound to cell lysate (BAB), GS4B beads after washed with PBS, and GS4B beads after thrombin cleavage (BAC). The 26-kDa bands shown in lane BAC represented cleaved GST, and the 10-kDa band indicated ProAgio.

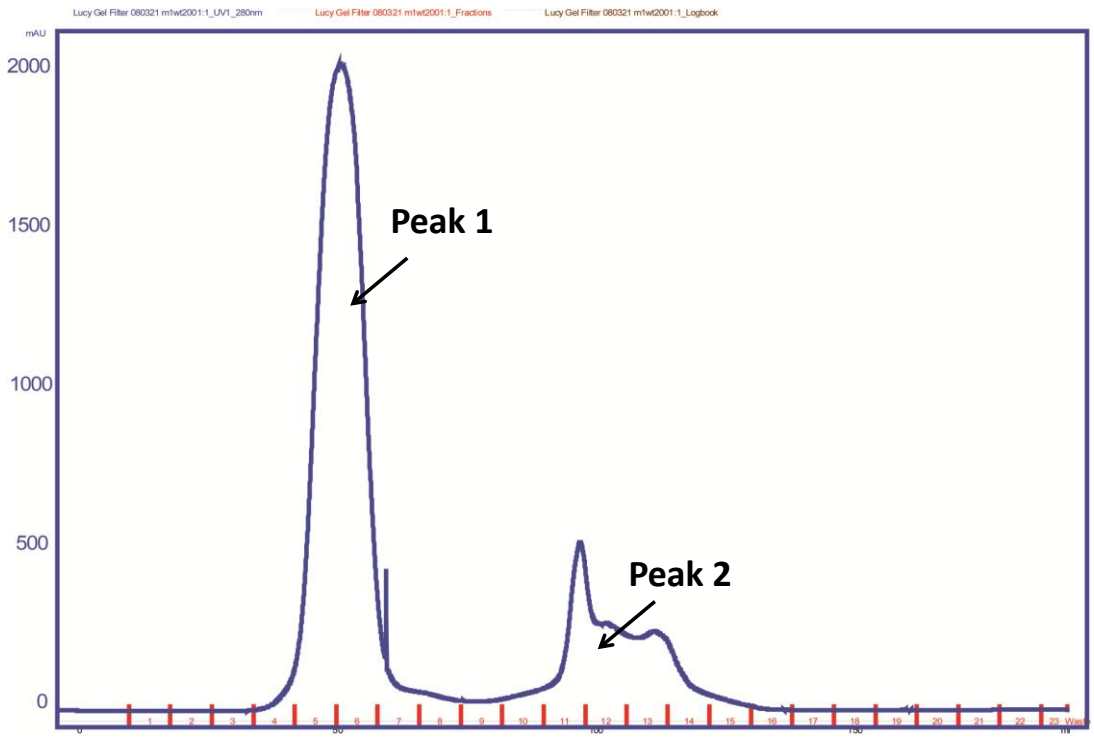

Figure 5. 7 Purification of ProAgio Using Gel Filtration Chromatography. ProAgio was eluted from GS4B column using elution buffer 10mM reduced glutathione, 50 mM Tris buffer, pH 8.0 and then subjected to gel filtration chromatography. Absorbances of eluted fractions were monitored using a UV detector at a wavelength of 280 nm. Peak 1 indicated GST eluates, and Peak 2 represents ProAgio eluates.

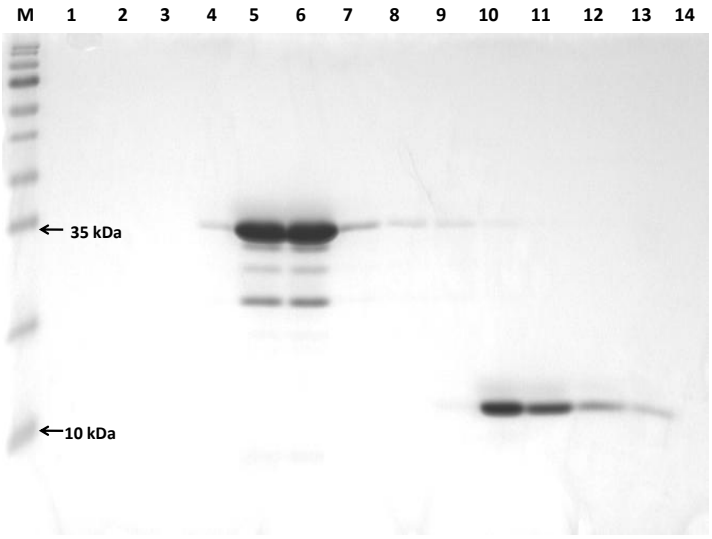

Figure 5.8 Elution fractions of ProAgio Using Gel Filtration Chromatography. Fractions (1 to 14) were examined by SDS-PAGE gel electrophoresis and coomassie blue staining. Upper bands (26-kDa) represented GST (Peak 1 in Figure 5.7). Lower bands (11-kDa) in fraction 10 – 14 were ProAgio (Peak 2 in Figure 5.7).

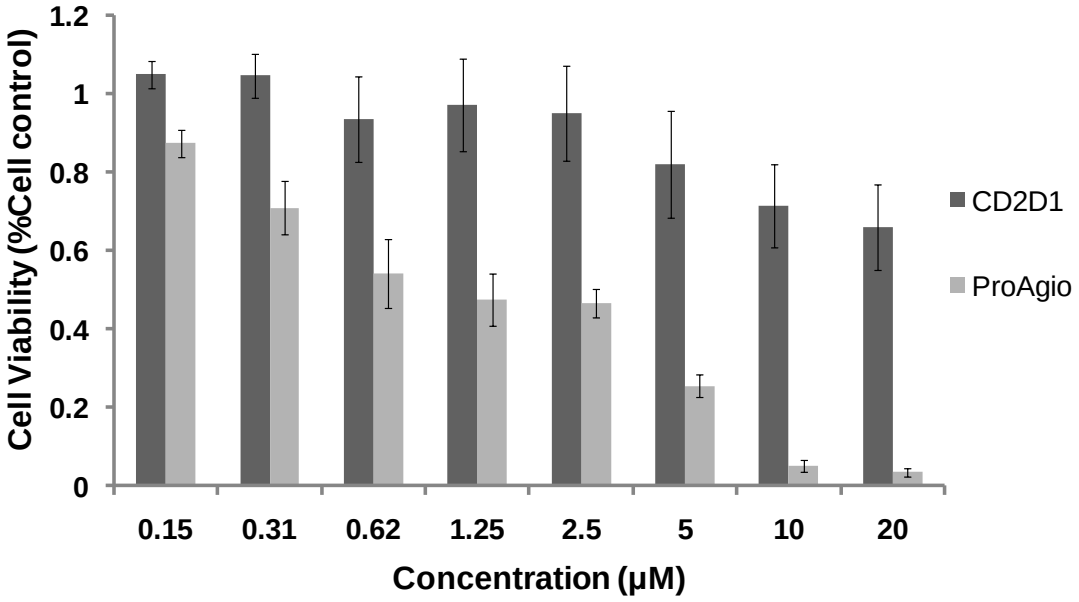

Figure 5.9 ProAgio Reduced Viability of HUVECs. HUVECs were seeded into 96-well plates and treated with CD2D1 and ProAgio at different concentration for 48 hours. A total 100 µL of ProAgio was added to each well and incubated for additional 4 hours. Viability was evaluated by the absorbance of MTT at wavelength of 490nm. The experiment was repeated three times.

Table 5.3 *Solubility Test for ProAgio.

Sample	Chemicals	Start Concentration	End Concentration	Soluble ProAgio in HEPS (µM)	Soluble ProAgio in PBS (µM)
1	NaCl	45 mM	450 mM	11.37	11.51
2	Glycerol	0.5%	5%	8.65	8.88
3	Glycerol	1%	10%	8.99	9.36
4	Sucrose	1.5%	15%	9.13	11.37
5	Lactose	0.8%	8%	7.43	11.17
6	Mannitol	0.8%	8%	8.3	8.33
7	Trehalose	1.5%	15%	10.04	10.55
8	Trehalose	0.6%	6%	16.0	16.68
	Tween 20	0.001%	0.01%		
	PEG 800	0.1%	1%		
9	Arginine	5 mM	50 mM	22.02	19.66
	Glycine	5 mM	50 mM		
	Tween 20	0.001%	0.01%		
	PEG800	0.1%	1%		

Table 5.3 *Solubility Test for ProAgio.

*Individual or a combination of sucrose, trehalose, lactose, mannitol, arginine, glutamatic acid, trehalose dehydrate, Tween 20, PEG8000 and NaCl were added to the diluted HEPES and PBS buffer solutions in a start concentrations indicated as column 3. After concentration, the end concentration of each solvent was indicated as column 4. The starting and end protein concentration using each buffer recipe were listed as column 5 and 6.

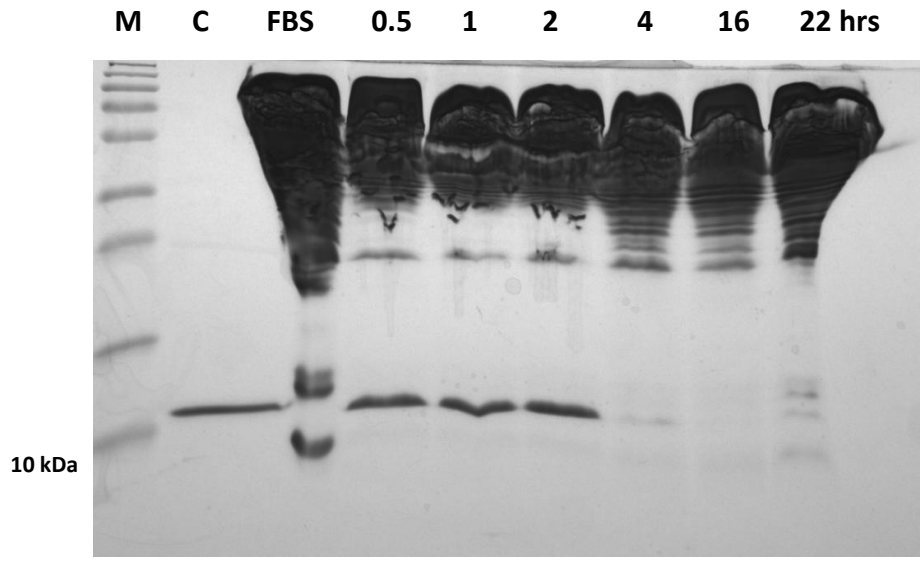

Figure 5.10 Protein Stability of ProAgio in FBS. Purified ProAgio was incubated with FBS at a 1:1 ratio (volume) at 37 ˚C for 0.5, 1, 2, 4, 16 and 22 hours. The second left lane represents the purified ProAgio without FBS, and the third lane is FBS alone. Degradation of ProAgio was started after 2 hours of incubation with FBS.

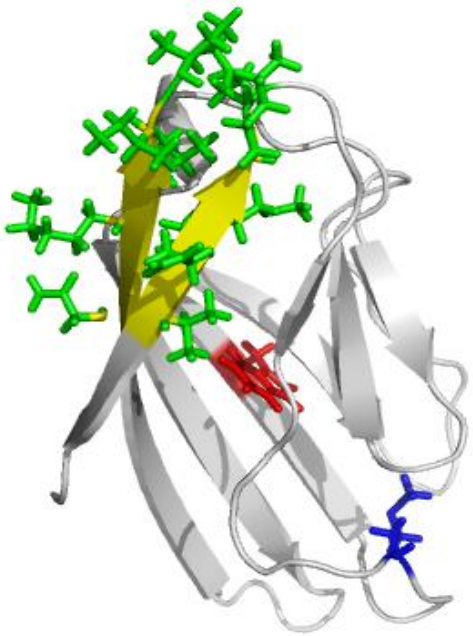

Figure 5.11 Simulated ProAgio Model for Site-specific PEGylation. The overall ribbon diagrams of ProAgio Met23Cys were built on the crystal structure of CD2D1 (PDB accession ID, 1hng). Side chains of amino acids (yellow color) involved in design of the anti-angiogenic sites are shown in green color. Trp32 and its only side chains are shown in red. Met23Cys is shown in blue. Sequences are aligned by Dr. Hsiau-Wei Lee using a computer program, Pymol.

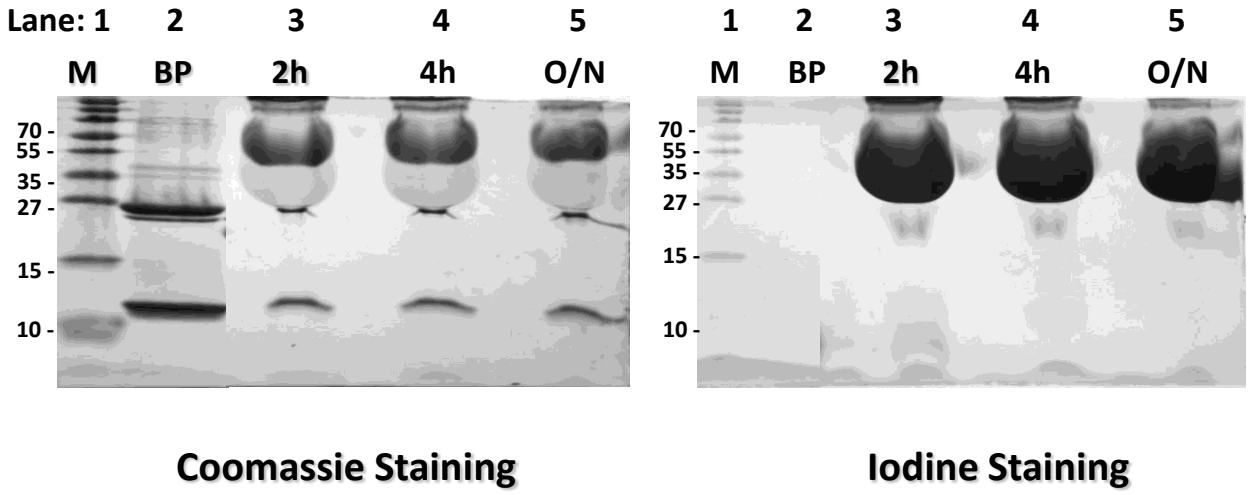

Figure 5.12 PEGylation of ProAgio.

Figure 5.12 PEGylation of ProAgio. ProAgio bearing a Met23Cys mutation were purified by GS4B affinity columns and eluted using PBS containing 500 mM L-arginine as shown in lane 2. Protein and a 20-kDa Y-shaped maleimide-PEG (one 10-kDa PEG chain in each arm) were mixed at 1:5 molar ratios. Different incubation conditions including 2 hours, 4 hours at room temperature, and overnight at 4˚C were shown in lane 3 to 5. SDS-PAGE gel was first stained with iodine isoproponol (right panel). Then it was destained by repeated wash with water, and re-stained with Coomassie staining (left panel). Iodine isoproponol stains the PEG chain, so that the right panel indicated that 2 hours at room temperature was sufficient to PEGylated ProAgio. The branched maleimide-PEG slowed down protein migration rates in SDS-PAGE gel. ProAgio-PEG bands were located between molecular markers of 55-KDa and 70-kDa (overlapped with excess maleimide-PEG in the right panel). GST has four cysteine residues, and it migrated slower than 250-kDa molecular marker. ProAgio-PEG was confirmed by Coomassie staining (left panel). Pure ProAgio-PEG protein was purified by cation-exchange chromatography as shown in Figure 3.1.SC.

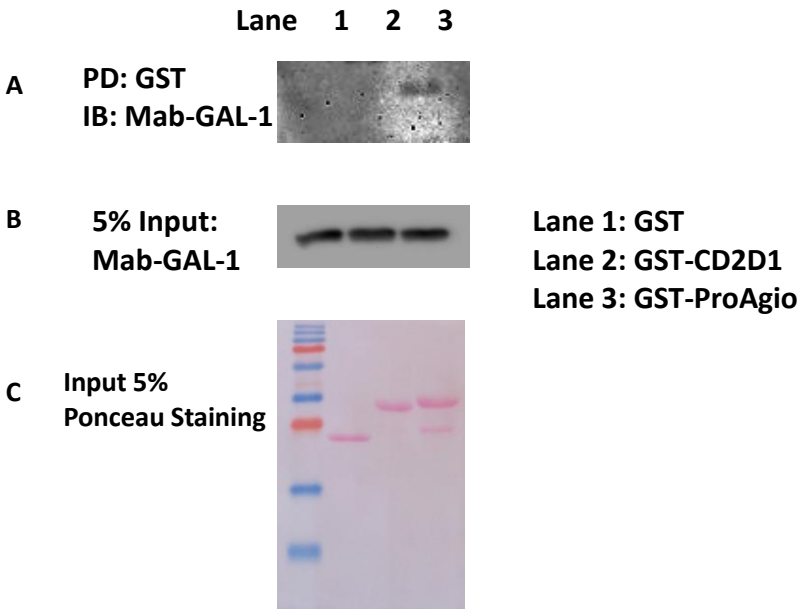

Figure 5.13 ProAgio Interacts with Galectin-1. Cell lysates from HUVECs were mixed with GST-ProAgio conjugated GS4B beads. Mixtures were incubated overnight at 4 ˚C. Panel A: Gal-1 pulled down by GST, GST-CD2D1, or GST-ProAgio conjugated GS4B beads and then detected by a monoclonal anti-Gal-1 antibody; Panel B: 5% input for Gal-1 expressed in whole cell lysate for each sample (detected by anti-Gal-1 antibody); and Panel C: 5% input for GST, GST-CD2D1, or GST-ProAgio added to each sample (detected by Ponceau staining). Lane 1: pull-down by GST conjugated GS4B beads; Lane 2: pull-down by CD2D1 conjugated GST-GS4B beads; and Lane 3: pull-down by ProAgio-GST conjugated GS4B beads.

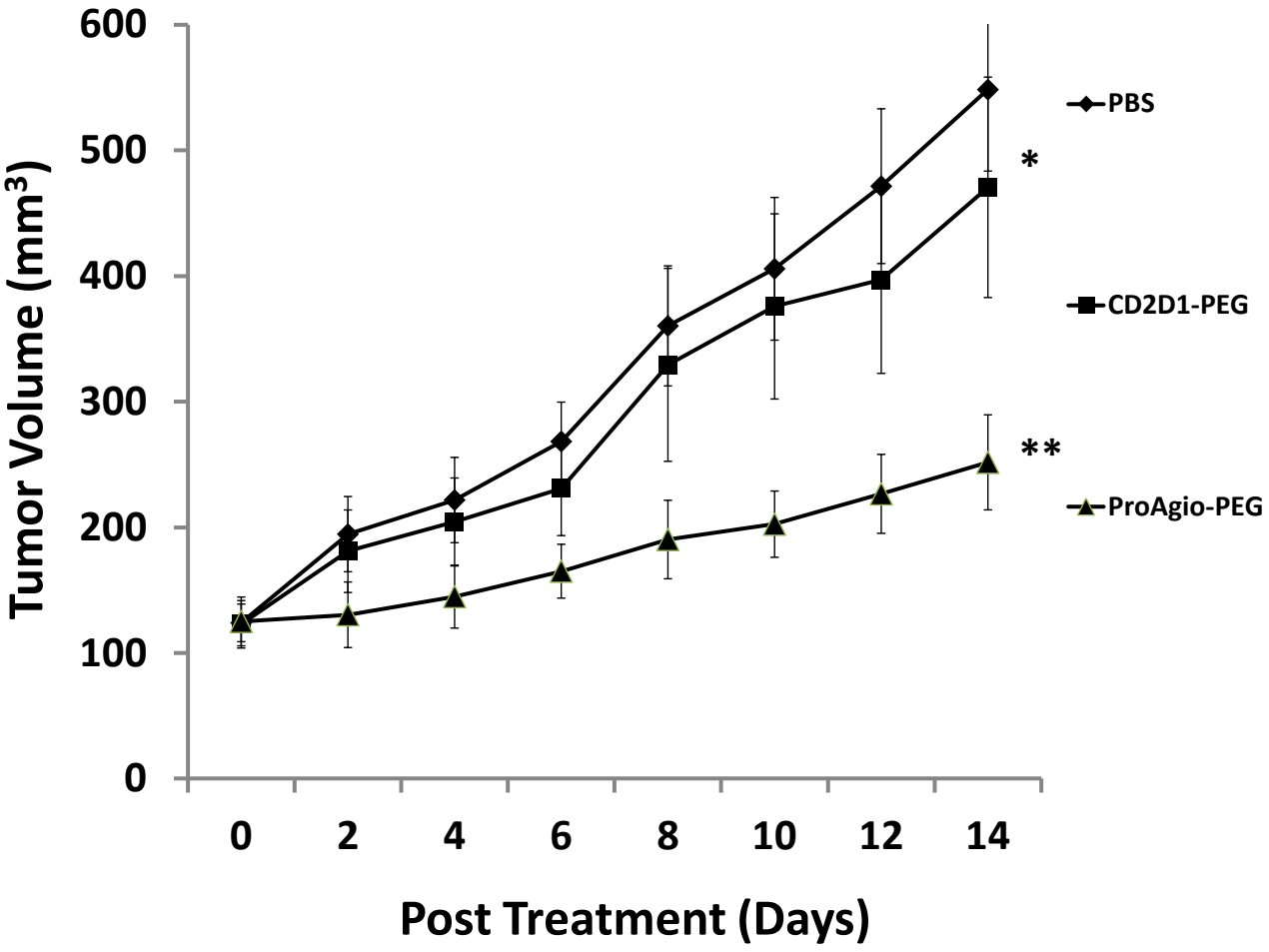

Figure 5.14A ProAgio-PEG Inhibits PC3 Xenograft Model.

Figure 5.14A ProAgio-PEG Inhibits PC3 Xenograft Model. A volume of 100 µL ($5X10^6$) PC3 cells were subcutaneously injected into nude mice. Treatments were initiated at the 4^{th} week after tumor inoculation. All agents were administered for 14 days by intraperitoneal injection (i.p.) at desired doses (buffer: 1 X PBS, pH 7.4, 200 µL/mouse/day; CD2D1-PEG: 10 mg/kg/day; and ProAgio-PEG 10 mg/kg/day). Tumor dimensions were measured using a digital caliper every other day. Tumor volume were calculated using formula: Tumor volume (mm^3) = $\pi/6$ x (length x width x height). Data were shown as mean ± S.E.. Statistic significances were evaluated using Welch's *t* test. $P < 0.05$ was considered significant.

*: CD2D1-PEG (n = 5, 10 mg/kg/day) versus Buffer treated group (n = 4) was not significantly different, $P > 0.05$.

**: ProAgio-PEG (n =5, 10 mg/kg/day) versus buffer treated group was significantly different, $P < 0.05$.

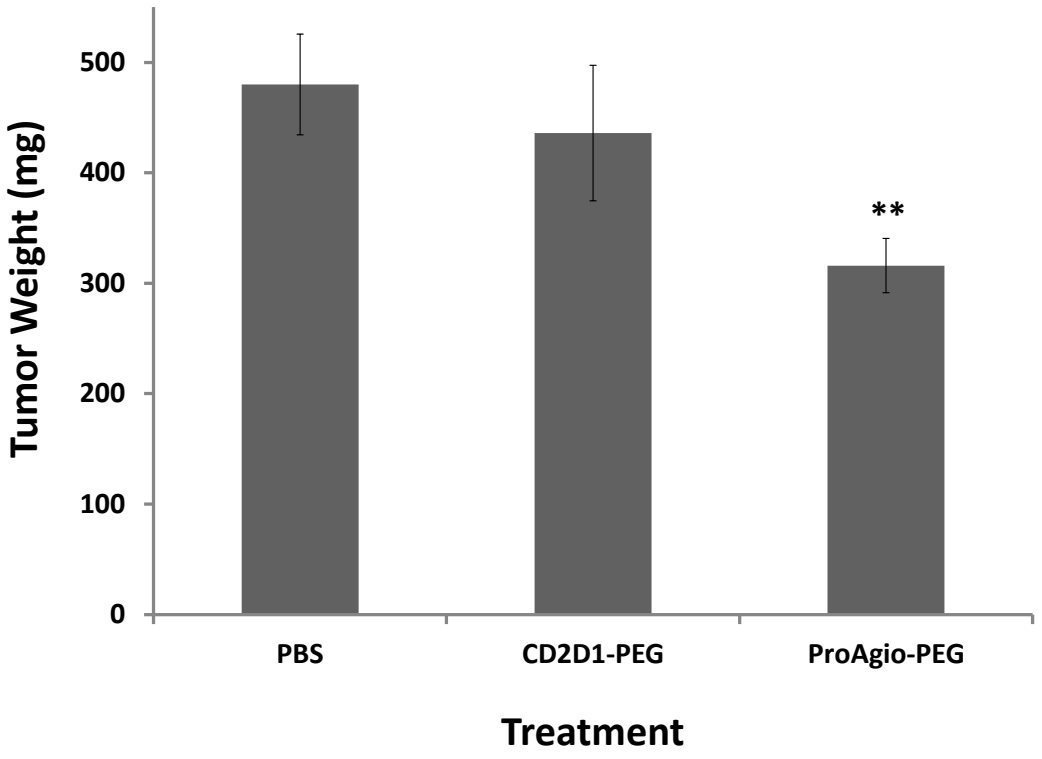

Figure 5.14B Tumor Weights of HuProAgio Treated Xenografts. A volume of 100 µL ($5X10^6$) PC3 cells were subcutaneously injected into nude mice. Treatments were initiated at the 4^{th} week after tumor inoculation. All agents were administered for 14 days by intraperitoneal injection (i.p.) at desired doses (buffer: 1 X PBS, pH 7.4, 200 µL/mouse/day; CD2D1-PEG: 10 mg/kg/day; and ProAgio-PEG 10 mg/kg/day). Tumor dimensions were measured using a digital caliper every other day. Tumor volume were calculated using formula: Tumor volume (mm^3) = π/6 x (length x width x height). Data were shown as mean ± S.E.. Statistic significances were evaluated using Student's *t* test (unpaired, two tailed). $P < 0.05$ was considered significant.

**: ProAgio-PEG (n =5, 10 mg/kg/day) versus buffer treated group (n = 4) was significantly different, $P < 0.05$.

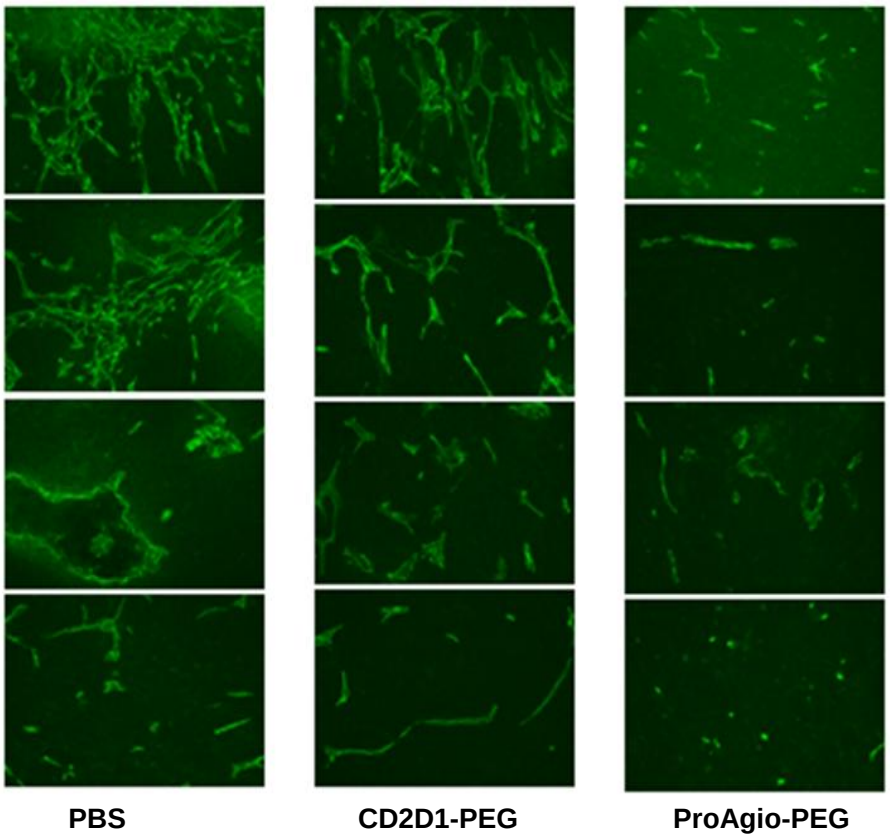

Figure 5.14C ProAgio-PEG Inhibits Xenograft Tumor Angiogenesis. Snap frozen tissue blocks were sliced into 20 µM thick sections using a cryostat. ECs were stained using a rat anti-mouse CD31 (BD Pharmingen, San Diego, CA) and a green fluorescence conjugated anti-rat IgG second antibody. This picture showed the ECpattern (labeled in green fluorescence) of microvessels in 1 X PBS buffer (pH 7.4, 200 µl/mice/day), CD2D1-PEG (10mg/kg/day), and ProAgio-PEG (10mg/kg/day) treated tumor tissues.

CHAPTER 6

CONCLUSION AND SIGNIFICANCE

6.1 Design Approach and Model Structure

Based on important structural features of endogenous anti-angiogenic proteins and peptides, we developed a *de novo* designed protein agent that inhibits tumor angiogenesis.

As reviewed in section 1.9.5, many endogenous anti-angiogenic proteins and peptides such as PF4, endostatin, and TSP-1 peptides share several characterized structures within areas of β-sheets. First, these β-sheet regions are composed of anti-parallel β-strands consisted with amino acids arranged by alterations between charge/polar and hydrophobic residues. Second, side chains of charge/polar amino acids are located on the opposite surface to that of hydrophobic residues. Last, most charged residues are lysines and arginines forming a positive-charged and solvent-exposed surface on the β-sheet region or on the whole protein surface. Furthermore, investigations performed with PF4, endostatin, TSP-1, and other extracellular matrix proteins have demonstrated that anti-angiogenic effects of these proteins depend on only small fragments of these proteins. These evidences led us to the hypothesis of designing and developing novel protein agent by crafting small anti-angiogenic peptides into a stable parental β-sheet protein domain.

Our designed protein models were described extensively in sections 1.10 and 4.2, separately. Both Figure 1.4 and 3.1 illustrated the computational simulated structure of our designed protein agent, ProAgio. Two peptides (TVQMKL and NLKVII) derived from endogenous anti-angiogenic proteins can mimic all three important structural features summarized as above

if they pair with each other to form a β-sheet structure. It was a challenge to choose a suitable protein to host these two peptides in order to maintain the specific β-sheet characters. The extracellular domain 1 of rat CD2 molecule, CD2D1 was chosen as the parental protein. This 99-amino-acid protein domain has been well studied and expressed using bacterial expressing systems. A total of 9 strands composed of this stable β-sheet protein with a solved 3D structure as introduced in Chapter 1. Within the 9 β-strands, the two anti-angiogenic peptides (TVQMKL and NLKVII) that mimic the β-sheet regions of endogenous anti-angiogenic proteins were crafted into N- and C- terminal β-strands of CD2D1, separately. Mutagenesis studies were performed using a cDNA of CD2D1 to achieve mutations listed in Table 1.1. The simulated 3D structure showed in Figure 3.1 clearly predicted that amino acids of TVQMKL in the N-terminus will pair with those of NLKVII in the C-terminus to produce a β-strand pair that stabilized these two short sequences.

Since β-sheet features are critical for the crafted peptides to inhibit angiogenesis, it is important to examine whether or not our designed protein, ProAgio forms a stable structure as predicted. Solving the unknown 3D structure of a protein requires complicated techniques such as NMR spectroscopy or X-ray crystallography. In our case, since the parental CD2D1 has a solved 3D structure, the comparison between 1D ^{1}H-NMR spectra of CD2D1 and ProAgio will be sufficient to support the predicted 3D structure. For this purpose, 1D ^{1}H-NMR spectra of bacterial expressed ProAgio was examined and compared with that of its parental protein, rat CD2D1. As shown in Figure 3.S1B, the aromatic amino Trp32 and another residue Val78 located in the hydrophobic core region of ProAgio formed same peaks as those of rat CD2D1, which indicated that the hydrophobic core region of ProAgio was well formed. The overall similarity be-

tween these two spectra suggested that rat ProAgio retains a similar fold as that of CD2D1. The differences between these two spectra in regions of 0.0 – 1.5 ppm showed that there were side chain changes, which was expected because there were a total of 8-amino-acid mutations.

6.2 ProAgio inhibits EC Proliferation and Tube Formation

In Chapter 3 and 4, evaluations of the drug effects using different *in vitro* bio-assays and a human PC3 tumor xenograft model in nude mice clearly demonstrated that our designed protein agent, ProAgio is a potential candidate for inhibition of tumor angiogenesis.

ECs are "building blocks" for the inner layer of blood vessels, so that EC proliferation is a prerequisite for the occurrence of angiogenesis. Different bio-assays such as cell counting, MTT, [^{3}H]thymidine, and BrdU assays that measure proliferation/viability rates of cultured ECs have been applied as major tools to evaluate of *in vitro* effects of pro- or anti- angiogenic agents (reviewed in [346, 347]). Usually a combination of two or more different methods will give more reliable conclusions. Two different methods including MTT and BrdU assays were used to evaluate the *in vitro* effect of ProAgio. MTT assays reflect the cell number, while BrdU assays measure DNA synthesis during the S-phase of cell cycles.

More than 19 kinds of primary ECs from different adult tissues are commercially available now as reviewed in reference [347]. ECs of different origins tend to behave differently, and primary cultured ECs are expensive and difficult to be maintained [348]. To date, HUVECs are still widely used ECs in *in vitro* angiogenesis bio-assays (reviewed in [347, 349]). Commercially available primary HUVECs were purchased and maintained in our laboratory as introduced in

2.1. Since HUVECs are primary cells that become senescent when cultured in medium, only HUVECs within 3 – 9 passages were used for *in vitro* assays.

As shown in Figure 3.1B, it was clear that ProAgio significantly reduced proliferation rates of HUVECs (72% reduction at concentration of 5 μM compared to cells treated with buffer controls). The inhibitory effects were further evaluated using MTT cell viability assays showing that IC_{50} of ProAgio was 2.6 μM. IC_{50} is an important indicator for drug efficacy, so that values of several most characterized anti-angiogenic protein or peptide agents reviewed in Chapter 1 were discussed in order to compare them to ProAgio. Avastin is a FDA approved monoclonal antibody that specifically neutralizes VEGF [138]. Wang and coworkers reported that avastin inhibited VEGF induced EC proliferation with an EC_{50} of 0.36 nM. Endostatin inhibits proliferation of HUVECs with IC_{50} values between 4 – 390 nM [208, 350, 351]. Another endogenous anti-angiogenic protein, angiostatin inhibits bovine capillary endothelial cells with an IC_{50} of 135 nM [222]. A 33-amino-acid β-sheet peptide inhibits proliferation of HUVECs with an IC_{50} of 2.5 μM, while its 11-amino-adic peptide derivative, 6DBF7 has an IC_{50} of 15 μM [281, 286]. Compared to these listed values, the inhibitory efficacy of ProAgio was comparable to peptides but less than these of avastin and endogenous proteins.

The IC_{50}/EC_{50} values drew from *in vitro* bio-assays for proteins or peptides are difficult to predict actual *in vivo* effects because each protein has unique molecular weight, 3D structure, resistance to protease degradation, and tissue penetration. Although ProAgio has weaker *in vitro* effects than other endogenous proteins and avastin in inhibition of EC proliferation, it is not necessary that the *in vivo* effects of ProAgio would not be comparable to these of avastin or

endogenous proteins. The *in vivo* effects of ProAgio were tested and compared to that of avastin, which will be discussed in this Chapter.

In addition to inhibition of EC-proliferation, ProAgio also reduced the ability of HUVECs to form endothelial tubes *in vitro*. In 1989, Lawley and Kubota found that HUVECs and human dermal microvascular ECs seeded onto the surfaces of matrigel coated cell-culture plates underwent morphologic change and differentiated into capillary-like tubes [352]. Unlike EC-proliferation and migration assays that focus on only one aspect of ECs, endothelial tube formation assay has become a popular *in vitro* angiogenesis assay that partially simulates the process of *in vivo* capillary formation. As reviewed in section 1.2, angiogenesis is a multi-step process that involves in a cascade of events such as EC-proliferation, migration toward chemoattractant, attachment, and formation of tubules. Since capillary structures are usually observed within 8 – 12 hours when a tube formation assay is performed, it mainly assesses EC-migration, attachment, and formation of tubules [352].

Besides ECs, the other major components of tube formation assay are matrices, such as fibronectins, collagens, and matrigels (reviewed in [347]). Matrigel potently induces ECs to form endothelial tube, and is composed of solubilized extracellular and basement membrane proteins extracted from Engelbreth-Holm-Swarm (EHS) sarcoma, a mouse tumor that rich in extracellular matrices [352]. Donovan and coworkers showed that a type of growth factor reduced (GFR) matrigel containing lower levels of cytokines and growth factors can avoid overstimulation of ECs that associates with standard matrigel [353]. In addition, they demonstrated that not only ECs but primary human fibroblasts and several non-EC human tumor cell lines in-

cluding MDA-MB (metastatic breast carcinoma), U87-MG (glioblastoma), and PC3 (human metastatic prostate carcinoma) also formed endothelial tubes on GFR matrigel [353].

In our animal studies, a human PC3 cell line was used to generate nude mice xenograft models. It has been shown that tumor angiogenesis not only predicts pathologic stage but also correlates with tumor metastasis of clinical prostate carcinomas [354, 355]. Ravindranath and coworkers found different level of VEGF expression in normal prostate, benign and malignant prostatic tumors, and cultured prostatic carcinoma cell lines including PC3 cells [356]. In order to simulate angiogenesis in PC3 tumors, we used HUVECs co-cultured with PC3 cells to perform tube formation studies. ProAgio dramatically reduced the amount of tubule formed and total tubular lengths under 5 X Objective fields in HUVECs and PC3 co-culture ($P < 0.001$, unpaired student's *t* test, two-tailed), as shown in Figure 3.1D. It also showed that the control drug, avastin, also inhibited the formation of tubules and tubular counts under the same experimental conditions. It has been demonstrated that avastin inhibits VEGF-stimulated formation of endothelial tubules [357]. Since avastin is a humanized anti-VEGF monoclonal antibody, avastin may neutralize VEGFs secreted by PC3 cells, therefore, inhibited ECs to form tubules. ProAgio, in the other hand, might inhibited tube formation by reducing the ability of ECs to migration or attach to each other. These findings indicated that ProAgio has potential to inhibit tumor angiogenesis.

Our preliminary data (not shown) indicated that ECs suspended in growth factor and FBS-deprived culture medium can form endothelial tubes after they were seeded on GFR-matrigel, but these capillary structures were quickly dismissed because by shrinkages of EC-formed branches. The possible reason might be that growth factor and serum-deprivation pro-

motes EC-apoptosis or reduced EC-migration. When a low concentration of FBS (2%) was added into the culture medium, ECs formed well-structured tubules. This condition was applied to tube formation studies used a co-culture of HUVECs and PC3 cells.

6.3 PEGylation of ProAgio

PEGylation is a process that covalently conjugates PEG polymeric chains to other molecules (reviewed in [344]). It has been widely adapted in bio-medical field, especially in modification of proteins and peptides. The most common PEG chains are ethylene oxide polymers. PEG chain casts a “mask” on the surface of the conjugates, and each ethylene oxide unit in PEG binds water molecules. Due to these characters, linkage of water soluble PEG chains to proteins or peptides not only increases their molecular sizes, but also provides many advantages including: i) preventing immunogenicity, ii) reducing renal filtration, iii) resisting protease degradation, iv) changing bio-distribution, and v) increasing stability and solubility (reviewed in [358]). Therefore, PEGylation is an important tool to improve PK/PD parameters of therapeutic protein and peptide drugs.

A PEG polymer has to be prepared into a derivative with an activate functional group that reacts with specific amino acids. Depending on the different types of functional group, PEG chains can be coupled to N-terminal amino group, lysine, arginine, aspartic acid, histidine, cysteine, C-terminal amino group, and others (reviewed in [344]). Most proteins are abundant in lysines, so that conjugating PEGs to –NH2 group of lysine and arginine is a commonly used PEGylation method. Bell and colleagues compared the impacts of different PEGylation methods on the biological activity of IFN-α2, a 20-kDa cytokine used for treatment of viral infection and

inhibition of tumor growth [359]. They concluded that a single 20- or 40-kDa maleimide-PEG coupled to a Met111Cys mutant of IFN-α2 is significantly more efficient in increasing protein half life and retaining anti-tumor activity than lysine- or histine-PEGylation [359].

For above reasons, a cysteine PEGylation site was introduced by a Met23Cys mutation in ProAgio. Because no native cysteine residues exist in ProAgio, this single mutation allowed site-specific PEGylation of ProAgio. A simulated model structure of Met23Cys-mutated ProAgio without PEG was illustrated in Figure 5.12 and introduced in section 5.8. The cysteine-PEGylated protein, ProAgio-PEG was highly soluble in PBS, pH 7.4. It was later used for animal studies.

Proteins PEGylated with long PEG chains migrated slower than these without PEGylation [359, 360]. The molecular weight (MW) of unmodified ProAgio is 11-kDa. After conjugated to a Y-shaped 20-kDa maleimide-PEG, the apparent MW of ProAgio-PEG was indicated between 55 – 70-kDa as shown in Figure 5.12, which was confirmed by iodine-staining of the PEG chain and coomassie protein staining. After it was further purified, the apparent MW remained consis-tently at the same location as shown in Figure 3.1SC.

6.4 ProAgio Inhibits Growth and Angiogenesis of Xenograft Tumors

Since tumor growth is dependent on angiogenesis, xenograft tumors have become a type of commonly used method to investigate tumor growth and angiogenesis [16-18]. There are several advantages to use xenograft models. First, the growth of subcutaneously-grown tumors in immunocompromised mice is easy to be monitored. Second, tumor xenografts can be easily dissected and used to evaluate tumor angiogenesis by different EC surface-marker stain-

ing techniques. Third, it allows studying drug uptakes and distribution. Pre- and clinical data has showed that tumor angiogenesis contributes to the pathogenesis of prostatic carcinoma, so that in this study the inhibitory effects of ProAgio were examined using a PC3 xenograft nude mice model [354-356].

Our preliminary data indicated that compared to buffer (PBS, pH 7.4) control-treated group, treatment with ProAgio-PEG (10 mg/kg/day) significantly inhibited the growth and angiogenesis of PC3 xenografts as shown in Figure 5.14A-C. Next, we examined the anti-tumor efficiency of the non-PEGylated ProAgio and the dose-dependence in ProAgio-PEG-treated groups. The mean tumor mass for each treatment group (n = 6) was measured on the 20^{th} day after the initial dose, and was statistically analyzed using AVONA (one way) Post Hoc tests. Treatment with the non-PEGylated ProAgio (5 mg/kg/day) resulted in a 45.72% ($P < 0.05$) reduction rate in tumor mass, indicating that ProAgio significantly inhibited tumor growth of PC3 xenografts. When the PEGylated protein was considered, the end-point mean tumor mass for treatments with ProAgio-PEG at a low dose (2.5 mg/kg/day) showed no significant difference ($P > 0.05$) from that of the buffer-treated group as shown in Figure 3.2B. Treatments with ProAgio-PEG at 5 mg/kg/day and 10 mg/kg/day strongly inhibited tumor growth compared to the buffer-treated group, resulting in 36% ($P < 0.05$) and 65% reduction ($P < 0.01$) in tumor masses, separately (shown in Figure 3.2B). Thus, it demonstrated that PC3 xenografts responded to ProAgio-PEG treatments in a dose-dependent manner. These statistic analyses indicated that the effective dose for ProAgio and ProAgio treatment is 5 mg/kg/day in nude mice models.

In this study, treatments with ProAgio and ProAgio-PEG at 5 mg/kg/day for 20 days resulted in a mean end-point tumor mass of 243.33 ± 53.14 mg and 285 ± 59.99 mg, separately,

which suggested no significant differences between these two groups. The tumor growth curves shown in Figure 3.2A also exhibited no differences. It has been shown that PEGylation has a tendency to decrease *in vitro* protein bio-activities (reviewed in [358]). ProAgio-PEG was site-specifically PEGylated in a cysteine residue, a method that has less impact on protein functions than non-specific ones [359]. The overall anti-angiogenic effect of ProAgio-PEG was expected to be less than that of ProAgio because the coupled PEG chain may mask the protein surface. *In vivo* effects, however, are not solely determined by *in vitro* bio-activities. One of the advantages of PEGylation of ProAgio was to improve PK/PD parameters, thus it may have equal-to-better *in vivo* effects compared to these of the non-PEGylated protein. Because ProAgio-PEG has longer circulating retention time compared to ProAgio, it is possible that increasing treatment course will demonstrate differences in anti-tumor efficiencies between these two proteins. Even if ProAgio showed better tumor-inhibitory effects, we still expect to use humanized ProAgio-PEG as a therapeutic agent in clinical studies due to protein solubility and less immune responses.

It is important to compare our designed protein agents directly to VEGF/VEGFR inhibitors, the most widely used category of anti-angiogenic agents. Therefore, animal studies were performed in order to compare treatments with ProAgio-PEG (20 mg/kg/day) to avastin (20 mg/kg/twice weekly) for 20 days. The reason for using avastin as a positive control was mainly because avastin is a protein drug that has been approved by FDA for the treatment of several types of solid tumors (reviewed in section 1.7.1.1.1). The circulating half-life for avastin is 23.1 days, so that avastin is commonly distributed in an interval of twice weekly [138]. Daily administration of ProAgio-PEG was determined by referring to circulating half-lives of literature-

reported PEGylated proteins. Proteins coupled with different length of PEG chains vary in circulating half-lives. Baker and coworkers reported that PEGylation of INFβ1, a 20-kDa cytokine coupled with a 20-kDa maleimide-PEG increased the protein circulating half-life from 0.98 minutes to 13 hours [360]. Rosendahl and colleagues showed that the half-lives of IFN-α2 were 22, 34, and 32 hours when it was modified with 10, 20, and 40-kDa maleimide-PEGs, separately [359]. ProAgio is an 11-kDa protein; therefore, we speculated that when it was coupled with a 20-kDa maleimide-PEG, its circulating half-life would be 13 – 30 hours. Thus a daily dose was necessary to maintain its ED_{50} *in vivo*.

When the end-point tumor masses were compared, both treatments with ProAgio-PEG and avastin dramatically reduced tumor masses ($P < 0.01$), while treatments with the buffer control and the parental protein (CD2D1-PEG, 20 mg/kg/day) showed no statistic significances. Treatment with ProAgio-PEG (20 mg/kg/day) for 20 days resulted in a 68% reduction rate in tumor mass, which was slightly higher than that of avastin (59%). As discussed above, the end-point tumor mass reduced 65% when mouse were treated with ProAgio-PEG at 10 mg/kg/day. In addition, when tumor growth curves for ProAgio-PEG (20 mg/kg/day), ProAgio-PEG (10 mg/kg/day), and avastin (20 mg/kg/twice weekly) were compared (shown in Figure 3.2A and 3.2C), it suggested that ProAgio-PEG achieved the same level of anti-tumor effect as avastin did at 10 mg/kg/day; however, it is an indirect comparison because of differences in circulating half-lives and anti-angiogenic mechanisms.

Cluster of differentiation 31 (CD31), also known as platelet endothelial cell adhesion molecule-1 (PECAM-1) is one of the major components in EC intercellular junctions [361]. Immunohistochemical staining of CD31 has been a useful method for identification of vasculatures

in different human and mouse tissues including tumors [362-364]. In order to determine the anti-angiogenic effects from treatments with our designed protein agents, CD31 IF-staining patterns of above tumor tissues dissected from different treatment groups were analyzed and data were listed in Table 3.1A and 3.1B. Three indicators including mean vessel length, mean vascular density (MVD), and mean branch points were statistically analyzed using unpaired student's *t* tests (n = 6, two-tailed). The treatment with the non-PEGylated ProAgio (5 mg/kg/day) resulted in a 65% reduction rate ($P < 0.05$) in mean vascular length and an 83% reduction rate ($P < 0.05$) in branch points in PC3 xenografts, which were significantly different from these treated with the buffer control. The MVD, however, failed to be effectively reduced by the treatment of ProAgio at 5 mg/kg/day (12.16 ± 1.75/counted-field) compared to buffer-treated group (15.83 ± 1.78/counted-field). The treatment with ProAgio-PEG at 5 and 10 mg/kg/day resulted in 36% ($P < 0.01$) and 46% ($P < 0.01$) reductions in MVD, separately. In addition, treatments with ProAgio-PEG not only substantially reduced mean vessel lengths and MVDs, but also dramatically inhibited the formation of new vascular branches. Reduction rates in branch points/counted-field for 2.5, 5, and 10 mg/kg/day of ProAgio-PEG treated xenograft groups were 30% ($P = 0.23$), 72% ($P < 0.05$), and 80% ($P < 0.01$), suggesting a strong dose-dependent effect. Angiogenesis is the process that new blood vessels form from existing ones, so that these statistic analyses demonstrated that our designed agents significantly inhibited tumor growth by preventing the occurrence of angiogenesis.

The anti-angiogenic effects of avastin (20 mg/kg/twice weekly), CD2D1-PEG (20 mg/kg/day), and ProAgio-PEG (20 mg/kg/day) were compared by statistic analyses of CD31 IF-staining patterns of tumor tissues from each treatment groups as indicated in Figure 3.2C and

Table 3.1B. Treatment with CD2D1-PEG (20 mg/kg/day) did not affect the mean vessel length, MVD, and mean branch points in tumor tissues. The treatment with ProAgio-PEG (20 mg/kg/day) resulted in a dramatic reduction rate in mean vessel length (80%, $P < 0.01$), MDV (65%, $P < 0.0001$), and near complete elimination of branch points (95%, $P < 0.0001$). Same as indicated by the mean end-point tumor mass, treatment with avastin (20 mg/kg/twice weekly) resulted in reduction rates of 58% ($P < 0.01$) in mean vessel length, 46% ($P < 0.05$) in MVD, and 73% ($P < 0.05$) in mean branch points, which were at the same levels as these of ProAgio-PEG (10 mg/kg/day) treated group (reduction rates of 67%, 46%, and 81% for mean vessel length, MVD, and mean branch points, separately).

In summary, the treatment with ProAgio (5 mg/kg/day) significantly inhibited tumor growth and angiogenesis in PC3 tumor xenografts. Treatments with ProAgio-PEG from 2.5 to 10 mg/kg/day showed dose-dependent anti-tumor and anti-angiogenic effects *in vivo*. A dose of 10 mg/kg was expected to be the optimal dose for future studies in nude mice models. Tumor growth and angiogenesis were inhibited at the same levels for treatments with 10 mg/kg/day of ProAgio-PEG and avastin 20 mg/kg/twice weekly. At 20 mg/kg/day, ProAgio dramatically inhibited tumor growth and near completely reduced tumor angiogenesis. These studies demonstrated that our design approaches have great potentials to be applied in the development of anti-angiogenic protein agents.

6.5 Targeting Mechanisms of ProAgio

As shown in Figure 3.1B, and 3.1C, ELISA assays using anti-BrdU antibody demonstrated that ProAgio inhibited proliferation of ECs but not that of a type of epithelium-original cells,

M4A1 (breast cancer). Compared to traditional cytotoxic drugs, targeting endothelial cells is one of the major advantages for anti-angiogenic agents. It is commonly reported that endogenous anti-angiogenic proteins and peptides specifically inhibit the growth of ECs, but the targeting mechanisms remain elusive (reviewed in [21, 196, 240, 365]). Galectin-1(Gal-1) belongs to a family of lectins with a conserved carbohydrate recognition domain (CRD) [366]. Gal-1 regulates a wide range of cellular processes including cell growth, migration, adhesion, invasion, and apoptosis (reviewed in [367]). As demonstrated by pull down assays, Gal-1 is a potential anti-angiogenic target for ProAgio.

ProAgio interact with Gal-1 expressed in HUVECs, whereas CD2D1 did not as shown in Figure 3.4. Over-expression of Gal-1 has been observed in a number of different types of tumor stroma, such as colon [368], lung [369], pancreas [370, 371], bladder [372], and prostate cancers [373]. Studies have suggested two major mechanisms of how Gal-1 contributes to tumor progression. First, Gal-1 promotes tumor metastasis by enhancing the cell-cell adhesion between tumor cells and ECs [374-377]. Second, Gal-1 facilitates tumor cells to escape from immune responses through immuno-suppressive functions [378, 379]. In addition to these two mechanisms, Thijssen and co-workers by using a Gal-1-null (Gal-$1^{-/-}$) mice model demonstrated that Gal-1 plays an essential role in promoting tumor angiogenesis, and it is a target for a synthetic anti-angiogenic peptide, anginex [345]. Since ProAgio interacts with Gal-1, it is possible that ProAgio exerts anti-angiogenic function via inhibition of Gal-1.

Gal-1 is a major immune-modulator that maintains T-cell homeostasis and survival by inhibiting T-cell activation [380], promoting cell-cycle arrests and apoptosis of activated but not quiescent T-cells [381-385], and reducing the secretion of IL-2 and IL-10 [383]. Since blockage of

Gal-1 expression inhibited tumor growth, studies suggested that Gal-1 promotes apoptosis of tumor-infiltration T-cells, resulting in immune suppressive environments that protect tumor cells from immune responses [378, 379]. Moreover, Zhou and coworkers demonstrated that cytotoxic T lymphocytes (CTLs) specifically kill proliferating ECs, which strongly inhibits tumor angiogenesis [386]. Therefore, inhibiting the immunosuppressive function of Gal-1 may be counted as one of the anti-angiogenic mechanisms for ProAgio. This theory can be applied to clinical patients or animal models with normal T lymphocytes except for the nude mice models that were used to study the *in vivo* activities of ProAgio in the present work. Because nude mice do not have thymus nor do them produce functioning T-cells, enhancing the function of CTLs cannot explain the anti-angiogenic function of ProAgio in these animal studies. Several similar nude mouse models have been used to prove anti-angiogenic effects of anginex, the synthetic peptide targeting Gal-1.

Based on previous studies, several signal pathways are speculated to explain possible anti-angiogenic mechanisms of ProAgio involved in these animal cases. Gal-1 is a typical cytoplasmic protein, but it is also exported to ECM [387-390]. Cytoplasmic Gal-1 has different binding partners from extracellular Gal-1. Firstly, the extracellular Gal-1 functions as a β-galactoside-binding protein with different affinities to various glycosylated cell surface receptors and ECM proteins (reviewed in [367]). It increases cell adhesion and migration capabilities of different types of cells [375-377]. As reviewed in section 1.2, EC migration and adhesion are critical processes required for angiogenesis, which can be evaluated by *in vitro* EC tube formation assays. ProAgio inhibited HUVECs to form endothelial tubules as shown in Figure 3.1D and discussed in section 6.2, so that ProAgio may inhibit angiogenesis by disrupting the interaction be-

tween Gal-1 and integrins. ProAgio may dissociate or prevent Gal-1 from interacting with integrins expressed in ECs, resulting in reduced EC adhesion and migration. Secondly, the cytoplasmic Gal-1 binds to H-Ras-GTP in a glycosylation-independent manner [391]. In human tumor cells, the cell-membrane-anchored H-RAs-GTP recruits cytoplasmic Gal-1 to form a stable complex that subsequently activates Raf-MEK-ERK pathway [392, 393]. It has been shown that tumor ECs in F9 teratocarcinoma and B16F10 mouse melanoma planted in $gal^{-/-}$ mice uptake Gal-1 secreted by these tumor cells [394]. ECs cultured *in vitro* also uptake Gal-1, which subsequently promotes EC proliferation and migration through activation of Raf-MEK-ERK pathway [394]. We have confirmed that ProAgio inhibited EC-proliferation. The anti-proliferative mechanism of ProAgio may lie on inhibition of ECs from uptaking extracellular Gal-1. Alternatively, ProAgio may be accompanied Gal-1 to enter ECs, blocking Gal-1 to be recruited by H-Ras-GTP, resulting in blockage of the Raf-MEK-ERK pathway.

6.6 Humanized ProAgio for Therapeutic Applications

The parental protein for ProAgio is the extracellular domain 1 part of rat CD2D1 (refer to 1.10.4). Table 4.1 compared amino acid sequences and side chain directions in these two proteins. The human counterpart of CD2D1, huCD2D1 forms a same 3D structure as rat CD2D1, but it is N-glycosylated. Because N-glycan is critical to the folding and stability of huCD1D1, expression of huCD2D1 requires either mammalian expression system or mutations that abolish the N-glycosylation site (refer to section 4.2.3). Compared to human CD2D1, rat CD2D1 is a non-glycosylated protein so that expression and purification of rat CD2D1 is more convenient and cost efficient in laboratory settings [300, 336, 338]. More importantly, the expressed rat CD2D1

is stable with many detailed structural studies on different site-mutations and insertion [298, 308, 311, 395]. For these reasons, rat CD2D1 was used to demonstrate our design approach and protein was expressed in a small scale for *in vitro* and *in vivo* studies shown in Chapter 3 and 5. As discussed in section 4.1.1, ProAgio was re-designed using the first 104-amino-acid fragment of human CD2 (huCD2$_{1\text{-}104}$) as the parental host protein. The detailed design strategy was listed in section 4.2.2. The re-designed protein was denoted as huProAgio in order to be differentiated from ProAgio. A number of human protein and peptide drugs has been successfully manufactured and applied in patients with different types of disease [396, 397]. With advances in protein drug production techniques, huProAgio is expected to be used in future clinical studies and treatment of cancer patients.

Rational for design the anti-angiogenic region of huProAgio and strategies for eliminating the N-glycosylation, facilitating cysteine-PEGylation, abolishing CD2-CD58 interaction was introduced in details in section 4.2 (also refer to section 4.2, Figure 4.2, and Figure 4.3). In order to facilitate protein expression in different systems, the N-glycosylation site was maintained for yeast expression. In order to express the protein in our laboratory using bacterial systems, three mutations (Lys61Glu, Phe63Leu, and Thr67Ala) were introduced. A simulated model structure of huProAgio without glycosylation was illustrated in Figure 4.1 and discussed in section 4.4. The cDNA for huProAgio were optimized for yeast and bacterial expression, separately (cDNA sequences shown in Figure 4.5 and 4.6). A BL-21 (DE3) bacterial stain expressed the non-glycosylated huProAgio with an N-terminal his-tag (his-huProAgio), and the protein was purified and further tested for *in vitro* and *in vivo* effects. As discussed in section 4.5.2, the purified his-huProAgio showed limited solubility. Optimization of buffer conditions showed that 50 mM ar-

ginine, 50 mM glycine, and 2 mM DTT increased protein solubility. Because the purified his-huProAgio is not PEGylated, the suspected reason for limited solubility without DTT, arginine, and glycine is that Cys28 originally designed for PEGylation was solvent-exposed and facilitated dimerization of the expressed protein. It is expected that the solubility issue will be solved by cysteine-PEGylation in future.

The *in vitro* and *in vivo* tests were preliminary using non-PEGylated his-huProAgio. As shown in Figure 4.10, at concentration of 10 μM, his-huProAgio exhibited stronger anti-proliferation effect compared to ProAgio. The anti-tumor effect of non-PEGylated his-huProAgio was examined using PC3 xenograft model described in previous Chapters. His-huProAgio showed significant tumor inhibitory effect compared to buffer control group ($t = 3.53$, $P = 0.0054$, paired student's *t* test) and induction of end-point tumor mass ($t = 2.78$, $p = 0.02$, paired student's *t* test). Different purification strategies, structural modification, and drug delivery methods are expected to optimize the solubility and structural stability of huProAgio; however, these preliminary data suggested that the recombinant huProAgio has potential to be developed into an anti-angiogenic protein agent.

Although the goal of present study was to demonstrate an effective strategy to design novel anti-angiogenic agents, it is valuable to discuss future clinical outlooks and pitfalls for hu-ProAgio. The following discussions were based on results showed in Chapter 3 and 4.

6.7 Human CD2-CD58 and Rat CD2-CD48 Interactions

The CD2-CD48 (in rat) and CD2-CD58 (in human) interactions was considered differently in the present study.

Firstly, the CD2-CD58 interaction was abolished during the design of huProAgio by a single Tyr86Ala mutation (refer to section 4.2.4). The intact CD2 molecule is a transmembrane glycoprotein expressed on T lymphocytes, NK cells, and thymocytes with cell adhesion and immuno-regulatory functions [293]. The first 104-amino-acid fragment used in this study is located in the extracellular domain part of CD2, and it has only been indicated in the cell adhesion function of CD2. In human species, CD58 is the natural ligand to CD2 [398]. Inhibition of CD2-CD58 interaction impairs the ability of T lymphocytes to recognize cell surface antigens [340] and blocks T lymphocytes activation [399], therefore; huProAgio will compromise immune response if it affects CD2-CD58 interaction in human. There are several reasons to choose a single mutation to abolish CD2-CD58 interaction. The CD2-CD58 interaction has been well studied using X-ray crystallography and NMR analysis, suggesting several hot spots involved in ligand recognition [338, 340]. Among these amino acids in the binding surface, disrupting the interaction between Tyr86 of CD2 and Lys34 of CD58 most sufficiently abolished the binding of these two molecules [340]. In addition, Tyr86 is located at the flexible loop region instead of the rigid β-sheet of huCD2, so that Tyr86Ala mutation was expected to bring the least effects on protein structural stability, which is confirmed by the NMR studies carried out by Kim and coworkers [340]. These previous studies facilitated us to use Tyr86Ala mutation as a strategy to avoid possible clinical side effects caused by change of T lymphocytes function/activation in cancer patients.

Although Tyr86 was mutated in huProAgio, it still necessary to confirm that huProAgio does not affect CD2-CD58 interaction. A classic method, E-Rosetting assay, can be performed to determine whether or not huProAgio will affect the cell-cell adhesion function of T lymphocytes mediated by CD2 [400]. Exogenously expressed CD58 adhesion domain can be used to deter-

mine huProAgio-CD58 binding *in vitro* [340, 401]. Since CD2-CD58 binding surface is disrupted by Tyr86Ala mutation, it is suggestive that huProAgio may not bind to CD58 *in vitro* and *in vivo*. CD2 binds to CD58 with a K_d of 1 – 10 μM, whereas Tyr86Ala mutation decreases the affinity of CD2 to CD58 by 100 – 1000 folds [340]. If huProAgio does bind to CD58 with a low affinity, activation and functions of T lymphocytes has to be examined using animal models. Otherwise the binding of huProAgio-CD58 could be further reduced or abolished by additional mutations in the binding surface.

Secondly, CD48 is the natural ligand of rat and mouse CD2 instead of CD58 in human [296, 341]. CD2-CD48 interaction of rat ProAgio was not taken into consideration because of two reasons. First, rat CD2 bind CD48 with a low affinity (K_d = 60 – 90 μM) [296, 297]. Theoretically, the experimental protein concentrations (50 – 100 μM of 200 μL for i.p. injection) used in animal model will not produce serum ProAgio concentrations that are sufficient to disrupt CD2-CD48 interaction. Second, nude mice were used for evaluation of *in vivo* effects of rat ProAgio, so that the anti-angiogenic and anti-tumor functions observed were less likely to be caused by suppressing activation or functions of T lymphocytes.

6.8 Advantages Using ProAgio as a Therapeutic Agent

After bevacizumab was approved by FDA, anti-angiogenic therapy has become a new line of treatment excepted to bring exceptional benefits to cancer patients, such as low toxicity, less drug resistance, and flexibility to inhibit a broad spectrum of tumors. In the past several decades, although a great body of knowledge regarding mechanisms of angiogenesis has provided valid targets for anti-angiogenic studies, a majority of current FDA approved anti-

angiogenic drugs are VEGF/VEGFR inhibitors (reviewed in sections 1.5 and 1.7). VEGF/VEGFR inhibitors such as anti-VEGF monoclonal antibody, bevacizumab (Avastin, Genentech/Roche), and small molecule VEGGR inhibitor, sunitinib (Sutent®, Pfizer) were ice-breakers for anti-angiogenic therapy and they have been applied to cancer patients with different types of tumors since 2004. As clinical and research data compiled within past a decade, several drawbacks of VEGF/VEGFR inhibitors have been suggested (reviewed in section 1.8). Other agents including EGFR inhibitor, mTOR inhibitors, and immuno-modulators have anti-angiogenic effects but do not specifically inhibit tumor angiogenesis (reviewed in section 1.7).

Compared to the above agents, ProAgio has several advantages. Firstly, these marked agents are indirect angiogenesis inhibitors by targeting one or several signaling pathways that mediate(s) EC proliferation or apoptosis. It has been shown that tumor cells intrinsically resist treatment with VEGF/VEGFR inhibitors by stimulating redundant pro-angiogenic factors such as FGF, PIGF or PDGF, resulting in drug resistance (reviewed in [181]). Growth factor triggered EC proliferation/migration is the key to this phenomenon. ProAgio directly target ECs to inhibit EC proliferation and formation of tubules. Direct angiogenesis inhibitors damages the “building block” for new blood vessels regardless of different sources of stimulants (reviewed in [136]), so that cancer patients treated with ProAgio will theoretically have less chance to experience drug resistance. Secondly, inhibition of multiple signal pathways has been considered as promising solution to solve above drug resistance; however, combination of anti-VEGF and anti-EGF monoclonal antibody drugs have produced controversial results about improving anti-tumor efficacy in different clinical trials [402, 403]. The combination of an anti-EGF antibody, panitumumab with bevacizumab increased toxicity and reduced progression-free survival (PFS) rate in

metastatic colorectal cancer [403]. Small molecule TKIs usually inhibits several signal pathways and more efficient at inhibiting angiogenesis, but they have higher toxicity compared to monoclonal antibodies (reviewed in [179]). The ant-angiogenic mechanisms of ProAgio are independent of growth factors, so that adverse effects can be avoided if ProAgio replaces these controversial combinational treatment regimes. Thirdly, our *in vitro* data showed that ProAgio inhibited EC-proliferation without significant effects on epithelium-original cells. One of the advantages of using ProAgio or other endogenous anti-angiogenesis proteins is low toxicity. Tumor vessels are structurally and functionally abnormal with less protected and disconnected ECs compared to normal vasculatures as reviewed in section 1. 4. These features allow direct anti-angiogenic agents specifically target proliferating tumor ECs, resulting in less side effects. Toxicities had not been observed ProAgio treated animals. In contrast, VEGF signaling have been shown to regulate normal organ homeostasis, and treatments with VEGF/VEGFR inhibitors associated with complications involved in multiple organ systems, especially heart and kidney (reviewed in [170]). In future studies, long-term toxicity of ProAgio is necessary to be examined in pre- and clinical trials.

All the above reasons led to a wave of discovery and development of endogenous anti-angiogenic proteins and peptides that directly target ECs with low toxicity and broad anti-tumor spectrum. As reviewed in section 1.9, to date, numerous investigations have documented a large number of matrix-derived or non-matrix-derived endogenous proteins, protein fragments, and peptides that sufficiently inhibit tumor angiogenesis in a variety of tumor models. Unfortunately, except for endostatin none has been successfully applied to treat cancer patients. It is not clear why these endogenous proteins or peptides failed clinical trials, however; three as-

pects could affect their activities and applications. Firstly, most of them are fragments or peptides derived from ECM proteins with limited structural stability and protein solubility. For example, endostatin is highly positively charged protein fragments that is soluble in low pH and forms precipitation in neutral pH [289]. Compared to endogenous anti-angiogenic protein or protein fragments derived from ECM proteins, ProAgio is soluble in isotonic buffer at neutral pH (PBS, pH7.4). Secondly, the "default" biological functions of endogenous proteins, such as TSP-1, PF4, ILs, and IFNs have high potential to cause side effects if used as anti-angiogenic agents. Although the humanized ProAgio (huProAgio) was derived from the extracellular domain 1 of CD2 (CD2D1), the cell adhesion function caused by CD2-CD58 interaction was crippled in order to avoid its "default" function in regulating immune responses. Thirdly, although dissecting endogenous proteins will avoid trigger non-angiogenesis related activities and in some cases increase solubility, but lack of pharmacological properties and high production cost usually hinder small peptides to be developed into anti-angiogenic drugs. NMR evidences suggested that ProAgio is protein with a stable β-sheet sandwich structure that not only conveys importance structural features, but also resists to protease degradation, resulting in a longer *in vivo* half life and higher targeting efficiency. With regard to expenses, bacterial or yeast fermentation techniques will facilitate the mass production of ProAgio in a relative lower cost compared to synthetic peptides.

In summary, ProAgio demonstrated a *de novo* designed methods to produce protein agents that can overcome not only the disadvantages of existing marked anti-angiogenic drugs (VEGF/VEGFR and EGFR inhibitors) but also the shortcomings of endogenous proteins and peptides undergoing drug development. Our studies highly suggested that the humanized ProAgio,

huProAgio is expected to produce higher anti-angiogenic efficiency, lower toxicity, and lower risk of drug resistance than these mentioned above. Backed up by low manufacture cost, simplicity in formulation, and proper modifications favoring *in vivo* pharmacokinetic parameters, huProAgio will have a high potential to become the next generation of anti-angiogenic drug.

6.9 Clinical Outlook of HuProAgio

To date, a large portion of anti-angiogenic drug research and development has focused on antibodies and proteins. Antibodies, proteins, and peptides remain as attractive drug candidates because they have high affinity, specificity, and safety. Like many of the endogenous anti-angiogenic proteins such as PF4, angiostatin, anastellin, and restin, studies used rat ProAgio proved that our designed agent specifically targeted ECs not epithelial cells. Studies with ProAgio and huProAgio indicated that both agents strongly inhibit tumor growth and angiogenesis in animal models. In addition, the ligand binding capability of CD2D1 (the parental protein of huProAgio) was crippled to avoid possible immune responses. These profiles will assure the efficacy and safety profiles of huProAgio.

In general, angiogenesis inhibitors are considered as a new category of low toxic and well-tolerable anti-cancer therapy. They lack cytotoxic anti-cancer drug related side effects such as alopecia, severe myelosuppression, neural, renal, and gastrointestinal toxicities (reviewed in [170]). The possible side effects of huProAgio are expected to be confined to complications caused by disruption of angiogenesis. Wound healing, bleeding, and gastrointestinal perforations are the most common complications when angiogenesis is perturbed (reviewed in [170]). The occurrences of these complications are expected in huProAgio-treated cancer patients, but

the incidences will depend on the serum concentration of huProAgio. As a protein agent that directly targets ECs, huProAgio is less likely to cause side effects related to inhibition of the physiological functions of pro-angiogenic signal pathways. For example, as reviewed in section 1.8, VEGF not only activates ECs, but also plays an important role in the maintenance of body homeostasis, especially in the cardiovascular system. The most common side effects associated VEGF/VEGFR inhibitors are hypertension, MI, and congestive heart failure. VEGF is highly expressed in renal glomeruli and tubules, and mediates renal functions, which may contribute to proteinuria is also commonly occurred in bevacizumab-treated cancer patients [404-406]. ProAgio is a *de novo* designed protein that is not involved in above physiological processes, suggesting it will have fewer chances to affect cardiovascular and renal systems compared to VEGF/VEGFR inhibitors.

If safety is demonstrated in pre- and clinical trials, huProAgio can be used to treat many types of tumors because angiogenesis is a general mechanism for growth of most solid tumors. As reviewed in section 1.7, anti-angiogenic drugs including VEGF/VEGFR and EGFR inhibitors have been approved to treat patients with NSCLC, glioblastoma, RCC, breast cancer, hepatocellular carcinoma, and others. Recombinant human endostatin (rh-endostatin, Endostar®) was approved to treat NSCLC in China in 2005 [190]. In animal models, human endostatin has been used to inhibit more than 15 different types of human tumor xenografts in mice models (reviewed in [196]). HuProAgio effectively inhibited the growth of PC3 xenograft models, but it is important to test it on animal models with different types of human tumors.

6.10 Clinical Challenges for HuProAgio

To date, hundreds of endogenous proteins and peptides have been discovered and investigated in pre- and different stages of clinical trials, but only rh-endostatin has succeeded to pass clinical approval. It is not clear why these proteins and peptides showed robust anti-cancer effects in experimental animal models, but failed to exhibit the same effect in humans. We expect huProAgio to be a highly efficient anti-angiogenic agent with low toxicity and a broad anti-cancer spectrum; however, clinical trials may demonstrate that huProAgio shows no significant inhibitory effects in inhibition of tumor growth and angiogenesis. Several aspects that might contribute to these circumstances are speculated and discussed as follows.

On one hand, as a protein drug, huProAgio has intrinsic challenges that will hinder the therapeutic applications. Torchilin and coworkers summarized major obstacles for protein and peptide drugs in a review: i) short circulation time generated by fast renal filtration and enzymatic degradation, ii) immune responses, and iii) uptake by non-target tissues [407]. Our design approach has taken these obstructive factors into consideration. First, ProAgio adapts a well-folded β-sheet sandwich structure that more resists to protease degradation than peptide do. Second, ProAgio was re-designed into huProAgio to avoid possible cross-species immune responses. Third, a site-specific PEGylation method was used to elongate circulation time, reduce immune responses, and improve pharmacokinetic and pharmacodynamic features of huProAgio with PEGylated L-asparaginase (Oncospar®, Enzon), IFN-2a and -2b as successful examples. If huProAgio fails to show expected clinical effects despite of these factors, exchanging PEGylation conjugates, modifying protein structure, or adapting advanced drug delivery methods are valuable avenues to further overcome these possible obstacles. For example, encapsulation of

huProAgio in tumor-vasculature-targeting liposomes is a promising delivery method. Liposomes are spherical vesicles composed of phospholipid bilayers with an inner aqueous space that is suitable for encapsulation of anti-cancer drugs, proteins, and peptides (reviewed in [407]). Chang and colleagues reported that coupling tumor vasculature homing peptides with a doxorubicin (Lipo-Dox; LD)-containing liposome as a methods that significantly promoted accumulation of doxorubicin in tumor endothelium and enhanced its anti-cancer activity [408]. This technique can avoid immunogenicity, prolong blood circulation time, increase drug concentration in tumor ECs, and reduce uptake by non-targeting tissues or organs (reviewed in [409]).

On the other hand, except for above impediments, lack of efficient targeting may play an essential role if our designed protein agents fail to show expected effects. It is important to clarify the anti-angiogenic mechanisms of huProAgio. As discussed in section 6.5, Gal-1 was a potential anti-angiogenic target for our designed protein agents, but it may not be the only protein that interacts with ProAgio *in vivo*. Further studies are necessary in order to portray the exact picture of how huProAgio exerts anti-angiogenic functions. These protein-protein interactions profiles will provide solid ground on monitoring and improving drug efficacy. By far our design approach has focused on importance β-sheet structural features of endogenous anti-angiogenic proteins and peptides including alternation of charge/polar and hydrophobic residues, constitution of amphipathic surfaces with the positive-charged surface exposed to solvent. Within the designed anti-angiogenic portion of huProAgio, it is critical to identify the most important residues that determine protein-protein binding between huProAgio and its partner. Substitutions of these amino acids will affect the binding affinity of huProAgio. Consequently, the anti-angiogenic effects of huProAgio will also be enhanced or reduced by different muta-

tions. Furthermore, identification of downstream targets will help to establish the anti-cancer spectrum of huProAgio. For example, if Gal-1 is the only target for huProAgio, it has to be applied to patients with cancers over-expressing Gal-1.

In addition, efficacies of novel anti-cancer drugs are constantly tested in patients with late stage cancers. Within advanced tumors, tumor vasculatures have established usually with the existence of necrotic and hypoxic areas. Under these circumstances, any anti-angiogenic drug may fail to demonstrate beneficial effects because at this stage angiogenesis contributes less to tumor growth. Regimens combining VEGF/VEGFR inhibitors with cytotoxic agents or radiotherapies are commonly used to treat cancer patients (reviewed in [410]). For these reasons, it is necessary to use huProAgio in combination with traditional anti-cancer therapies instead of being applied as a single agent. Since exponential tumor growth only occurs after new blood vessels are established, it is critical to apply anti-angiogenic therapy in early stage of cancer growth [5, 18]. Future advances in early cancer diagnosis will greatly expand the therapeutic prospective of anti-angiogenic agents.

Furthermore, tumor angiogenesis is a multi-step process choreographed by a number of cellular signal pathways, a large amount of proteins, and different types of cells. Compelling pre-clinical investigations have demonstrated that combining agents with different anti-angiogenic mechanisms can significantly reduce tumor angiogenesis than a single one does [411-413]. As discussed in section 6.8, current available VEGF/VEGFR and EGFR inhibitors exhibit limited anti-cancer effects as a single agent, and combination of these two have not produced consistent clinical outcomes. ProAgio is a direct anti-angiogenic agent targeting ECs. Combination of ProAgio with VEGF/VEGFR or EGFR inhibitors will curb tumor angiogenesis from

two independent angles, which will enhance treatment efficacy. Besides, it is possible that combination of ProAgio with other direct anti-angiogenic agents will also be more effective. For example, studies have shown that endostatin and anastellin have addictive *in vitro* effects [414].

6.11 Conclusions and Future Directions

We have successfully developed an anti-angiogenesis agent by rational protein design. Most current available anti-angiogenesis agents target VEGF/VEGFR or other RTK pathways. Such agents often cause unwanted biological side effects. In addition, many cancers are resistant to the inhibition of VEGF/VEGFR. Our developed protein is one of a very few examples that do not act through targeting VEGF/VEGFR or any other RTK pathways. Importantly, our study provides an example of proof-of-concept to harness the natural anti-angiogenesis activity to starve cancers. In addition, our study introduced a new strategy to integrate a small bio-active structural motif or an unstable short circulating peptide into a stable host protein. The resultant protein overcomes the major disadvantage of therapeutically peptides, e.g. *in vivo* instability and unfavorable pharmacological properties.

In vitro models showed that ProAgio effectively inhibit HUVEC cell growth and formation of endothelial tubes. The drug efficacy of ProAgio was further examined in a xenograft model. It was demonstrated that ProAgio inhibits tumor growth in a dose dependent manner. ProAgio also surpassed avastin in inhibition of tumor growth using the same model. These effects were further confirmed by MVD count in tumor tissues from different treated group. These *in vitro* and *in vivo* experiments demonstrate the effectiveness of our designed protein. The developed

agent is not toxic to non-cancerous blood vessels and other tissue/organs, providing for future potential clinical applications.

In addition, humanization of ProAgio was also carried out in this study utilizing the same strategy as with rat CD2D1. The designed huProAgio protein was expressed and purified in bacterial with an N-terminal his-tag. Anti-angiogenic effect of designed huProAgio is also examined in *in vitro* and *in vivo* models same as ProAgio. The refolded protein showed proliferation-inhibitory effect toward HUVECs. Further treatment of PC3 xenograft tumor model using huProAgio demonstrated its strong anti-angiogenic activity. Since human and rat CD2D1 share 40% amino acid similarity, it was evident that host protein did not significantly affect the designed anti-angiogenic effects of designed agents. In addition, these findings in huProAgio further demonstrated the efficacy of our design strategies.

The concept of this study can be extended to the design and development of other protein drugs. Our system certainly will create a new platform for design of therapeutic agents by *de novo* protein design.

REFERENCE

1. Carmeliet, P., *Angiogenesis in life, disease and medicine.* Nature, 2005. **438**(7070): p. 932-6.
2. Yancopoulos, G.D., et al., *Vascular-specific growth factors and blood vessel formation.* Nature, 2000. **407**(6801): p. 242-8.
3. Risau, W., *Mechanisms of angiogenesis.* Nature, 1997. **386**(6626): p. 671-4.
4. Carmeliet, P., *Mechanisms of angiogenesis and arteriogenesis.* Nat Med, 2000. **6**(4): p. 389-95.
5. Hanahan, D. and J. Folkman, *Patterns and emerging mechanisms of the angiogenic switch during tumorigenesis.* Cell, 1996. **86**(3): p. 353-64.
6. Hobson, B. and J. Denekamp, *Endothelial proliferation in tumours and normal tissues: continuous labelling studies.* Br J Cancer, 1984. **49**(4): p. 405-13.
7. Folkman, J., *Angiogenesis in cancer, vascular, rheumatoid and other disease.* Nat Med, 1995. **1**(1): p. 27-31.
8. Ferrara, N. and R.S. Kerbel, *Angiogenesis as a therapeutic target.* Nature, 2005. **438**(7070): p. 967-74.
9. Khong, T.L., et al., *Angiogenesis as a therapeutic target in arthritis: learning the lessons of the colorectal cancer experience.* Angiogenesis, 2007. **10**(4): p. 243-58.
10. Cao, Y., *Adipose tissue angiogenesis as a therapeutic target for obesity and metabolic diseases.* Nat Rev Drug Discov, 2010. **9**(2): p. 107-15.

11. Wong, M.L., et al., *Tumour angiogenesis: its mechanism and therapeutic implications in malignant gliomas.* J Clin Neurosci, 2009. **16**(9): p. 1119-30.

12. Senger, D.R., et al., *Tumor cells secrete a vascular permeability factor that promotes accumulation of ascites fluid.* Science, 1983. **219**(4587): p. 983-5.

13. Dvorak, H.F., *Vascular permeability factor/vascular endothelial growth factor: a critical cytokine in tumor angiogenesis and a potential target for diagnosis and therapy.* J Clin Oncol, 2002. **20**(21): p. 4368-80.

14. Hanahan, D. and R.A. Weinberg, *The hallmarks of cancer.* Cell, 2000. **100**(1): p. 57-70.

15. Bergers, G. and L.E. Benjamin, *Tumorigenesis and the angiogenic switch.* Nat Rev Cancer, 2003. **3**(6): p. 401-10.

16. Folkman, J., *Tumor angiogenesis: therapeutic implications.* N Engl J Med, 1971. **285**(21): p. 1182-6.

17. Gimbrone, M.A., Jr., et al., *Tumor dormancy in vivo by prevention of neovascularization.* J Exp Med, 1972. **136**(2): p. 261-76.

18. Knighton, D., et al., *Avascular and vascular phases of tumour growth in the chick embryo.* Br J Cancer, 1977. **35**(3): p. 347-56.

19. Brem, S., et al., *Prolonged tumor dormancy by prevention of neovascularization in the vitreous.* Cancer Res, 1976. **36**(8): p. 2807-12.

20. Holmgren, L., M.S. O'Reilly, and J. Folkman, *Dormancy of micrometastases: balanced proliferation and apoptosis in the presence of angiogenesis suppression.* Nat Med, 1995. **1**(2): p. 149-53.

21. Nyberg, P., L. Xie, and R. Kalluri, *Endogenous inhibitors of angiogenesis.* Cancer Res, 2005. **65**(10): p. 3967-79.

22. Brouty-Boye, D. and B.R. Zetter, *Inhibition of cell motility by interferon.* Science, 1980. **208**(4443): p. 516-8.

23. Taylor, S. and J. Folkman, *Protamine is an inhibitor of angiogenesis.* Nature, 1982. **297**(5864): p. 307-12.

24. Sato, Y., M. Abe, and R. Takaki, *Platelet factor 4 blocks the binding of basic fibroblast growth factor to the receptor and inhibits the spontaneous migration of vascular endothelial cells.* Biochem Biophys Res Commun, 1990. **172**(2): p. 595-600.

25. Good, D.J., et al., *A tumor suppressor-dependent inhibitor of angiogenesis is immunologically and functionally indistinguishable from a fragment of thrombospondin.* Proc Natl Acad Sci U S A, 1990. **87**(17): p. 6624-8.

26. O'Reilly, M.S., et al., *Endostatin: an endogenous inhibitor of angiogenesis and tumor growth.* Cell, 1997. **88**(2): p. 277-85.

27. O'Reilly, M.S., et al., *Angiostatin: a novel angiogenesis inhibitor that mediates the suppression of metastases by a Lewis lung carcinoma.* Cell, 1994. **79**(2): p. 315-28.

28. Ferrara, N., et al., *Discovery and development of bevacizumab, an anti-VEGF antibody for treating cancer.* Nat Rev Drug Discov, 2004. **3**(5): p. 391-400.

29. Lee, S., et al., *Processing of VEGF-A by matrix metalloproteinases regulates bioavailability and vascular patterning in tumors.* J Cell Biol, 2005. **169**(4): p. 681-91.

30. Carmeliet, P. and R.K. Jain, *Angiogenesis in cancer and other diseases.* Nature, 2000. **407**(6801): p. 249-57.

31. Dvorak, H.F., *Tumors: wounds that do not heal. Similarities between tumor stroma generation and wound healing.* N Engl J Med, 1986. **315**(26): p. 1650-9.

32. Brown, L.F., et al., *Vascular stroma formation in carcinoma in situ, invasive carcinoma, and metastatic carcinoma of the breast.* Clin Cancer Res, 1999. **5**(5): p. 1041-56.

33. Baluk, P., et al., *Abnormalities of basement membrane on blood vessels and endothelial sprouts in tumors.* Am J Pathol, 2003. **163**(5): p. 1801-15.

34. Morikawa, S., et al., *Abnormalities in pericytes on blood vessels and endothelial sprouts in tumors.* Am J Pathol, 2002. **160**(3): p. 985-1000.

35. McDonald, D.M., L. Munn, and R.K. Jain, *Vasculogenic mimicry: how convincing, how novel, and how significant?* Am J Pathol, 2000. **156**(2): p. 383-8.

36. Leung, D.W., et al., *Vascular endothelial growth factor is a secreted angiogenic mitogen.* Science, 1989. **246**(4935): p. 1306-9.

37. Olofsson, B., et al., *Vascular endothelial growth factor B, a novel growth factor for endothelial cells.* Proc Natl Acad Sci U S A, 1996. **93**(6): p. 2576-81.

38. Joukov, V., et al., *A novel vascular endothelial growth factor, VEGF-C, is a ligand for the Flt4 (VEGFR-3) and KDR (VEGFR-2) receptor tyrosine kinases.* EMBO J, 1996. **15**(7): p. 1751.

39. Achen, M.G., et al., *Vascular endothelial growth factor D (VEGF-D) is a ligand for the tyrosine kinases VEGF receptor 2 (Flk1) and VEGF receptor 3 (Flt4).* Proc Natl Acad Sci U S A, 1998. **95**(2): p. 548-53.

40. Gerber, H.P., V. Dixit, and N. Ferrara, *Vascular endothelial growth factor induces expression of the antiapoptotic proteins Bcl-2 and A1 in vascular endothelial cells.* J Biol Chem, 1998. **273**(21): p. 13313-6.

41. Benjamin, L.E., et al., *Selective ablation of immature blood vessels in established human tumors follows vascular endothelial growth factor withdrawal.* J Clin Invest, 1999. **103**(2): p. 159-65.

42. Yuan, F., et al., *Time-dependent vascular regression and permeability changes in established human tumor xenografts induced by an anti-vascular endothelial growth factor/vascular permeability factor antibody.* Proc Natl Acad Sci U S A, 1996. **93**(25): p. 14765-70.

43. Ferrara, N., et al., *Heterozygous embryonic lethality induced by targeted inactivation of the VEGF gene.* Nature, 1996. **380**(6573): p. 439-42.

44. Houck, K.A., et al., *The vascular endothelial growth factor family: identification of a fourth molecular species and characterization of alternative splicing of RNA.* Mol Endocrinol, 1991. **5**(12): p. 1806-14.

45. Tischer, E., et al., *The human gene for vascular endothelial growth factor. Multiple protein forms are encoded through alternative exon splicing.* J Biol Chem, 1991. **266**(18): p. 11947-54.

46. Vincenti, V., et al., *Assignment of the vascular endothelial growth factor gene to human chromosome 6p21.3.* Circulation, 1996. **93**(8): p. 1493-5.

47. Poltorak, Z., et al., *VEGF145, a secreted vascular endothelial growth factor isoform that binds to extracellular matrix.* J Biol Chem, 1997. **272**(11): p. 7151-8.

48. Jingjing, L., et al., *Human Muller cells express VEGF183, a novel spliced variant of vascular endothelial growth factor.* Invest Ophthalmol Vis Sci, 1999. **40**(3): p. 752-9.

49. Whittle, C., et al., *Heterogeneous vascular endothelial growth factor (VEGF) isoform mRNA and receptor mRNA expression in human glomeruli, and the identification of VEGF148 mRNA, a novel truncated splice variant.* Clin Sci (Lond), 1999. **97**(3): p. 303-12.

50. Ferrara, N., H.P. Gerber, and J. LeCouter, *The biology of VEGF and its receptors.* Nat Med, 2003. **9**(6): p. 669-76.

51. Houck, K.A., et al., *Dual regulation of vascular endothelial growth factor bioavailability by genetic and proteolytic mechanisms.* J Biol Chem, 1992. **267**(36): p. 26031-7.

52. Park, J.E., G.A. Keller, and N. Ferrara, *The vascular endothelial growth factor (VEGF) isoforms: differential deposition into the subepithelial extracellular matrix and bioactivity of extracellular matrix-bound VEGF.* Mol Biol Cell, 1993. **4**(12): p. 1317-26.

53. Plouet, J., et al., *Extracellular cleavage of the vascular endothelial growth factor 189-amino acid form by urokinase is required for its mitogenic effect.* J Biol Chem, 1997. **272**(20): p. 13390-6.

54. Keyt, B.A., et al., *The carboxyl-terminal domain (111-165) of vascular endothelial growth factor is critical for its mitogenic potency.* J Biol Chem, 1996. **271**(13): p. 7788-95.

55. Grunstein, J., et al., *Isoforms of vascular endothelial growth factor act in a coordinate fashion To recruit and expand tumor vasculature.* Mol Cell Biol, 2000. **20**(19): p. 7282-91.

56. Carmeliet, P., et al., *Impaired myocardial angiogenesis and ischemic cardiomyopathy in mice lacking the vascular endothelial growth factor isoforms VEGF164 and VEGF188.* Nat Med, 1999. **5**(5): p. 495-502.

57. Ruhrberg, C., et al., *Spatially restricted patterning cues provided by heparin-binding VEGF-A control blood vessel branching morphogenesis.* Genes Dev, 2002. **16**(20): p. 2684-98.

58. Shibuya, M., et al., *Nucleotide sequence and expression of a novel human receptor-type tyrosine kinase gene (flt) closely related to the fms family.* Oncogene, 1990. **5**(4): p. 519-24.

59. Terman, B.I., et al., *Identification of a new endothelial cell growth factor receptor tyrosine kinase.* Oncogene, 1991. **6**(9): p. 1677-83.

60. Terman, B.I., et al., *Identification of the KDR tyrosine kinase as a receptor for vascular endothelial cell growth factor.* Biochem Biophys Res Commun, 1992. **187**(3): p. 1579-86.

61. Quinn, T.P., et al., *Fetal liver kinase 1 is a receptor for vascular endothelial growth factor and is selectively expressed in vascular endothelium.* Proc Natl Acad Sci U S A, 1993. **90**(16): p. 7533-7.

62. Millauer, B., et al., *High affinity VEGF binding and developmental expression suggest Flk-1 as a major regulator of vasculogenesis and angiogenesis.* Cell, 1993. **72**(6): p. 835-46.

63. Soker, S., et al., *Neuropilin-1 is expressed by endothelial and tumor cells as an isoform-specific receptor for vascular endothelial growth factor.* Cell, 1998. **92**(6): p. 735-45.

64. Guo, D., et al., *Vascular endothelial cell growth factor promotes tyrosine phosphorylation of mediators of signal transduction that contain SH2 domains. Association with endothelial cell proliferation.* J Biol Chem, 1995. **270**(12): p. 6729-33.

65. Eliceiri, B.P., et al., *Selective requirement for Src kinases during VEGF-induced angiogenesis and vascular permeability.* Mol Cell, 1999. **4**(6): p. 915-24.

66. Takahashi, T., H. Ueno, and M. Shibuya, *VEGF activates protein kinase C-dependent, but Ras-independent Raf-MEK-MAP kinase pathway for DNA synthesis in primary endothelial cells.* Oncogene, 1999. **18**(13): p. 2221-30.

67. Gerber, H.P., et al., *Vascular endothelial growth factor regulates endothelial cell survival through the phosphatidylinositol 3'-kinase/Akt signal transduction pathway. Requirement for Flk-1/KDR activation.* J Biol Chem, 1998. **273**(46): p. 30336-43.

68. Kevil, C.G., et al., *Vascular permeability factor/vascular endothelial cell growth factor-mediated permeability occurs through disorganization of endothelial junctional proteins.* J Biol Chem, 1998. **273**(24): p. 15099-103.

69. Pepper, M.S., et al., *Vascular endothelial growth factor (VEGF) induces plasminogen activators and plasminogen activator inhibitor-1 in microvascular endothelial cells.* Biochem Biophys Res Commun, 1991. **181**(2): p. 902-6.

70. Mandriota, S.J., et al., *Vascular endothelial growth factor increases urokinase receptor expression in vascular endothelial cells.* J Biol Chem, 1995. **270**(17): p. 9709-16.

71. Goto, H., et al., *Identification of a novel phosphorylation site on histone H3 coupled with mitotic chromosome condensation.* J Biol Chem, 1999. **274**(36): p. 25543-9.

72. Asahara, T., et al., *Bone marrow origin of endothelial progenitor cells responsible for postnatal vasculogenesis in physiological and pathological neovascularization.* Circ Res, 1999. **85**(3): p. 221-8.

73. Gao, D., et al., *Bone marrow-derived endothelial progenitor cells contribute to the angiogenic switch in tumor growth and metastatic progression.* Biochim Biophys Acta, 2009. **1796**(1): p. 33-40.

74. Park, J.E., et al., *Placenta growth factor. Potentiation of vascular endothelial growth factor bioactivity, in vitro and in vivo, and high affinity binding to Flt-1 but not to Flk-1/KDR.* J Biol Chem, 1994. **269**(41): p. 25646-54.

75. Olofsson, B., et al., *Vascular endothelial growth factor B (VEGF-B) binds to VEGF receptor-1 and regulates plasminogen activator activity in endothelial cells.* Proc Natl Acad Sci U S A, 1998. **95**(20): p. 11709-14.

76. Hiratsuka, S., et al., *MMP9 induction by vascular endothelial growth factor receptor-1 is involved in lung-specific metastasis.* Cancer Cell, 2002. **2**(4): p. 289-300.

77. Kaplan, R.N., et al., *VEGFR1-positive haematopoietic bone marrow progenitors initiate the pre-metastatic niche.* Nature, 2005. **438**(7069): p. 820-7.

78. Dawson, M.R., et al., *VEGFR1-activity-independent metastasis formation.* Nature, 2009. **461**(7262): p. E4; discussion E5.

79. Orlandini, M., et al., *Identification of a c-fos-induced gene that is related to the platelet-derived growth factor/vascular endothelial growth factor family.* Proc Natl Acad Sci U S A, 1996. **93**(21): p. 11675-80.

80. Davis, S., et al., *Isolation of angiopoietin-1, a ligand for the TIE2 receptor, by secretion-trap expression cloning.* Cell, 1996. **87**(7): p. 1161-9.

81. Sato, T.N., et al., *Distinct roles of the receptor tyrosine kinases Tie-1 and Tie-2 in blood vessel formation.* Nature, 1995. **376**(6535): p. 70-4.

82. Puri, M.C., et al., *The receptor tyrosine kinase TIE is required for integrity and survival of vascular endothelial cells.* EMBO J, 1995. **14**(23): p. 5884-91.

83. Suri, C., et al., *Requisite role of angiopoietin-1, a ligand for the TIE2 receptor, during embryonic angiogenesis.* Cell, 1996. **87**(7): p. 1171-80.

84. Schnurch, H. and W. Risau, *Expression of tie-2, a member of a novel family of receptor tyrosine kinases, in the endothelial cell lineage.* Development, 1993. **119**(3): p. 957-68.

85. Thurston, G., et al., *Angiopoietin-1 protects the adult vasculature against plasma leakage.* Nat Med, 2000. **6**(4): p. 460-3.

86. Gavard, J., V. Patel, and J.S. Gutkind, *Angiopoietin-1 prevents VEGF-induced endothelial permeability by sequestering Src through mDia.* Dev Cell, 2008. **14**(1): p. 25-36.

87. Maisonpierre, P.C., et al., *Angiopoietin-2, a natural antagonist for Tie2 that disrupts in vivo angiogenesis.* Science, 1997. **277**(5322): p. 55-60.

88. Gale, N.W., et al., *Angiopoietin-2 is required for postnatal angiogenesis and lymphatic patterning, and only the latter role is rescued by Angiopoietin-1.* Dev Cell, 2002. **3**(3): p. 411-23.

89. Zhu, Y., et al., *Angiopoietin-2 facilitates vascular endothelial growth factor-induced angiogenesis in the mature mouse brain.* Stroke, 2005. **36**(7): p. 1533-7.

90. Hata, K., et al., *Expression of the angopoietin-1, angopoietin-2, Tie2, and vascular endothelial growth factor gene in epithelial ovarian cancer.* Gynecol Oncol, 2004. **93**(1): p. 215-22.

91. Loges, S., et al., *Analysis of concerted expression of angiogenic growth factors in acute myeloid leukemia: expression of angiopoietin-2 represents an independent prognostic factor for overall survival.* J Clin Oncol, 2005. **23**(6): p. 1109-17.

92. Helfrich, I., et al., *Angiopoietin-2 levels are associated with disease progression in metastatic malignant melanoma.* Clin Cancer Res, 2009. **15**(4): p. 1384-92.

93. Falcon, B.L., et al., *Contrasting actions of selective inhibitors of angiopoietin-1 and angiopoietin-2 on the normalization of tumor blood vessels.* Am J Pathol, 2009. **175**(5): p. 2159-70.

94. Huang, H., et al., *Specifically Targeting Angiopoietin-2 Inhibit Angiogenesis, Tie2 Expressing Monocyte Infiltration and Tumor Growth.* Clin Cancer Res, 2011.

95. Folkman, J. and M. Klagsbrun, *Angiogenic factors.* Science, 1987. **235**(4787): p. 442-7.

96. Beenken, A. and M. Mohammadi, *The FGF family: biology, pathophysiology and therapy.* Nat Rev Drug Discov, 2009. **8**(3): p. 235-53.

97. Dunn, I.F., O. Heese, and P.M. Black, *Growth factors in glioma angiogenesis: FGFs, PDGF, EGF, and TGFs.* J Neurooncol, 2000. **50**(1-2): p. 121-37.

98. Pardo, O.E., et al., *Fibroblast growth factor-2 induces translational regulation of Bcl-XL and Bcl-2 via a MEK-dependent pathway: correlation with resistance to etoposide-induced apoptosis.* J Biol Chem, 2002. **277**(14): p. 12040-6.

99. Alavi, A., et al., *Role of Raf in vascular protection from distinct apoptotic stimuli.* Science, 2003. **301**(5629): p. 94-6.

100. Sato, Y. and D.B. Rifkin, *Autocrine activities of basic fibroblast growth factor: regulation of endothelial cell movement, plasminogen activator synthesis, and DNA synthesis.* J Cell Biol, 1988. **107**(3): p. 1199-205.

101. Matsuzaki, K., et al., *Monoclonal antibodies against heparin-binding growth factor II/basic fibroblast growth factor that block its biological activity: invalidity of the antibodies for tumor angiogenesis.* Proc Natl Acad Sci U S A, 1989. **86**(24): p. 9911-5.

102. Casanovas, O., et al., *Drug resistance by evasion of antiangiogenic targeting of VEGF signaling in late-stage pancreatic islet tumors.* Cancer Cell, 2005. **8**(4): p. 299-309.

103. Andrae, J., R. Gallini, and C. Betsholtz, *Role of platelet-derived growth factors in physiology and medicine.* Genes Dev, 2008. **22**(10): p. 1276-312.

104. Hoch, R.V. and P. Soriano, *Roles of PDGF in animal development.* Development, 2003. **130**(20): p. 4769-84.

105. Wang, Z., et al., *Emerging roles of PDGF-D signaling pathway in tumor development and progression.* Biochim Biophys Acta, 2010. **1806**(1): p. 122-30.

106. Lindahl, P., et al., *Pericyte loss and microaneurysm formation in PDGF-B-deficient mice.* Science, 1997. **277**(5323): p. 242-5.

107. Skobe, M. and N.E. Fusenig, *Tumorigenic conversion of immortal human keratinocytes through stromal cell activation.* Proc Natl Acad Sci U S A, 1998. **95**(3): p. 1050-5.

108. Dong, J., et al., *VEGF-null cells require PDGFR alpha signaling-mediated stromal fibroblast recruitment for tumorigenesis.* EMBO J, 2004. **23**(14): p. 2800-10.

109. Tejada, M.L., et al., *Tumor-driven paracrine platelet-derived growth factor receptor alpha signaling is a key determinant of stromal cell recruitment in a model of human lung carcinoma.* Clin Cancer Res, 2006. **12**(9): p. 2676-88.

110. Guo, P., et al., *Platelet-derived growth factor-B enhances glioma angiogenesis by stimulating vascular endothelial growth factor expression in tumor endothelia and by promoting pericyte recruitment.* Am J Pathol, 2003. **162**(4): p. 1083-93.

111. Wang, D., et al., *Induction of vascular endothelial growth factor expression in endothelial cells by platelet-derived growth factor through the activation of phosphatidylinositol 3-kinase.* Cancer Res, 1999. **59**(7): p. 1464-72.

112. Roberts, W.G., et al., *Antiangiogenic and antitumor activity of a selective PDGFR tyrosine kinase inhibitor, CP-673,451.* Cancer Res, 2005. **65**(3): p. 957-66.

113. Chiang, H.S., et al., *Lycopene inhibits PDGF-BB-induced signaling and migration in human dermal fibroblasts through interaction with PDGF-BB.* Life Sci, 2007. **81**(21-22): p. 1509-17.

114. Suzuki, S., et al., *Clinicopathological significance of platelet-derived growth factor (PDGF)-B and vascular endothelial growth factor-A expression, PDGF receptor-beta phosphorylation, and microvessel density in gastric cancer.* BMC Cancer, 2010. **10**: p. 659.

115. Hou, X., et al., *PDGF-CC blockade inhibits pathological angiogenesis by acting on multiple cellular and molecular targets.* Proc Natl Acad Sci U S A, 2010. **107**(27): p. 12216-21.

116. Nussenbaum, F. and I.M. Herman, *Tumor angiogenesis: insights and innovations.* J Oncol, 2010. **2010**: p. 132641.

117. Pardali, E., M.J. Goumans, and P. ten Dijke, *Signaling by members of the TGF-beta family in vascular morphogenesis and disease.* Trends Cell Biol, 2010. **20**(9): p. 556-67.

118. Roberts, A.B. and L.M. Wakefield, *The two faces of transforming growth factor beta in carcinogenesis.* Proc Natl Acad Sci U S A, 2003. **100**(15): p. 8621-3.

119. Serrati, S., et al., *TGFbeta1 antagonistic peptides inhibit TGFbeta1-dependent angiogenesis.* Biochem Pharmacol, 2009. **77**(5): p. 813-25.

120. Avraamides, C.J., B. Garmy-Susini, and J.A. Varner, *Integrins in angiogenesis and lymphangiogenesis.* Nat Rev Cancer, 2008. **8**(8): p. 604-17.

121. Garmy-Susini, B. and J.A. Varner, *Roles of integrins in tumor angiogenesis and lymphangiogenesis.* Lymphat Res Biol, 2008. **6**(3-4): p. 155-63.

122. Brooks, P.C., R.A. Clark, and D.A. Cheresh, *Requirement of vascular integrin alpha v beta 3 for angiogenesis.* Science, 1994. **264**(5158): p. 569-71.

123. Kim, S., et al., *Regulation of angiogenesis in vivo by ligation of integrin alpha5beta1 with the central cell-binding domain of fibronectin.* Am J Pathol, 2000. **156**(4): p. 1345-62.

124. Friedlander, M., et al., *Definition of two angiogenic pathways by distinct alpha v integrins.* Science, 1995. **270**(5241): p. 1500-2.

125. Desgrosellier, J.S. and D.A. Cheresh, *Integrins in cancer: biological implications and therapeutic opportunities.* Nat Rev Cancer, 2010. **10**(1): p. 9-22.

126. van Hinsbergh, V.W. and P. Koolwijk, *Endothelial sprouting and angiogenesis: matrix metalloproteinases in the lead.* Cardiovasc Res, 2008. **78**(2): p. 203-12.

127. Kessenbrock, K., V. Plaks, and Z. Werb, *Matrix metalloproteinases: regulators of the tumor microenvironment.* Cell, 2010. **141**(1): p. 52-67.

128. Gialeli, C., A.D. Theocharis, and N.K. Karamanos, *Roles of matrix metalloproteinases in cancer progression and their pharmacological targeting.* FEBS J, 2011. **278**(1): p. 16-27.

129. Bergers, G., et al., *Matrix metalloproteinase-9 triggers the angiogenic switch during carcinogenesis.* Nat Cell Biol, 2000. **2**(10): p. 737-44.

130. Yu, Q. and I. Stamenkovic, *Cell surface-localized matrix metalloproteinase-9 proteolytically activates TGF-beta and promotes tumor invasion and angiogenesis.* Genes Dev, 2000. **14**(2): p. 163-76.

131. Ardi, V.C., et al., *Neutrophil MMP-9 proenzyme, unencumbered by TIMP-1, undergoes efficient activation in vivo and catalytically induces angiogenesis via a basic fibroblast growth factor (FGF-2)/FGFR-2 pathway.* J Biol Chem, 2009. **284**(38): p. 25854-66.

132. Hurwitz, H., et al., *Bevacizumab plus irinotecan, fluorouracil, and leucovorin for metastatic colorectal cancer.* N Engl J Med, 2004. **350**(23): p. 2335-42.

133. Duda, D.G., R.K. Jain, and C.G. Willett, *Antiangiogenics: the potential role of integrating this novel treatment modality with chemoradiation for solid cancers.* J Clin Oncol, 2007. **25**(26): p. 4033-42.

134. Huber, P.E., et al., *Trimodal cancer treatment: beneficial effects of combined antiangiogenesis, radiation, and chemotherapy.* Cancer Res, 2005. **65**(9): p. 3643-55.

135. Jain, R.K., *Normalization of tumor vasculature: an emerging concept in antiangiogenic therapy.* Science, 2005. **307**(5706): p. 58-62.

136. Abdollahi, A. and J. Folkman, *Evading tumor evasion: current concepts and perspectives of anti-angiogenic cancer therapy.* Drug Resist Updat, 2010. **13**(1-2): p. 16-28.

137. Kim, K.J., et al., *Inhibition of vascular endothelial growth factor-induced angiogenesis suppresses tumour growth in vivo.* Nature, 1993. **362**(6423): p. 841-4.

138. Presta, L.G., et al., *Humanization of an anti-vascular endothelial growth factor monoclonal antibody for the therapy of solid tumors and other disorders.* Cancer Res, 1997. **57**(20): p. 4593-9.

139. Holash, J., et al., *VEGF-Trap: a VEGF blocker with potent antitumor effects.* Proc Natl Acad Sci U S A, 2002. **99**(17): p. 11393-8.

140. Fukasawa, M. and M. Korc, *Vascular endothelial growth factor-trap suppresses tumorigenicity of multiple pancreatic cancer cell lines.* Clin Cancer Res, 2004. **10**(10): p. 3327-32.

141. Kim, E.S., et al., *Potent VEGF blockade causes regression of coopted vessels in a model of neuroblastoma.* Proc Natl Acad Sci U S A, 2002. **99**(17): p. 11399-404.

142. Hu, L., et al., *Vascular endothelial growth factor trap combined with paclitaxel strikingly inhibits tumor and ascites, prolonging survival in a human ovarian cancer model.* Clin Cancer Res, 2005. **11**(19 Pt 1): p. 6966-71.

143. Byrne, A.T., et al., *Vascular endothelial growth factor-trap decreases tumor burden, inhibits ascites, and causes dramatic vascular remodeling in an ovarian cancer model.* Clin Cancer Res, 2003. **9**(15): p. 5721-8.

144. Frischer, J.S., et al., *Effects of potent VEGF blockade on experimental Wilms tumor and its persisting vasculature.* Int J Oncol, 2004. **25**(3): p. 549-53.

145. Huang, J., et al., *Regression of established tumors and metastases by potent vascular endothelial growth factor blockade.* Proc Natl Acad Sci U S A, 2003. **100**(13): p. 7785-90.

146. Twardowski, P., et al., *Phase II study of Aflibercept (VEGF-Trap) in patients with recurrent or metastatic urothelial cancer, a California Cancer Consortium Trial.* Urology, 2010. **76**(4): p. 923-6.

147. Leighl, N.B., et al., *A multicenter, phase 2 study of vascular endothelial growth factor trap (Aflibercept) in platinum- and erlotinib-resistant adenocarcinoma of the lung.* J Thorac Oncol, 2010. **5**(7): p. 1054-9.

148. de Groot, J.F., et al., *Phase II study of aflibercept in recurrent malignant glioma: a North American Brain Tumor Consortium study.* J Clin Oncol, 2011. **29**(19): p. 2689-95.

149. Peter, F., P. Nguyen Van, and H.D. Soling, *Different sorting of Lys-Asp-Glu-Leu proteins in rat liver.* J Biol Chem, 1992. **267**(15): p. 10631-7.

150. Singh, N., et al., *Flt-1 intraceptors inhibit hypoxia-induced VEGF expression in vitro and corneal neovascularization in vivo.* Invest Ophthalmol Vis Sci, 2005. **46**(5): p. 1647-52.

151. Jani, P.D., et al., *Nanoparticles sustain expression of Flt intraceptors in the cornea and inhibit injury-induced corneal angiogenesis.* Invest Ophthalmol Vis Sci, 2007. **48**(5): p. 2030-6.

152. Singh, S.R., et al., *Intravenous transferrin, RGD peptide and dual-targeted nanoparticles enhance anti-VEGF intraceptor gene delivery to laser-induced CNV.* Gene Ther, 2009. **16**(5): p. 645-59.

153. Soltau, J. and J. Drevs, *Mode of action and clinical impact of VEGF signaling inhibitors.* Expert Rev Anticancer Ther, 2009. **9**(5): p. 649-62.

154. D'Amico, D.J., et al., *Pegaptanib sodium for neovascular age-related macular degeneration: two-year safety results of the two prospective, multicenter, controlled clinical trials.* Ophthalmology, 2006. **113**(6): p. 992-1001 e6.

155. Rosenfeld, P.J., et al., *Ranibizumab for neovascular age-related macular degeneration.* N Engl J Med, 2006. **355**(14): p. 1419-31.

156. Goodman, V.L., et al., *Approval summary: sunitinib for the treatment of imatinib refractory or intolerant gastrointestinal stromal tumors and advanced renal cell carcinoma.* Clin Cancer Res, 2007. **13**(5): p. 1367-73.

157. Motzer, R.J., et al., *Sunitinib efficacy against advanced renal cell carcinoma.* J Urol, 2007. **178**(5): p. 1883-7.

158. Rossi, A., et al., *Angiogenesis inhibitors and vascular disrupting agents in non-small cell lung cancer.* Curr Med Chem, 2009. **16**(30): p. 3919-30.

159. Sherman, S.I., *Targeted therapy of thyroid cancer.* Biochem Pharmacol, 2010. **80**(5): p. 592-601.

160. Wilhelm, S.M., et al., *BAY 43-9006 exhibits broad spectrum oral antitumor activity and targets the RAF/MEK/ERK pathway and receptor tyrosine kinases involved in tumor progression and angiogenesis.* Cancer Res, 2004. **64**(19): p. 7099-109.

161. Wilhelm, S.M., et al., *Preclinical overview of sorafenib, a multikinase inhibitor that targets both Raf and VEGF and PDGF receptor tyrosine kinase signaling.* Mol Cancer Ther, 2008. **7**(10): p. 3129-40.

162. Del Bufalo, D., et al., *Antiangiogenic potential of the Mammalian target of rapamycin inhibitor temsirolimus.* Cancer Res, 2006. **66**(11): p. 5549-54.

163. Bellmunt, J., et al., *Temsirolimus safety profile and management of toxic effects in patients with advanced renal cell carcinoma and poor prognostic features.* Ann Oncol, 2008. **19**(8): p. 1387-92.

164. Wheeler, D.L., E.F. Dunn, and P.M. Harari, *Understanding resistance to EGFR inhibitors-impact on future treatment strategies.* Nat Rev Clin Oncol, 2010. **7**(9): p. 493-507.

165. Goldman, C.K., et al., *Epidermal growth factor stimulates vascular endothelial growth factor production by human malignant glioma cells: a model of glioblastoma multiforme pathophysiology.* Mol Biol Cell, 1993. **4**(1): p. 121-33.

166. De Luca, A., et al., *The role of the EGFR ligand/receptor system in the secretion of angiogenic factors in mesenchymal stem cells.* J Cell Physiol, 2010.

167. Pennell, N.A. and T.J. Lynch, Jr., *Combined inhibition of the VEGFR and EGFR signaling pathways in the treatment of NSCLC.* Oncologist, 2009. **14**(4): p. 399-411.

168. List, A., et al., *Efficacy of lenalidomide in myelodysplastic syndromes.* N Engl J Med, 2005. **352**(6): p. 549-57.

169. Tamilarasan, K.P., et al., *Thalidomide attenuates nitric oxide mediated angiogenesis by blocking migration of endothelial cells.* BMC Cell Biol, 2006. **7**: p. 17.

170. Verheul, H.M. and H.M. Pinedo, *Possible molecular mechanisms involved in the toxicity of angiogenesis inhibition.* Nat Rev Cancer, 2007. **7**(6): p. 475-85.

171. Bhargava, P., *VEGF kinase inhibitors: how do they cause hypertension?* Am J Physiol Regul Integr Comp Physiol, 2009. **297**(1): p. R1-5.

172. Ku, D.D., et al., *Vascular endothelial growth factor induces EDRF-dependent relaxation in coronary arteries.* Am J Physiol, 1993. **265**(2 Pt 2): p. H586-92.

173. Hood, J.D., et al., *VEGF upregulates ecNOS message, protein, and NO production in human endothelial cells.* Am J Physiol, 1998. **274**(3 Pt 2): p. H1054-8.

174. Tille, J.C., et al., *Vascular endothelial growth factor (VEGF) receptor-2 signaling mediates VEGF-C(deltaNdeltaC)- and VEGF-A-induced angiogenesis in vitro.* Exp Cell Res, 2003. **285**(2): p. 286-98.

175. Lee, S., et al., *Autocrine VEGF signaling is required for vascular homeostasis.* Cell, 2007. **130**(4): p. 691-703.

176. Matsuura, A., et al., *Stimulatory interaction between vascular endothelial growth factor and endothelin-1 on each gene expression.* Hypertension, 1998. **32**(1): p. 89-95.

177. Veronese, M.L., et al., *Mechanisms of hypertension associated with BAY 43-9006.* J Clin Oncol, 2006. **24**(9): p. 1363-9.

178. Higa, G.M. and J. Abraham, *Biological mechanisms of bevacizumab-associated adverse events.* Expert Rev Anticancer Ther, 2009. **9**(7): p. 999-1007.

179. Eskens, F.A. and J. Verweij, *The clinical toxicity profile of vascular endothelial growth factor (VEGF) and vascular endothelial growth factor receptor (VEGFR) targeting angiogenesis inhibitors; a review.* Eur J Cancer, 2006. **42**(18): p. 3127-39.

180. Shimizu, A., et al., *Vascular endothelial growth factor165 resolves glomerular inflammation and accelerates glomerular capillary repair in rat anti-glomerular basement membrane glomerulonephritis.* J Am Soc Nephrol, 2004. **15**(10): p. 2655-65.

181. Bergers, G. and D. Hanahan, *Modes of resistance to anti-angiogenic therapy.* Nat Rev Cancer, 2008. **8**(8): p. 592-603.

182. Ferrara, N., *Pathways mediating VEGF-independent tumor angiogenesis.* Cytokine Growth Factor Rev, 2010. **21**(1): p. 21-6.

183. Kindler, H.L., et al., *Axitinib plus gemcitabine versus placebo plus gemcitabine in patients with advanced pancreatic adenocarcinoma: a double-blind randomised phase 3 study.* Lancet Oncol, 2011.

184. Gridelli, C. and A. Rossi, *Unanswered questions: monoclonal antibodies in the treatment of advanced non-small-cell lung cancer.* Oncology (Williston Park), 2010. **24**(13): p. 1216-23.

185. Baselga, J. and J. Tabernero, *Combined antiangiogenesis and antiepidermal growth factor receptor targeting in the treatment of cancer: hold back, we are not there yet.* J Clin Oncol, 2007. **25**(29): p. 4516-8.

186. Timke, C., et al., *Combination of vascular endothelial growth factor receptor/platelet-derived growth factor receptor inhibition markedly improves radiation tumor therapy.* Clin Cancer Res, 2008. **14**(7): p. 2210-9.

187. Bullock, K.E., et al., *A phase I study of bevacizumab (B) in combination with everolimus (E) and erlotinib (E) in advanced cancer (BEE).* Cancer Chemother Pharmacol, 2011. **67**(2): p. 465-74.

188. Bouck, N.P. and B.K. Benton, *Loss of cancer suppressors, a driving force in carcinogenesis.* Chem Res Toxicol, 1989. **2**(1): p. 1-11.

189. Folkman, J. and D. Hanahan, *Switch to the angiogenic phenotype during tumorigenesis.* Princess Takamatsu Symp, 1991. **22**: p. 339-47.

190. Wang, J., et al., *[Results of randomized, multicenter, double-blind phase III trial of rh-endostatin (YH-16) in treatment of advanced non-small cell lung cancer patients.].* Zhongguo Fei Ai Za Zhi, 2005. **8**(4): p. 283-290.

191. O'Reilly, M.S., et al., *Angiostatin induces and sustains dormancy of human primary tumors in mice.* Nat Med, 1996. **2**(6): p. 689-92.

192. Oh, S.P., et al., *Isolation and sequencing of cDNAs for proteins with multiple domains of Gly-Xaa-Yaa repeats identify a distinct family of collagenous proteins.* Proc Natl Acad Sci U S A, 1994. **91**(10): p. 4229-33.

193. Wen, W., et al., *The generation of endostatin is mediated by elastase.* Cancer Res, 1999. **59**(24): p. 6052-6.

194. Felbor, U., et al., *Secreted cathepsin L generates endostatin from collagen XVIII.* EMBO J, 2000. **19**(6): p. 1187-94.

195. Rege, T.A., C.Y. Fears, and C.L. Gladson, *Endogenous inhibitors of angiogenesis in malignant gliomas: nature's antiangiogenic therapy.* Neuro Oncol, 2005. **7**(2): p. 106-21.

196. Folkman, J., *Antiangiogenesis in cancer therapy--endostatin and its mechanisms of action.* Exp Cell Res, 2006. **312**(5): p. 594-607.

197. Wilson, R.F., et al., *Endostatin inhibits migration and invasion of head and neck squamous cell carcinoma cells.* Anticancer Res, 2003. **23**(2B): p. 1289-95.

198. Mallery, S.R., et al., *AIDS-related Kaposi's sarcoma cells rapidly internalize endostatin, which co-localizes to tropomysin microfilaments and inhibits cytokine-mediated migration and invasion.* J Cell Biochem, 2003. **89**(1): p. 133-43.

199. Zorick, T.S., et al., *High serum endostatin levels in Down syndrome: implications for improved treatment and prevention of solid tumours.* Eur J Hum Genet, 2001. **9**(11): p. 811-4.

200. Sund, M., et al., *Function of endogenous inhibitors of angiogenesis as endothelium-specific tumor suppressors.* Proc Natl Acad Sci U S A, 2005. **102**(8): p. 2934-9.

201. Dhanabal, M., et al., *Endostatin induces endothelial cell apoptosis.* J Biol Chem, 1999. **274**(17): p. 11721-6.

202. Hanai, J., et al., *Endostatin causes G1 arrest of endothelial cells through inhibition of cyclin D1.* J Biol Chem, 2002. **277**(19): p. 16464-9.

203. Nyberg, P., et al., *Endostatin inhibits human tongue carcinoma cell invasion and intravasation and blocks the activation of matrix metalloprotease-2, -9, and -13.* J Biol Chem, 2003. **278**(25): p. 22404-11.

204. Kim, Y.M., et al., *Endostatin blocks vascular endothelial growth factor-mediated signaling via direct interaction with KDR/Flk-1.* J Biol Chem, 2002. **277**(31): p. 27872-9.

205. Dixelius, J., et al., *Endostatin regulates endothelial cell adhesion and cytoskeletal organization.* Cancer Res, 2002. **62**(7): p. 1944-7.

206. Wickstrom, S.A., K. Alitalo, and J. Keski-Oja, *Endostatin associates with integrin alpha5beta1 and caveolin-1, and activates Src via a tyrosyl phosphatase-dependent pathway in human endothelial cells.* Cancer Res, 2002. **62**(19): p. 5580-9.

207. Sudhakar, A., et al., *Human tumstatin and human endostatin exhibit distinct antiangiogenic activities mediated by alpha v beta 3 and alpha 5 beta 1 integrins.* Proc Natl Acad Sci U S A, 2003. **100**(8): p. 4766-71.

208. Sasaki, T., et al., *Structural basis and potential role of heparin/heparan sulfate binding to the angiogenesis inhibitor endostatin.* EMBO J, 1999. **18**(22): p. 6240-8.

209. Abdollahi, A., et al., *Endostatin's antiangiogenic signaling network.* Mol Cell, 2004. **13**(5): p. 649-63.

210. Chen, H., M.E. Herndon, and J. Lawler, *The cell biology of thrombospondin-1.* Matrix Biol, 2000. **19**(7): p. 597-614.

211. Haviv, F., et al., *Thrombospondin-1 mimetic peptide inhibitors of angiogenesis and tumor growth: design, synthesis, and optimization of pharmacokinetics and biological activities.* J Med Chem, 2005. **48**(8): p. 2838-46.

212. Tolsma, S.S., et al., *Peptides derived from two separate domains of the matrix protein thrombospondin-1 have anti-angiogenic activity.* J Cell Biol, 1993. **122**(2): p. 497-511.

213. Hohenester, E. and J. Engel, *Domain structure and organisation in extracellular matrix proteins.* Matrix Biol, 2002. **21**(2): p. 115-28.

214. Petitclerc, E., et al., *New functions for non-collagenous domains of human collagen type IV. Novel integrin ligands inhibiting angiogenesis and tumor growth in vivo.* J Biol Chem, 2000. **275**(11): p. 8051-61.

215. Colorado, P.C., et al., *Anti-angiogenic cues from vascular basement membrane collagen.* Cancer Res, 2000. **60**(9): p. 2520-6.

216. Kamphaus, G.D., et al., *Canstatin, a novel matrix-derived inhibitor of angiogenesis and tumor growth.* J Biol Chem, 2000. **275**(2): p. 1209-15.

217. Maeshima, Y., et al., *Identification of the anti-angiogenic site within vascular basement membrane-derived tumstatin.* J Biol Chem, 2001. **276**(18): p. 15240-8.

218. Morla, A. and E. Ruoslahti, *A fibronectin self-assembly site involved in fibronectin matrix assembly: reconstruction in a synthetic peptide.* J Cell Biol, 1992. **118**(2): p. 421-9.

219. Ramchandran, R., et al., *Antiangiogenic activity of restin, NC10 domain of human collagen XV: comparison to endostatin.* Biochem Biophys Res Commun, 1999. **255**(3): p. 735-9.

220. Claesson-Welsh, L., et al., *Angiostatin induces endothelial cell apoptosis and activation of focal adhesion kinase independently of the integrin-binding motif RGD.* Proc Natl Acad Sci U S A, 1998. **95**(10): p. 5579-83.

221. Cornelius, L.A., et al., *Matrix metalloproteinases generate angiostatin: effects on neovascularization.* J Immunol, 1998. **161**(12): p. 6845-52.

222. Cao, Y., et al., *Kringle domains of human angiostatin. Characterization of the anti-proliferative activity on endothelial cells.* J Biol Chem, 1996. **271**(46): p. 29461-7.

223. Cao, Y., et al., *Kringle 5 of plasminogen is a novel inhibitor of endothelial cell growth.* J Biol Chem, 1997. **272**(36): p. 22924-8.

224. Tombran-Tink, J. and L.V. Johnson, *Neuronal differentiation of retinoblastoma cells induced by medium conditioned by human RPE cells.* Invest Ophthalmol Vis Sci, 1989. **30**(8): p. 1700-7.

225. Steele, F.R., et al., *Pigment epithelium-derived factor: neurotrophic activity and identification as a member of the serine protease inhibitor gene family.* Proc Natl Acad Sci U S A, 1993. **90**(4): p. 1526-30.

226. Taniwaki, T., et al., *Pigment epithelium-derived factor is a survival factor for cerebellar granule cells in culture.* J Neurochem, 1995. **64**(6): p. 2509-17.

227. Dawson, D.W., et al., *Pigment epithelium-derived factor: a potent inhibitor of angiogenesis.* Science, 1999. **285**(5425): p. 245-8.

228. Yang, H., et al., *Angiostatin decreases cell migration and vascular endothelium growth factor (VEGF) to pigment epithelium derived factor (PEDF) RNA ratio in vitro and in a murine ocular melanoma model.* Mol Vis, 2006. **12**: p. 511-7.

229. Elayappan, B., et al., *PEDF inhibits VEGF- and EPO- induced angiogenesis in retinal endothelial cells through interruption of PI3K/Akt phosphorylation.* Angiogenesis, 2009. **12**(4): p. 313-24.

230. Cai, J., et al., *Pigment epithelium-derived factor inhibits angiogenesis via regulated intracellular proteolysis of vascular endothelial growth factor receptor 1.* J Biol Chem, 2006. **281**(6): p. 3604-13.

231. Gao, G., et al., *Unbalanced expression of VEGF and PEDF in ischemia-induced retinal neovascularization.* FEBS Lett, 2001. **489**(2-3): p. 270-6.

232. Takenaka, K., et al., *Pigment epithelium-derived factor (PEDF)-induced apoptosis and inhibition of vascular endothelial growth factor (VEGF) expression in MG63 human osteosarcoma cells.* Life Sci, 2005. **77**(25): p. 3231-41.

233. Abe, R., et al., *Overexpression of pigment epithelium-derived factor decreases angiogenesis and inhibits the growth of human malignant melanoma cells in vivo.* Am J Pathol, 2004. **164**(4): p. 1225-32.

234. Garcia, M., et al., *Inhibition of xenografted human melanoma growth and prevention of metastasis development by dual antiangiogenic/antitumor activities of pigment epithelium-derived factor.* Cancer Res, 2004. **64**(16): p. 5632-42.

235. Zhang, Y., et al., *Pigment epithelium-derived factor inhibits angiogenesis and growth of gastric carcinoma by down-regulation of VEGF.* Oncol Rep, 2011. **26**(3): p. 681-6.

236. Yang, J., et al., *Growth suppression of cervical carcinoma by pigment epithelium-derived factor via anti-angiogenesis.* Cancer Biol Ther, 2010. **9**(12): p. 967-74.

237. Ek, E.T., et al., *Pigment epithelium-derived factor overexpression inhibits orthotopic osteosarcoma growth, angiogenesis and metastasis.* Cancer Gene Ther, 2007. **14**(7): p. 616-26.

238. Uehara, H., et al., *Expression of pigment epithelium-derived factor decreases liver metastasis and correlates with favorable prognosis for patients with ductal pancreatic adenocarcinoma.* Cancer Res, 2004. **64**(10): p. 3533-7.

239. Yang, H. and H.E. Grossniklaus, *Constitutive overexpression of pigment epithelium-derived factor inhibition of ocular melanoma growth and metastasis.* Invest Ophthalmol Vis Sci, 2010. **51**(1): p. 28-34.

240. Folkman, J., *Endogenous angiogenesis inhibitors.* APMIS, 2004. **112**(7-8): p. 496-507.

241. Streck, C.J., et al., *Restriction of neuroblastoma angiogenesis and growth by interferon-alpha/beta.* Surgery, 2004. **136**(2): p. 183-9.

242. Tanabe, T., et al., *Inhibition of the glioblastoma cell cycle by type I IFNs occurs at both the G1 and S phases and correlates with the upregulation of p21(WAF1/CIP1).* J Neurooncol, 2000. **48**(3): p. 225-32.

243. Slaton, J.W., et al., *Interferon-alpha-mediated down-regulation of angiogenesis-related genes and therapy of bladder cancer are dependent on optimization of biological dose and schedule.* Clin Cancer Res, 1999. **5**(10): p. 2726-34.

244. von Marschall, Z., et al., *Effects of interferon alpha on vascular endothelial growth factor gene transcription and tumor angiogenesis.* J Natl Cancer Inst, 2003. **95**(6): p. 437-48.

245. Slaton, J.W., et al., *Treatment with low-dose interferon-alpha restores the balance between matrix metalloproteinase-9 and E-cadherin expression in human transitional cell carcinoma of the bladder.* Clin Cancer Res, 2001. **7**(9): p. 2840-53.

246. Wigginton, J.M., et al., *IFN-gamma and Fas/FasL are required for the antitumor and antiangiogenic effects of IL-12/pulse IL-2 therapy.* J Clin Invest, 2001. **108**(1): p. 51-62.

247. Cao, R., et al., *Interleukin-18 acts as an angiogenesis and tumor suppressor.* FASEB J, 1999. **13**(15): p. 2195-202.

248. Bar, D., et al., *A continuous delivery system of IL-1 receptor antagonist reduces angiogenesis and inhibits tumor development.* FASEB J, 2004. **18**(1): p. 161-3.

249. Volpert, O.V., et al., *Inhibition of angiogenesis by interleukin 4.* J Exp Med, 1998. **188**(6): p. 1039-46.

250. Belperio, J.A., et al., *CXC chemokines in angiogenesis.* J Leukoc Biol, 2000. **68**(1): p. 1-8.

251. Keeley, E.C., B. Mehrad, and R.M. Strieter, *Chemokines as mediators of tumor angiogenesis and neovascularization.* Exp Cell Res, 2011. **317**(5): p. 685-90.

252. Strieter, R.M., et al., *Cancer CXC chemokine networks and tumour angiogenesis.* Eur J Cancer, 2006. **42**(6): p. 768-78.

253. Barinaga, M., *Designing therapies that target tumor blood vessels.* Science, 1997. **275**(5299): p. 482-4.

254. Maione, T.E., et al., *Inhibition of angiogenesis by recombinant human platelet factor-4 and related peptides.* Science, 1990. **247**(4938): p. 77-9.

255. Bikfalvi, A., *Platelet factor 4: an inhibitor of angiogenesis.* Semin Thromb Hemost, 2004. **30**(3): p. 379-85.

256. Gentilini, G., et al., *Inhibition of human umbilical vein endothelial cell proliferation by the CXC chemokine, platelet factor 4 (PF4), is associated with impaired downregulation of p21(Cip1/WAF1).* Blood, 1999. **93**(1): p. 25-33.

257. Jiang, Y., I.D. Goldberg, and Y.E. Shi, *Complex roles of tissue inhibitors of metalloproteinases in cancer.* Oncogene, 2002. **21**(14): p. 2245-52.

258. Seo, D.W., et al., *TIMP-2 mediated inhibition of angiogenesis: an MMP-independent mechanism.* Cell, 2003. **114**(2): p. 171-80.

259. Patterson, B.C. and Q.A. Sang, *Angiostatin-converting enzyme activities of human matrilysin (MMP-7) and gelatinase B/type IV collagenase (MMP-9).* J Biol Chem, 1997. **272**(46): p. 28823-5.

260. Brew, K., D. Dinakarpandian, and H. Nagase, *Tissue inhibitors of metalloproteinases: evolution, structure and function.* Biochim Biophys Acta, 2000. **1477**(1-2): p. 267-83.

261. Brooks, P.C., et al., *Disruption of angiogenesis by PEX, a noncatalytic metalloproteinase fragment with integrin binding activity.* Cell, 1998. **92**(3): p. 391-400.

262. Doll, J.A., et al., *Pigment epithelium-derived factor regulates the vasculature and mass of the prostate and pancreas.* Nat Med, 2003. **9**(6): p. 774-80.

263. Yao, L., S.E. Pike, and G. Tosato, *Laminin binding to the calreticulin fragment vasostatin regulates endothelial cell function.* J Leukoc Biol, 2002. **71**(1): p. 47-53.

264. Pan, H., et al., *Molecular targeting of antiangiogenic factor 16K hPRL inhibits oxygen-induced retinopathy in mice.* Invest Ophthalmol Vis Sci, 2004. **45**(7): p. 2413-9.

265. Karagiannis, E.D. and A.S. Popel, *Peptides derived from type I thrombospondin repeat-containing proteins of the CCN family inhibit proliferation and migration of endothelial cells.* Int J Biochem Cell Biol, 2007. **39**(12): p. 2314-23.

266. Dawson, D.W., et al., *Three distinct D-amino acid substitutions confer potent antiangiogenic activity on an inactive peptide derived from a thrombospondin-1 type 1 repeat.* Mol Pharmacol, 1999. **55**(2): p. 332-8.

267. Reiher, F.K., et al., *Inhibition of tumor growth by systemic treatment with thrombospondin-1 peptide mimetics.* Int J Cancer, 2002. **98**(5): p. 682-9.

268. Baker, L.H., et al., *Randomized, phase II study of the thrombospondin-1-mimetic angiogenesis inhibitor ABT-510 in patients with advanced soft tissue sarcoma.* J Clin Oncol, 2008. **26**(34): p. 5583-8.

269. Nabors, L.B., et al., *A phase 1 trial of ABT-510 concurrent with standard chemoradiation for patients with newly diagnosed glioblastoma.* Arch Neurol, 2010. **67**(3): p. 313-9.

270. Ebbinghaus, S., et al., *Phase 2 study of ABT-510 in patients with previously untreated advanced renal cell carcinoma.* Clin Cancer Res, 2007. **13**(22 Pt 1): p. 6689-95.

271. Maeshima, Y., et al., *Distinct antitumor properties of a type IV collagen domain derived from basement membrane.* J Biol Chem, 2000. **275**(28): p. 21340-8.

272. Maeshima, Y., et al., *Extracellular matrix-derived peptide binds to alpha(v)beta(3) integrin and inhibits angiogenesis.* J Biol Chem, 2001. **276**(34): p. 31959-68.

273. Deuel, T.F., et al., *Amino acid sequence of human platelet factor 4.* Proc Natl Acad Sci U S A, 1977. **74**(6): p. 2256-8.

274. Aidoudi, S. and A. Bikfalvi, *Interaction of PF4 (CXCL4) with the vasculature: a role in atherosclerosis and angiogenesis.* Thromb Haemost, 2010. **104**(5): p. 941-8.

275. Lippi, G. and E.J. Favaloro, *Recombinant platelet factor 4: a therapeutic, anti-neoplastic chimera?* Semin Thromb Hemost, 2010. **36**(5): p. 558-69.

276. Gupta, S.K., T. Hassel, and J.P. Singh, *A potent inhibitor of endothelial cell proliferation is generated by proteolytic cleavage of the chemokine platelet factor 4.* Proc Natl Acad Sci U S A, 1995. **92**(17): p. 7799-803.

277. Jouan, V., et al., *Inhibition of in vitro angiogenesis by platelet factor-4-derived peptides and mechanism of action.* Blood, 1999. **94**(3): p. 984-93.

278. Butcher, D.J., et al., *A natural motif approach to protein design: a synthetic leucine zipper peptide mimics the biological function of the platelet factor 4 protein.* FEBS Lett, 1997. **409**(2): p. 183-7.

279. Nesmelova, I.V., et al., *Platelet factor 4 and interleukin-8 CXC chemokine heterodimer formation modulates function at the quaternary structural level.* J Biol Chem, 2005. **280**(6): p. 4948-58.

280. van der Schaft, D.W., et al., *The designer anti-angiogenic peptide anginex targets tumor endothelial cells and inhibits tumor growth in animal models.* FASEB J, 2002. **16**(14): p. 1991-3.

281. Griffioen, A.W., et al., *Anginex, a designed peptide that inhibits angiogenesis.* Biochem J, 2001. **354**(Pt 2): p. 233-42.

282. Mayo, K.H., et al., *Designed beta-sheet-forming peptide 33mers with potent human bactericidal/permeability increasing protein-like bactericidal and endotoxin neutralizing activities.* Biochim Biophys Acta, 1998. **1425**(1): p. 81-92.

283. Mayo, K.H., E. Ilyina, and H. Park, *A recipe for designing water-soluble, beta-sheet-forming peptides.* Protein Sci, 1996. **5**(7): p. 1301-15.

284. Brandwijk, R.J., et al., *Anti-angiogenesis and anti-tumor activity of recombinant anginex.* Biochem Biophys Res Commun, 2006. **349**(3): p. 1073-8.

285. Dings, R.P., et al., *Beta-sheet is the bioactive conformation of the anti-angiogenic anginex peptide.* Biochem J, 2003. **373**(Pt 1): p. 281-8.

286. Mayo, K.H., et al., *Design of a partial peptide mimetic of anginex with antiangiogenic and anticancer activity.* J Biol Chem, 2003. **278**(46): p. 45746-52.

287. Otvos, L., Jr., *Peptide-based drug design: here and now.* Methods Mol Biol, 2008. **494**: p. 1-8.

288. Dings, R.P., et al., *Discovery and development of anti-angiogenic peptides: A structural link.* Angiogenesis, 2003. **6**(2): p. 83-91.

289. Hohenester, E., et al., *Crystal structure of the angiogenesis inhibitor endostatin at 1.5 A resolution.* EMBO J, 1998. **17**(6): p. 1656-64.

290. Zhang, X., et al., *Crystal structure of recombinant human platelet factor 4.* Biochemistry, 1994. **33**(27): p. 8361-6.

291. Wilkins, A.L., W. Yang, and J.J. Yang, *Structural biology of the cell adhesion protein CD2: from molecular recognition to protein folding and design.* Curr Protein Pept Sci, 2003. **4**(5): p. 367-73.

292. Yang, J.J., et al., *Structural biology of the cell adhesion protein CD2: alternatively folded states and structure-function relation.* Curr Protein Pept Sci, 2001. **2**(1): p. 1-17.

293. Arulanandam, A.R., S. Koyasu, and E.L. Reinherz, *T cell receptor-independent CD2 signal transduction in FcR+ cells.* J Exp Med, 1991. **173**(4): p. 859-68.

294. Bierer, B.E. and W.C. Hahn, *T cell adhesion, avidity regulation and signaling: a molecular analysis of CD2.* Semin Immunol, 1993. **5**(4): p. 249-61.

295. Gollob, J.A. and J. Ritz, *CD2-CD58 interaction and the control of T-cell interleukin-12 responsiveness. Adhesion molecules link innate and acquired immunity.* Ann N Y Acad Sci, 1996. **795**: p. 71-81.

296. Brown, M.H., S. Preston, and A.N. Barclay, *A sensitive assay for detecting low-affinity interactions at the cell surface reveals no additional ligands for the adhesion pair rat CD2 and CD48.* Eur J Immunol, 1995. **25**(12): p. 3222-8.

297. Qin, L., et al., *Anti-CD2 receptor and anti-CD2 ligand (CD48) antibodies synergize to prolong allograft survival.* J Exp Med, 1994. **179**(1): p. 341-6.

298. Driscoll, P.C., et al., *Structure of domain 1 of rat T lymphocyte CD2 antigen.* Nature, 1991. **353**(6346): p. 762-5.

299. McAlister, M.S., et al., *NMR analysis of interacting soluble forms of the cell-cell recognition molecules CD2 and CD48.* Biochemistry, 1996. **35**(19): p. 5982-91.

300. Bodian, D.L., et al., *Crystal structure of the extracellular region of the human cell adhesion molecule CD2 at 2.5 A resolution.* Structure, 1994. **2**(8): p. 755-66.

301. Jones, E.Y., et al., *Crystal structure at 2.8 A resolution of a soluble form of the cell adhesion molecule CD2.* Nature, 1992. **360**(6401): p. 232-9.

302. Withka, J.M., et al., *Structure of the glycosylated adhesion domain of human T lymphocyte glycoprotein CD2.* Structure, 1993. **1**(1): p. 69-81.

303. Wyss, D.F., et al., *Conformation and function of the N-linked glycan in the adhesion domain of human CD2.* Science, 1995. **269**(5228): p. 1273-8.

304. Yang, J.J., et al., *Nonnative intermediate state of acid-stable beta-sheet protein.* Cell Biochem Biophys, 2000. **33**(3): p. 253-73.

305. Arulanandam, A.R., et al., *The CD58 (LFA-3) binding site is a localized and highly charged surface area on the AGFCC'C" face of the human CD2 adhesion domain.* Proc Natl Acad Sci U S A, 1993. **90**(24): p. 11613-7.

306. Davis, S.J., et al., *The role of charged residues mediating low affinity protein-protein recognition at the cell surface by CD2.* Proc Natl Acad Sci U S A, 1998. **95**(10): p. 5490-4.

307. Yang, W., et al., *Rational design of a calcium-binding protein.* J Am Chem Soc, 2003. **125**(20): p. 6165-71.

308. Ye, Y., et al., *A grafting approach to obtain site-specific metal-binding properties of EF-hand proteins.* Protein Eng, 2003. **16**(6): p. 429-34.

309. Pfuhl, M., et al., *When a module is also a domain: the role of the N terminus in the stability and the dynamics of immunoglobulin domains from titin.* J Mol Biol, 1997. **265**(2): p. 242-56.

310. Yang, W., et al., *The effects of Ca2+ binding on the dynamic properties of a designed Ca2+-binding protein.* Biochemistry, 2005. **44**(23): p. 8267-73.

311. Li, S., et al., *Rational design of a conformation-switchable Ca2+- and Tb3+-binding protein without the use of multiple coupled metal-binding sites.* FEBS J, 2008. **275**(20): p. 5048-61.

312. Kaelin, W.G., Jr., et al., *Identification of cellular proteins that can interact specifically with the T/E1A-binding region of the retinoblastoma gene product.* Cell, 1991. **64**(3): p. 521-32.

313. Weidner, N., et al., *Tumor angiogenesis and metastasis--correlation in invasive breast carcinoma.* N Engl J Med, 1991. **324**(1): p. 1-8.

314. Ruegg, C. and N. Mutter, *Anti-angiogenic therapies in cancer: achievements and open questions.* Bull Cancer, 2007. **94**(9): p. 753-62.

315. Carmeliet, P. and D. Collen, *Molecular basis of angiogenesis. Role of VEGF and VE-cadherin.* Ann N Y Acad Sci, 2000. **902**: p. 249-62; discussion 262-4.

316. Jain, R.K., et al., *Lessons from phase III clinical trials on anti-VEGF therapy for cancer.* Nat Clin Pract Oncol, 2006. **3**(1): p. 24-40.

317. Gotink, K.J. and H.M. Verheul, *Anti-angiogenic tyrosine kinase inhibitors: what is their mechanism of action?* Angiogenesis, 2010. **13**(1): p. 1-14.

318. Heng, D.Y. and R.M. Bukowski, *Anti-angiogenic targets in the treatment of advanced renal cell carcinoma.* Curr Cancer Drug Targets, 2008. **8**(8): p. 676-82.

319. Demetri, G.D., et al., *Efficacy and safety of sunitinib in patients with advanced gastrointestinal stromal tumour after failure of imatinib: a randomised controlled trial.* Lancet, 2006. **368**(9544): p. 1329-38.

320. Motzer, R.J. and R.M. Bukowski, *Targeted therapy for metastatic renal cell carcinoma.* J Clin Oncol, 2006. **24**(35): p. 5601-8.

321. Abou-Alfa, G.K., et al., *Phase II study of sorafenib in patients with advanced hepatocellular carcinoma.* J Clin Oncol, 2006. **24**(26): p. 4293-300.

322. Escudier, B., et al., *Sorafenib in advanced clear-cell renal-cell carcinoma.* N Engl J Med, 2007. **356**(2): p. 125-34.

323. Mundel, T.M. and R. Kalluri, *Type IV collagen-derived angiogenesis inhibitors.* Microvasc Res, 2007. **74**(2-3): p. 85-9.

324. Keshet, E. and S.A. Ben-Sasson, *Anticancer drug targets: approaching angiogenesis.* J Clin Invest, 1999. **104**(11): p. 1497-501.

325. Fukumura, D. and R.K. Jain, *Tumor microvasculature and microenvironment: targets for anti-angiogenesis and normalization.* Microvasc Res, 2007. **74**(2-3): p. 72-84.

326. Sudhakar, A. and C.S. Boosani, *Inhibition of tumor angiogenesis by tumstatin: insights into signaling mechanisms and implications in cancer regression.* Pharm Res, 2008. **25**(12): p. 2731-9.

327. Damber, J.E., et al., *The anti-tumour effect of low-dose continuous chemotherapy may partly be mediated by thrombospondin.* Cancer Chemother Pharmacol, 2006. **58**(3): p. 354-60.

328. Wu, S., et al., *Bevacizumab increases risk for severe proteinuria in cancer patients.* J Am Soc Nephrol, 2010. **21**(8): p. 1381-9.

329. Yardley, D.A., *Integrating bevacizumab into the treatment of patients with early-stage breast cancer: focus on cardiac safety.* Clin Breast Cancer, 2010. **10**(2): p. 119-29.

330. Weidner, N., et al., *Tumor angiogenesis: a new significant and independent prognostic indicator in early-stage breast carcinoma.* J Natl Cancer Inst, 1992. **84**(24): p. 1875-87.

331. Moingeon, P., et al., *The structural biology of CD2.* Immunol Rev, 1989. **111**: p. 111-44.

332. Moingeon, P., et al., *CD2-mediated adhesion facilitates T lymphocyte antigen recognition function.* Nature, 1989. **339**(6222): p. 312-4.

333. Hunig, T., et al., *Alternative pathway activation of T cells by binding of CD2 to its cell-surface ligand.* Nature, 1987. **326**(6110): p. 298-301.

334. Chang, H.C., et al., *Dissection of the human CD2 intracellular domain. Identification of a segment required for signal transduction and interleukin 2 production.* J Exp Med, 1989. **169**(6): p. 2073-83.

335. Recny, M.A., et al., *Structural and functional characterization of the CD2 immunoadhesion domain. Evidence for inclusion of CD2 in an alpha-beta protein folding class.* J Biol Chem, 1990. **265**(15): p. 8542-9.

336. Hanson, S.R., et al., *The core trisaccharide of an N-linked glycoprotein intrinsically accelerates folding and enhances stability.* Proc Natl Acad Sci U S A, 2009. **106**(9): p. 3131-6.

337. Recny, M.A., et al., *N-glycosylation is required for human CD2 immunoadhesion functions.* J Biol Chem, 1992. **267**(31): p. 22428-34.

338. Wang, J.H., et al., *Structure of a heterophilic adhesion complex between the human CD2 and CD58 (LFA-3) counterreceptors.* Cell, 1999. **97**(6): p. 791-803.

339. Dustin, M.L., et al., *Anchoring mechanisms for LFA-3 cell adhesion glycoprotein at membrane surface.* Nature, 1987. **329**(6142): p. 846-8.

340. Kim, M., et al., *Molecular dissection of the CD2-CD58 counter-receptor interface identifies CD2 Tyr86 and CD58 Lys34 residues as the functional "hot spot".* J Mol Biol, 2001. **312**(4): p. 711-20.

341. van der Merwe, P.A., et al., *Human cell-adhesion molecule CD2 binds CD58 (LFA-3) with a very low affinity and an extremely fast dissociation rate but does not bind CD48 or CD59.* Biochemistry, 1994. **33**(33): p. 10149-60.

342. Arulanandam, A.R., et al., *A soluble multimeric recombinant CD2 protein identifies CD48 as a low affinity ligand for human CD2: divergence of CD2 ligands during the evolution of humans and mice.* J Exp Med, 1993. **177**(5): p. 1439-50.

343. Murasugi, A., *Secretory expression of human protein in the Yeast Pichia pastoris by controlled fermentor culture.* Recent Pat Biotechnol, 2010. **4**(2): p. 153-66.

344. Roberts, M.J., M.D. Bentley, and J.M. Harris, *Chemistry for peptide and protein PEGylation.* Adv Drug Deliv Rev, 2002. **54**(4): p. 459-76.

345. Thijssen, V.L., et al., *Galectin-1 is essential in tumor angiogenesis and is a target for antiangiogenesis therapy.* Proc Natl Acad Sci U S A, 2006. **103**(43): p. 15975-80.

346. Staton, C.A., et al., *Current methods for assaying angiogenesis in vitro and in vivo.* Int J Exp Pathol, 2004. **85**(5): p. 233-48.

347. Staton, C.A., M.W. Reed, and N.J. Brown, *A critical analysis of current in vitro and in vivo angiogenesis assays.* Int J Exp Pathol, 2009. **90**(3): p. 195-221.

348. Jackson, C.J. and M. Nguyen, *Human microvascular endothelial cells differ from macrovascular endothelial cells in their expression of matrix metalloproteinases.* Int J Biochem Cell Biol, 1997. **29**(10): p. 1167-77.

349. Bouis, D., et al., *Endothelium in vitro: a review of human vascular endothelial cell lines for blood vessel-related research.* Angiogenesis, 2001. **4**(2): p. 91-102.

350. Rehn, M., et al., *Interaction of endostatin with integrins implicated in angiogenesis.* Proc Natl Acad Sci U S A, 2001. **98**(3): p. 1024-9.

351. Yokoyama, Y., et al., *Synergy between angiostatin and endostatin: inhibition of ovarian cancer growth.* Cancer Res, 2000. **60**(8): p. 2190-6.

352. Lawley, T.J. and Y. Kubota, *Induction of morphologic differentiation of endothelial cells in culture.* J Invest Dermatol, 1989. **93**(2 Suppl): p. 59S-61S.

353. Donovan, D., et al., *Comparison of three in vitro human 'angiogenesis' assays with capillaries formed in vivo.* Angiogenesis, 2001. **4**(2): p. 113-21.

354. Brawer, M.K., et al., *Predictors of pathologic stage in prostatic carcinoma. The role of neovascularity.* Cancer, 1994. **73**(3): p. 678-87.

355. Weidner, N., et al., *Tumor angiogenesis correlates with metastasis in invasive prostate carcinoma.* Am J Pathol, 1993. **143**(2): p. 401-9.

356. Ravindranath, N., et al., *Epidermal growth factor modulates the expression of vascular endothelial growth factor in the human prostate.* J Androl, 2001. **22**(3): p. 432-43.

357. Wang, Y., et al., *Biological activity of bevacizumab, a humanized anti-VEGF antibody in vitro.* Angiogenesis, 2004. **7**(4): p. 335-45.

358. Veronese, F.M., *Peptide and protein PEGylation: a review of problems and solutions.* Biomaterials, 2001. **22**(5): p. 405-17.

359. Bell, S.J., et al., *Enhanced circulating half-life and antitumor activity of a site-specific pegylated interferon-alpha protein therapeutic.* Bioconjug Chem, 2008. **19**(1): p. 299-305.

360. Baker, D.P., et al., *N-terminally PEGylated human interferon-beta-1a with improved pharmacokinetic properties and in vivo efficacy in a melanoma angiogenesis model.* Bioconjug Chem, 2006. **17**(1): p. 179-88.

361. Newman, P.J., et al., *PECAM-1 (CD31) cloning and relation to adhesion molecules of the immunoglobulin gene superfamily.* Science, 1990. **247**(4947): p. 1219-22.

362. Miettinen, M., A.E. Lindenmayer, and A. Chaubal, *Endothelial cell markers CD31, CD34, and BNH9 antibody to H- and Y-antigens--evaluation of their specificity and sensitivity in the diagnosis of vascular tumors and comparison with von Willebrand factor.* Mod Pathol, 1994. **7**(1): p. 82-90.

363. Muller, A.M., et al., *Expression of the endothelial markers PECAM-1, vWf, and CD34 in vivo and in vitro.* Exp Mol Pathol, 2002. **72**(3): p. 221-9.

364. Pusztaszeri, M.P., W. Seelentag, and F.T. Bosman, *Immunohistochemical expression of endothelial markers CD31, CD34, von Willebrand factor, and Fli-1 in normal human tissues.* J Histochem Cytochem, 2006. **54**(4): p. 385-95.

365. Rosca, E.V., et al., *Anti-angiogenic peptides for cancer therapeutics.* Curr Pharm Biotechnol, 2011. **12**(8): p. 1101-16.

366. Barondes, S.H., et al., *Galectins. Structure and function of a large family of animal lectins.* J Biol Chem, 1994. **269**(33): p. 20807-10.

367. Camby, I., et al., *Galectin-1: a small protein with major functions.* Glycobiology, 2006. **16**(11): p. 137R-157R.

368. Nagy, N., et al., *Refined prognostic evaluation in colon carcinoma using immunohistochemical galectin fingerprinting.* Cancer, 2003. **97**(8): p. 1849-58.

369. Szoke, T., et al., *Prognostic significance of endogenous adhesion/growth-regulatory lectins in lung cancer.* Oncology, 2005. **69**(2): p. 167-74.

370. Grutzmann, R., et al., *Gene expression profiling of microdissected pancreatic ductal carcinomas using high-density DNA microarrays.* Neoplasia, 2004. **6**(5): p. 611-22.

371. Shen, J., et al., *Protein expression profiles in pancreatic adenocarcinoma compared with normal pancreatic tissue and tissue affected by pancreatitis as detected by two-dimensional gel electrophoresis and mass spectrometry.* Cancer Res, 2004. **64**(24): p. 9018-26.

372. Cindolo, L., et al., *galectin-1 and galectin-3 expression in human bladder transitional-cell carcinomas.* Int J Cancer, 1999. **84**(1): p. 39-43.

373. van den Brule, F.A., D. Waltregny, and V. Castronovo, *Increased expression of galectin-1 in carcinoma-associated stroma predicts poor outcome in prostate carcinoma patients.* J Pathol, 2001. **193**(1): p. 80-7.

374. van den Brule, F., et al., *Galectin-1 accumulation in the ovary carcinoma peritumoral stroma is induced by ovary carcinoma cells and affects both cancer cell proliferation and adhesion to laminin-1 and fibronectin.* Lab Invest, 2003. **83**(3): p. 377-86.

375. Tinari, N., et al., *Glycoprotein 90K/MAC-2BP interacts with galectin-1 and mediates galectin-1-induced cell aggregation.* Int J Cancer, 2001. **91**(2): p. 167-72.

376. Clausse, N., et al., *Galectin-1 expression in prostate tumor-associated capillary endothelial cells is increased by prostate carcinoma cells and modulates heterotypic cell-cell adhesion.* Angiogenesis, 1999. **3**(4): p. 317-25.

377. Glinsky, V.V., et al., *Effects of Thomsen-Friedenreich antigen-specific peptide P-30 on beta-galactoside-mediated homotypic aggregation and adhesion to the endothelium of MDA-MB-435 human breast carcinoma cells.* Cancer Res, 2000. **60**(10): p. 2584-8.

378. Le, Q.T., et al., *Galectin-1: a link between tumor hypoxia and tumor immune privilege.* J Clin Oncol, 2005. **23**(35): p. 8932-41.

379. Rubinstein, N., et al., *Targeted inhibition of galectin-1 gene expression in tumor cells results in heightened T cell-mediated rejection; A potential mechanism of tumor-immune privilege.* Cancer Cell, 2004. **5**(3): p. 241-51.

380. Chung, C.D., et al., *Galectin-1 induces partial TCR zeta-chain phosphorylation and antagonizes processive TCR signal transduction.* J Immunol, 2000. **165**(7): p. 3722-9.

381. Blaser, C., et al., *Beta-galactoside-binding protein secreted by activated T cells inhibits antigen-induced proliferation of T cells.* Eur J Immunol, 1998. **28**(8): p. 2311-9.

382. Perillo, N.L., et al., *Apoptosis of T cells mediated by galectin-1.* Nature, 1995. **378**(6558): p. 736-9.

383. Rabinovich, G.A., et al., *Specific inhibition of T-cell adhesion to extracellular matrix and proinflammatory cytokine secretion by human recombinant galectin-1.* Immunology, 1999. **97**(1): p. 100-6.

384. Rabinovich, G.A., et al., *Activated rat macrophages produce a galectin-1-like protein that induces apoptosis of T cells: biochemical and functional characterization.* J Immunol, 1998. **160**(10): p. 4831-40.

385. Rabinovich, G.A., et al., *Induction of allogenic T-cell hyporesponsiveness by galectin-1-mediated apoptotic and non-apoptotic mechanisms.* Cell Death Differ, 2002. **9**(6): p. 661-70.

386. Zhou, H., et al., *T cell-mediated suppression of angiogenesis results in tumor protective immunity.* Blood, 2005. **106**(6): p. 2026-32.

387. Clerch, L.B., et al., *Sequence of a full-length cDNA for rat lung beta-galactoside-binding protein: primary and secondary structure of the lectin.* Biochemistry, 1988. **27**(2): p. 692-9.

388. Cooper, D.N. and S.H. Barondes, *Evidence for export of a muscle lectin from cytosol to extracellular matrix and for a novel secretory mechanism.* J Cell Biol, 1990. **110**(5): p. 1681-91.

389. Van den Brule, F.A., et al., *Differential expression of galectin-1 and galectin-3 during first trimester human embryogenesis.* Dev Dyn, 1997. **209**(4): p. 399-405.

390. von Wolff, M., et al., *Galectin fingerprinting in human endometrium and decidua during the menstrual cycle and in early gestation.* Mol Hum Reprod, 2005. **11**(3): p. 189-94.

391. Paz, A., et al., *Galectin-1 binds oncogenic H-Ras to mediate Ras membrane anchorage and cell transformation.* Oncogene, 2001. **20**(51): p. 7486-93.

392. Prior, I.A., et al., *Direct visualization of Ras proteins in spatially distinct cell surface microdomains.* J Cell Biol, 2003. **160**(2): p. 165-70.

393. Elad-Sfadia, G., et al., *Galectin-1 augments Ras activation and diverts Ras signals to Raf-1 at the expense of phosphoinositide 3-kinase.* J Biol Chem, 2002. **277**(40): p. 37169-75.

394. Thijssen, V.L., et al., *Tumor cells secrete galectin-1 to enhance endothelial cell activity.* Cancer Res, 2010. **70**(15): p. 6216-24.

395. Yang, J.J., et al., *Rational design of protein-based MRI contrast agents.* J Am Chem Soc, 2008. **130**(29): p. 9260-7.

396. Ruegg, C., et al., *Antiangiogenic peptides and proteins: from experimental tools to clinical drugs.* Biochim Biophys Acta, 2006. **1765**(2): p. 155-77.

397. Pasut, G. and F.M. Veronese, *PEG conjugates in clinical development or use as anticancer agents: an overview.* Adv Drug Deliv Rev, 2009. **61**(13): p. 1177-88.

398. Somoza, C., et al., *Mutational analysis of the CD2/CD58 interaction: the binding site for CD58 lies on one face of the first domain of human CD2.* J Exp Med, 1993. **178**(2): p. 549-58.

399. Xu, Y., et al., *The anti-CD2 monoclonal antibody BTI-322 generates unresponsiveness by activation-associated T cell depletion.* Clin Exp Immunol, 2004. **138**(3): p. 476-83.

400. Jondal, M., G. Holm, and H. Wigzell, *Surface markers on human T and B lymphocytes. I. A large population of lymphocytes forming nonimmune rosettes with sheep red blood cells.* J Exp Med, 1972. **136**(2): p. 207-15.

401. Sun, Z.Y., et al., *Functional glycan-free adhesion domain of human cell surface receptor CD58: design, production and NMR studies.* EMBO J, 1999. **18**(11): p. 2941-9.

402. Saltz, L.B., et al., *Randomized phase II trial of cetuximab, bevacizumab, and irinotecan compared with cetuximab and bevacizumab alone in irinotecan-refractory colorectal cancer: the BOND-2 study.* J Clin Oncol, 2007. **25**(29): p. 4557-61.

403. Bukowski, R.M., et al., *Randomized phase II study of erlotinib combined with bevacizumab compared with bevacizumab alone in metastatic renal cell cancer.* J Clin Oncol, 2007. **25**(29): p. 4536-41.

404. Masuda, Y., et al., *Vascular endothelial growth factor enhances glomerular capillary repair and accelerates resolution of experimentally induced glomerulonephritis.* Am J Pathol, 2001. **159**(2): p. 599-608.

405. Sugimoto, H., et al., *Neutralization of circulating vascular endothelial growth factor (VEGF) by anti-VEGF antibodies and soluble VEGF receptor 1 (sFlt-1) induces proteinuria.* J Biol Chem, 2003. **278**(15): p. 12605-8.

406. Yang, J.C., et al., *A randomized trial of bevacizumab, an anti-vascular endothelial growth factor antibody, for metastatic renal cancer.* N Engl J Med, 2003. **349**(5): p. 427-34.

407. Torchilin, V.P. and A.N. Lukyanov, *Peptide and protein drug delivery to and into tumors: challenges and solutions.* Drug Discov Today, 2003. **8**(6): p. 259-66.

408. Chang, D.K., et al., *Antiangiogenic targeting liposomes increase therapeutic efficacy for solid tumors.* J Biol Chem, 2009. **284**(19): p. 12905-16.

409. Wu, H.C. and D.K. Chang, *Peptide-mediated liposomal drug delivery system targeting tumor blood vessels in anticancer therapy.* J Oncol, 2010. **2010**: p. 723798.

410. Gasparini, G., et al., *Combination of antiangiogenic therapy with other anticancer therapies: results, challenges, and open questions.* J Clin Oncol, 2005. **23**(6): p. 1295-311.

411. Strieth, S., et al., *Antiangiogenic combination tumor therapy blocking alpha(v)-integrins and VEGF-receptor-2 increases therapeutic effects in vivo.* Int J Cancer, 2006. **119**(2): p. 423-31.

412. Awasthi, N., et al., *The efficacy of a novel, dual PI3K/mTOR inhibitor NVP-BEZ235 to enhance chemotherapy and antiangiogenic response in pancreatic cancer.* J Cell Biochem, 2011.

413. Zhang, W., et al., *Bevacizumab With Angiostatin-armed oHSV Increases Antiangiogenesis and Decreases Bevacizumab-induced Invasion in U87 Glioma.* Mol Ther, 2011.

414. Neskey, D.M., et al., *Endostatin and anastellin inhibit distinct aspects of the angiogenic process.* J Exp Clin Cancer Res, 2008. **27**: p. 61.

APPENDIX

LIST OF COMMON BUFFERS

Lysate buffer, Preparation for 250 mL:

1% sarcosyl (N-lauroyl sarcosine)	2.5 g
10 mM DTT	0.385 g
1 mM EDTA	0.10 g
5 μM inhibitor (AEBSF)	2.5 mL

Fill to 250 mL with 1x PBS pH 7.3

10x PBS, Preparation for 1 L:

NaCl	81.750 g
KCl	2.009 g
$Na_2HPO_4*7H_2O$	27.075 g
KH_2PO_4	2.448 g

Add 1 L ddH_2O. Verify pH at or near 7.3

Luria-Bertani (LB) broth medium (1L)

Bacto-tryptone	10 g
Bactone-yeast extract	5 g
NaCl	10 g

Add distilled water to 1 L

Adjust pH to 7.0 with NaOH and autoclave